NASA Contractor Report 178147

Near-Field Testing of the 5-Meter Model of the Tetrahedral Truss Antenna

Final Report

Martin Marietta Denver Aerospace
Denver, CO 80201

Contract NAS1-18016
August 1986

National Aeronautics and
Space Administration

Langley Research Center
Hampton, Virginia 23665

MCR-85-640

Contract No. NAS1-18016

Final
Report August 1986

Technical Report

NEAR-FIELD TESTING OF THE 5-METER MODEL OF THE TETRAHEDRAL TRUSS ANTENNA

To

NASA Langley Research Center
Antenna and Microwave Research Branch

Authors:

Neill Kefauver
Tom Cencich

Jim Osborn
Program Manager and Author

J. T. Osmanski
Manager
Environmental & Test Technologies

MARTIN MARIETTA
DENVER AEROSPACE
P.O. Box 179
Denver, Colorado 80201

FOREWORD

This report, prepared by Martin Marietta Denver Aerospace, is submitted to the NASA Langley Research Center, Antenna and Microwave Research Branch, in response to Contract NAS1-18016, Near-Field Testing of the 15-Meter Model of the Hoop Column Antenna, CDRL Line Item I.D. This report covers only the contract add-on for Near-Field Testing of the 5-Meter Model of the Tetrahedral Truss Antenna.

CONTENTS

Figure

GLOSSARY

f/d	Ratio of Focus to Diameter
FFT	Fast Fourier Transform
GDC	General Dynamics Corporation
LaRC	NASA Langley Research Center
NFTL	Near-Field Test Laboratory
rms	Root Mean Square
VSWR	Voltage Standing Wave Ratio

1.0 INTRODUCTION

On February 3, 1986, the Martin Marietta Denver Aerospace Near-Field Test Laboratory (NFTL) began a series of tests on the General Dynamics Corporation (GDC) 5-Meter Tetrahedral Truss Antenna for NASA Langley Research Center (LaRC) as an add-on task to NASA Contract NAS1-18016. For the new task, NASA LaRC provided the same set of feeds used in testing the 15-Meter Hoop Column Antenna earlier under the contract (Refs 1,2,3). The tests performed with these feeds used four frequencies: 2.27, 4.26, 7.73, and 11.60 GHz. Because the antenna was installed in the NFTL under a separate contract between Martin Marietta and General Dynamics, no deployment or dismantling activities were performed for the add-on task; only feed installation and testing were performed.

The goals of this task included establishing reflector performance throughout the microwave frequency band, taking metric camera and theodolite measurements of the surface, and performing complete analysis of the electrical data. This analysis summarized the limiting errors in the measurements and isolated major sources of antenna performance degradation. The analysis helped to isolate the effects that exclusively depended on the specific feed tested, the effects that depended on frequency, and the effects that were controlled by the system accuracy. The following report covers the results of this detailed analysis of the electrical properties of the 5-Meter Tetrahedral Truss Antenna.

The final report is composed of six sections containing information in a logical sequence. The first section is the introduction. The second section describes the acquisition of the raw data needed to calculate antenna performance. The third defines the system measurement accuracy. The fourth section compiles the collected near-field data and calculated far-field data. The fifth covers the diagnostics used to isolate the different causes of actual pattern performance. The final section summarizes the results of the program.

This Page Intentionally Left Blank

2.0 TEST PROGRAM

The data collected on this program include RF measurements, metric camera photography, and theodolite sightings. Figures 1 and 2 show the reflector configured for testing in the NFTL. During the tests the antenna is pointed upward, the near-field of the antenna being measured in a horizontal plane with overhead sampling probes. Figure 1 shows the antenna from the floor, focusing on the tetrahedral trusswork and graphite cords used to control the reflector surface. It also shows the booms supporting the reflector and the offset feed. The photograph in Figure 2 was taken above the reflector and shows the metric camera targets as bright spots on the reflector surface. Figure 2 also includes the three lateral reflector seams, the major one located at the reflector center. Figures 3-6 show the four feeds used to illuminate the reflector for the LaRC tests. The large boom structure in Figure 1 supported the feeds in the focal plane above the reflector while the tests were conducted.

We organized the test schedule to optimize data acquisition. Table 1 shows this schedule. The tests at 7.73 GHz required reconfiguration of the feed mount assembly, and because of this reconfiguration the NFTL performed these tests last. Before the 7.73-GHz tests, personnel from Martin Marietta and NASA completed the set of metric camera photos and theodolite measurements needed to determine both the reflector surface tolerance and the feed position.

Metric photos were taken by Richard Adams of NASA LaRC with the NFTL Reachall (man-lifting device shown in Figure 1) at eight positions above the reflector surface. The turntable supporting the mounting tower was rotated, and the height from the Reachall to the reflector surface was set to approximately 20 ft. Next, using the two-way optical targets that NASA provided, we sighted the surface and the 11.60-GHz and 7.73-GHz feed horns using theodolites. These data, combined with the data obtained from processing the metric photos, provided the measured position of both the reflector surface and the feed.

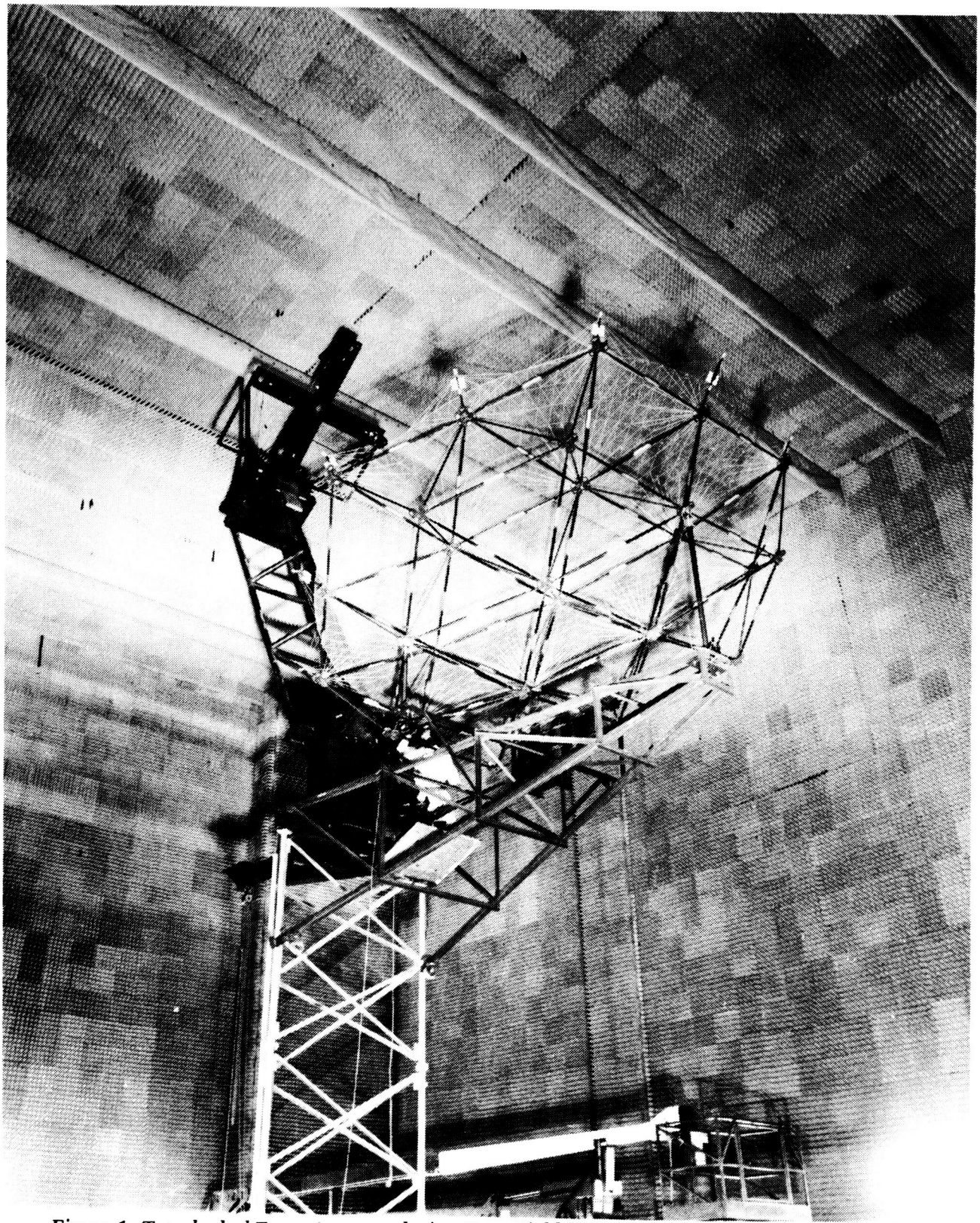

Figure 1 Tetrahedral Truss Antenna during Near-Field Measurements (Rear View)

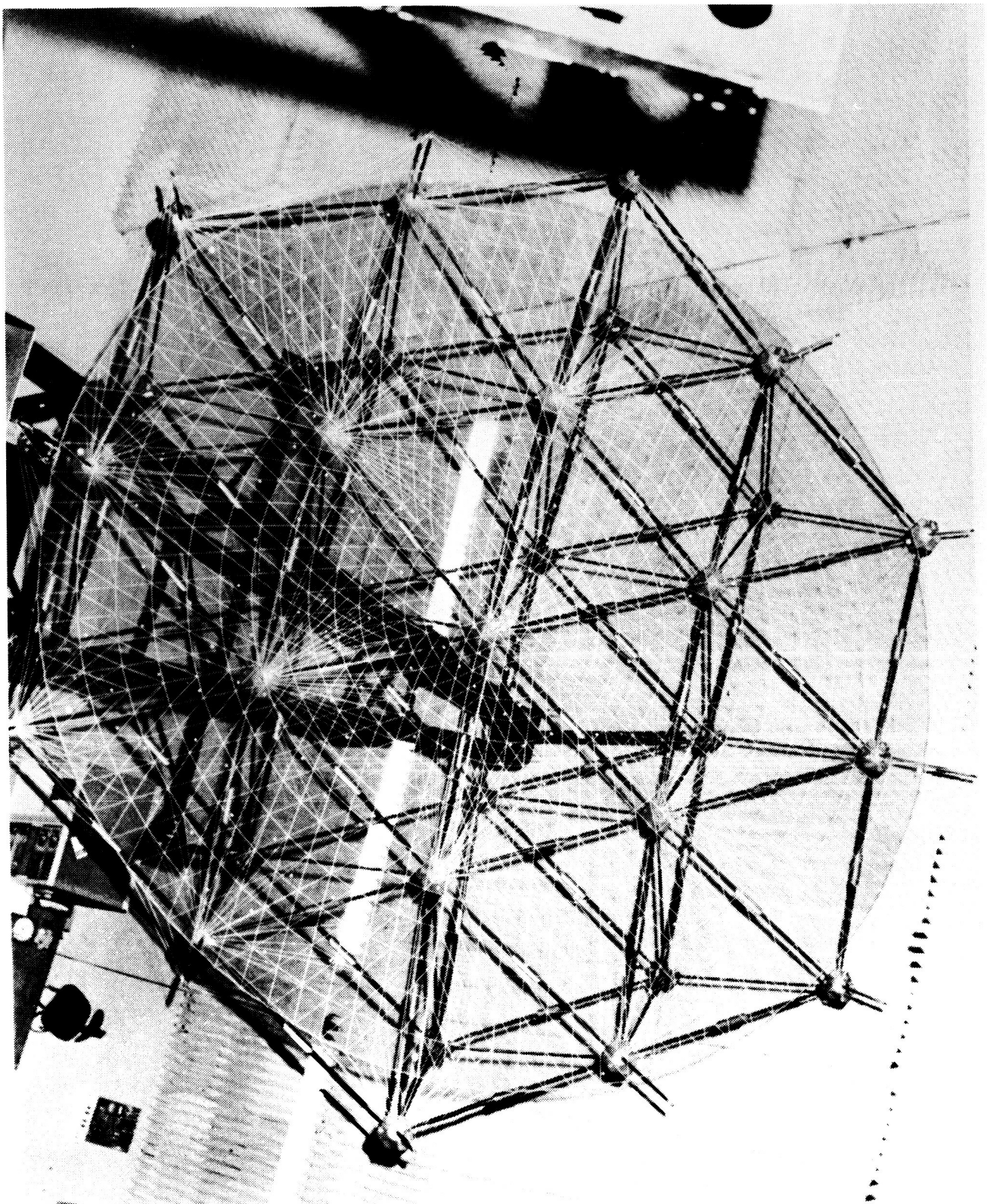

Figure 2 Tetrahedral Truss Antenna during Near-Field Measurements (Front View)

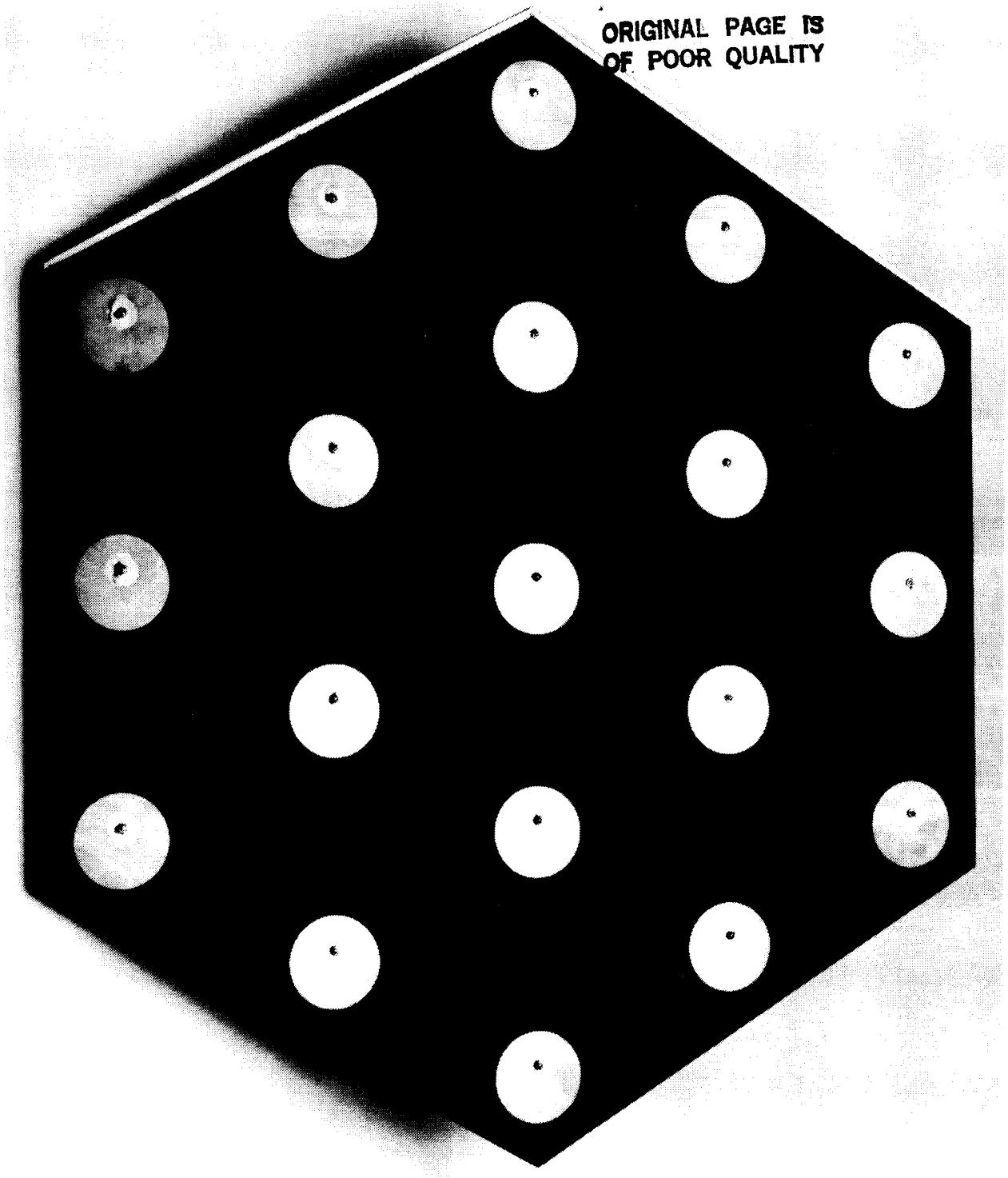

Figure 3 2.27-GHz Feed

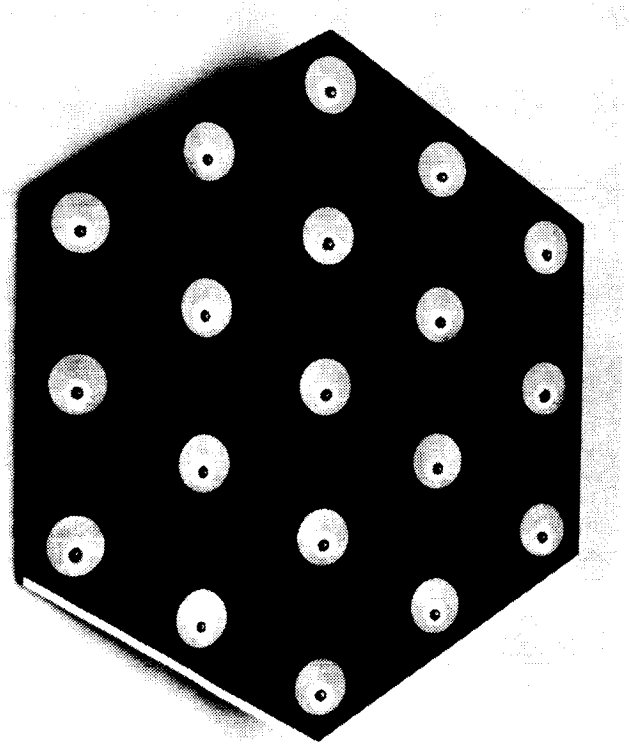

Figure 4 4.26-GHz Feed

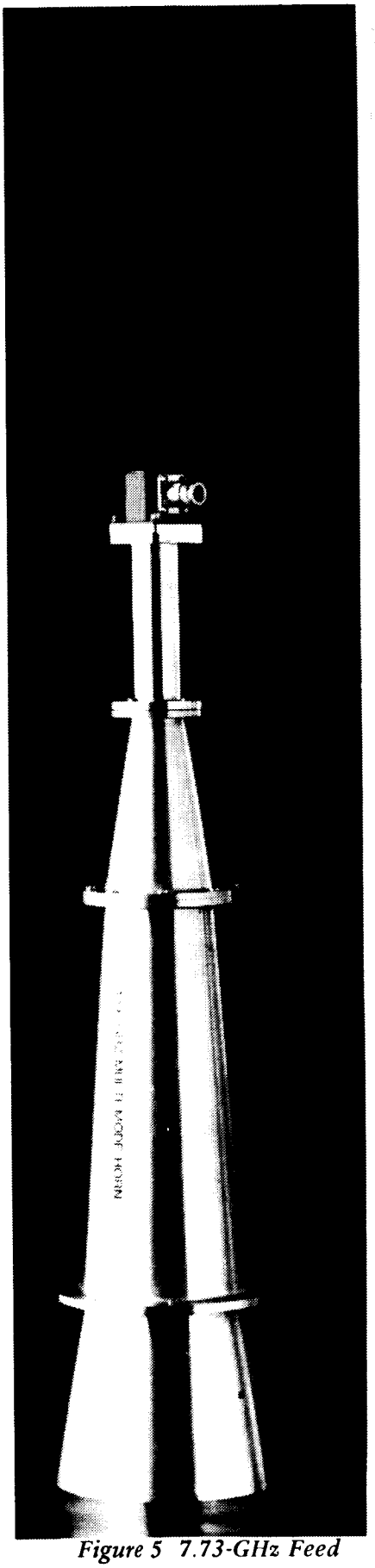

Figure 5 7.73-GHz Feed

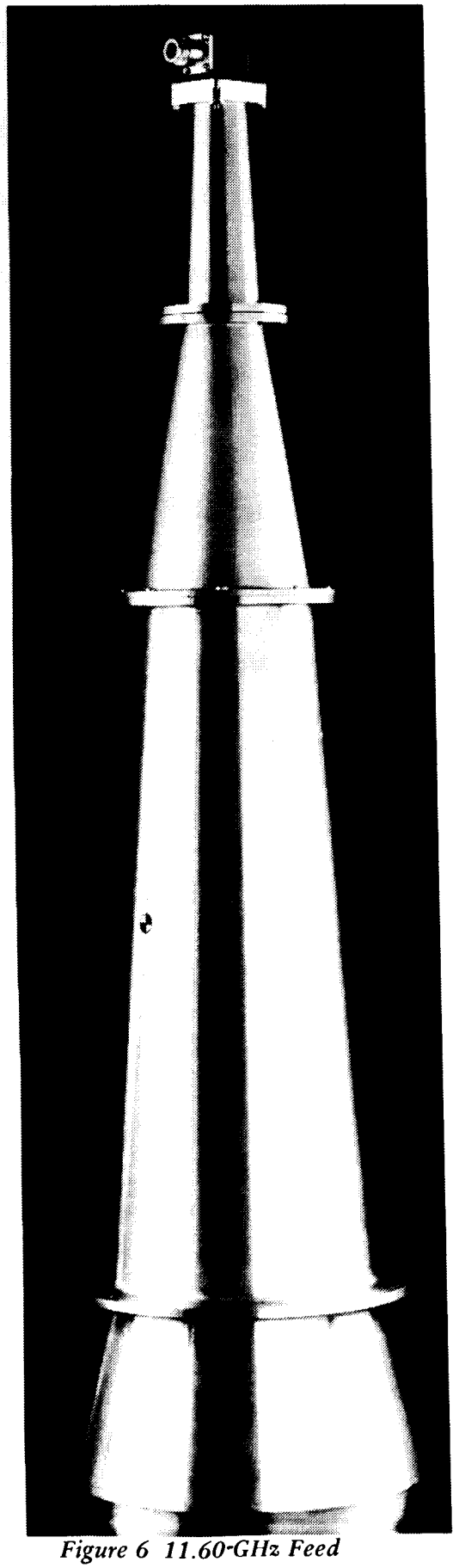

Figure 6 11.60-GHz Feed

Table 1 Test Plan

Test	Frequency (GHz)	Scan Angle (Degrees)	Scan Size Polarization	Array Size (Data Points)	Feed Pointed
1	4.26	0	Co	256 x 256	Yes
2	4.26	0	Cross	256 x 256	Yes
3	2.27	0	Co	138 x 138	Yes
4	2.27	0	Cross	138 x 138	Yes
5	11.60	0	Co	707 x 707	Yes
6	11.60	0	Cross	707 x 707	Yes
7	7.73	0	Co	471 x 471	Yes
8	7.73	0	Cross	471 x 471	Yes
9	7.73	8.5	Co	471 x 471	No
10	7.73	8.5	Cross	471 x 471	No
11	7.73	8.5	Co	471 x 471	Yes
12	7.73	8.5	Cross	471 x 471	Yes

Figures 7 and 8 show the two scanning modes used at the NFTL, rectangular and quadrant. To collect the data in the most efficient manner, NFTL used rectangular scans. One basis for determining the needed scan size arises from the physical optics approximation in antenna theory; the approximation states that all fields beyond the aperture edge in the plane of the aperture will be assumed to equal zero. In near-field scanning this approximation yields the equation

$$\theta = \tan^{-1} ((L-D)/2d)$$

where

- θ equals the maximum valid angle off boresight when a physical optics approximation is used to determine scan size
- L equals scan length
- D equals aperture diameter
- d equals distance separating scan plane from aperture.

This equation results in a maximum angle off boresight of 10° using the physical optics approximation for rectangular scans. Under the previous program using the General Dynamics Tetrahedral Truss, a comparison of quadrant and rectangular scans established that rectangular scans produced virtually identical data over angles up to 30° for this antenna. If any of the LaRC program test data had shown significant energy outside of the 10° region, larger scans would have been performed to guarantee data accuracy to 30°. This did not occur for any of LaRC tests; therefore, rectangular scans were used throughout the program.

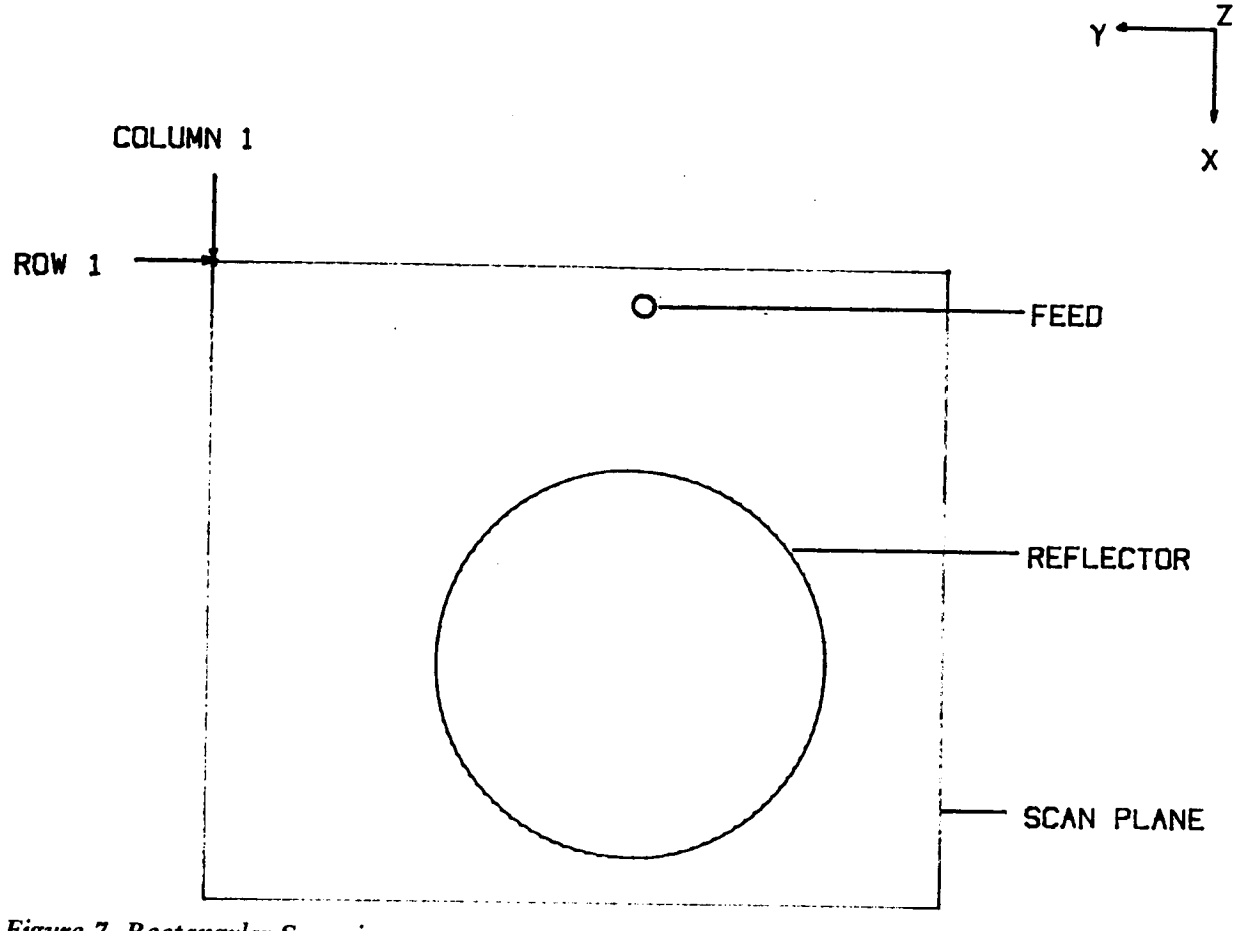

Figure 7 Rectangular Scanning

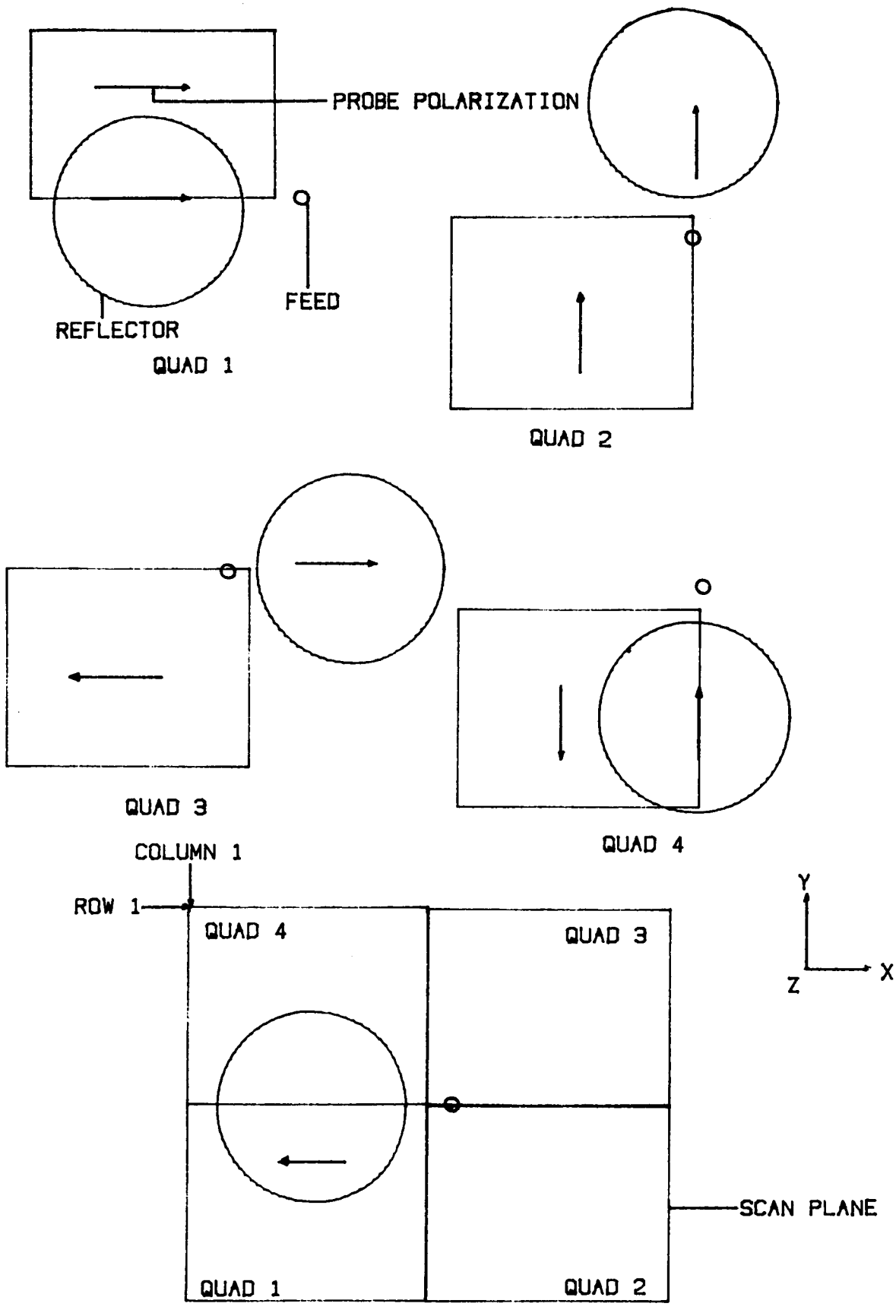

Figure 8 Quadrant Scanning

The antenna was tested at four frequencies, 2.27, 4.26, 7.73 and 11.60 GHz. For each of these frequencies both co- and cross-pol were measured. Measurement of the absolute gain helped to show the major sources of antenna performance degradation, including feed internal ohmic losses, surface rms, and focusing of the feed. Tests 9-12 helped to determine the advantages of boresighting a steered feed instead of simply mounting the feed parallel to the unsteered feed. Further analysis revealed that the major source of performance degradation was cubic phase error. We will examine this source under the diagnostic section (See Section 5.4). We checked all RF measurements for consistency with reference to frequency scaling, correlation between directivity and gain, and absolute value of gain based on known performance parameters. The next section will summarize the limiting errors on the RF measurements at the NFTL.

3.0 MEASUREMENT ERROR ANALYSIS

The near-field method of measuring antenna patterns, like all measurement techniques, has several accuracy-limiting errors in application. Although none of these errors caused misleading results, we will quantify them in this section to establish a basis for measurement accuracy. The errors covered in this section include scan plane truncation, system stability, chamber reflections, probe position error, and gain error.

For all pattern plots that follow we refer the far-field components and angles to the coordinate system shown in Figure 9. This figure identifies the near-field components by two vectors, E_x and E_y. After transformation into the far-field, the components are identified as A_{az} and A_{el} on a sphere defined by an azimuth and elevation coordinate system. In these coordinates, the far-field patterns are referenced to the antenna by placing its vertex in the x, y plane with the active aperture and its co-polarized field vector aligned with the negative x-axis. In all the far-field pattern plots that follow, the H-plane and E-plane correspond to azimuth and elevation planes, respectively (Ref 4).

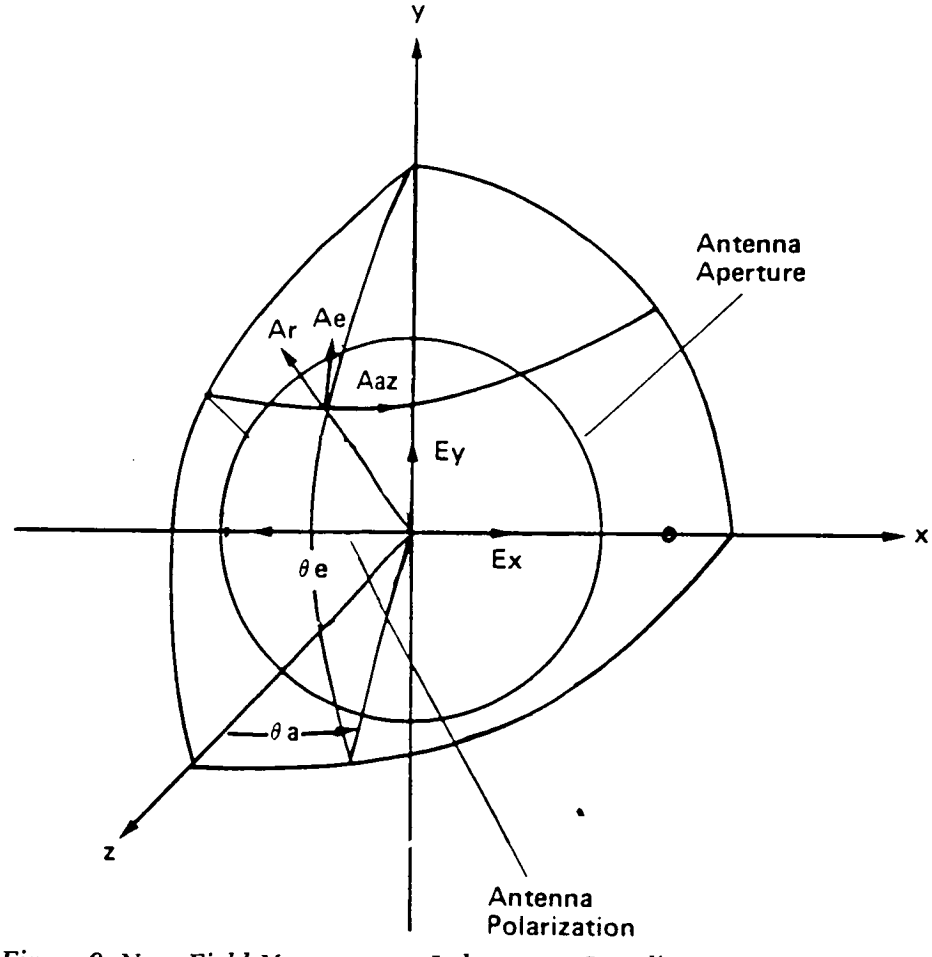

Figure 9 Near-Field Measurement Laboratory Coordinate System

3.1 SCAN PLANE TRUNCATION

Scan plane truncation is always a critical concern in determining the time spent to scan an antenna. According to the physical optics approximation commonly used in near-field scanning, the collections done for LaRC are valid over a maximum angle of 10°. However, if a more accurate method of defining valid angle is used that includes the actual energy distribution over the aperture, this angle will increase.

A comparison between quadrant and rectangular scans accomplished during the initial setup for General Dynamics had demonstrated virtually identical patterns for these two scan types, although the valid angle increased to 45° for quadrant scans. These two scan types differ in hardware configuration used in the actual collections. For a rectangular scan, the antenna is translated once in x while the scanning is completed in y, as defined in Figure 7. Quadrant scanning needs four separate scans of the antenna when rotating to four different angular positions (0°, 90°, 180°, 270°). The computer then reconstructs a scan plane from these data and places the data in a single file on disk. Although quadrant scan increases the scan area by four times, this increase in area did not change the antenna patterns in the General Dynamics comparison. Therefore, using only rectangular scans, total scan time (including setup, collection, and processing) could be cut by 65% without inducing significant error from truncation.

3.2 SYSTEM STABILITY

The long-term electrical stability of a near-field scanner can determine both gain and pattern accuracy when all other error sources are less significant. The NFTL system has demonstrated exceptional long-term stability over periods greater than 48 hours of $\pm$0.05 dB and $\pm$3° in the near-field amplitude and phase measurement; this error source has negligible effect on the pattern above levels of -60 dB. Even at the extremely low levels, the pattern accuracy degrades only on principal planes of the far field because long-term drift varies too slowly to affect the remaining envelope. Once measurement moves away from the two principal planes, this error becomes negligible. Chamber reflections and probe positioning accuracy limit the measurement accuracy over the entire far-field pattern. For all tests during this task for LaRC, system drift did not appear in any of the collections as a significant error contributor.

3.3 CHAMBER REFLECTIONS

No matter how precisely an electrical system measures the response of the antenna, reflections always remain a limit to data accuracy. The NFTL minimizes reflections by placing the antenna inside an anechoic chamber. The errors caused by the remaining reflections of the chamber

tend to appear at -15 dBi or less on an absolute scale in the far-field. Figures 10-17 show where this error bound lies relative to the antenna peak gain. As these figures demonstrate, for all measurements done with the LaRC feeds, this error never contributed significantly to the far-field pattern. Although the LaRC tests result in the conclusion that reflections did not limit the measurement accuracy, the level of this error determines the ultimate limitations of near-field measurement.

3.4 PROBE POSITION ERROR

Under normal operation, the most significant NFTL error source is probe positioning accuracy in the direction of propagation (z direction in the case of the unsteered antenna). Figures 10-17 show the upper bound for this error source. This error source still remains far below the far-field pattern envelope for all test frequencies. In addition, knowledge of the true probe position will allow removal of the probe position errors from near-field if they ever become significant. The only component of probe position error that significantly affects far-field pattern performance must occur along the direction of propagation of the mainbeam. In the unsteered collections virtually all power propagates in the vertical direction because the antenna has a high gain; therefore, the effect of probe position errors on the far-field pattern can be represented by out-of-plane errors in the collection. Figures 10-17 use this spectral distribution model for probe position error (Ref 5). Probe position error will also have some effect on the absolute gain measurement of the antenna because it has a nonzero rms value and affects the gain in much the same way as do reflector surface errors.

3.5 GAIN ERRORS

The absolute gain measurement accuracy of an antenna differs from the pattern measurement accuracy because the gain measurement relies on knowledge of absolute probe gain and reflection coefficients in the near-field circuit (Ref 6). The two factors limiting the absolute accuracy of the system, probe gain and insertion loss, need a hardware substitution to accomplish the measurement. To measure insertion loss, a fixed precision attenuator with known performance replaces the antenna in the transmission system. This measurement requires breaking of a minimum of two connections and the addition of the attenuator. Virtually any connector in the microwave frequency band has limited repeatability. The errors in this connection are the basis for the insertion loss error shown in Table 2.

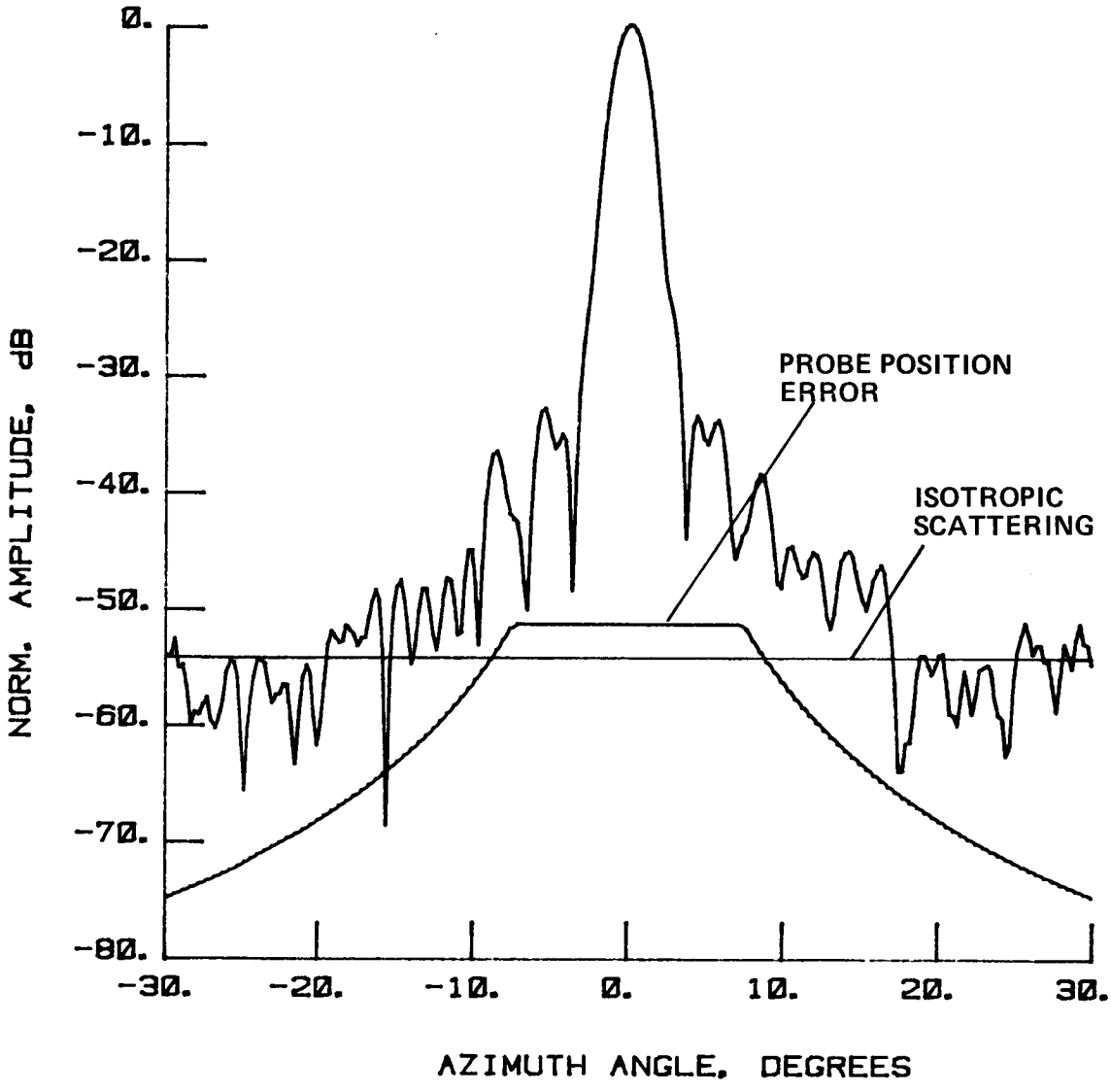

Figure 10 2.27 GHz, H-Plane, Error Curve

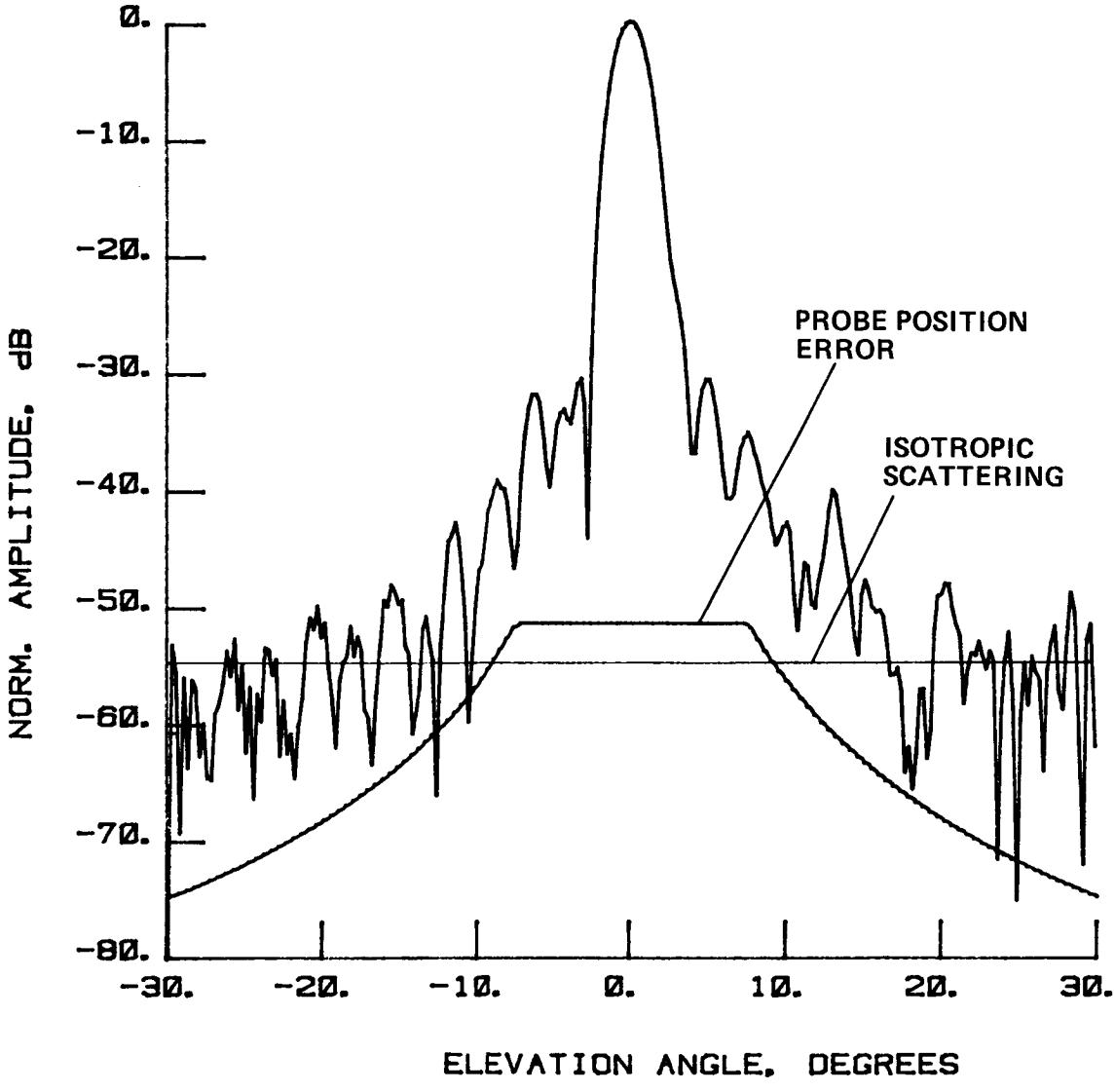

Figure 11 2.27 GHz, E-Plane, Error Curve

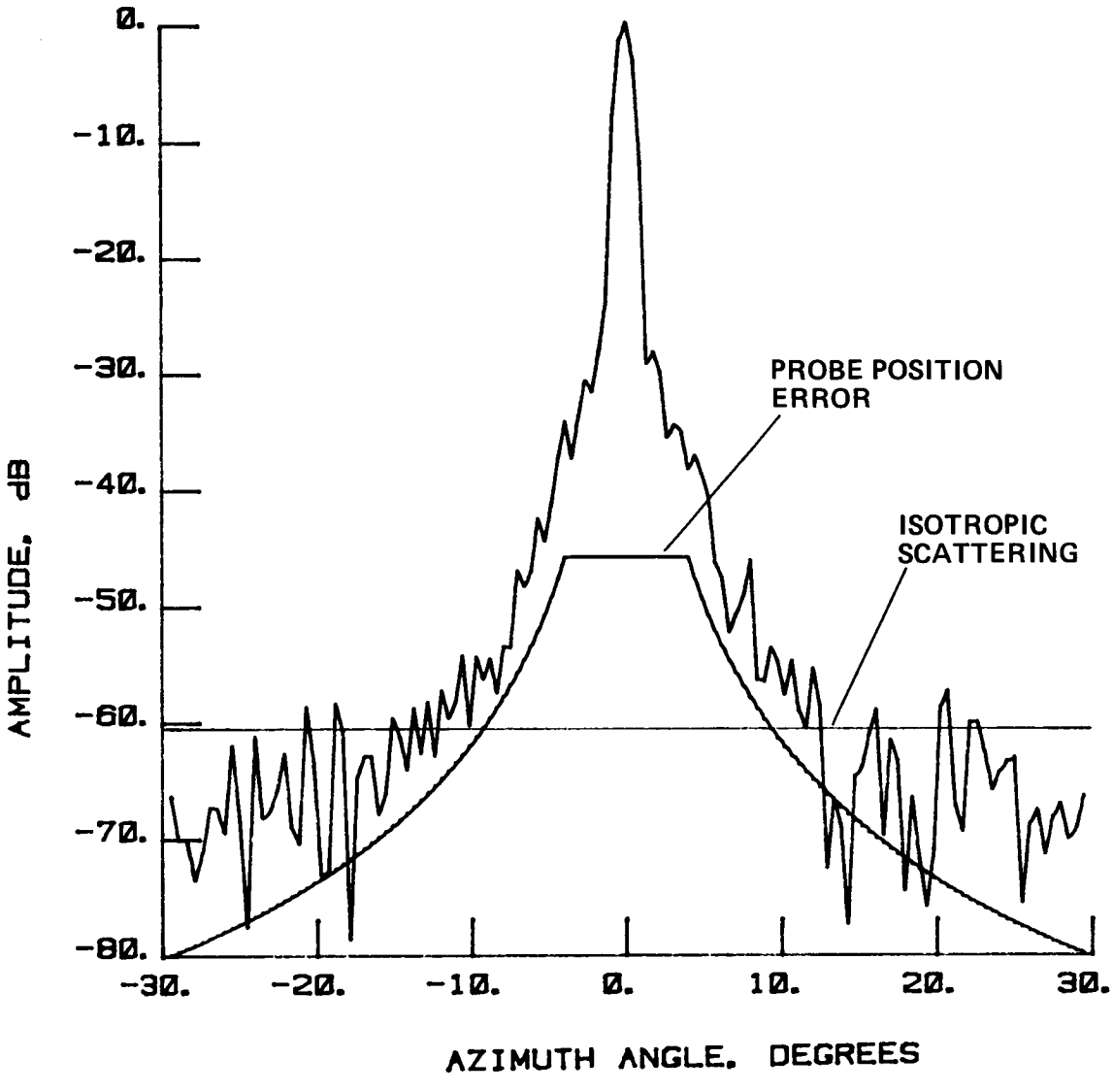

Figure 12 4.26 GHz, H-Plane, Error Curve

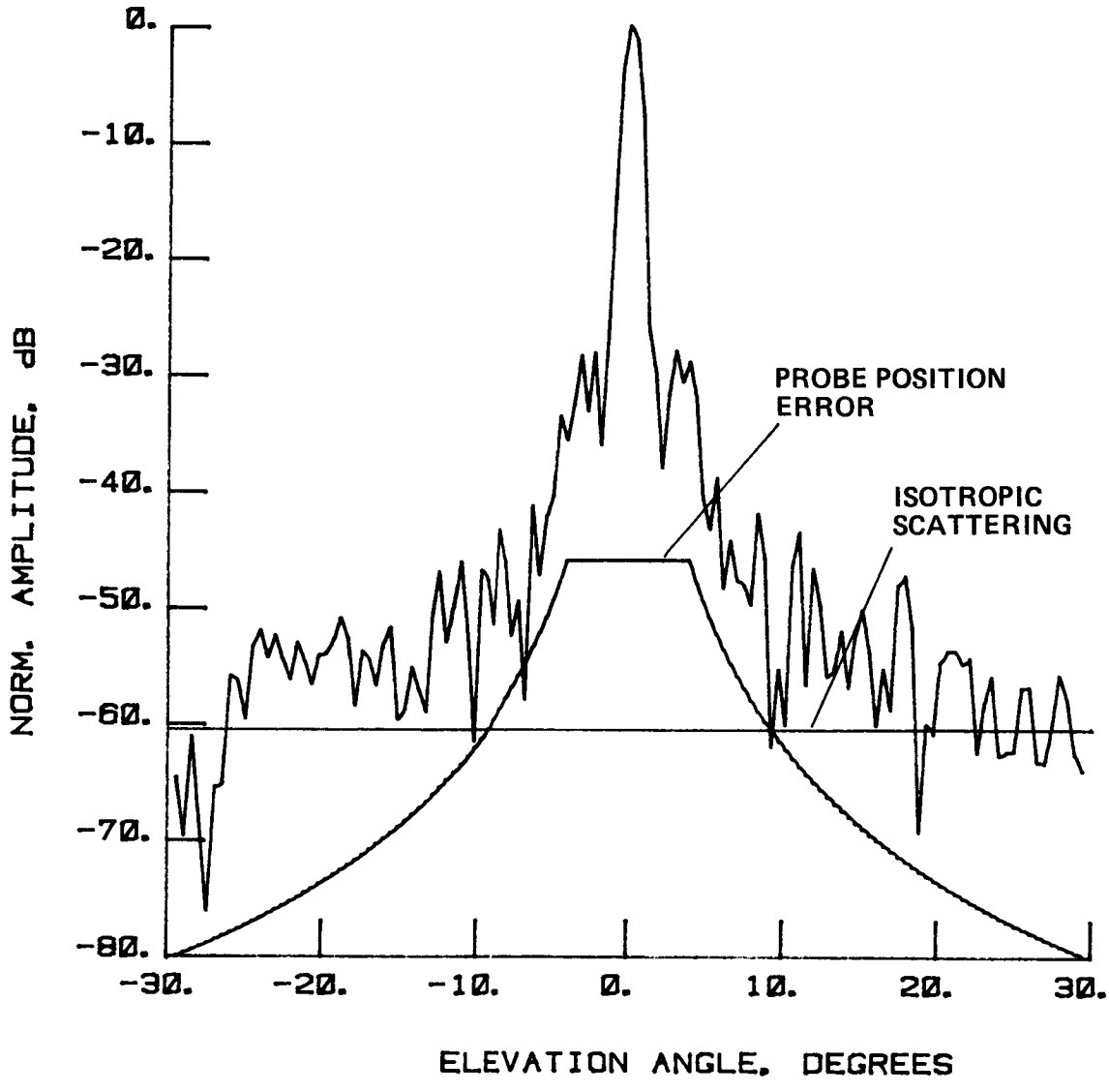

Figure 13 4.26 GHz, E-Plane, Error Curve

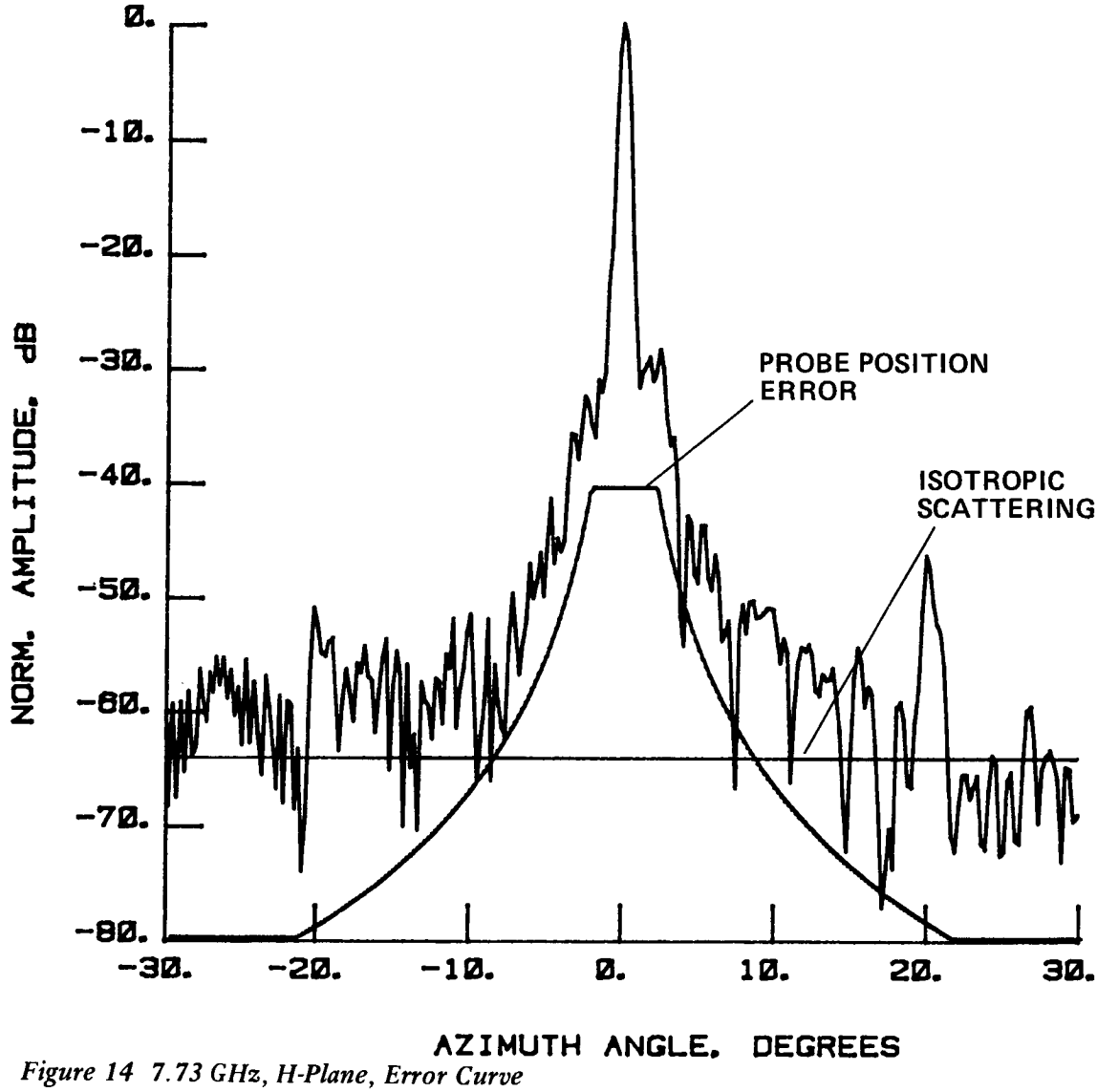

Figure 14 7.73 GHz, H-Plane, Error Curve

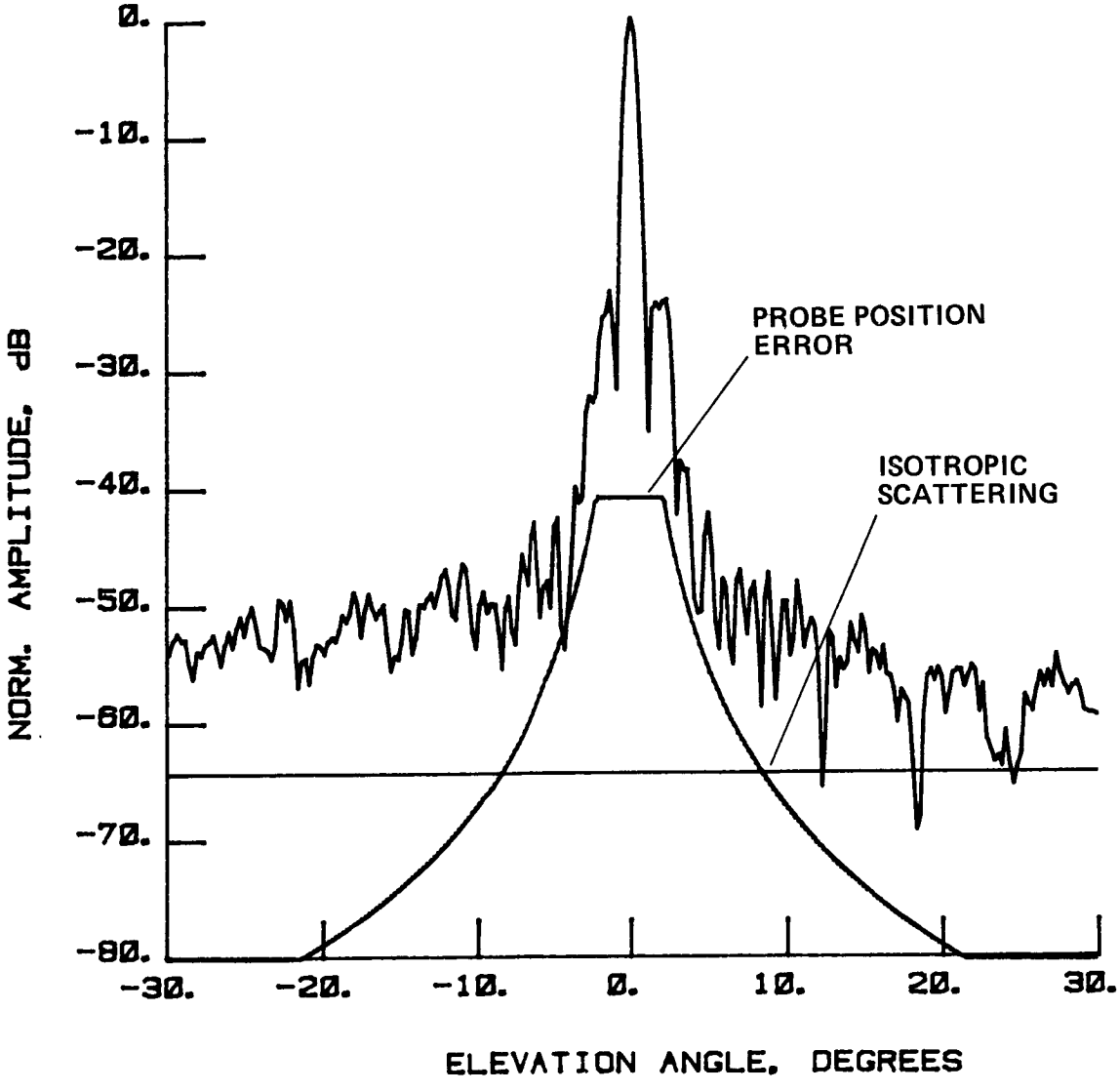

Figure 15 7.73 GHz, E-Plane, Error Curve

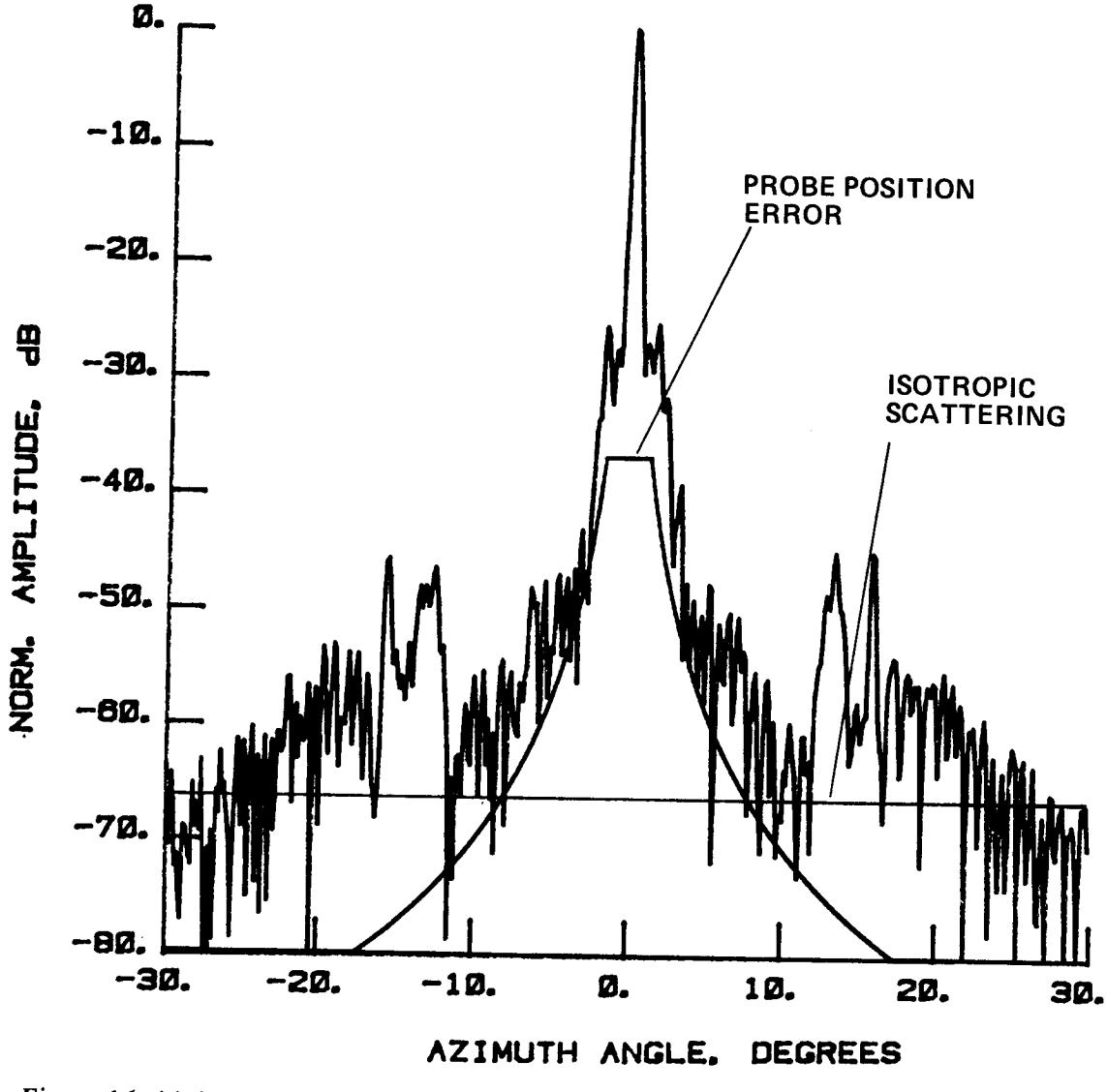

Figure 16 11.6 GHz, H-Plane, Error Curve

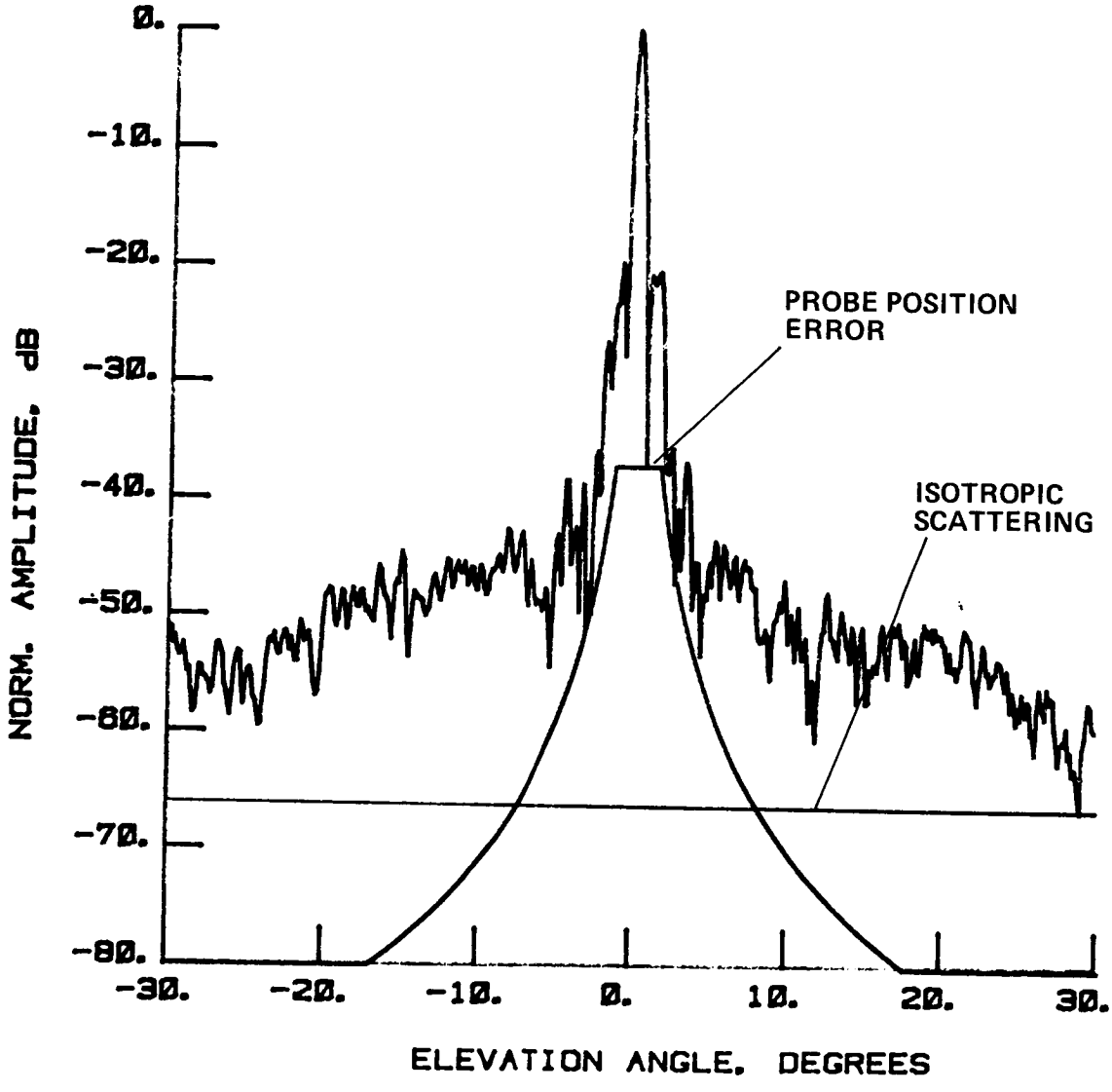

Figure 17 11.6 GHz, E-Plane, Error Curve

Table 2 Gain Error Analysis Summary

Frequency, GHz	Insertion Loss, dB	Probe Position, dB	Probe Gain, dB	Return Losses, dB	Total Gain Accuracy, dB*
2.27	±0.10	±0.003	±0.1	±0.01	±0.14
4.26	±0.15	±0.010	±0.1	±0.10	±0.21
7.73	±0.20	±0.030	±0.1	±0.01	±0.23
11.60	±0.25	±0.070	±0.1	±0.01	±0.28

*Root Sum Square

The probe gain error shown in the table arises from two sources, connector repeatability and accuracy of the standard gain horn used for a reference. The accuracy of the return loss measurement will usually cause negligible error in the gain calculation; however, for the 4.26-GHz tests, the probe that measured the response of the antenna had an unusually high return loss. Therefore, even an error of 0.05 dB in the measurement of the return loss of this probe would cause the error shown in the table. The probe position error effect on gain is based on a conservative estimate of maximum system deviation from the scan plane of 20 mils and uses the error bound defined by Yaghjian (Ref 7). By doing a root sum square averaging of the anticipated system errors, the total error bound for the absolute gain measurement results in the final values shown in Table 2.

4.0 TEST DATA

This task consisted of 12 tests on the antenna, covering four frequencies: 2.27, 4.26, 7.73, and 11.60 GHz. The data obtained from these tests allowed rapid analysis of the electrical performance of the antenna. Because the antenna had a feed offset, the diagnostic techniques developed at NFTL easily isolated any direct feed radiation from radiation of the reflector. Isolation of the reflector from all other electrical sources helped to make reliable analyses of this antenna and aided in establishing the actual performance parameters of the feed and the reflector. These parameters included surface trueness, aperture taper, direct radiation pattern of the feed, defocusing effects of steering, the effects of surface tolerance on the far-field pattern, and gain losses caused by not pointing the feed toward the aperture center.

These 12 tests used the feeds designed by LaRC for the 15-Meter Hoop Column Antenna. Although the f/d decreased from 1.5 to 1.3 when using the 5-meter reflector, this decrease caused only a slight increase in the aperture taper. Since the maximum sidelobe level is usually determined by surface errors on the reflector, this increased taper causes little change to the sidelobe envelope. The four frequencies chosen for the feeds cover 2.6 octaves and demonstrate both the versatility and the performance of this reflector. The 2.27- and 4.26-GHz feeds shown in Figures 3 and 4 are frequency-scaled versions of the same stripline and patch array feed. Both feed arrays have phase-matched elements with the amplitude taper being generated by a stripline network that distributes power to the 19 patches. The 7.73- and 11.60-GHz tests used the multimode horns shown in Figures 5 and 6, again with appropriate frequency scaling. Because of length constraints, the feeds used for lower frequencies were not horn designs.

4.1 TEST DATA PLOT FORMAT

The pattern plots that follow (Fig. 18-125) are organized in the format shown in Table 3. The table defines each of the plot types used in the figures covered in the test data section. These figures will have labels specifying the figure number, test number, frequency, polarization, type of data plotted, and plot type, all as shown in Table 3. The labeling convention covers only Figures 18-125, the test data. The geometry used to plot the data of the far-field patterns is shown in Figure 9.

These figures are arranged by test number, with the cross-pol test immediately following the co-pol test for that particular antenna configuration. The principal plane plots show far-field patterns to 30°. Although these scans were small, previous tests had confirmed negligible error from truncation; therefore, these data can be considered valid. These angles also make the data easy to correlate with the data in the previous reports from this contract on the 15-Meter Hoop Column Antenna (Ref 1-3) delivered earlier.

Table 3 Test Data Plot Format

Plot Type	Polarization	Far-Field Plot	Dynamic Range, dB	Angle, °
1	Co	H-Plane	-80 to 0	-30 to 30
2	Co	E-Plane	-80 to 0	-30 to 30
3	Co	H-Plane	-60 to 0	-10 to 10
4	Co	E-Plane	-60 to 0	-10 to 10
5	Co	Contour	-40, -30, -20, -10	Determined by Sidelobe Structure
6	Co	Contour	-30, - 20, -10, -3	
7	Co	3-D	-40 to 0	
		Near-Field Plot		
8	Co	H-Plane	-80 to 0	NA
9	Co	E-Plane	-80 to 0	NA
		Far-Field Plot		
10	Overlay	H-Plane	-80 to 0	-30 to 30
11	Overlay	E-Plane	-80 to 0	-30 to 30
12	Cross	H-Plane	-80 to 0	-30 to 30
13	Cross	E-Plane	-80 to 0	-30 to 30
14	Overlay	H-Plane	-60 to 0	-10 to 10
15	Overlay	E-Plane	-60 to 0	-10 to 10
16	Cross	H-Plane	-60 to 0	-10 to 10
17	Cross	E-Plane	-60 to 0	-10 to 10
18	Cross	Contour	-50, -40, -30	Determined by Sidelobe Structure

4.2 TESTS 1 AND 2, 4.26 GHz

The patch array (shown in Fig. 4 above) used in these tests measured approximately 11.6 in. across the flats and had 19 linearly polarized elements. We tested this feed first because extensive previous NFTL General Dynamics Tetrahedral Truss tests were performed at 4.2 GHz. The initial data demonstrated that the LaRC array achieved an illumination similar to that of the 4.2-GHz GDC horn, a taper of approximately 17 dB; but, because of the internal losses of the patch array, the absolute gain of the antenna dropped 2 dB from that of the GDC horn. The surface errors probably caused all significant degradation in the co-pol pattern inside 30°. Although the reflector design generated no major grating lobes inside 40°, the surface contained several distortions that increased the sidelobe envelope approximately 5 dB in the angular sector within 10° of the mainbeam. The 42.5-dB gain of the antenna at 4.26 GHz implied an aperture efficiency of 34% when compared to the gain of the same size aperture illuminated with a uniform amplitude and phase. However, because the feed has 2.9-dB internal loss and because the aperture area is approximately 219 sq ft, the efficiency of

the reflector aperture approaches 67%. Another major contributor to decreased efficiency of the antenna arises from the high illumination taper used to achieve low first sidelobe performance, the taper causing the effective aperture area to decrease to approximately 166 sq ft, thus increasing the efficiency of the reflector, without the taper, to 89%.

Data for Tests 1 and 2 (4.26-GHz series) are shown in Figures 18-35. Because of surface distortions in the mesh, the first sidelobe approaches -24 dB at its peak located at (1,1) in azimuth and elevation. The entire sidelobe envelope shows the effects of surface distortion both by increased amplitude and by the lack of nulls in the antenna pattern. The lack of nulls in a pattern near the mainbeam implies antenna defocusing. Two possible sources of this problem, feed defocusing and surface distortions, exhibit different behavior on the aperture phase front even though the far-field effects may appear indistinguishable. A surface distortion localizes to a small area on the reflector surface, whereas a defocusing of the feed will affect the entire phase front of the aperture by either bowing (axial defocusing) or tilting (lateral mispositioning) the phase front. The antenna design chosen by General Dynamics to facilitate beam steering has an f/d of 1.3, making the effects of feed defocusing, if it did occur, negligible. Therefore, the data indicates that the reflector surface distortion may cause the lack of nulls in the far-field. The surface distortions causing the increased sidelobe envelope do not always represent a high surface rms. Because the surface rms weights all surface errors evenly, errors at the center and edge of the reflector affect surface rms equally even though they do not affect the antenna performance equally. We could obtain a more appropriate rms value by weighting the surface errors by the taper value for that region of the reflector. This weighting would result in an rms value that accurately defines both the gain loss due to surface errors and the quality of the reflector for predicting sidelobe envelope degradation. Near-field measurements can then demonstrate that if the rms from the aperture illumination is calculated, it should correspond to an actual gain loss measured by processing the electrical data.

When comparing the performance shown by Figures 18-35 to that of the 15-Meter Hoop Column Antenna (Ref 1-3), several differences emerge. The smaller aperture of the GDC reflector had approximately 3 dB less gain than the 15-Meter Hoop Column Antenna. However, since GDC used a single aperture antenna design, the surface was illuminated more efficiently than that of the quad-aperture 15-Meter Hoop Column Antenna. Since the GDC surface had an aperiodic tie point spacing, no significant grating lobes appeared in the GDC antenna pattern. Also, the first sidelobe performance improved for the GDC antenna, probably because the GDC surface control used a denser tiepoint spacing than did the 15-Meter Hoop Column Antenna.

The cross-pol component of the feed controlled the cross-pol pattern of the antenna as seen in Figures 27-35. The characteristic pattern of null on boresight between two peaks shows a good linear polarization for a microstrip array. Significant reduction of this cross-pol component can only occur through use of a more ideally polarized feed. This polarization improvement would probably require a corrugated horn

such as the horn General Dynamics provided. The maximum cross-pol of the antenna is -22 dB at (1,0). The two cross-pol peaks do not balance; but since this test showed lack of sensitivity to the probe alignment, the conclusion of the test is that the feed has an unbalanced cross-pol pattern. This probably arises from patch elements used in the feed design. The surface degrades the cross-pol only minimally because of two factors: the low gain of the cross-pol and the small region of the reflector actually illuminated by the cross-pol. Figures 30 and 31 show the cross-pol insensitivity to surface; when compared to the co-pol pattern, the cross-pol has a much less defocused appearance (with much deeper nulls) than does the co-pol.

4.3 TESTS 3 AND 4, 2.27 GHz

This pair of tests showed no appreciable change in response from that of the 4.26-GHz feed except for frequency scaling. The major changes caused by this scaling include reduction in gain, lower sidelobes, and main beam distortion. The gain was 36.54 dB for this test, and the peak sidelobe did not exceed -28 dB; however, the main beam distorted, possibly because of the defocusing effect of the surface. The surface effects on the sidelobe envelope in the 2.27-GHz tests appeared to decrease approximately 5.5 dB from those seen in the 4.26-GHz tests. The filling-in of the nulls greatly decreased from the previous test. The surface distortions at 2.27 GHz controlled the sidelobe envelope over wider angles than at 4.26 GHz. Figures 36-53 show the antenna performance measured at 2.27 GHz as referred to in this section.

The cross-pol for this frequency closely resembles that of the 4.26-GHz feed. This resemblance results from using the same feed design and from scaling the feed by frequency. The cross-pol peak, -24 dB, the same as the 4.26-GHz feed, occurs at almost twice the angle from boresight because of the frequency change. Because the collection scanned over the feed, it quickly became apparent that the feed radiated a considerable cross-pol component directly into the scan plane. The fields from this component cause the interference patterns seen in the far-field cross-pol contour in Figure 53. This direct radiation from the feed could also cause electrical interference problems, depending upon the application of the feed.

The 2.27-GHz test did demonstrate that the antenna performance increases as the effects of the surface distortion scale down by frequency. Other factors affecting the reflector performance, such as use of mesh material, have become negligible. For apertures of this size (greater than 40 wavelengths) the offset reflector can be qualitatively examined by near-field measurements because it has no aperture blockage--this analysis normally reduces the sidelobe envelope to a function of the feed taper and surface accuracy. Focusing of the feed for this high-f/d ratio has no significant effect on the pattern; nevertheless, according to the electrical and photogrammetric data, the feed was focused. At 2.27 GHz the surface defocusing effects also dropped so low that individual sidelobes appeared in the pattern; this implies

that further surface improvements gain little at 2.27 GHz for this reflector, except for improving mainbeam symmetry and slightly reducing first sidelobes. Gain losses because of the surface roughness at this frequency are less than 0.1 dB; therefore, surface improvement is of little significance at this frequency.

4.4 TESTS 5 AND 6, 11.60 GHz

The feed used at 11.60 GHz had a multimode design in which different modes arose inside the horn because of abrupt transitions. The feed, 23 in. long, had three of these transitions. The horn produced an illumination for this aperture with an approximate taper of 15 dB at the aperture edge. The NFTL used the cross-pol component of the antenna to align the antenna for optimal polarization. Using single line near-field scans of the aperture, the NFTL optimized the polarization alignment based on the sharpest observed null in the aperture fields. This method has always worked well when a horn is used to illuminate the aperture because the horn will normally have a well-defined cross-pol null with which to align the near-field measurement probe.

As frequency increases, the existing surface accuracy causes some pattern degradation. Figures 54-71 show these effects. For the 11.60-GHz tests, the surface caused a peak first sidelobe of -19 dB and a sizeable loss in gain, approximately 1 dB. The surface accuracy limited antenna performance significantly at this frequency. The peak cross-pol again approached -24 dB; however, the cross-pol pattern at 11.60 GHz of the GDC antenna had four separate peaks as opposed to the two for the 15-Meter Hoop Column Antenna. This difference arises because the 15-Meter Hoop Column reflector had a pie shape while this antenna used a circular reflector. This reflector geometry difference changed the cross-pol aperture fields greatly because the fields of the feed cross-pol increase close to the edge of the aperture. This change in the cross-pol aperture fields resulted in a significant change in the far-field cross-pol.

An interesting feature of this horn compared to the other LaRC feeds is that, because there are different tapers in the E- and H-Planes of the 11.60-GHz feed pattern, the main beam asymmetry increased from that of the other feeds. As Figure 59 shows, the main beam covers a different angle in the two principal planes because of a wider horn beamwidth in the E-plane than in the H-plane. This difference in angle consequently caused a narrower beamwidth in the E-plane of the antenna pattern. LaRC developed this horn for use with the 15-Meter Hoop Column Antenna quad aperture design; therefore, the pattern taper differed along the two axes to compensate for the aperture geometry. For the symmetric GDC reflector, this feed pattern resulted in an asymmetric aperture illumination that caused an asymmetric main beam in the far-field pattern.

The gain of the antenna (51.4 dB) increased because of the negligible ohmic losses of the feed and because of the increased frequency. However, the antenna efficiency, whose measurement is based on aperture size and directivity, remains virtually unchanged because the losses,

caused by the surface roughness effects, increase with frequency and approach the ohmic feed losses of the patch arrays used at the lower frequencies. With the present surface, the GDC reflector will have losses at any higher frequency that probably outweigh the increased gain of this large reflector. The GDC antenna should have no problem in operating at frequencies higher than 11.60 GHz except that the current surface accuracy will cause large gain losses and high sidelobes. Therefore, measurement indicates that in the present configuration the antenna aperture gain may not increase above 12 GHz because the surface errors of the reflector cause gain losses that increase rapidly with frequency.

4.5 TESTS 7 AND 8, 7.73 GHz

These tests used a larger horn than did the 11.60-GHz tests (33.5 in. long as compared to 23 in. for 11.60 GHz), but the horn was symmetrical in all dimensions and geometrically scaled by frequency to the 11.60-GHz horn. To use this horn on the GDC antenna, NFTL personnel had to refocus the feed by axially raising the mounting fixture for the feed 7.5 in. After raising the feed, the antenna needed further alignment, and these adjustments were then completed using near-field measurements. Next, the antenna and the probe were aligned for polarization based on the near-field cross-pol measurements. The scanner then measured the near field of the antenna and yielded the results shown in Figures 72-89.

As Figure 75 shows, the peak sidelobe measures approximately -22.5 dB from the pattern maximum. The gain obtained from the measurements at 7.73 GHz, 49.2 dB showed the highest aperture efficiency of the four LaRC feeds--approximately 49%. This increased efficiency arises because the 7.73-GHz feed has minimal internal losses and because the reflector remains smooth enough to prevent significant gain losses. However, the surface errors do cause most of the pattern effects which yield the far-field sidelobe envelope. This frequency also happens to have the first appearance of grating lobes inside 30°. Figure 72 shows these grating lobes at 20°; they occur only in co-pol H-Plane. They also appear in the 4.26-GHz and 11.60-GHz tests at 30° and 13°, respectively, in the same plane. These angles for the grating lobes imply that, although the surface tie points are aperiodic, some portion of the surface has an average spacing of 4.5 inches. This distance approximately matches the average spacing between tiepoints; however, because the grating lobes occur in only one plane, the periodicity of the surface tiepoints apparently corresponds to the symmetric axis of the reflector.

Figure 73 shows another feature of both the 7.73-GHz and the 11.60-GHz co-pol patterns. This feature, a virtually constant 50-dB sidelobe envelope, was determined after thorough testing to be a high-frequency function of the reflector. Because this feature occurs in only one plane, and because the beamwidth of the sidelobe envelope approximates the main beam, this feature probably arises from a line source near the reflector surface. This line source should have the same length as the

reflector diameter in order for the effect to isolate to only one plane. This feature does not appear at lower frequencies, possibly because the overall sidelobe envelope is higher than -50 dB. If this feature arises from a surface discontinuity, the discontinuity may occur over an area small enough to vary faster than a radiating wave can vary at lower frequencies, creating an evanescent wave that would never reach the far field.

The antenna performed very well at 7.73 GHz. The gain shows the high efficiency that this reflector can produce. The peak sidelobe of -22 dB demonstrates that the surface roughness (calculated as 30-mils rms) does not degrade reflector performance to the degree seen in many mesh antennas, especially deployables. Because the surface had deployed repeatedly in earlier tests to a much lower roughness value (approximately 13-mils rms), much lower first sidelobes could probably be attained by this antenna. This conclusion is consistent with comparisons of the GDC results with those of the 15-Meter Hoop Column Antenna. Metric camera data acquired for both of these reflectors during the measurements at NFTL show that the surface deviation of the General Dynamics reflector was approximately 50% less than that achieved by the 15-Meter Hoop Column Antenna. A 6-dB-lower peak sidelobe (when compared to tests on the 15-Meter Hoop Column Antenna) for the GDC antenna was obtained during the pattern measurements. Another 50% reduction in surface deviation from approximately 30 to approximately 13-mils rms may again result in a 6-dB reduction of the peak sidelobe. Therefore, the 7.73-GHz operation of this antenna could probably improve dramatically if surface deviations could be reduced to the level measured at GDC facilities.

4.6 TESTS 9-12, STEERED 7.73-GHz TESTS

For the steered tests with the LaRC feeds, the cruciform (mechanical structure supporting the feed) remained in the position achieved by the focusing of Tests 7 and 8; the feed moved 44 in. laterally from boresight. This movement steered the mainbeam of the antenna 8.5° in the H-plane, resulting in dramatic changes in the antenna pattern. The NFTL steered the feed two ways for comparison. For the first, the NFTL simply bolted the feed into the steered position on the cruciform. For the second configuration, using an alignment laser provided by NASA, the NFTL adjusted the feed until it pointed to the center of the reflector. The results of these two configurations, Figures 90-125, show a very high level of pattern degradation compared to steering results of the Hoop Column Antenna.

The cause of the pattern degradation, defocusing, arises from the large steering angle. For the 15-Meter Hoop Column Antenna, the maximum angle for steering the antenna (4.8°) resulted in only minor pattern degradation. However, for the General Dynamics reflector the steering angle nearly doubled. This approximately 9° steering (approximately 10 beamwidths) resulted in a dramatic distortion of the phasefront from the reflector that drastically degraded both antenna pattern and gain. Pointing the feed toward the aperture center did not significantly improve the antenna pattern, although the pattern did change greatly.

The gain of the pointed feed configuration (45.6 dB) was higher by 0.7 dB than the unpointed configuration (44.9 dB) because of more efficient aperture usage. However, for both configurations the pattern degradation includes mainbeam distortion, increased sidelobe levels, and increased cross-pol. Pointing the feed reduced the peak cross-pol from -19.9 dB to -20.7 dB, a level still 3.6 dB higher than that for the boresighted case. The peak sidelobes for both configurations approach -19 dB, while the remainder of the sidelobe envelope remains slightly higher than in the boresighted case because of the gain lost by steering.

The mainbeam distorts during steering because of two factors. The first source of distortion comes from aperture illumination amplitude. Figures 95 and 113 show the change in the antenna pattern arising from the different aperture illuminations. The second and more important factor, known as cubic phase-front distortion, which causes pattern distortion, results in the 4-dB gain loss and the mainbeam distortion. This cubic phase error, sometimes known as coma lobing, occurs by steering an antenna with its feed until the phasefront distorts enough to raise the sidelobe envelope. To avoid this problem, a large f/d and an adaptive feed design are commonly employed. Since the antenna already had a large f/d (1.3), decreasing the cubic phase error would require modifying the feed to compensate for this error (by changing the phase front of the feed from a point source to a distributed source).

Steering this antenna 8.5° at 7.73 GHz caused a 4-dB gain loss in the co-pol and drastic pattern distortion. At lower frequencies or smaller angles, these effects will be reduced. However, because of the large f/d, coma lobing is much lower than the coma lobing observed on conventional antennas. The highest coma lobing measured in either Test 9 or 11 was slightly above -10 dB. Steering also degraded the cross-pol performance, raising it over 5 dB above levels measured for the boresight test. Pointing did decrease the cross-pol peak from -19 dB to -20.4 dB relative to the co-pol peak. The cross-pol patterns in the steered collections result primarily from the reflector, because the reflector aperture no longer has the field symmetry of the boresight cross-pol necessary to produce low cross-pol levels. Therefore, when electrically steered with a linear polarization to wide angles (greater than 10 beamwidths), this antenna's performance degrades; this degradation affects the gain, beamwidth, sidelobe envelope, and cross-pol. Pointing does result in modest improvements over strict planar steering.

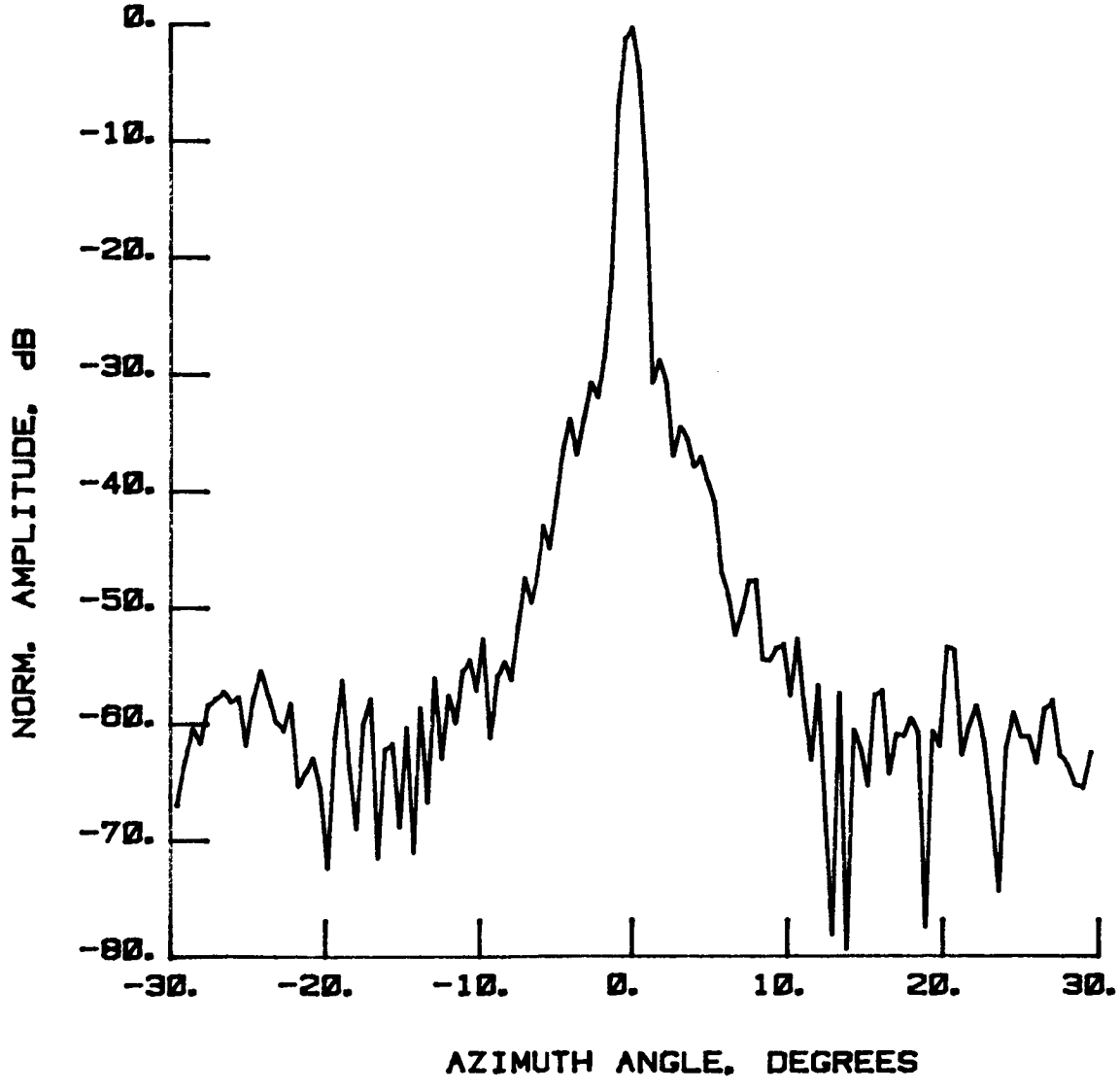

Figure 18 Test 1, 4.26 GHz, Co-Pol, H-Plane, Type 1

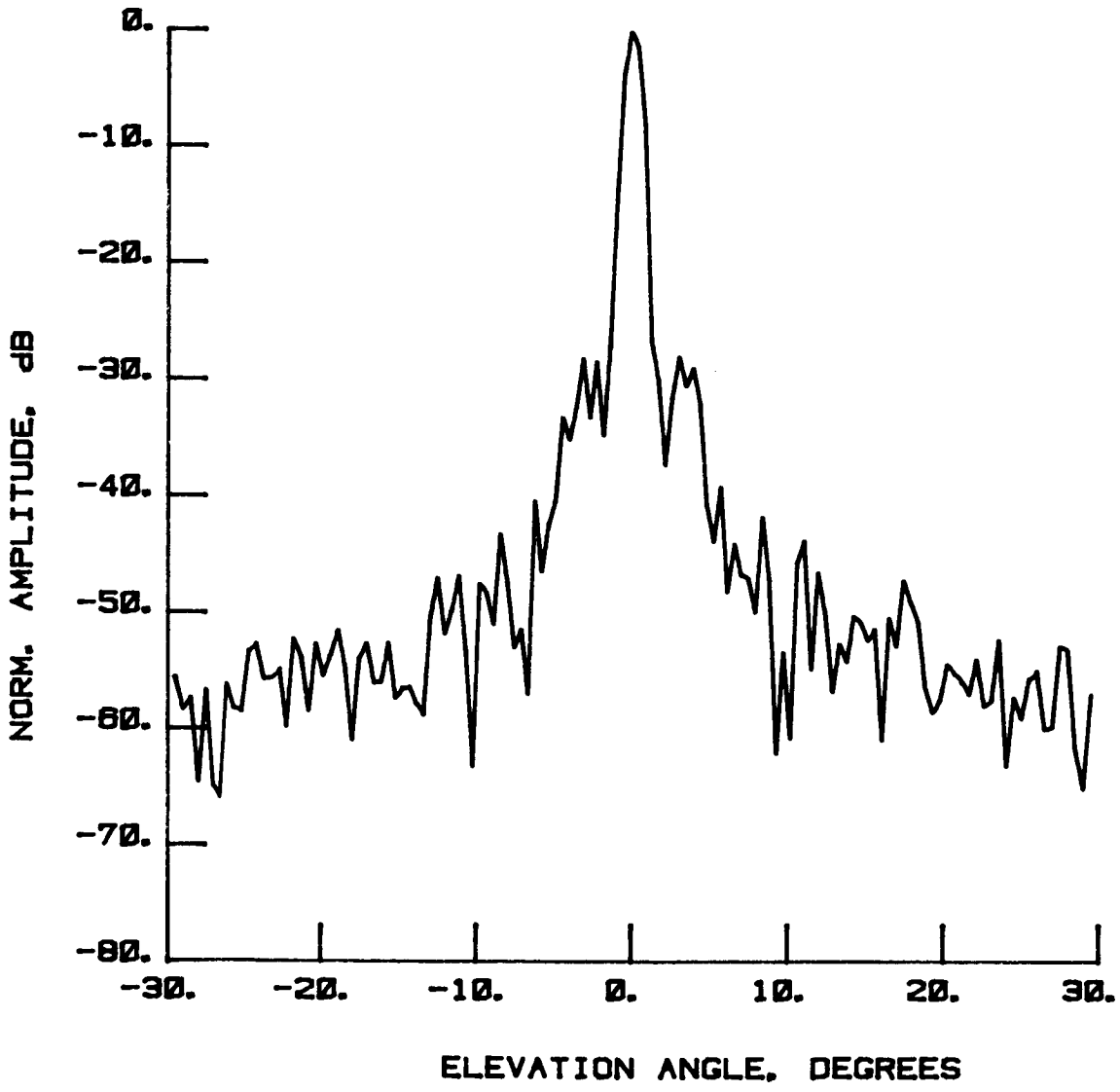

Figure 19 Test 1, 4.26 GHz, Co-Pol, E-Plane, Type 2

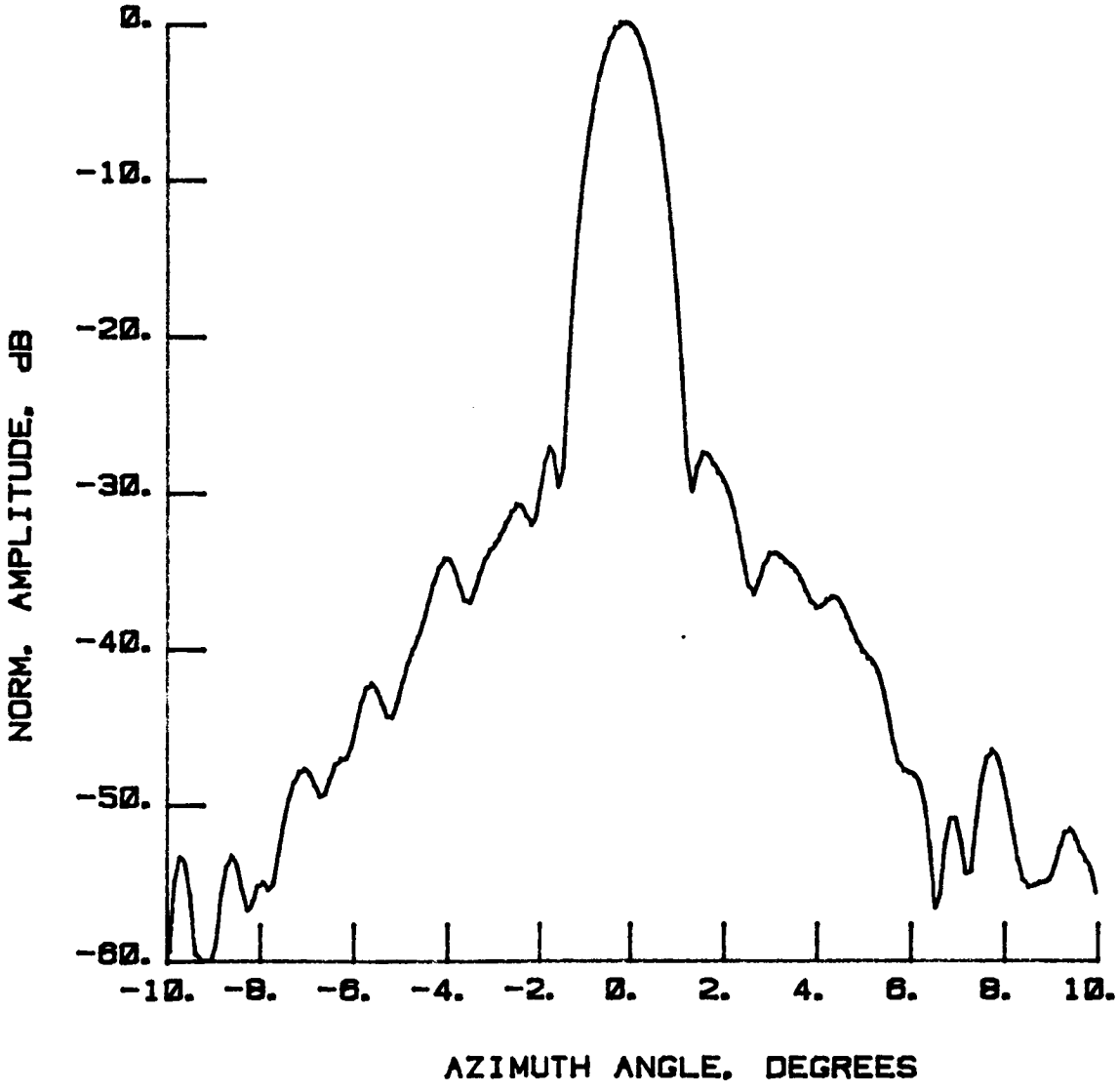

Figure 20 Test 1, 4.26 GHz, Co-Pol, H-Plane, Type 3

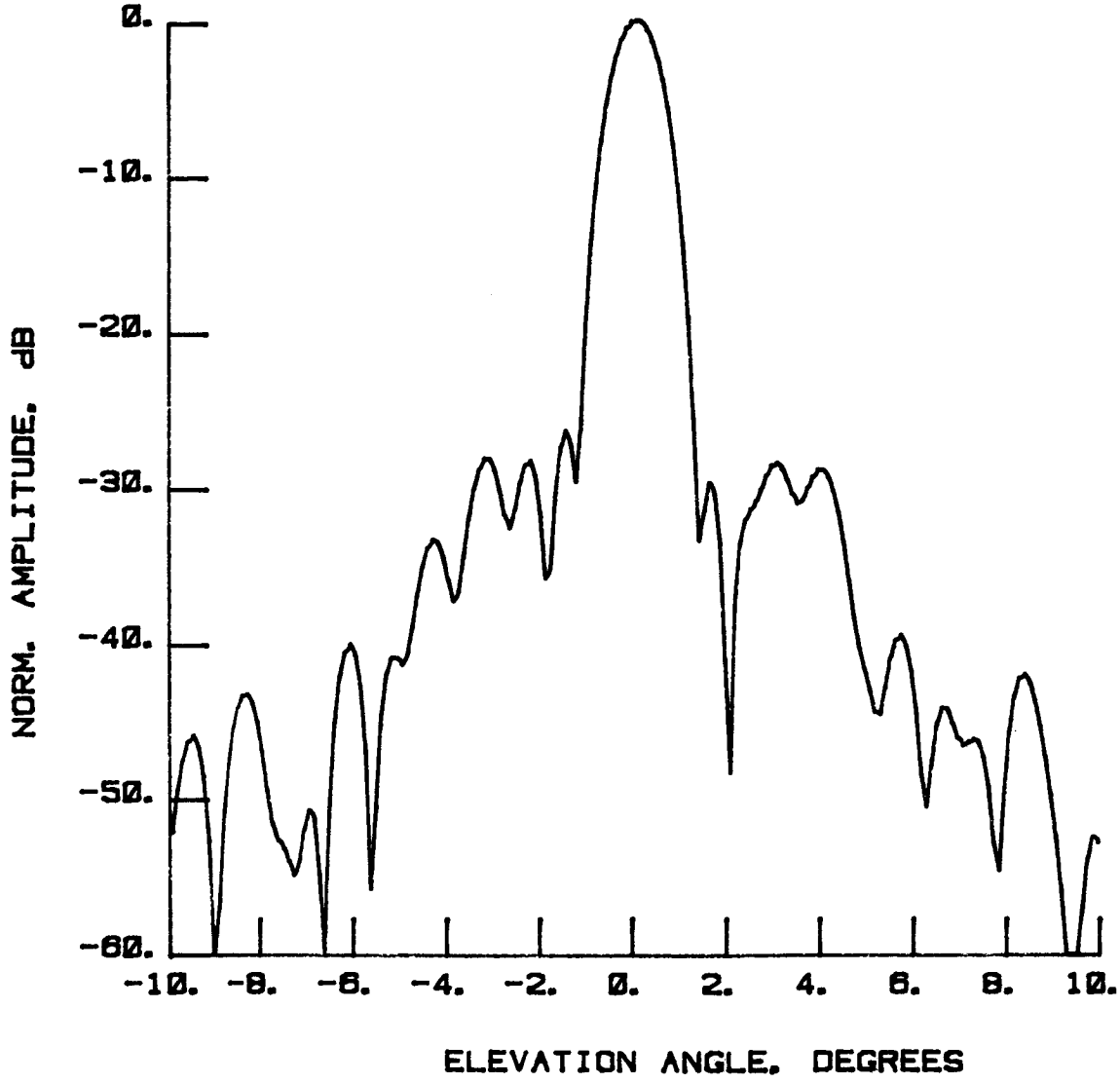

Figure 21 Test 1, 4.26 GHz, Co-Pol, E-Plane, Type 4

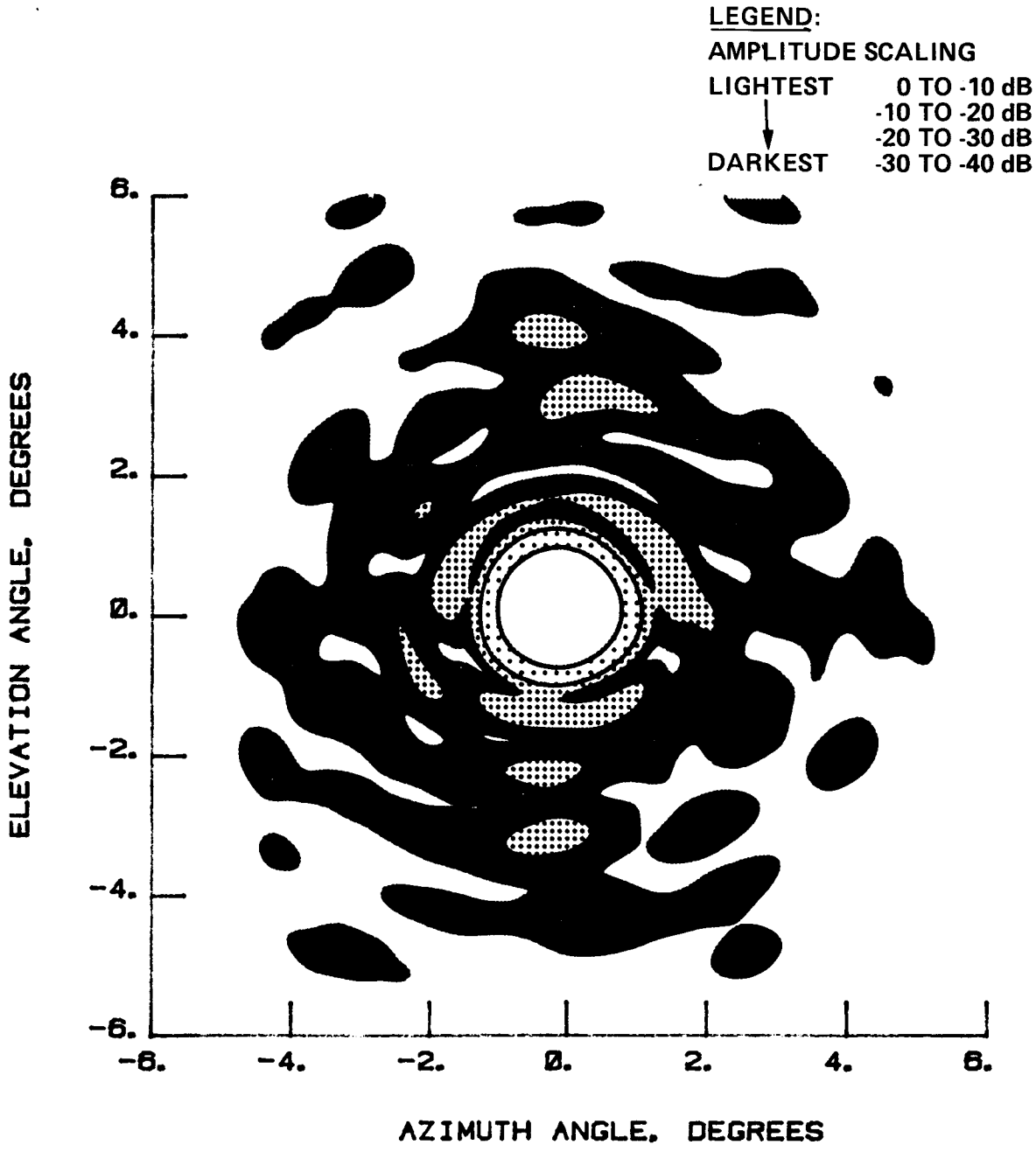

Figure 22 Test 1, 4.26 GHz, Co-Pol, Contour, Type 5

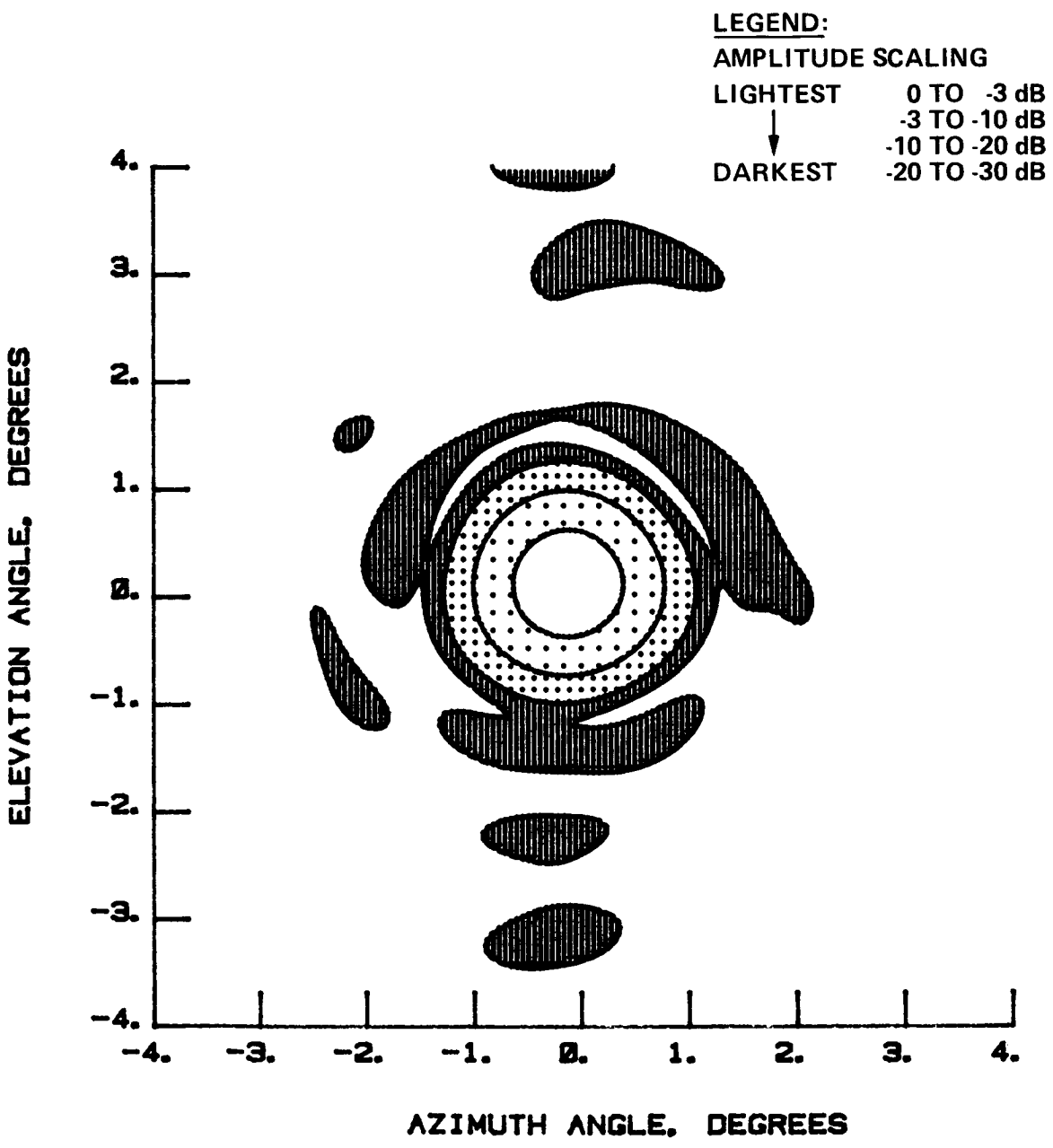

Figure 23 Test 1, 4.26 GHz, Co-Pol, Contour, Type 6

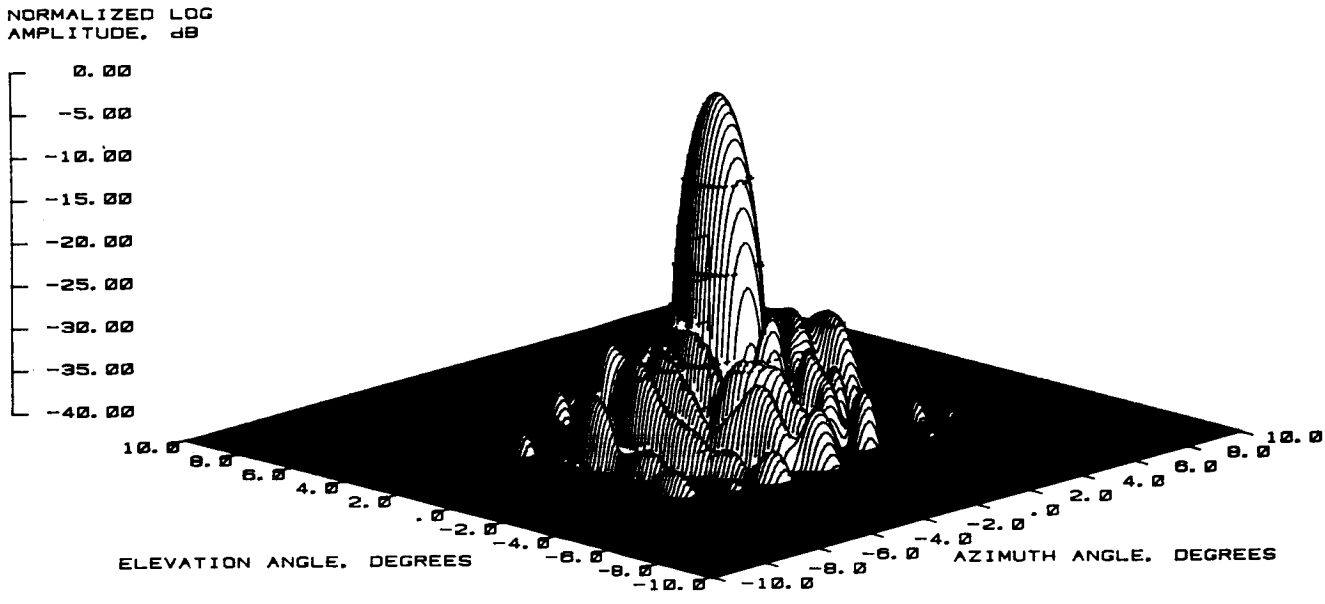

Figure 24 Test 1, 4.26 GHz, Co-Pol, 3-D, Type 7

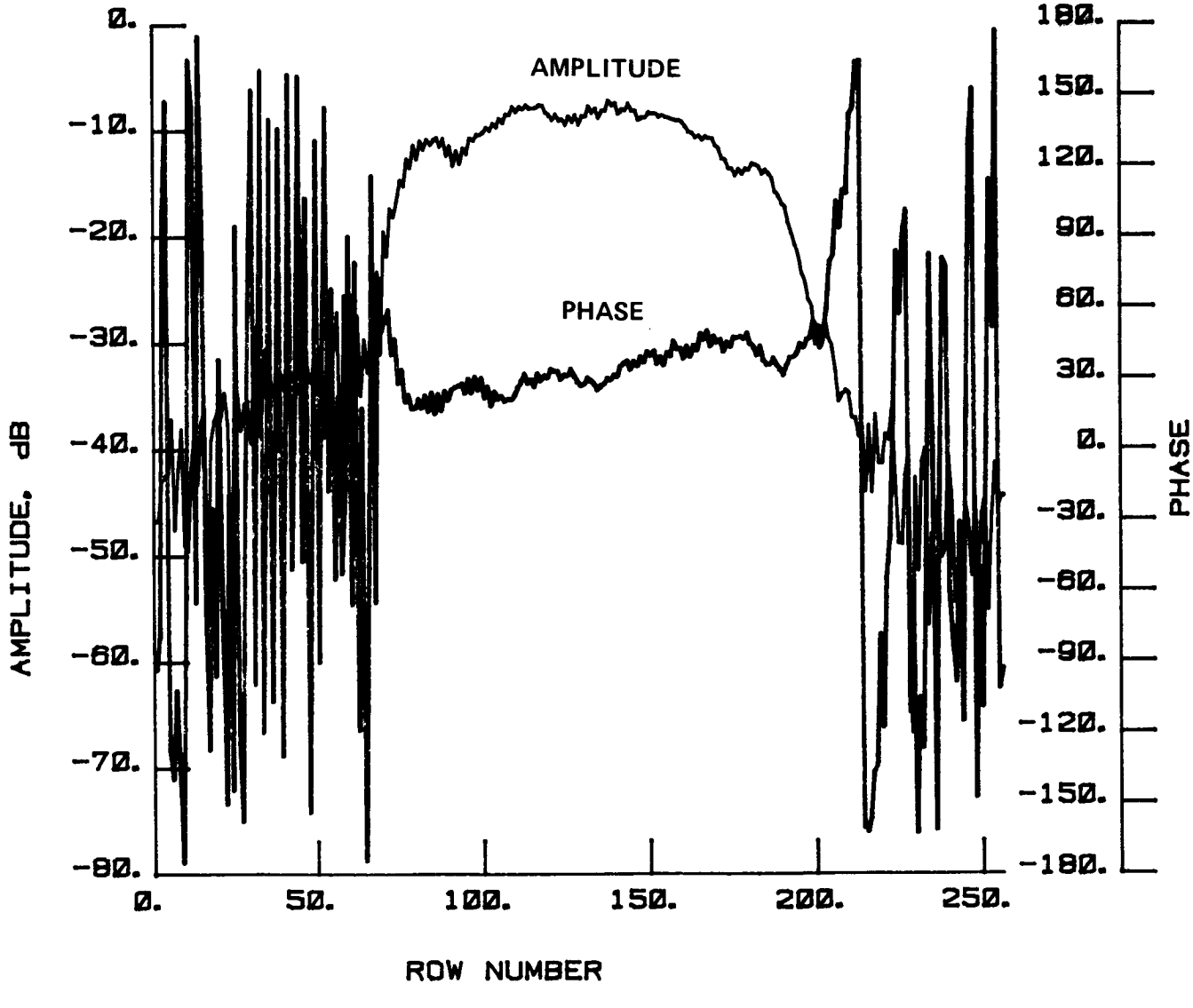

Figure 25 Test 1, 4.26 GHz, Co-Pol, H-Plane, Type 8

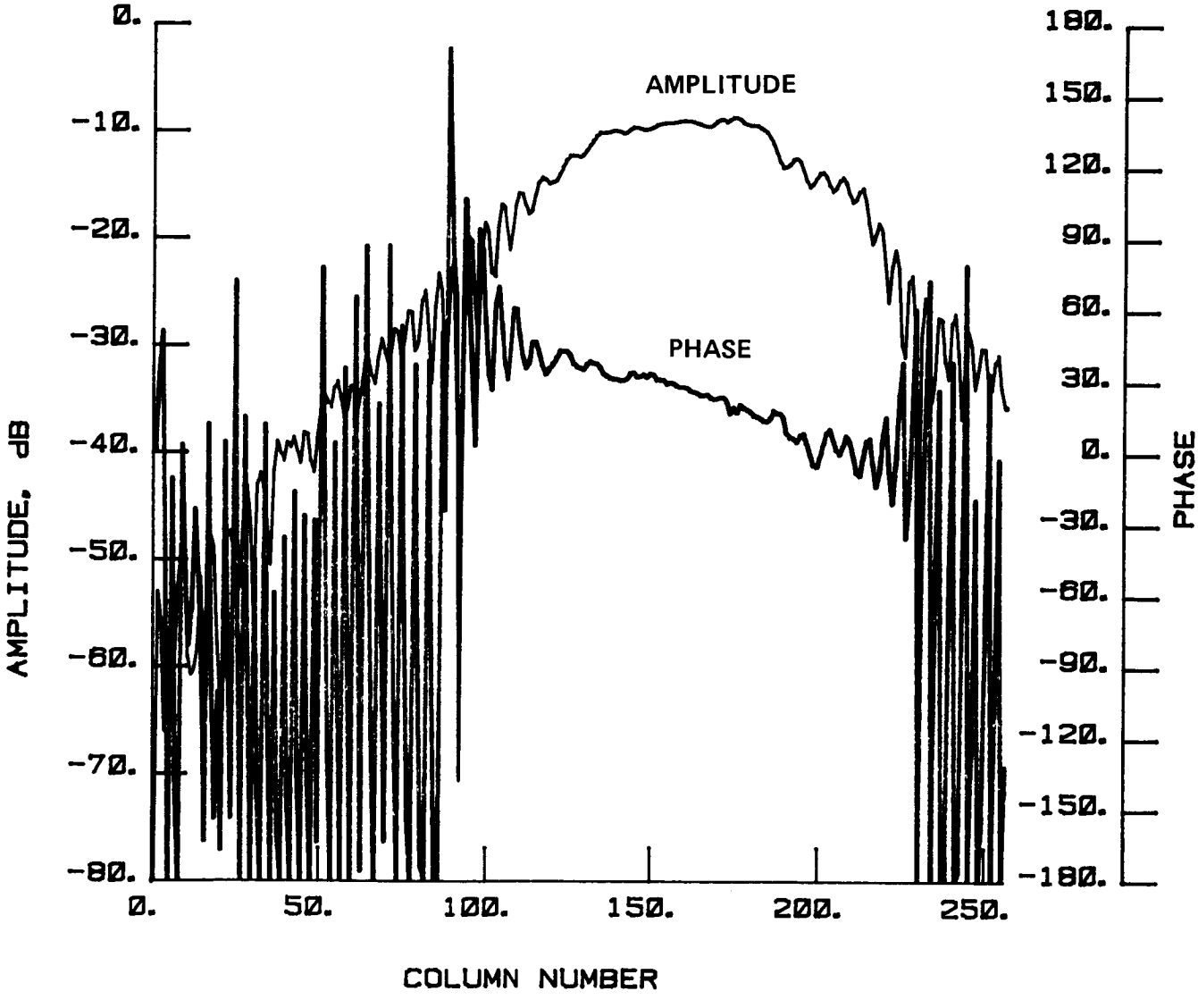

Figure 26 Test 1, 4.26 GHz, Co-Pol, E-Plane, Type 9

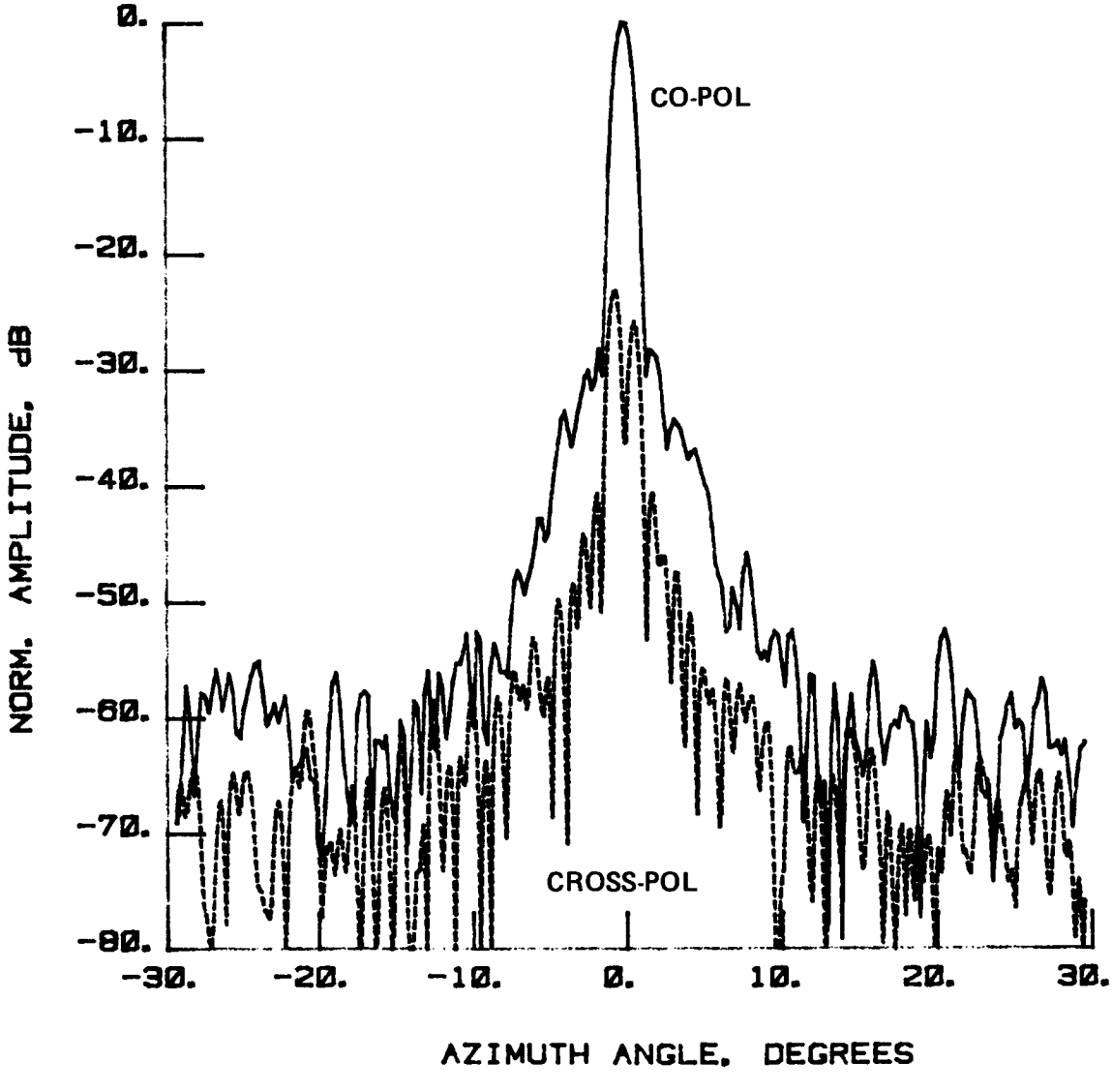

Figure 27 Test 2, 4.26 GHz, Overlay, H-Plane, Type 10

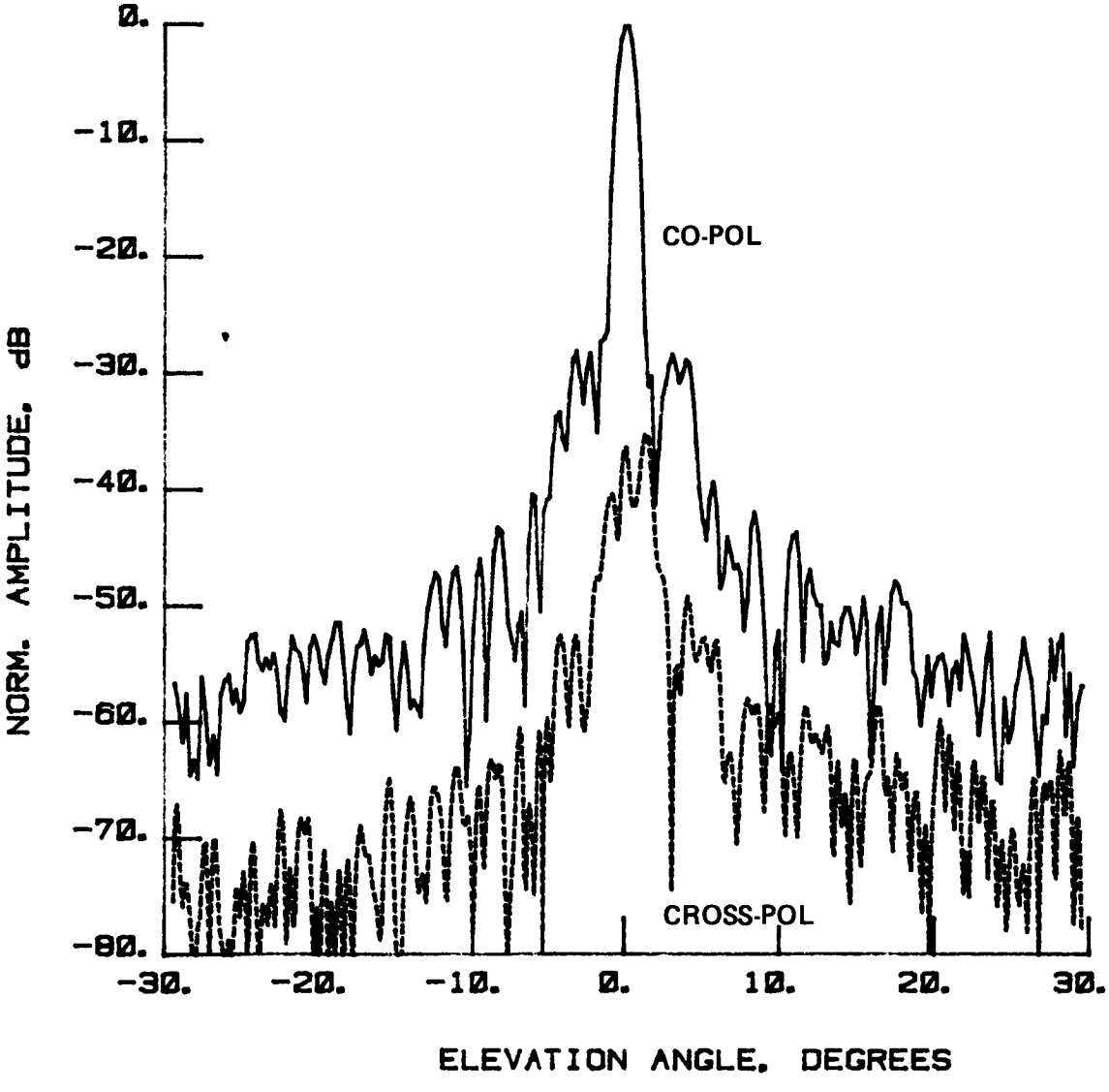

Figure 28 Test 2, 4.26 GHz, Overlay, E-Plane, Type 11

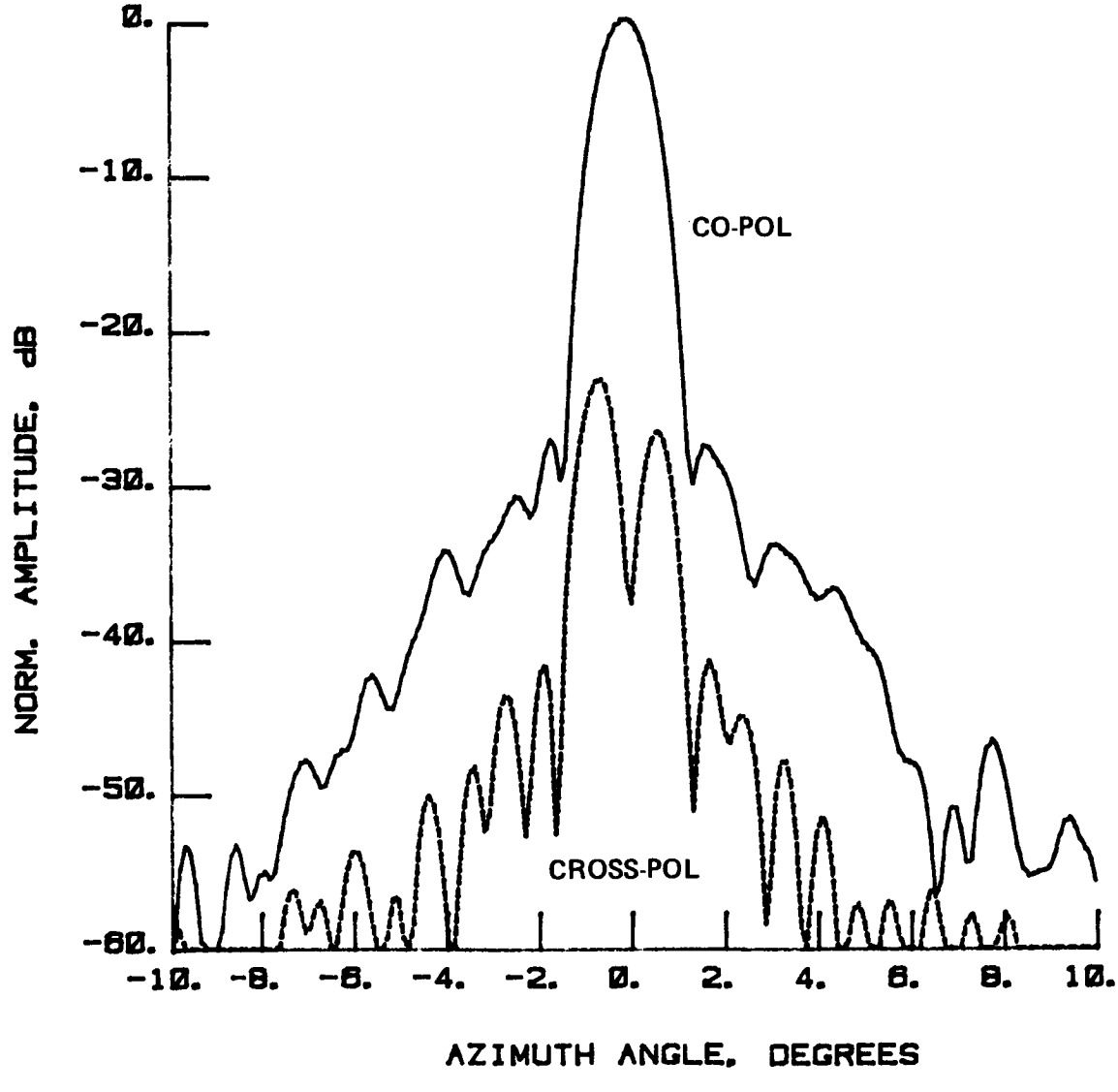

Figure 29 Test 2, 4.26 GHz, Overlay, H-Plane, Type 12

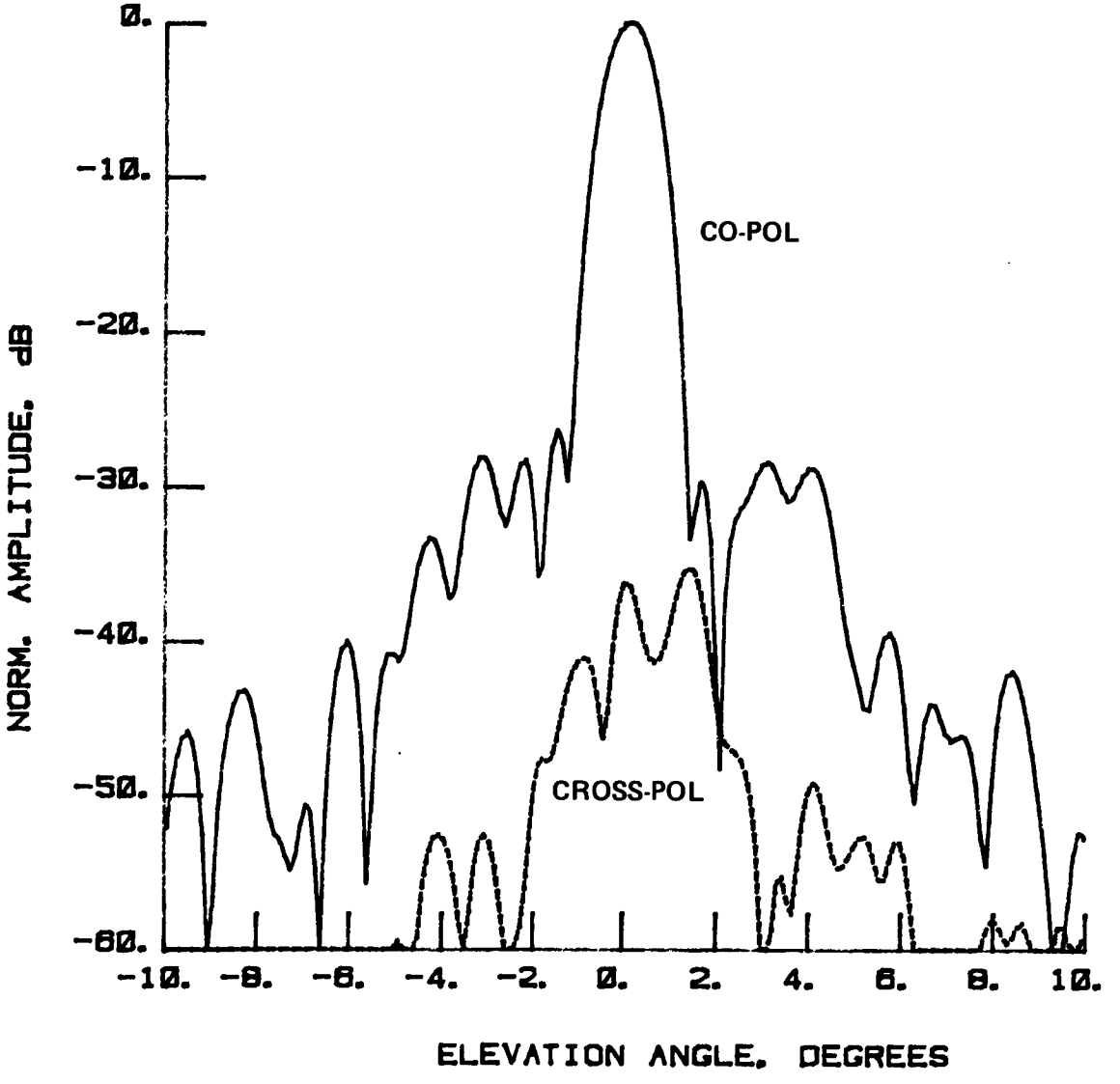

Figure 30 Test 2, 4.26 GHz, Overlay, E-Plane, Type 13

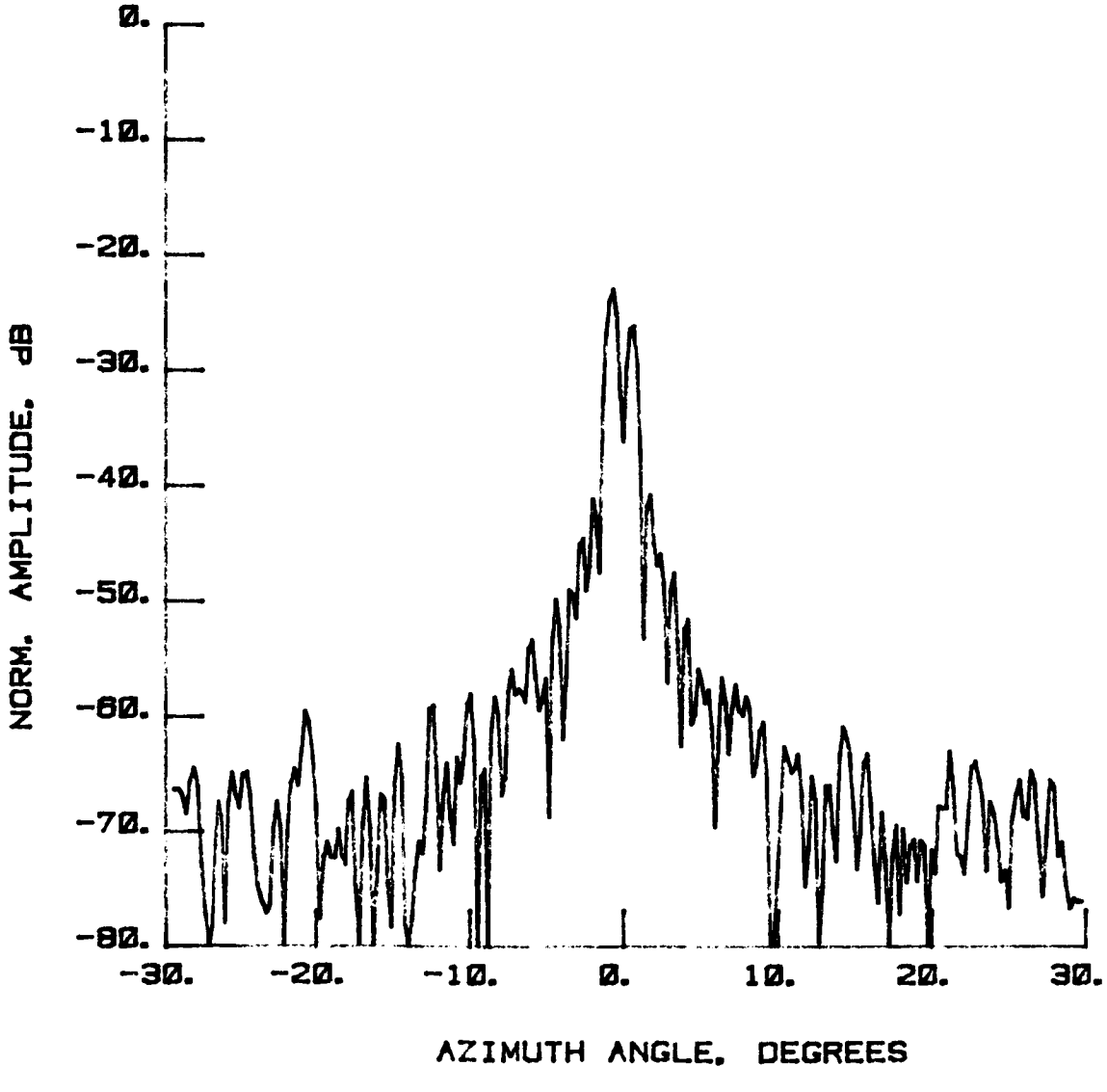

Figure 31 Test 2, 4.26 GHz, Cross-Pol, H-Plane, Type 14

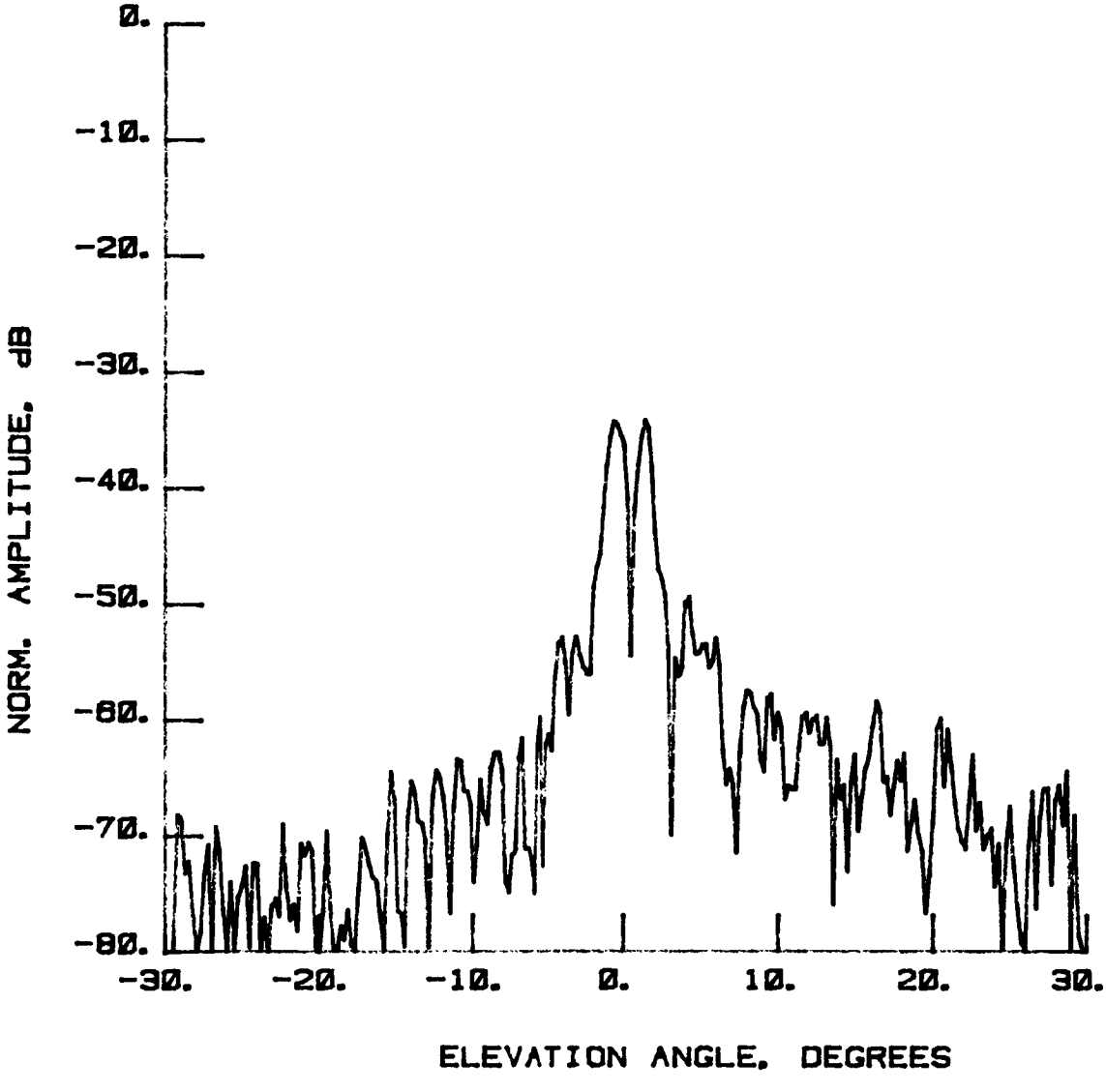

Figure 32 Test 2, 4.26 GHz, Cross-Pol, E-Plane, Type 15

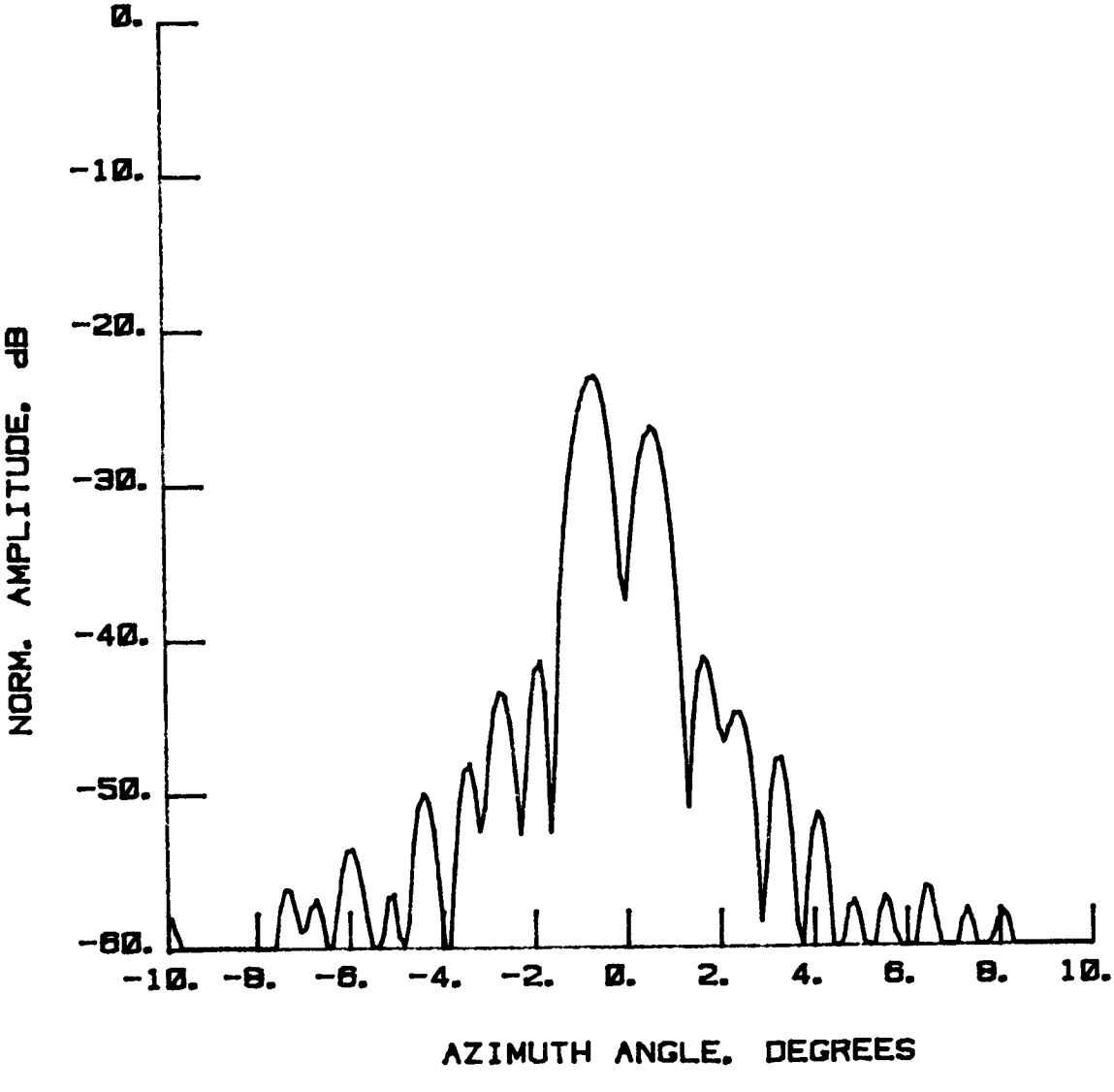

Figure 33 Test 2, 4.26 GHz, Cross-Pol, H-Plane, Type 16

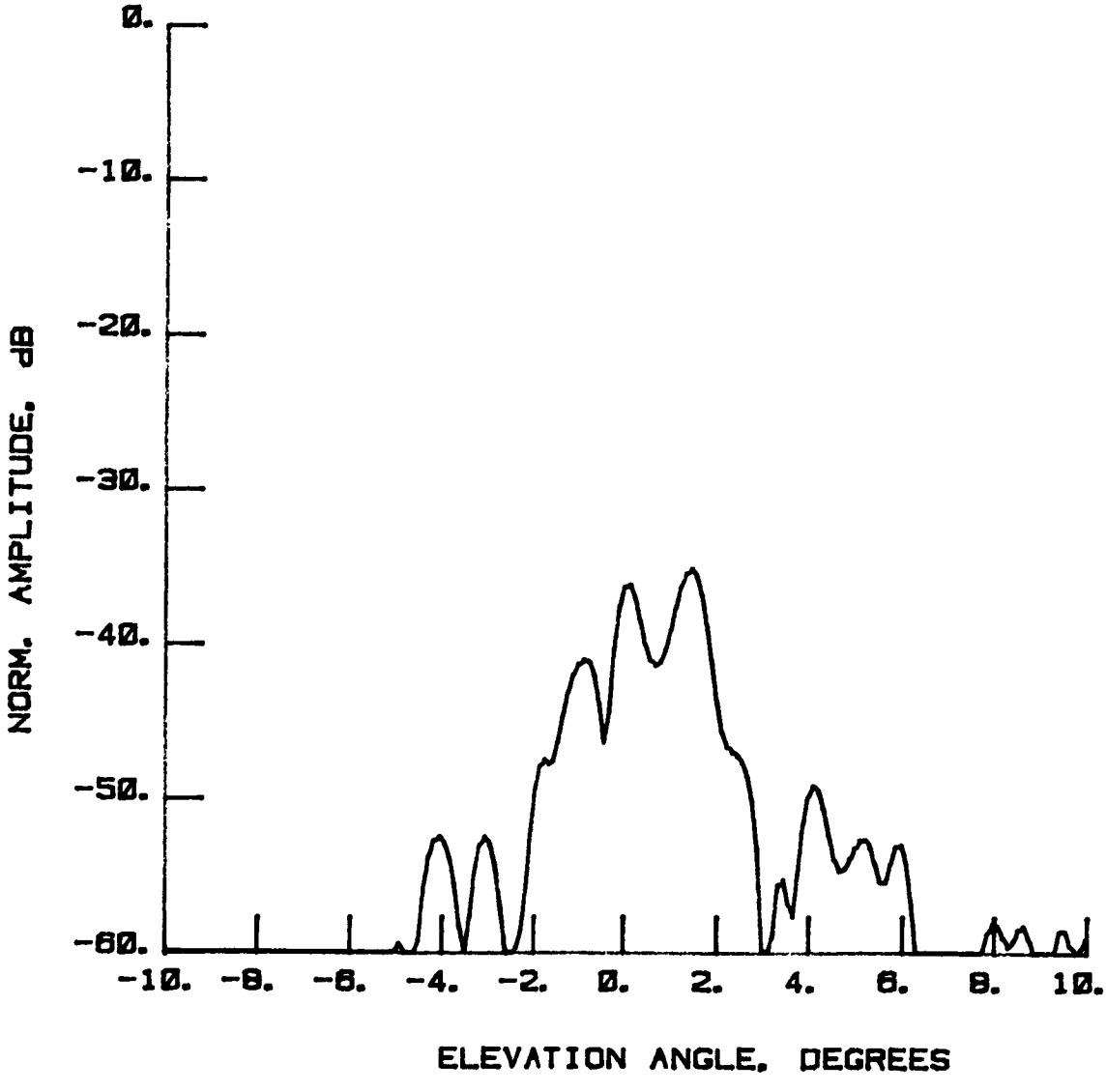

Figure 34 Test 2, 4.26 GHz, Cross-Pol, E-Plane, Type 17

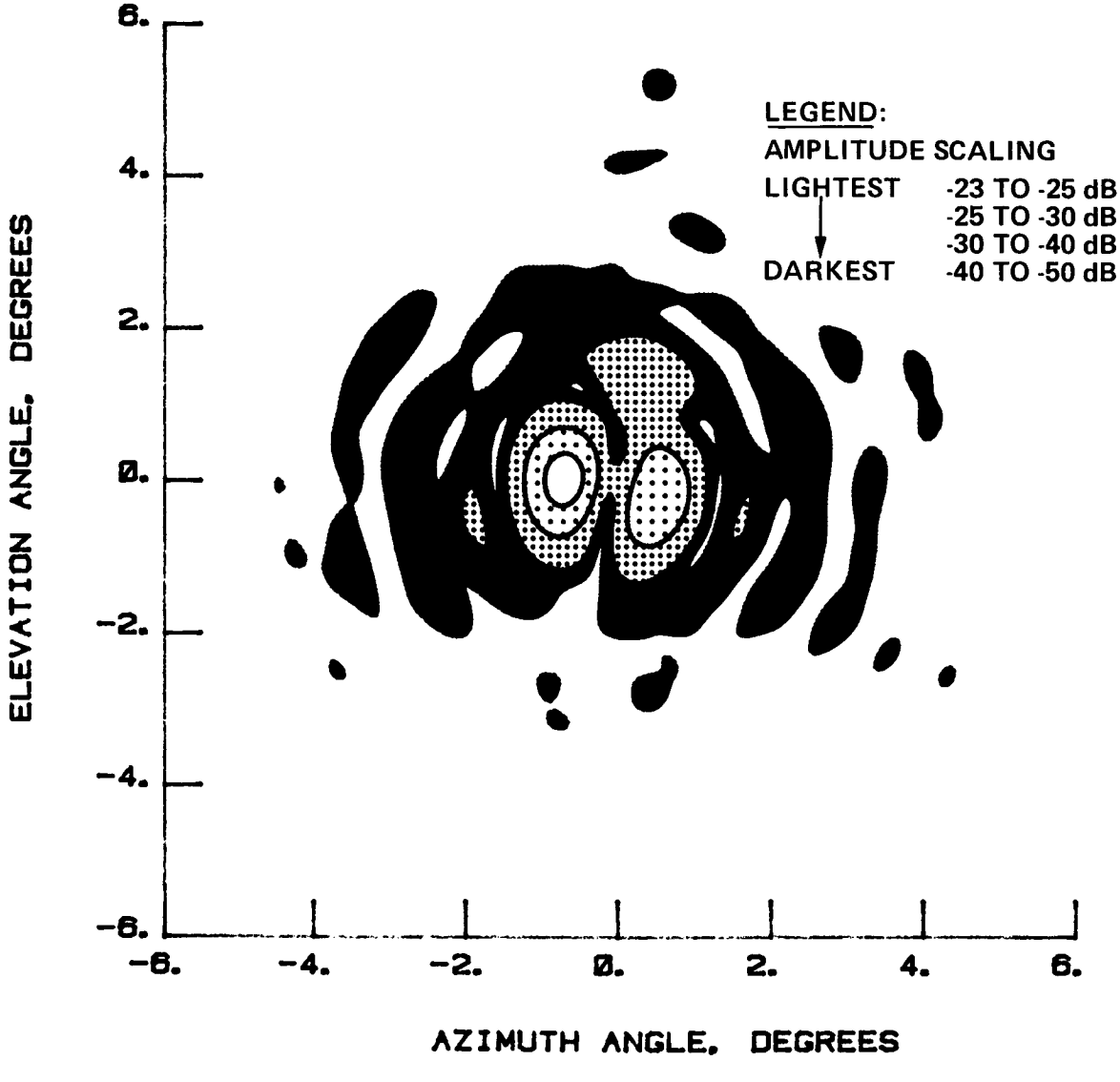

Figure 35 Test 2, 4.26 GHz, Cross-Pol, Contour, Type 18

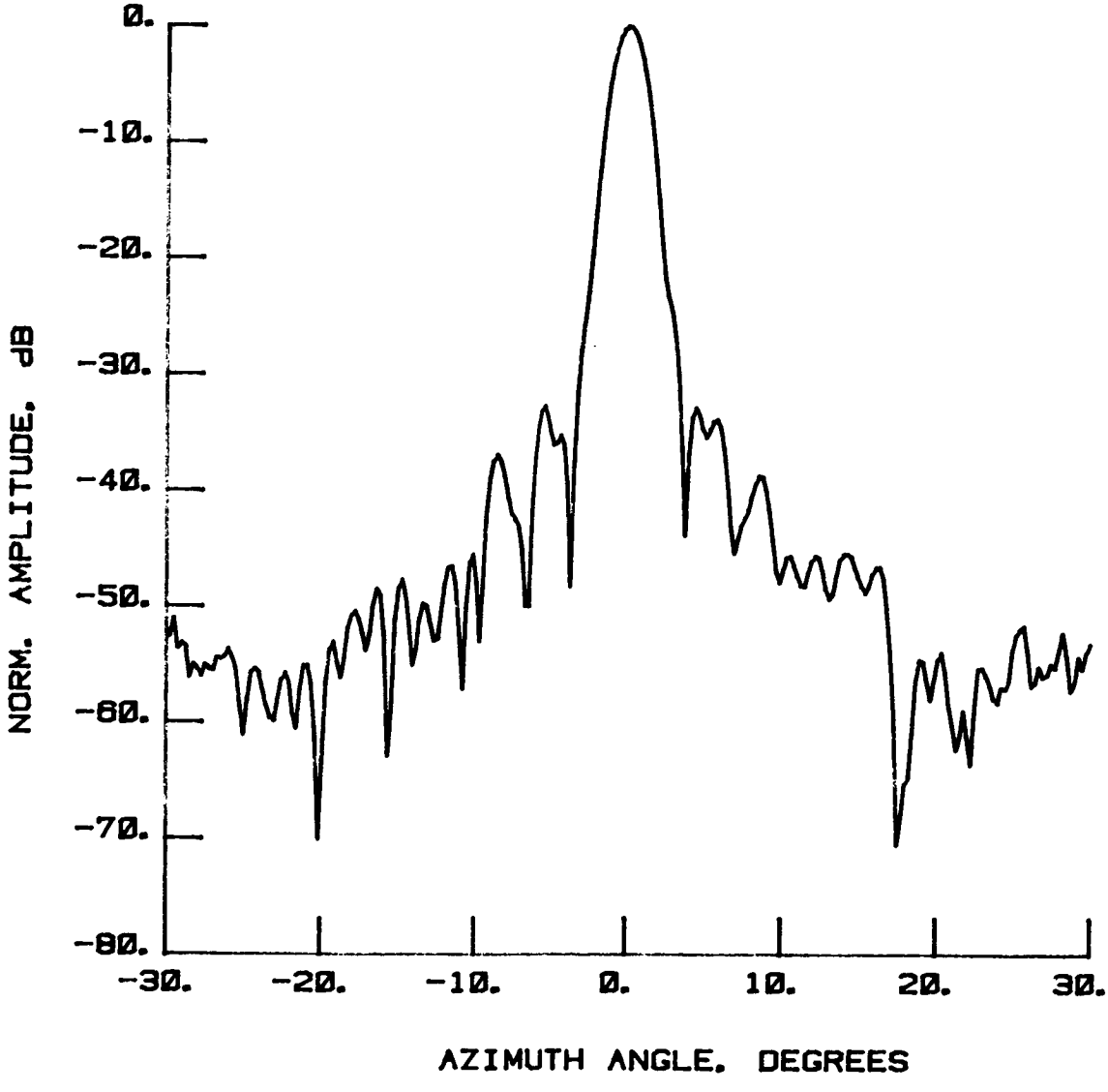

Figure 36 Test 3, 2.27 GHz, Co-Pol, H-Plane, Type 1

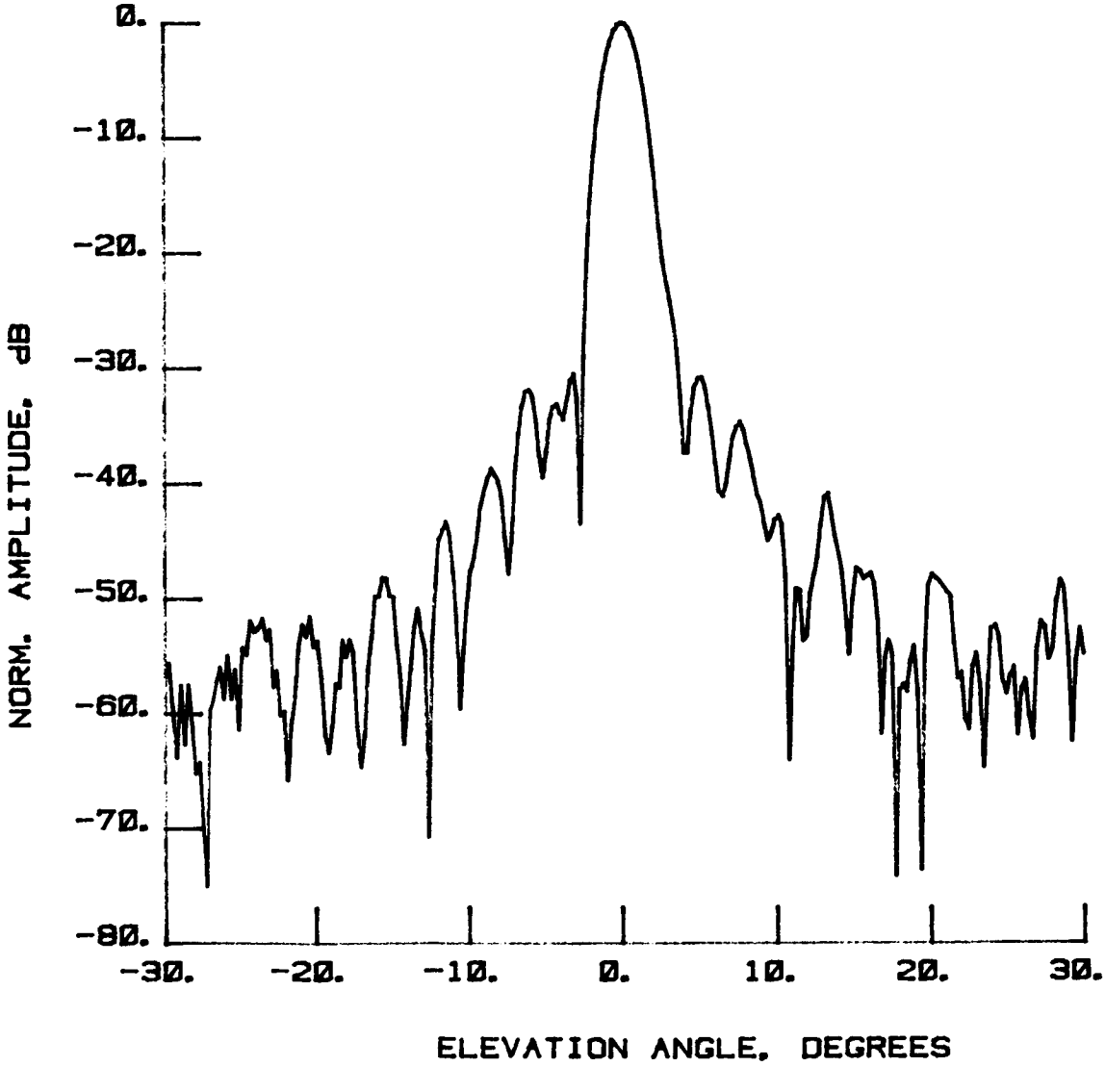

Figure 37 Test 3, 2.27 GHz, Co-Pol, E-Plane, Type 2

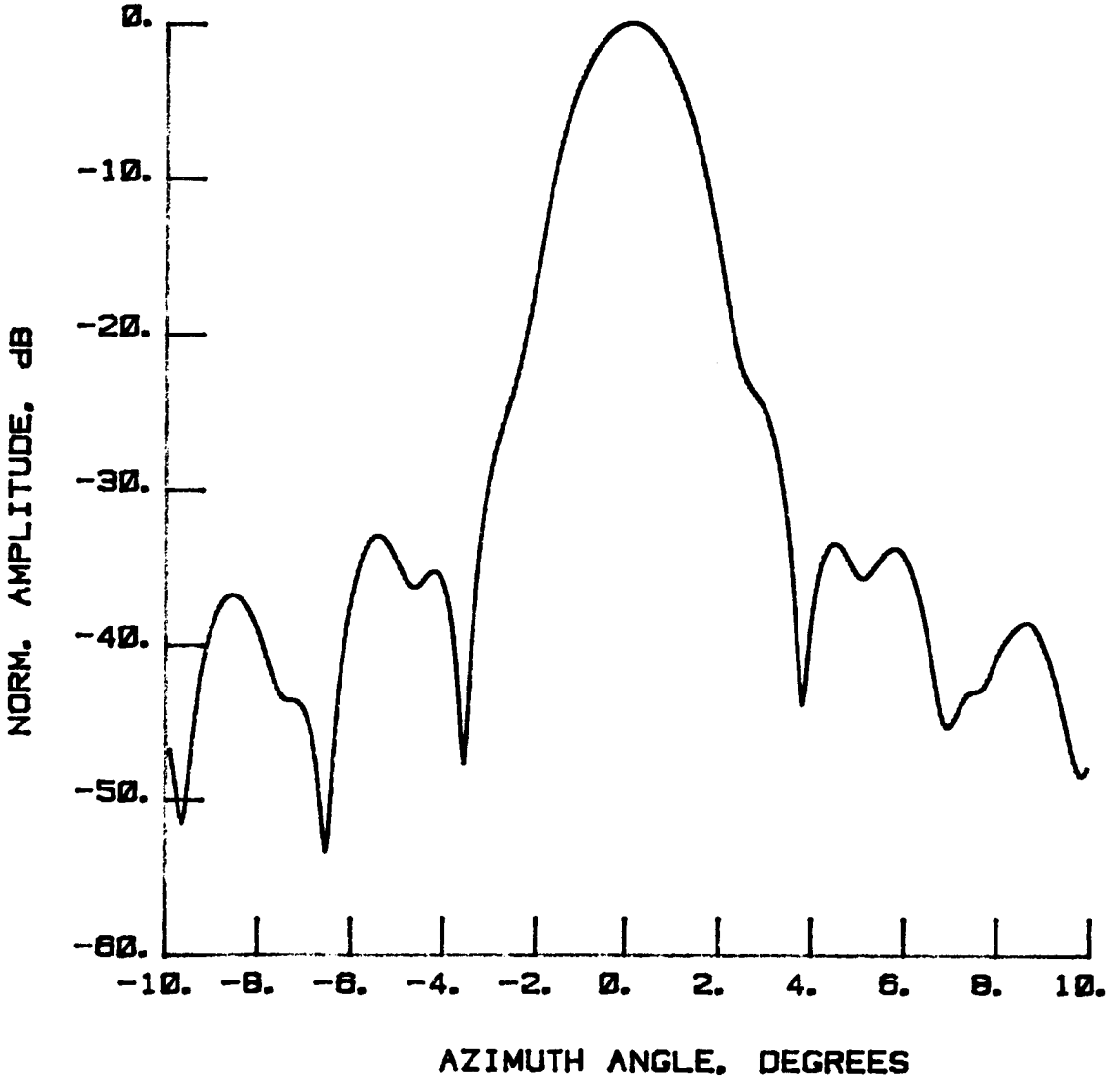

Figure 38 Test 3, 2.27 GHz, Co-Pol, H-Plane, Type 3

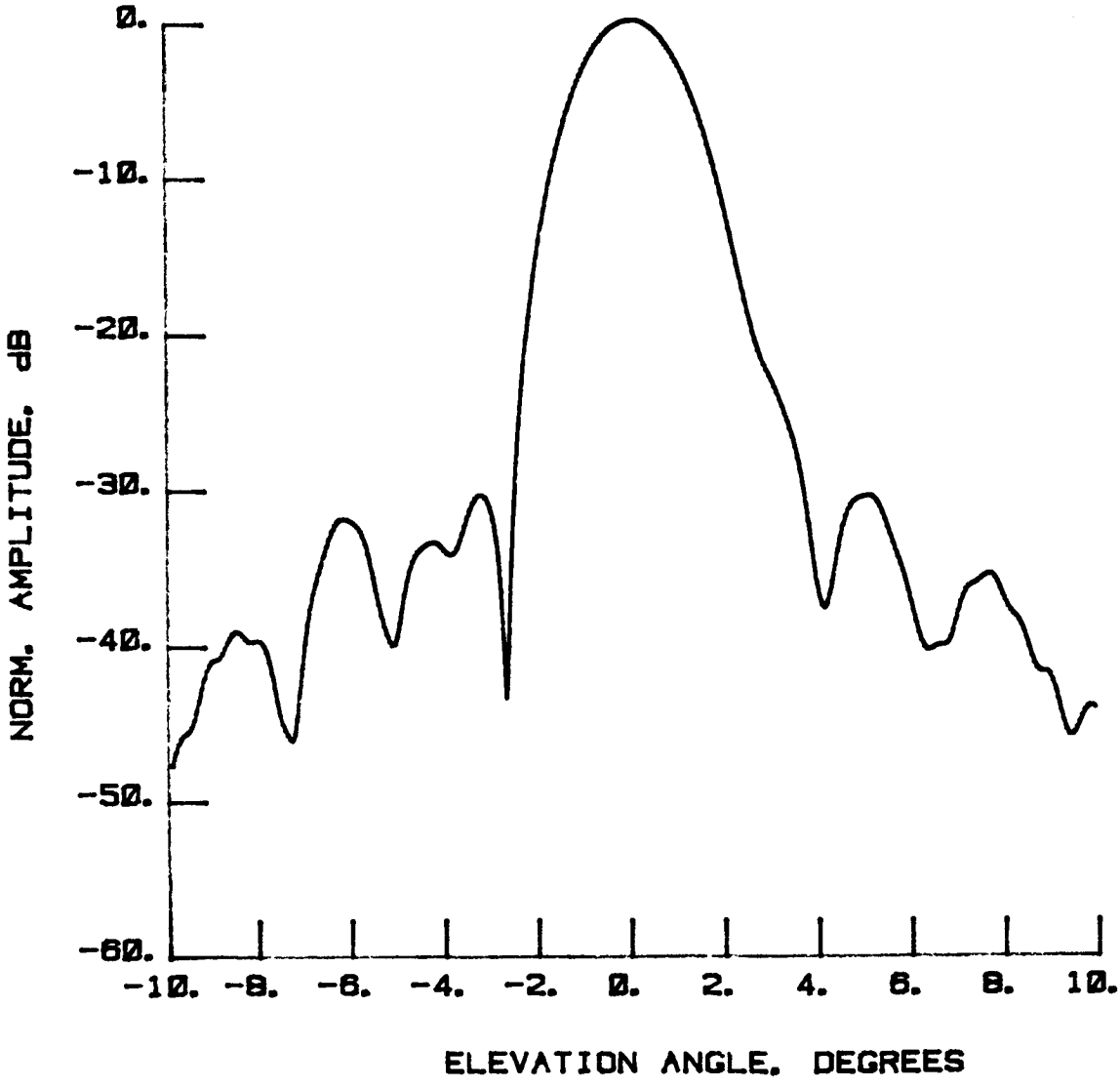

Figure 39 Test 3, 2.27 GHz, Co-Pol, E-Plane, Type 4

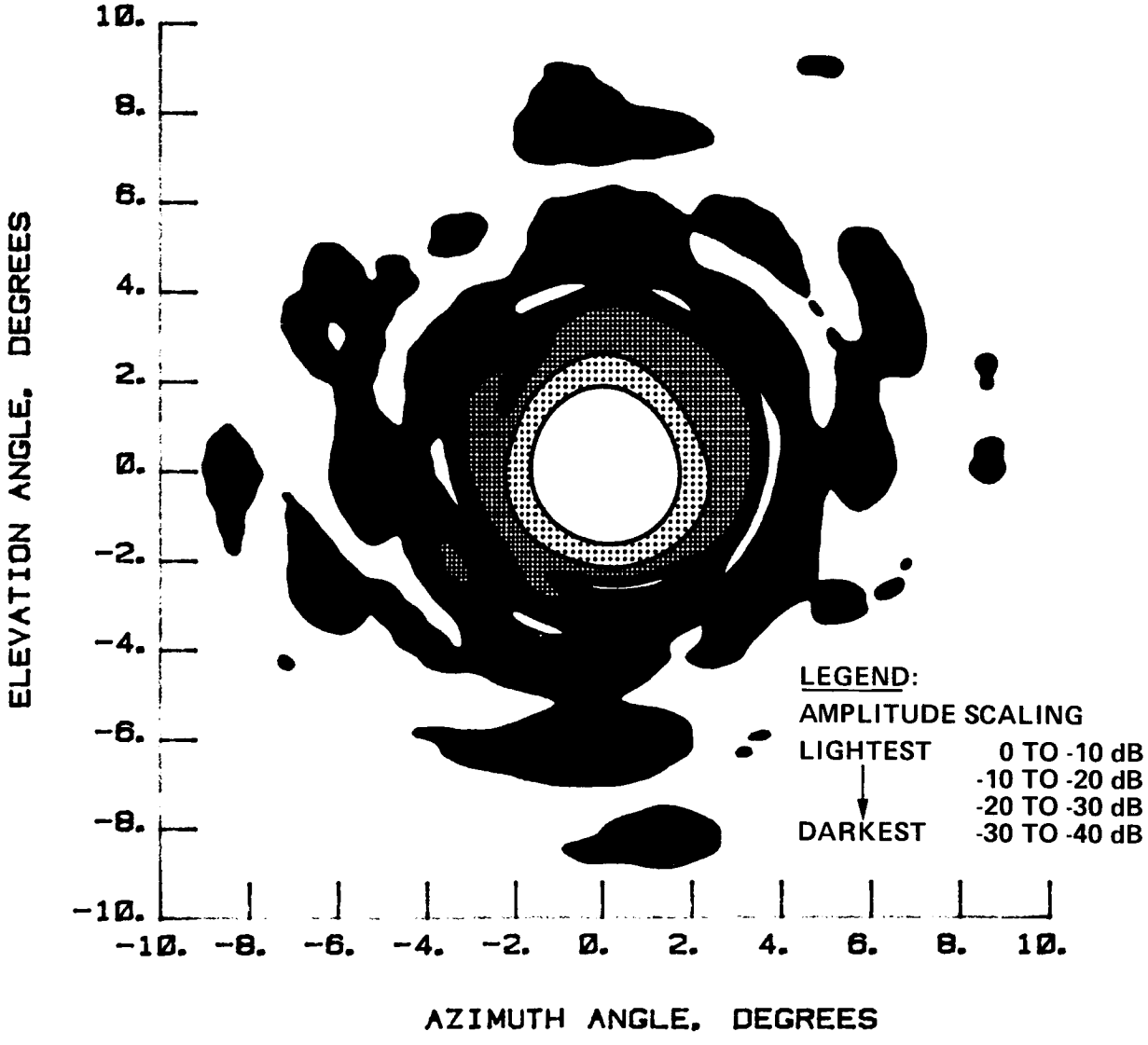

Figure 40 Test 3, 2.27 GHz, Co-Pol, Contour, Type 5

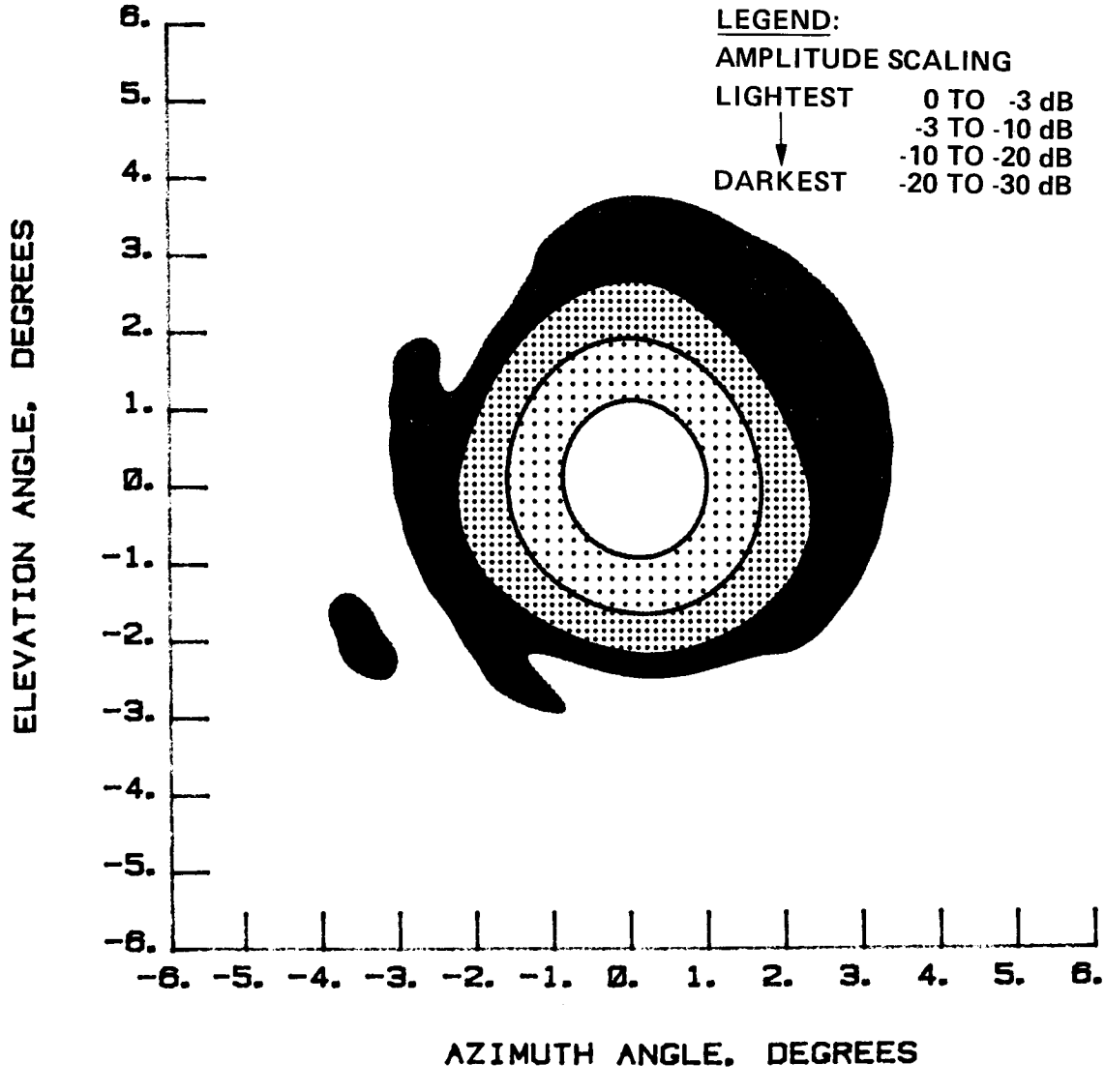

Figure 41 Test 3, 2.27 GHz, Co-Pol, Contour, Type 6

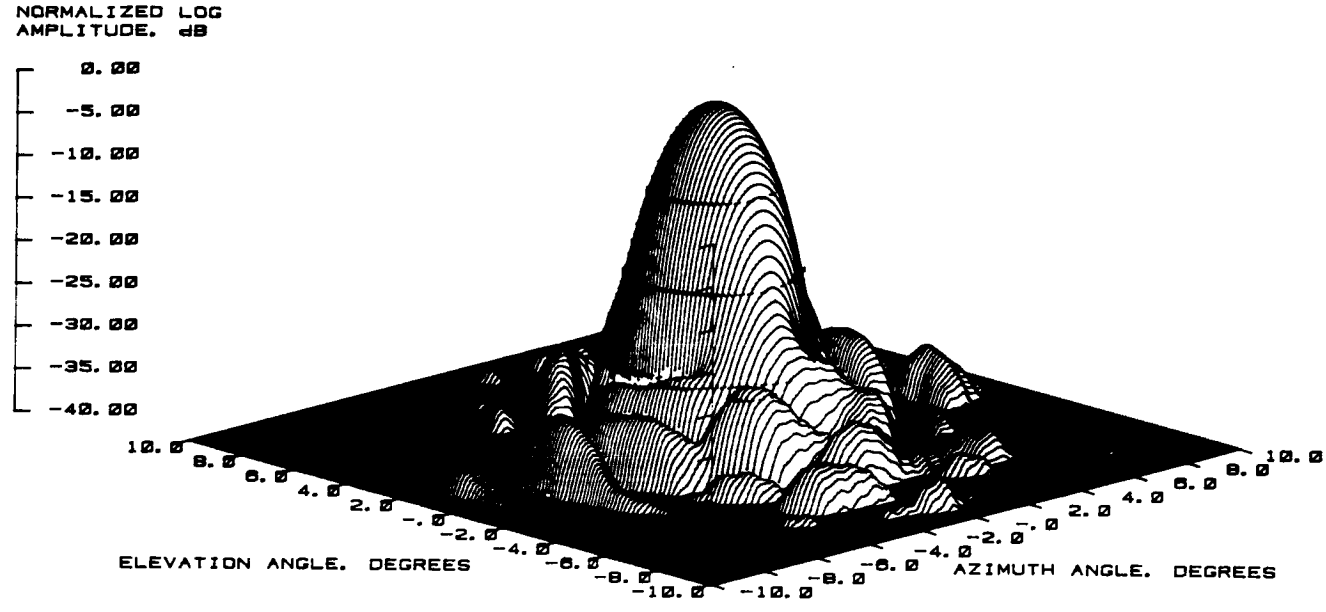

Figure 42 Test 3, 2.27 GHz, Co-Pol, 3-D, Type 7

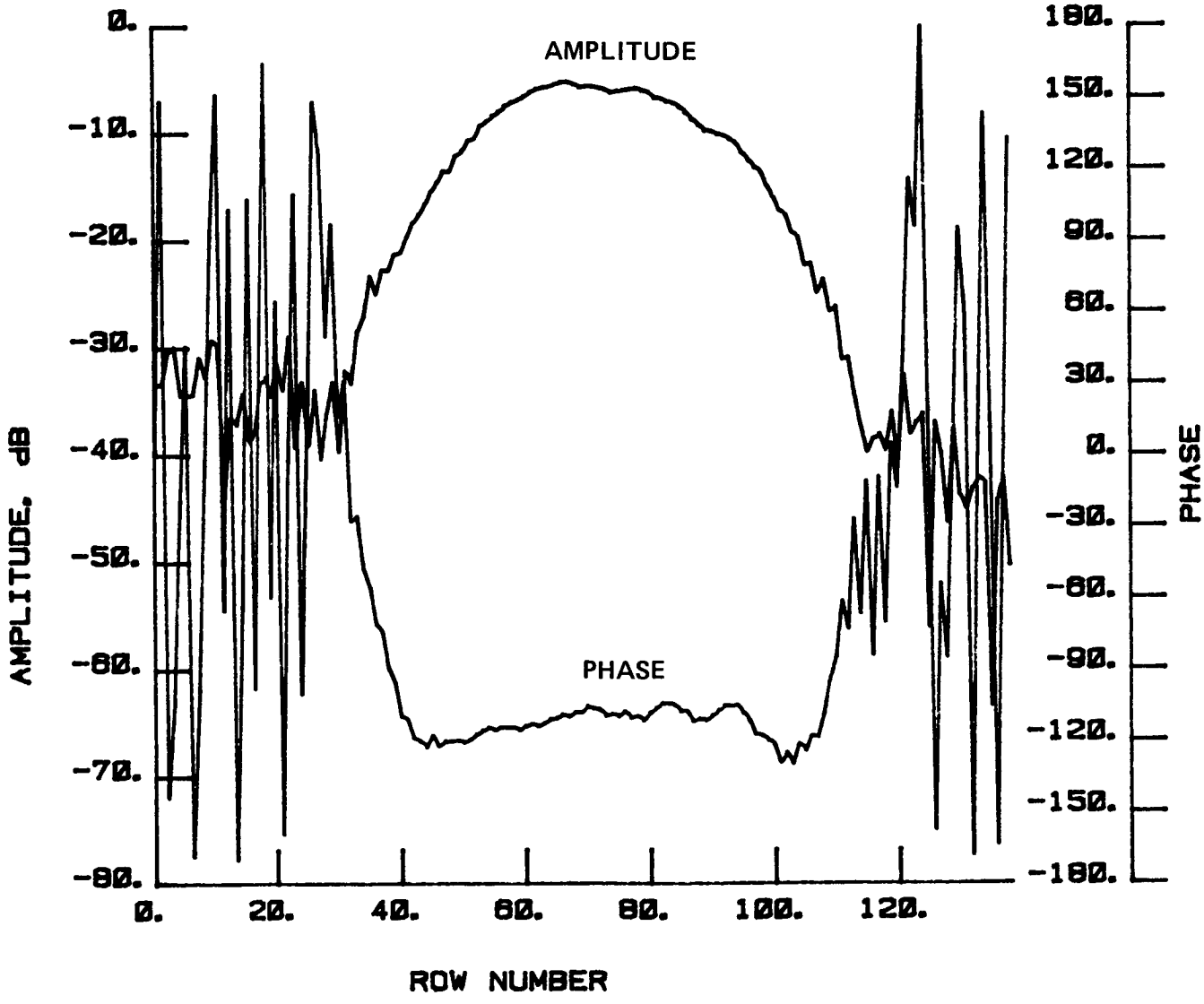

Figure 43 Test 3, 2.27 GHz, Co-Pol, H-Plane, Type 8

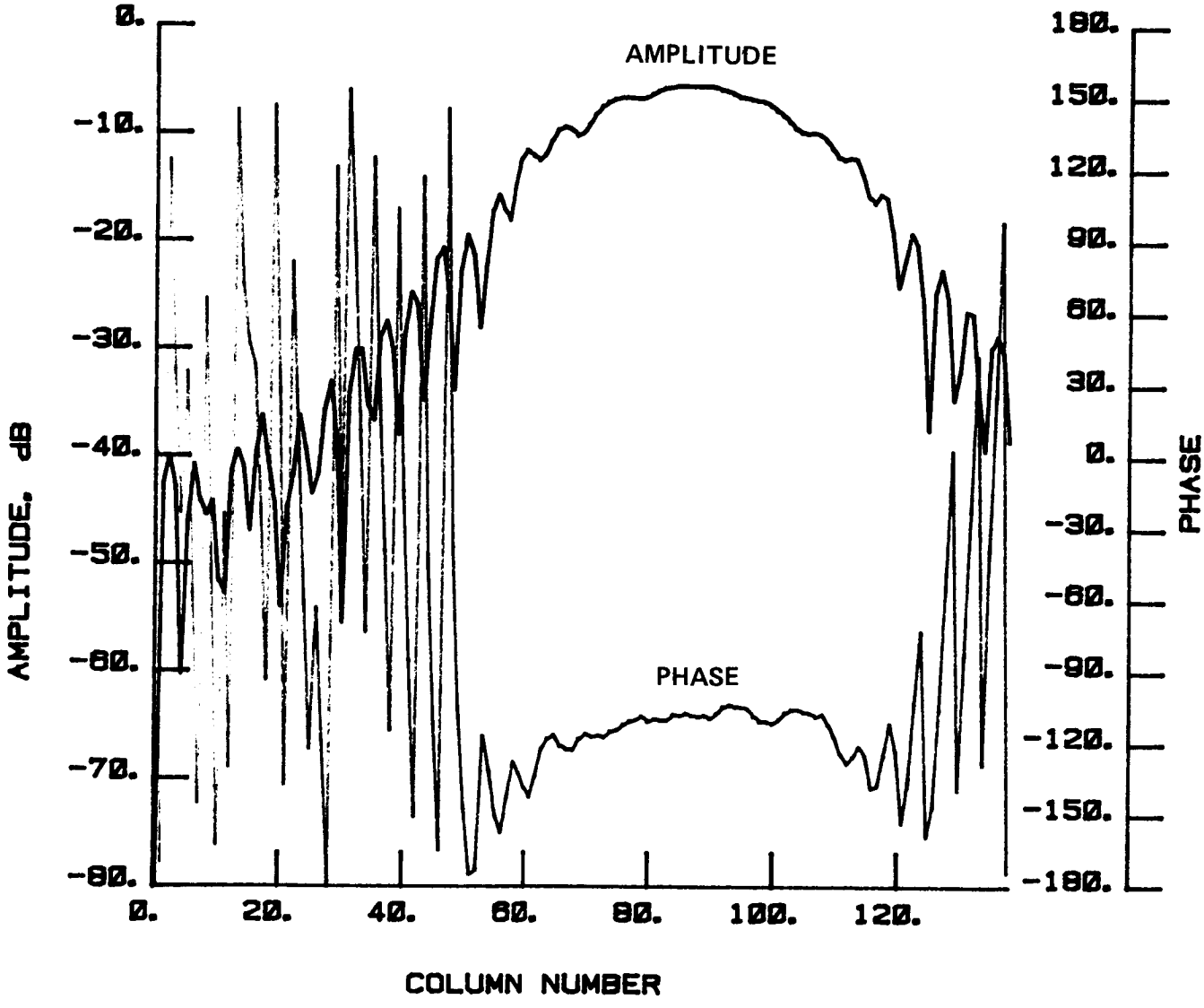

Figure 44 Test 3, 2.27 GHz, Co-Pol, E-Plane, Type 9

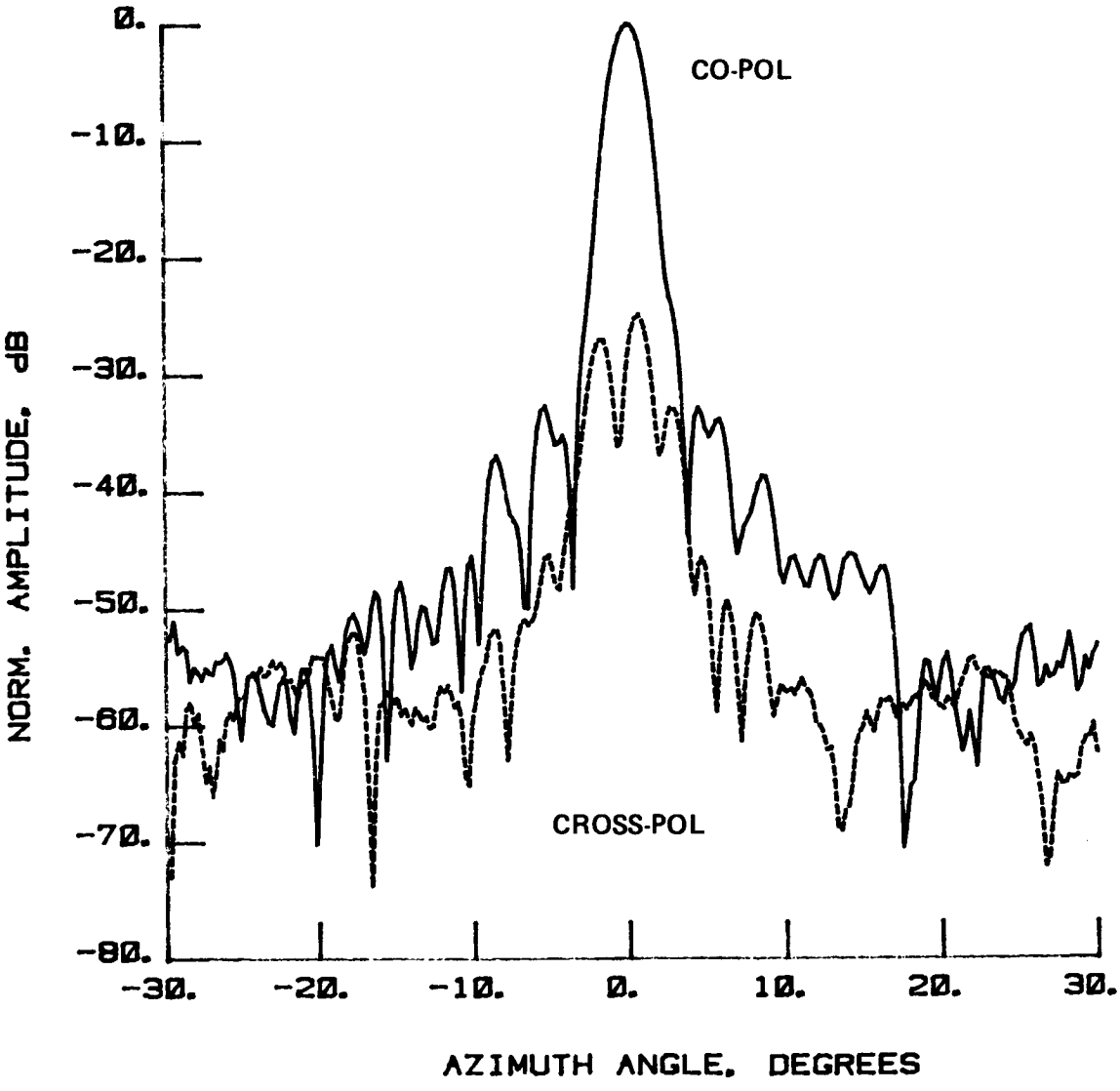

Figure 45 Test 4, 2.27 GHz, Overlay, H-Plane, Type 10

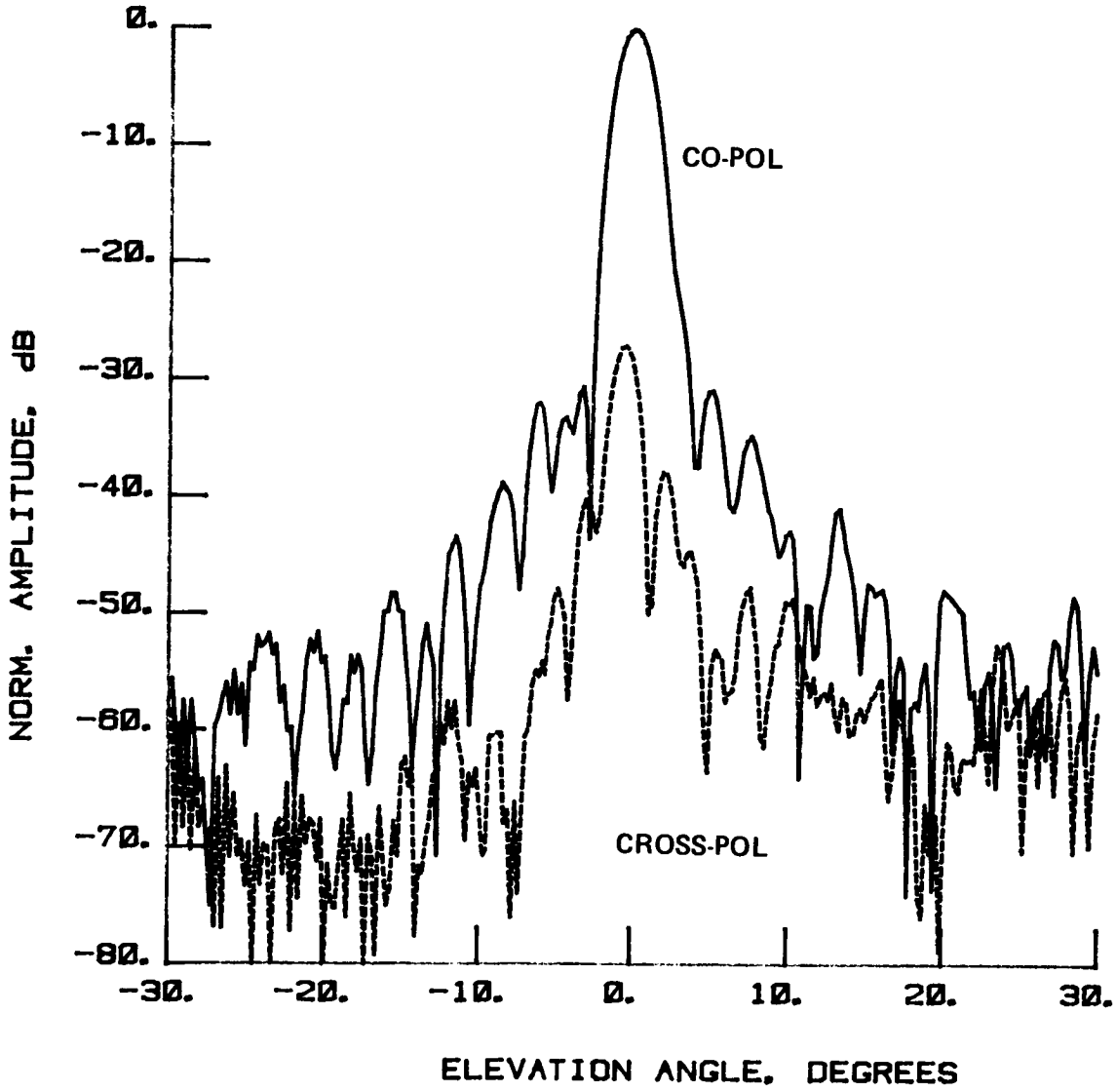

Figure 46 Test 4, 2.27 GHz, Overlay, E-Plane, Type 11

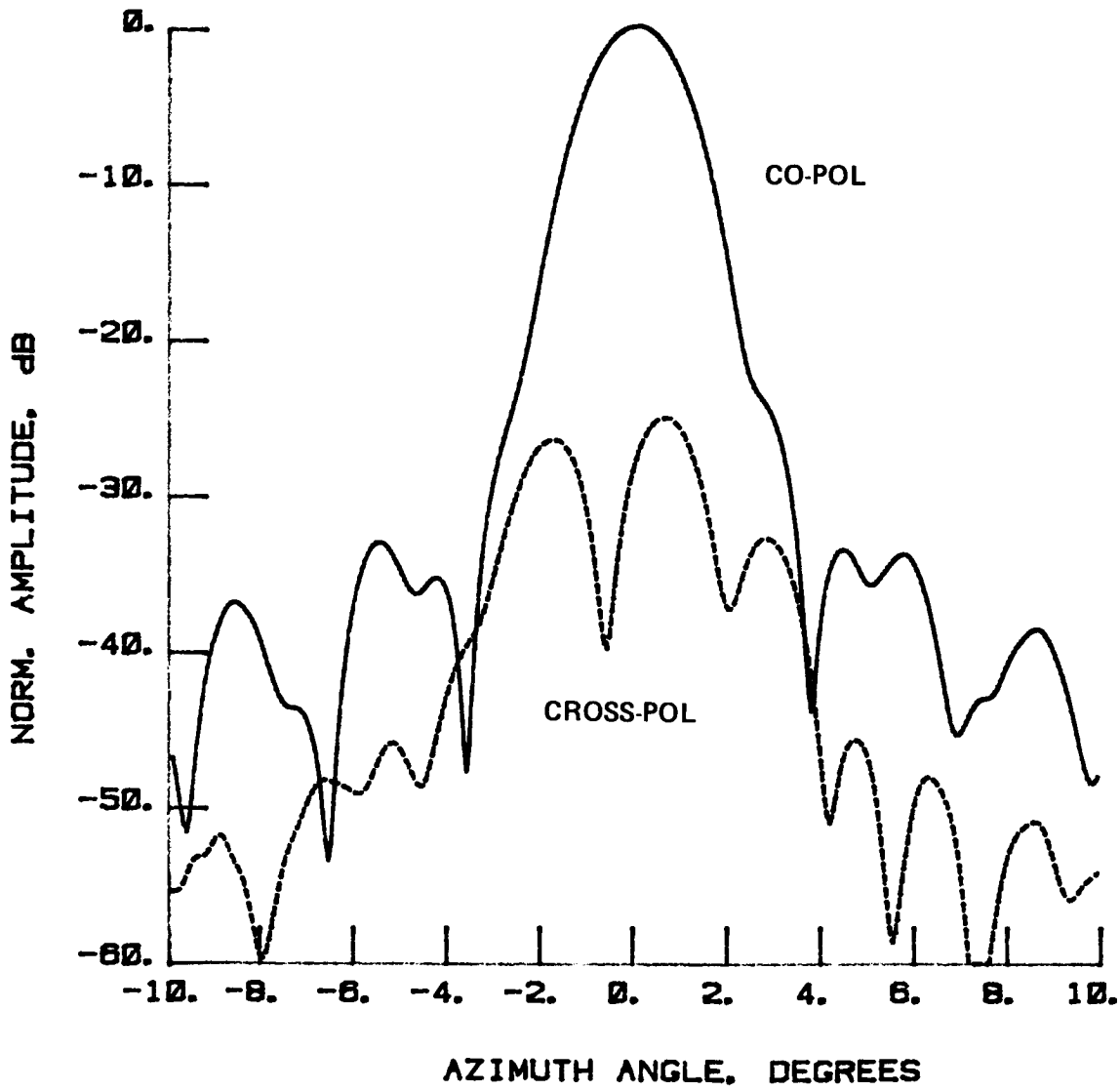

Figure 47 Test 4, 2.27 GHz, Overlay, H-Plane, Type 12

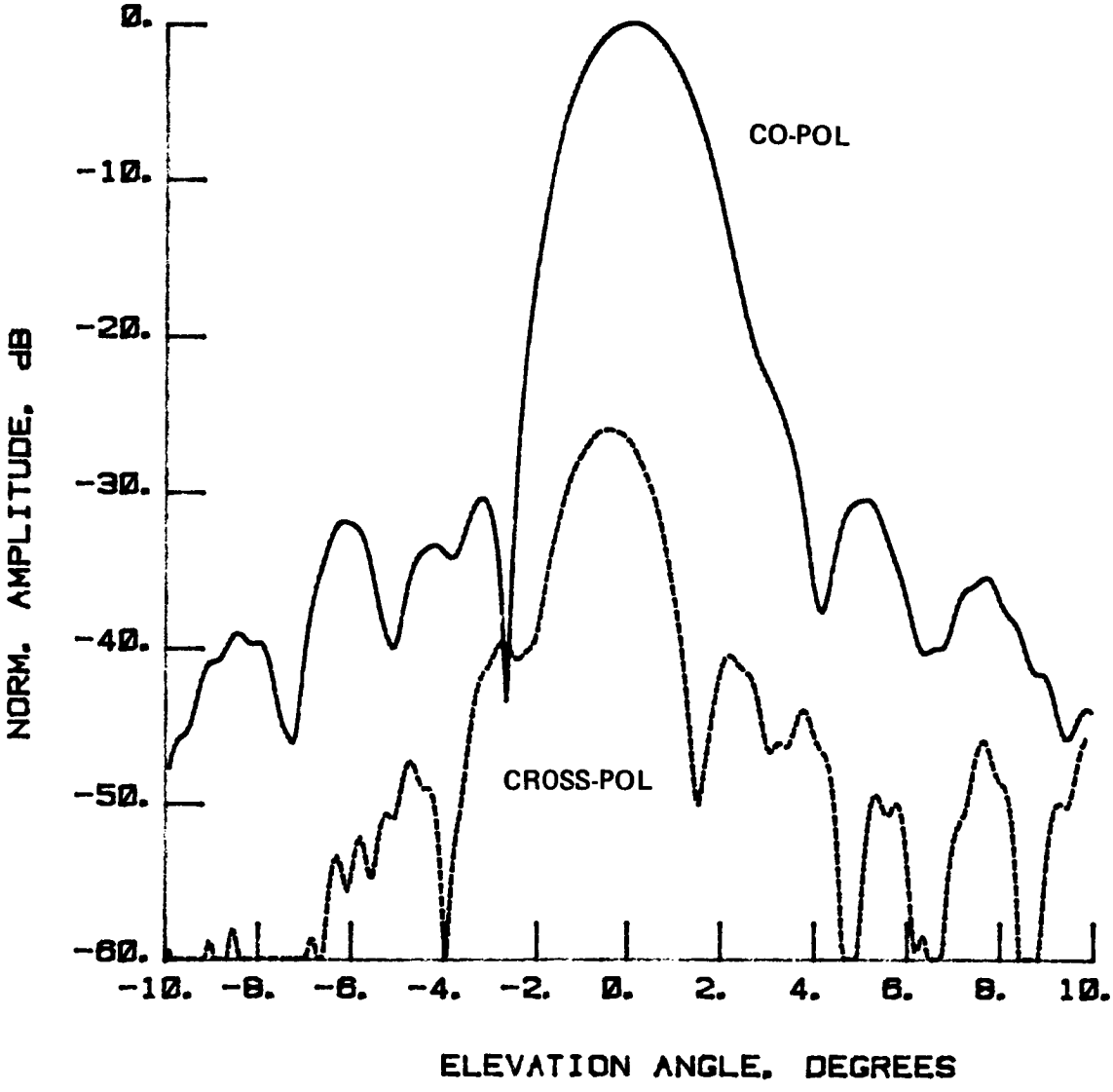

Figure 48 Test 4, 2.27 GHz, Overlay, E-Plane, Type 13

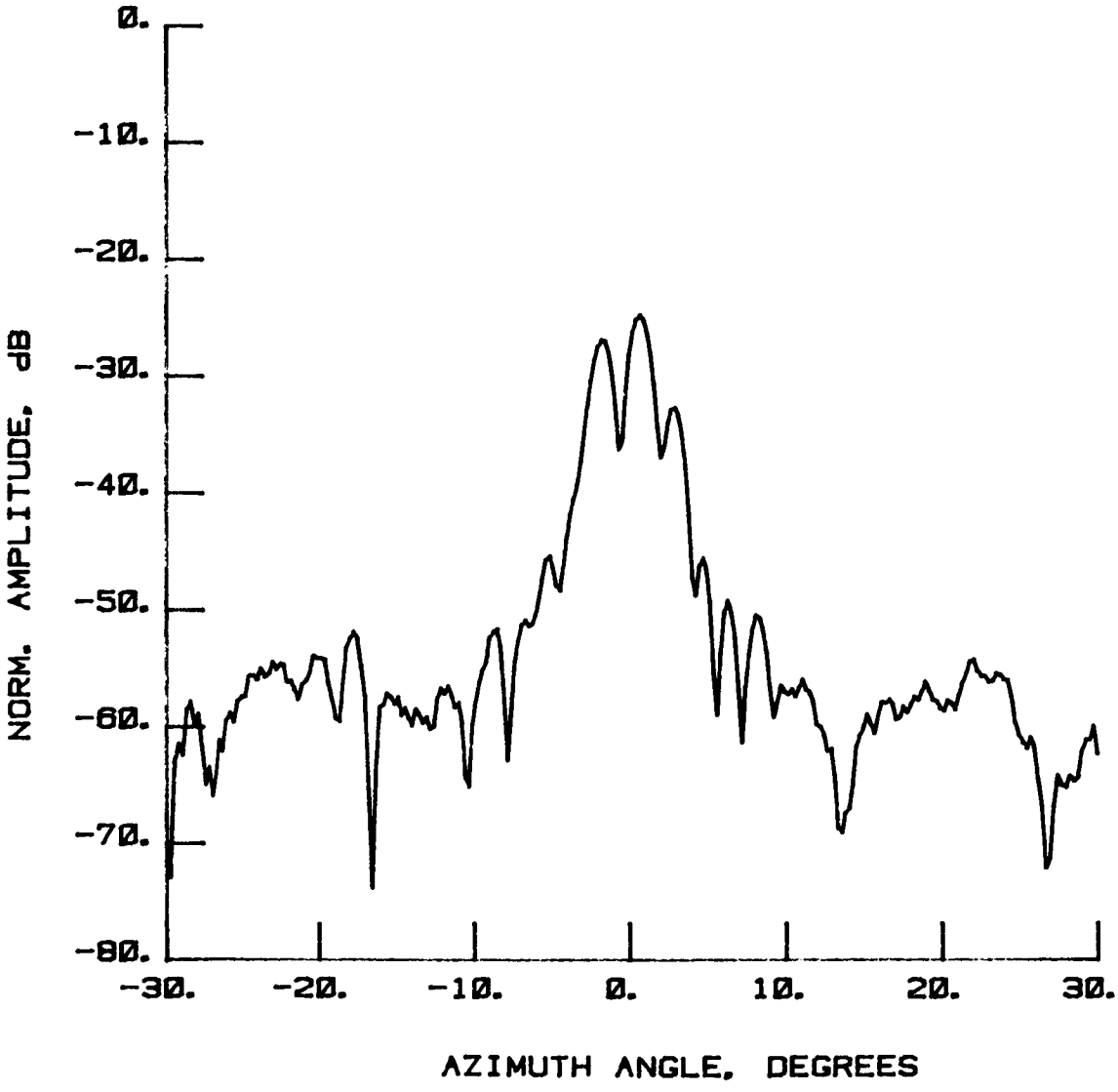

Figure 49 Test 4, 2.27 GHz, Cross-Pol, H-Plane, Type 14

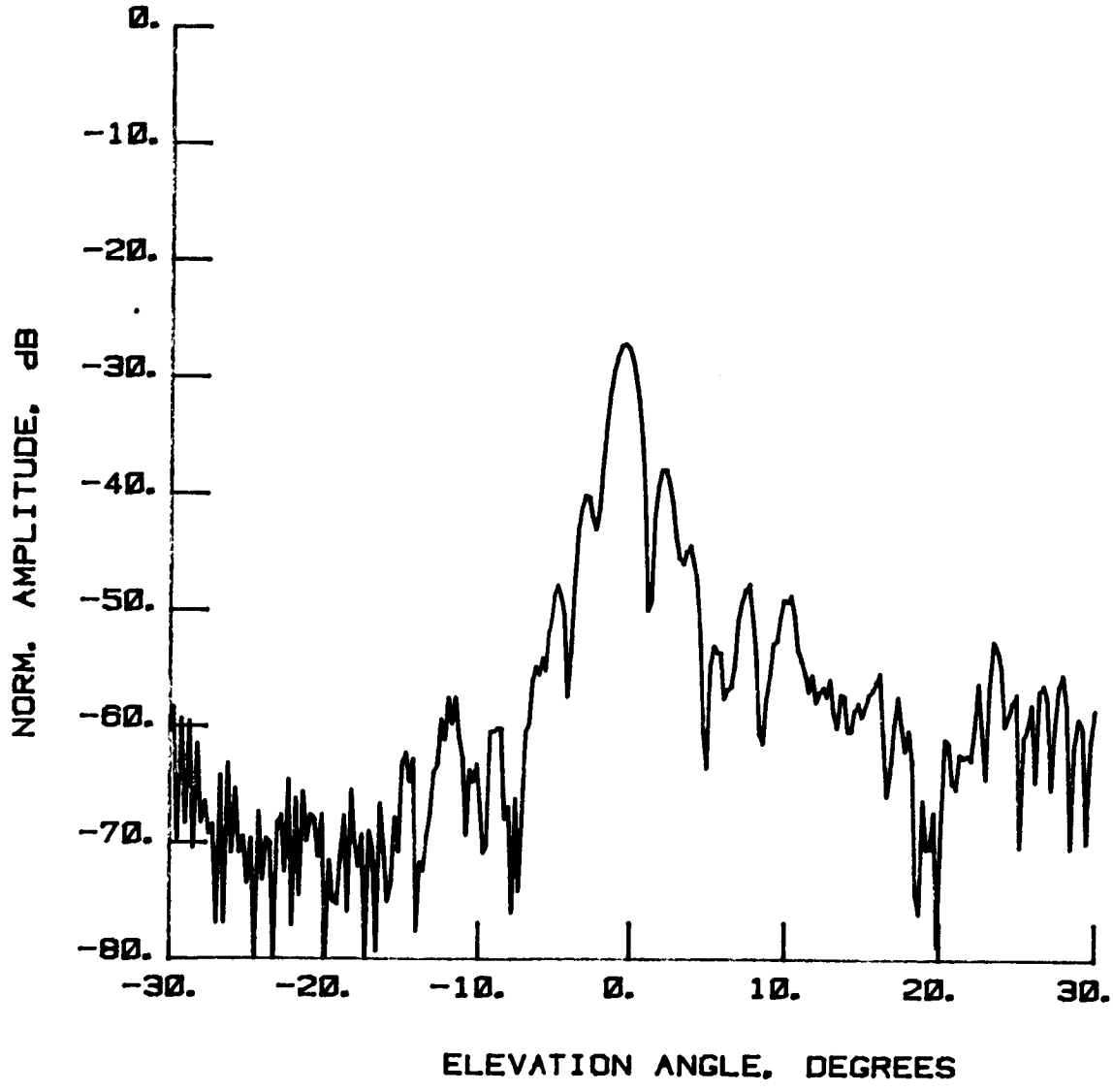

Figure 50 Test 4, 2.27 GHz, Cross-Pol, E-Plane, Type 15

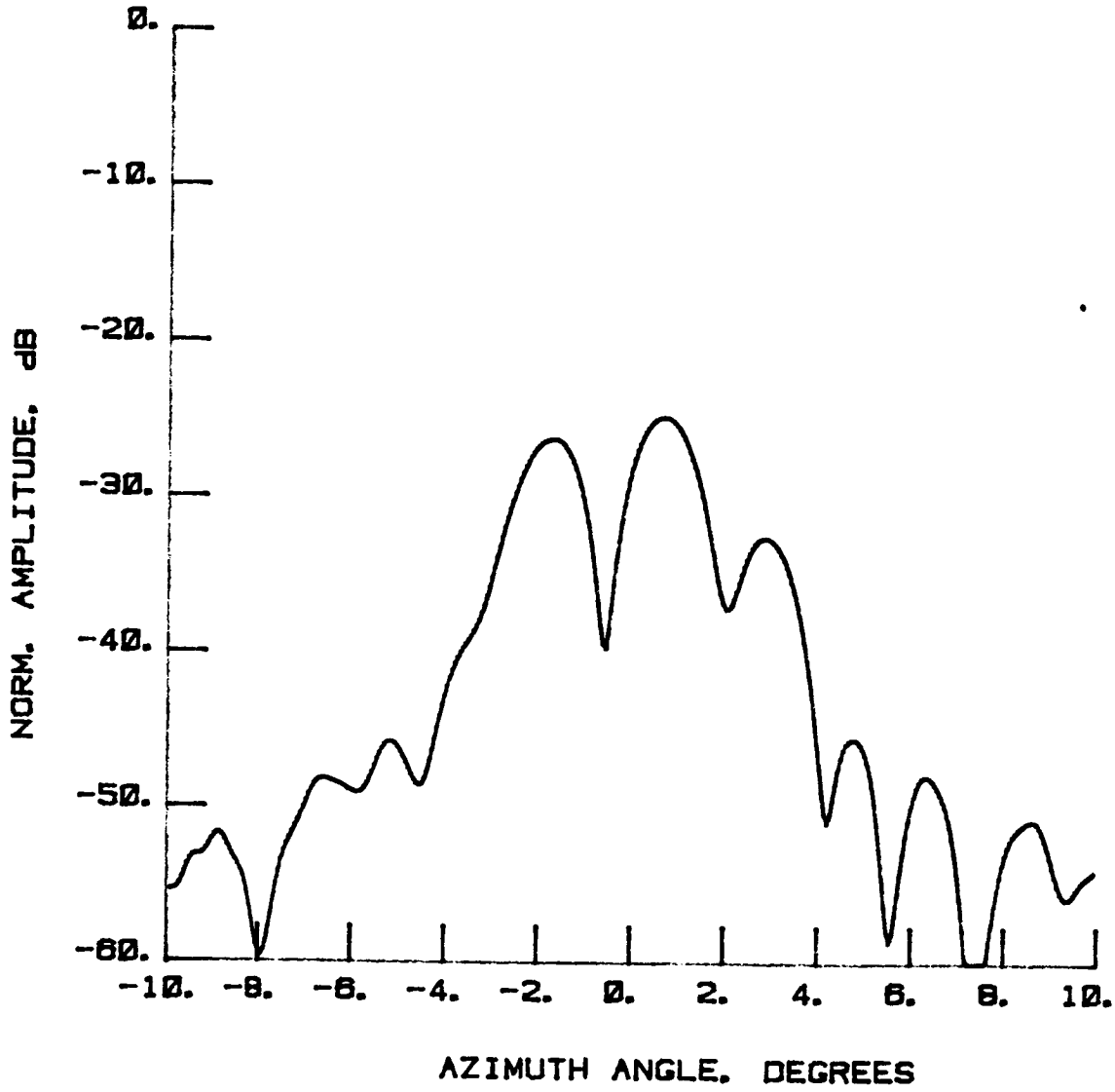

Figure 51 Test 4, 2.27 GHz, Cross-Pol, H-Plane, Type 16

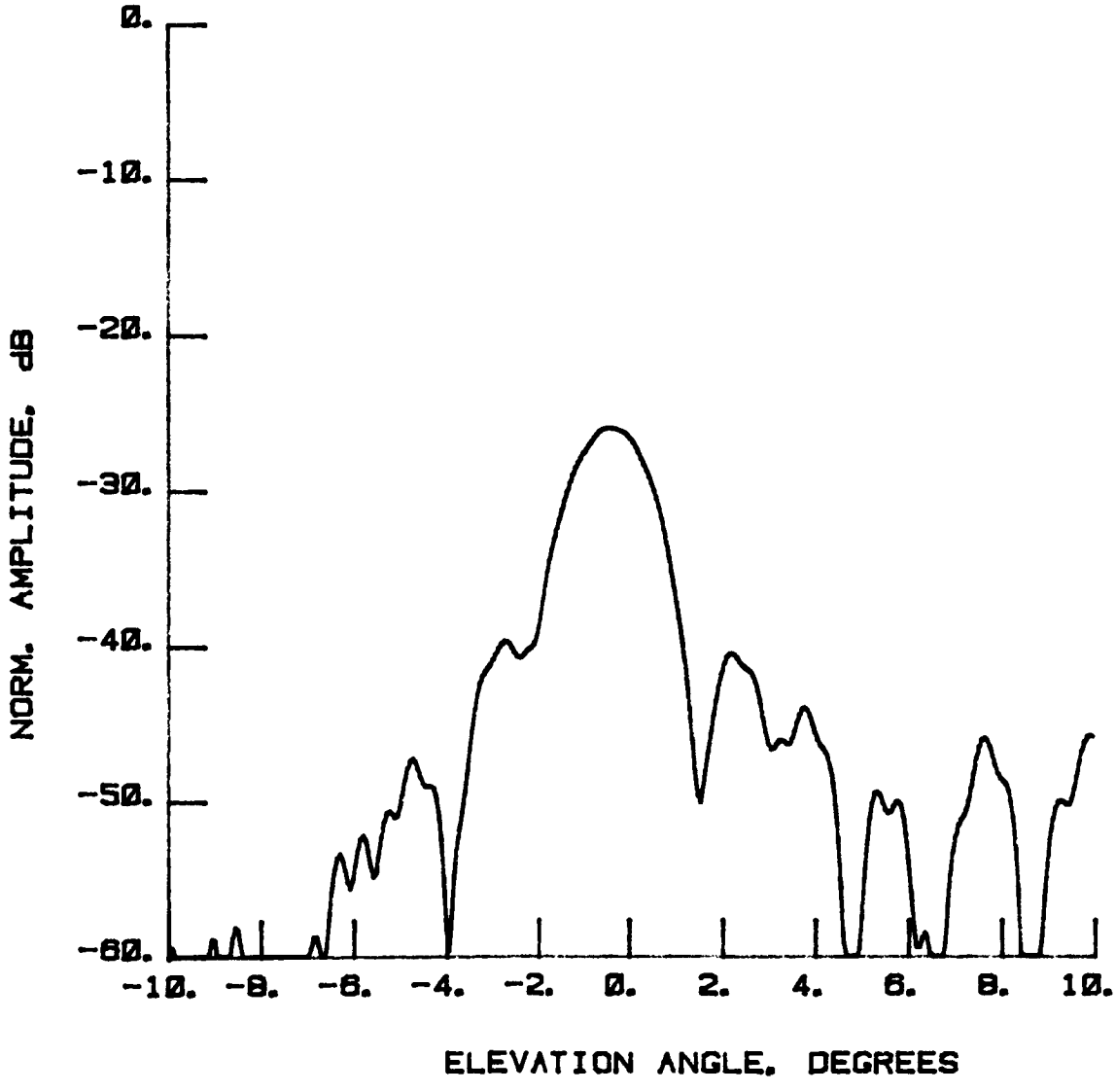

Figure 52 Test 4, 2.27 GHz, Cross-Pol, E-Plane, Type 17

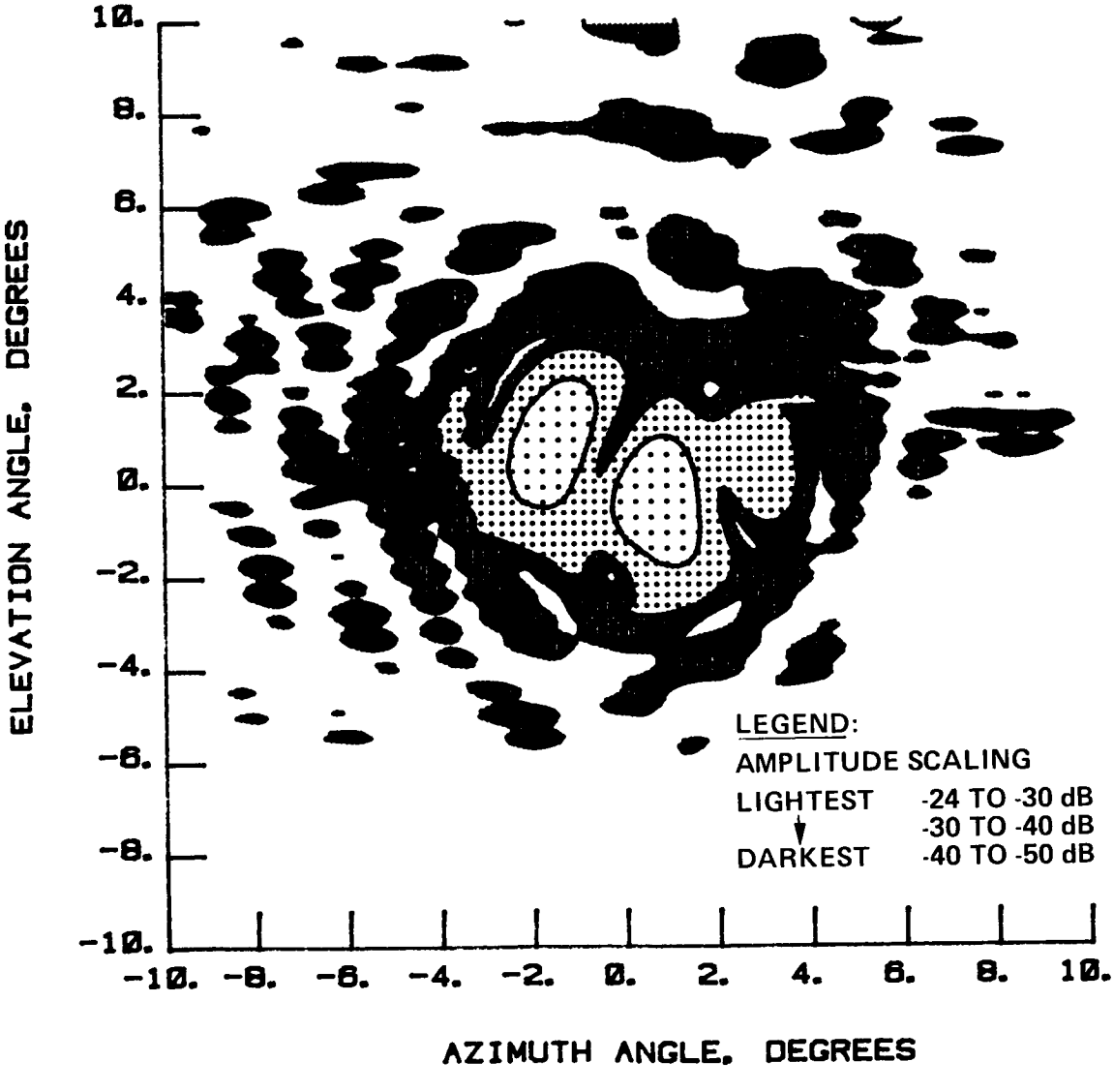

Figure 53 Test 4, 2.27 GHz, Cross-Pol, Contour, Type 18

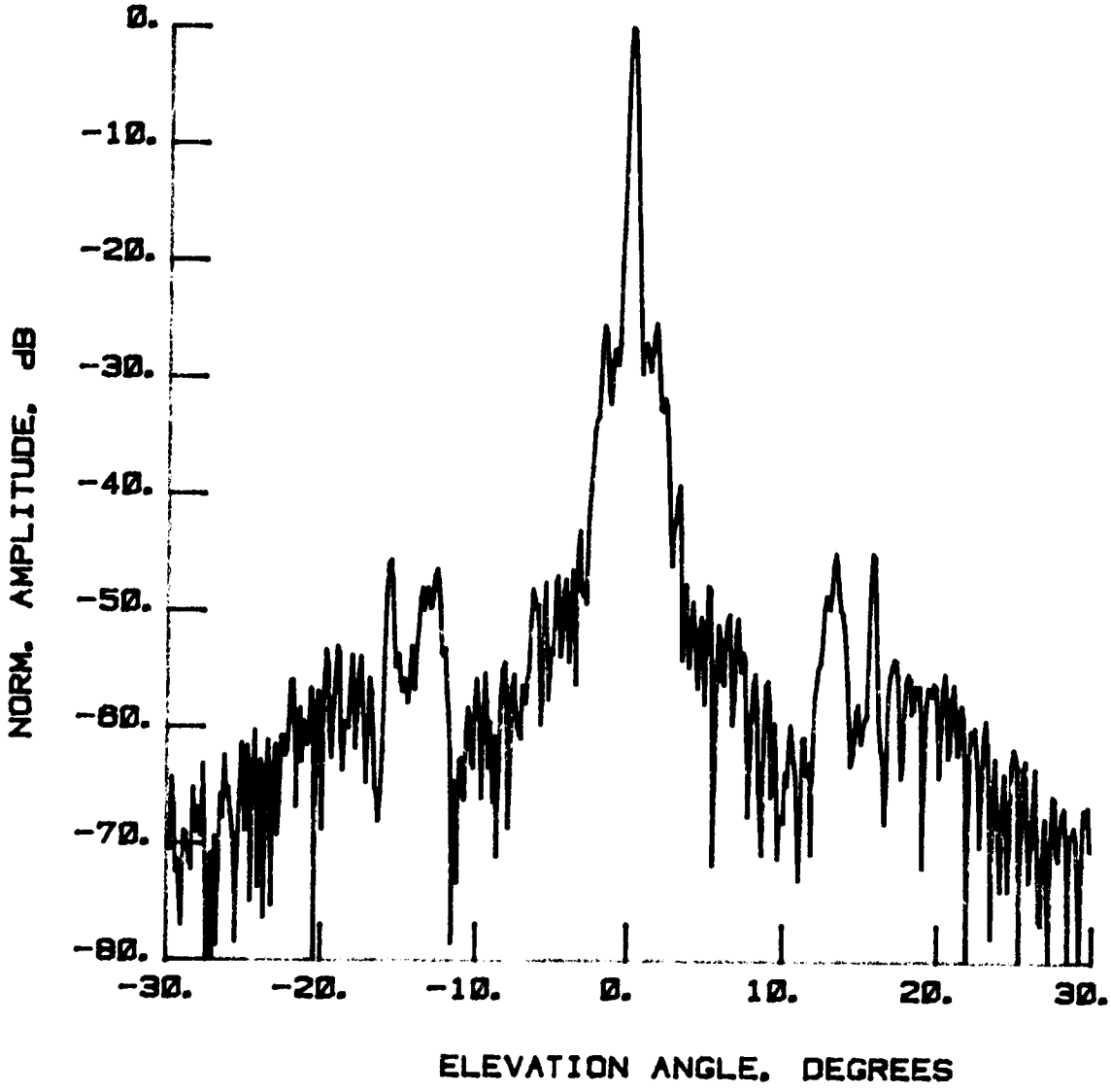

Figure 54 Test 5, 11.60 GHz, Co-Pol, H-Plane, Type 1

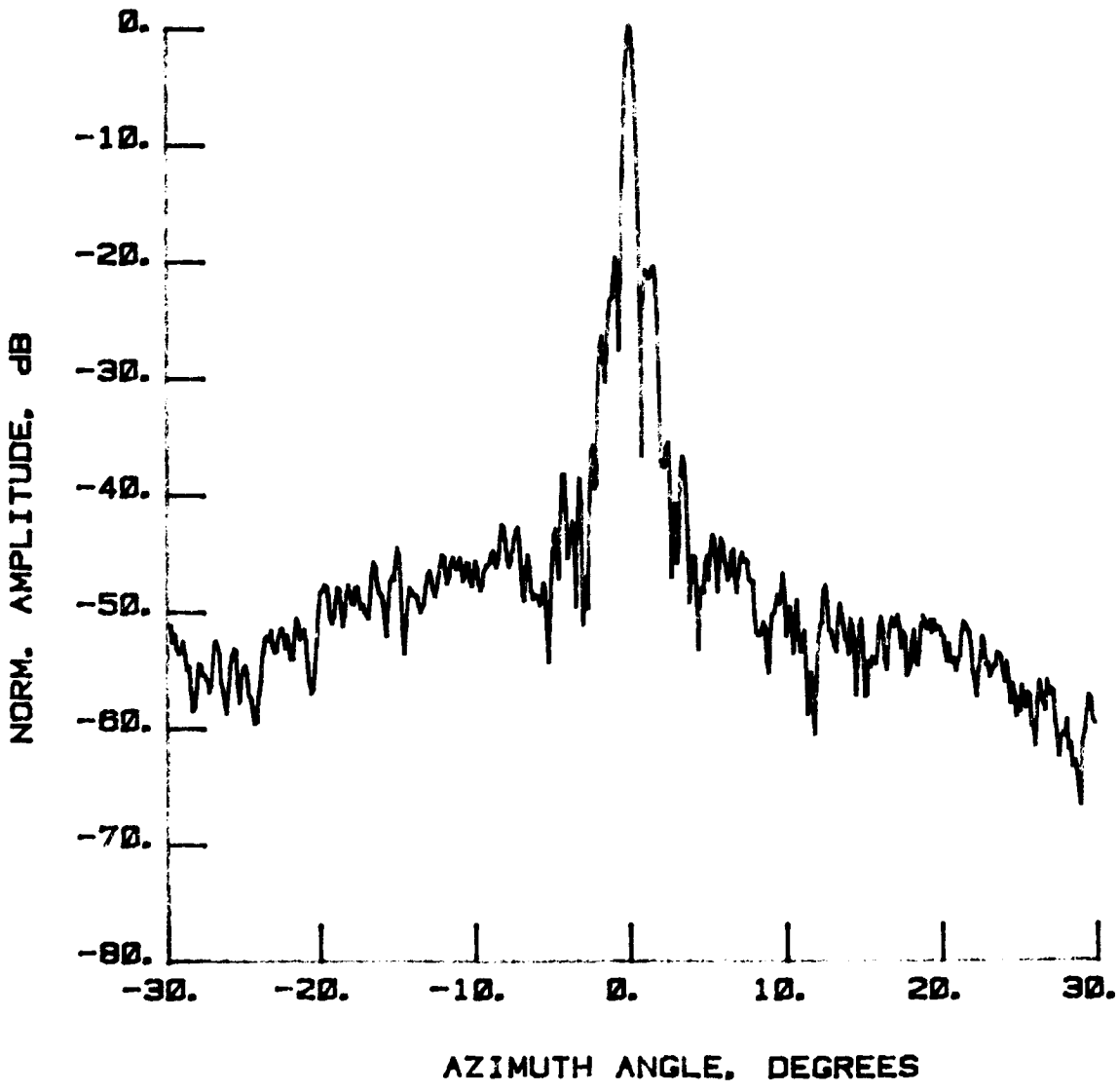

Figure 55 Test 5, 11.60 GHz, Co-Pol, E-Plane, Type 2

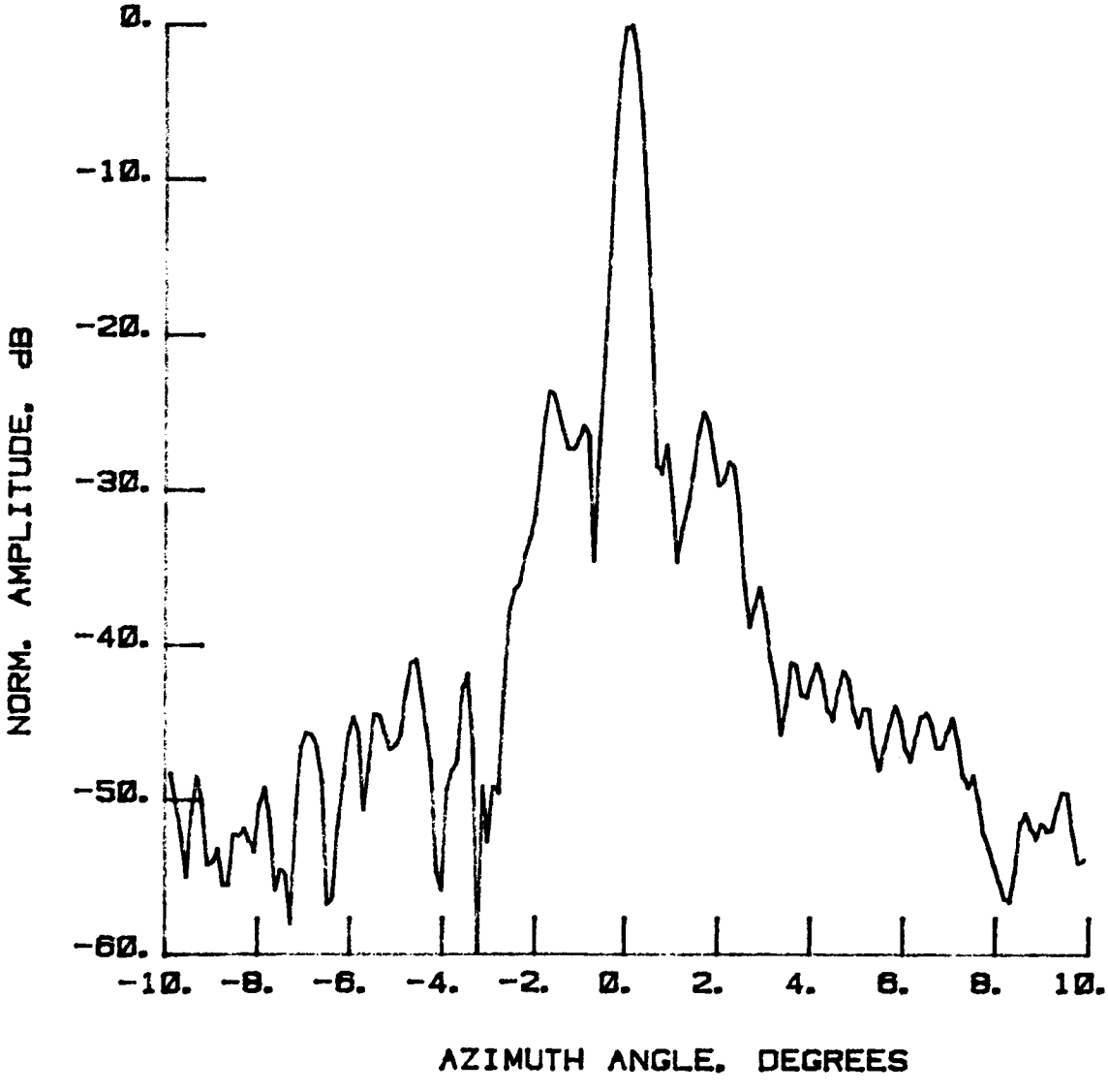

Figure 56 Test 5, 11.60 GHz, Co-Pol, H-Plane, Type 3

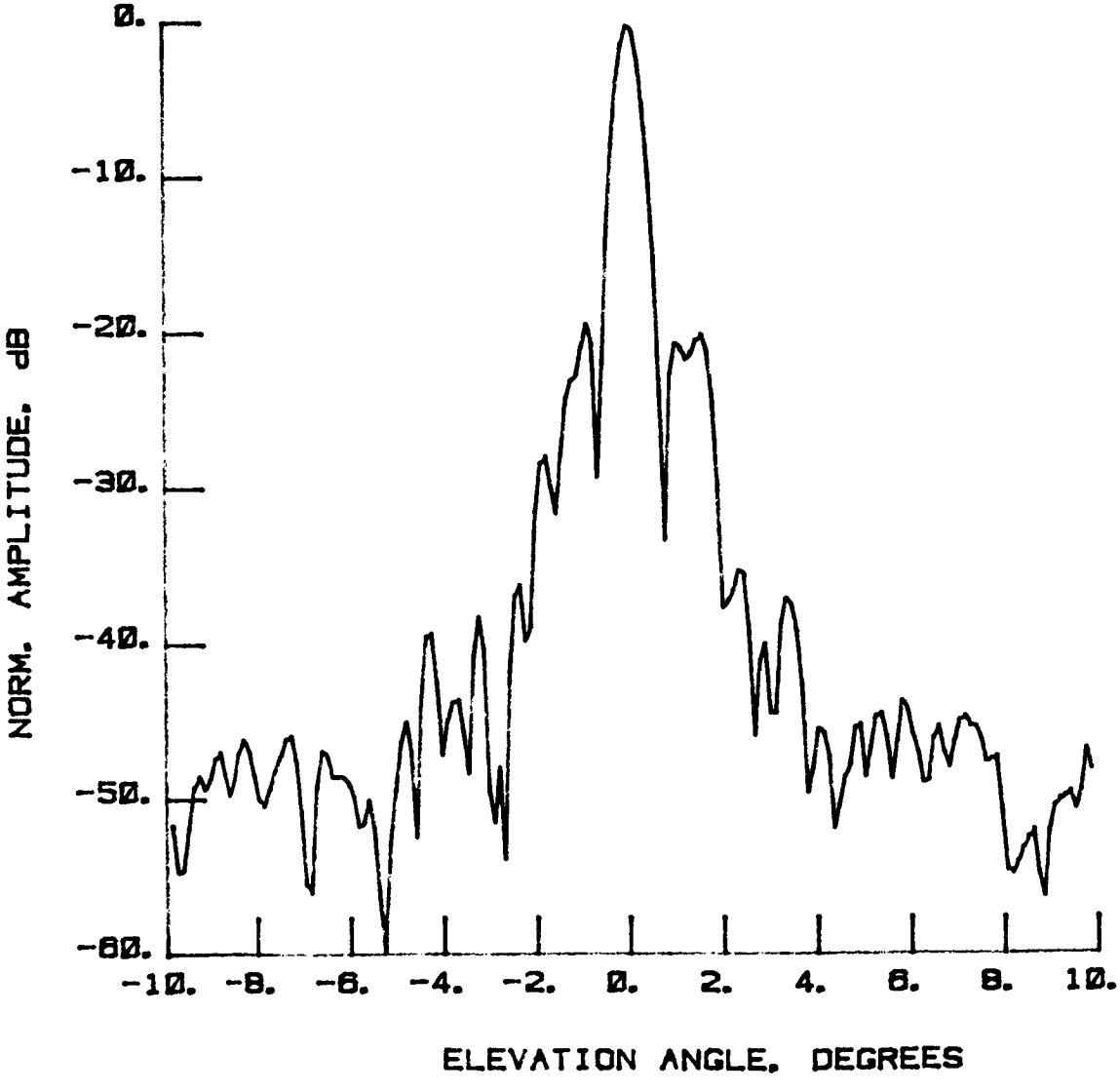

Figure 57 Test 5, 11.60 GHz, Co-Pol, E-Plane, Type 4

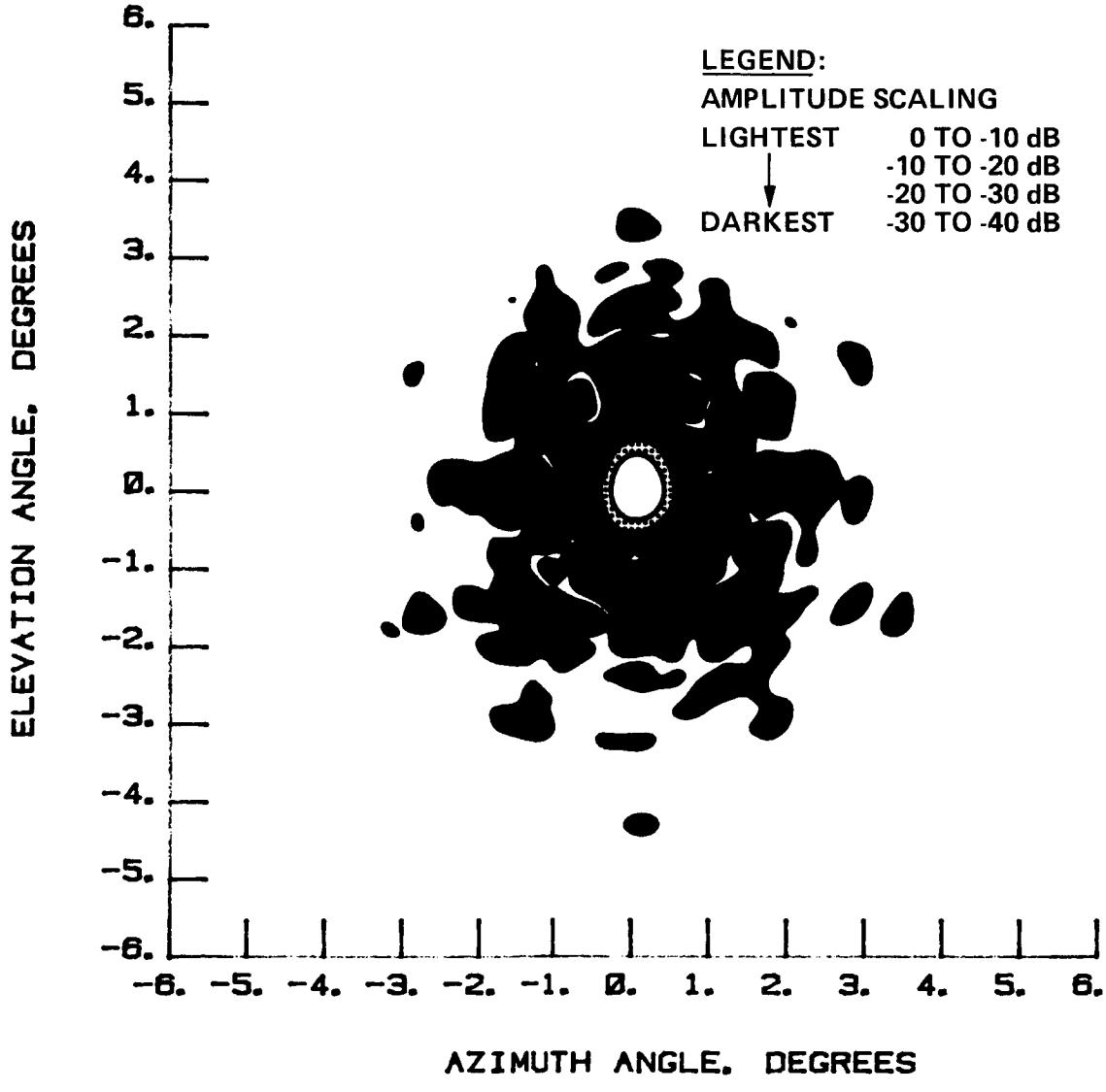

Figure 58 Test, 5, 11.60 GHz, Co-Pol, Contour, Type 5

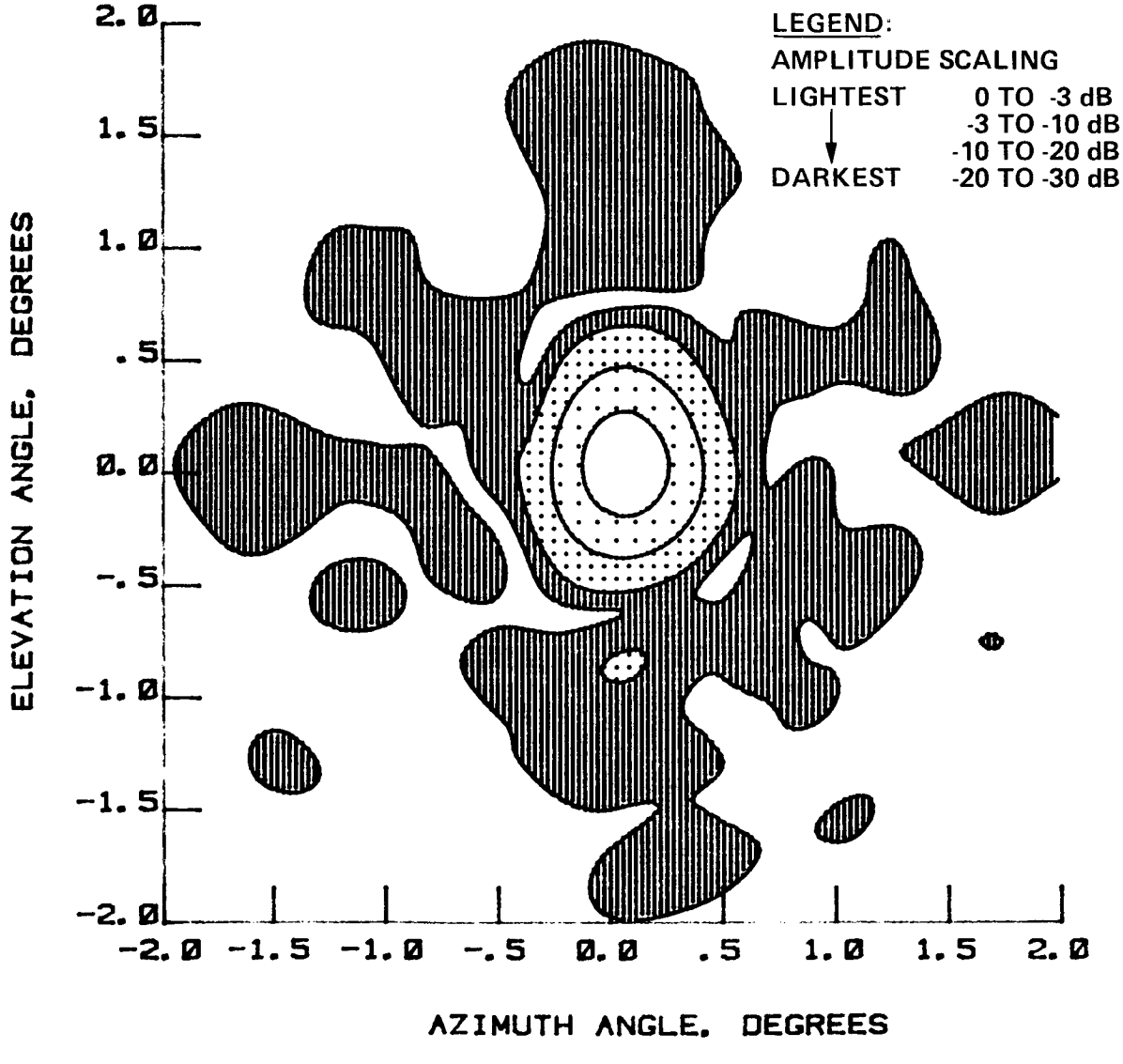

Figure 59 Test 5, 11.60 GHz, Co-Pol, Contour, Type 6

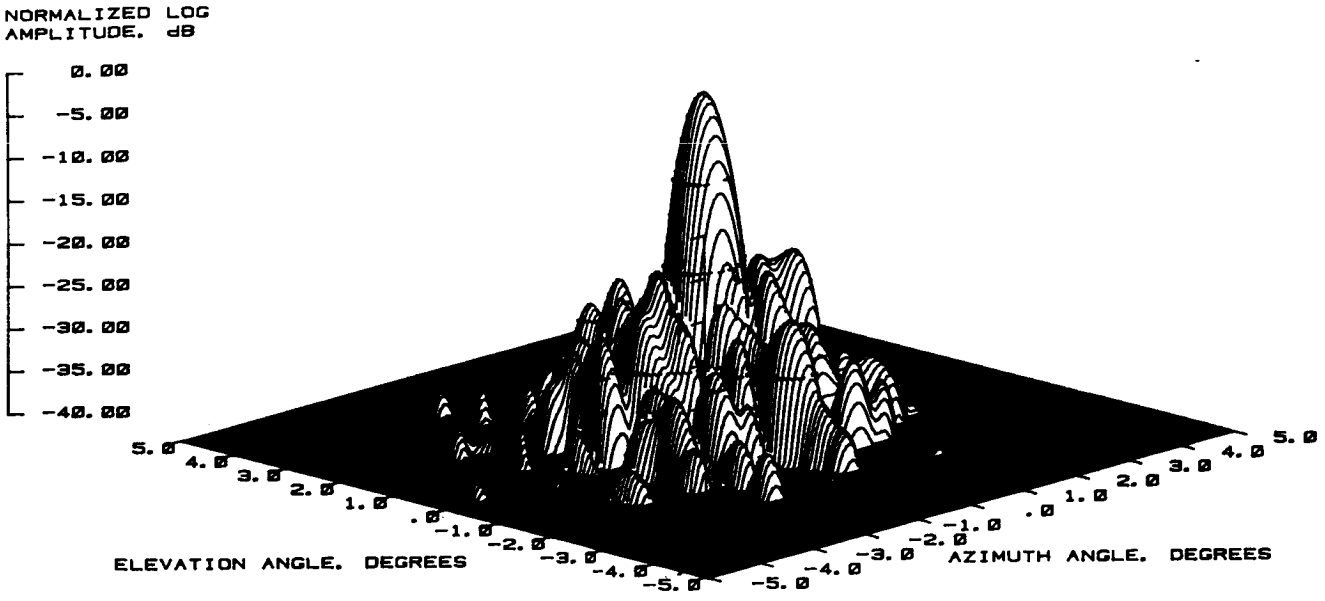

Figure 60 Test 5, 11.60 GHz, Co-Pol, 3-D, Type 7

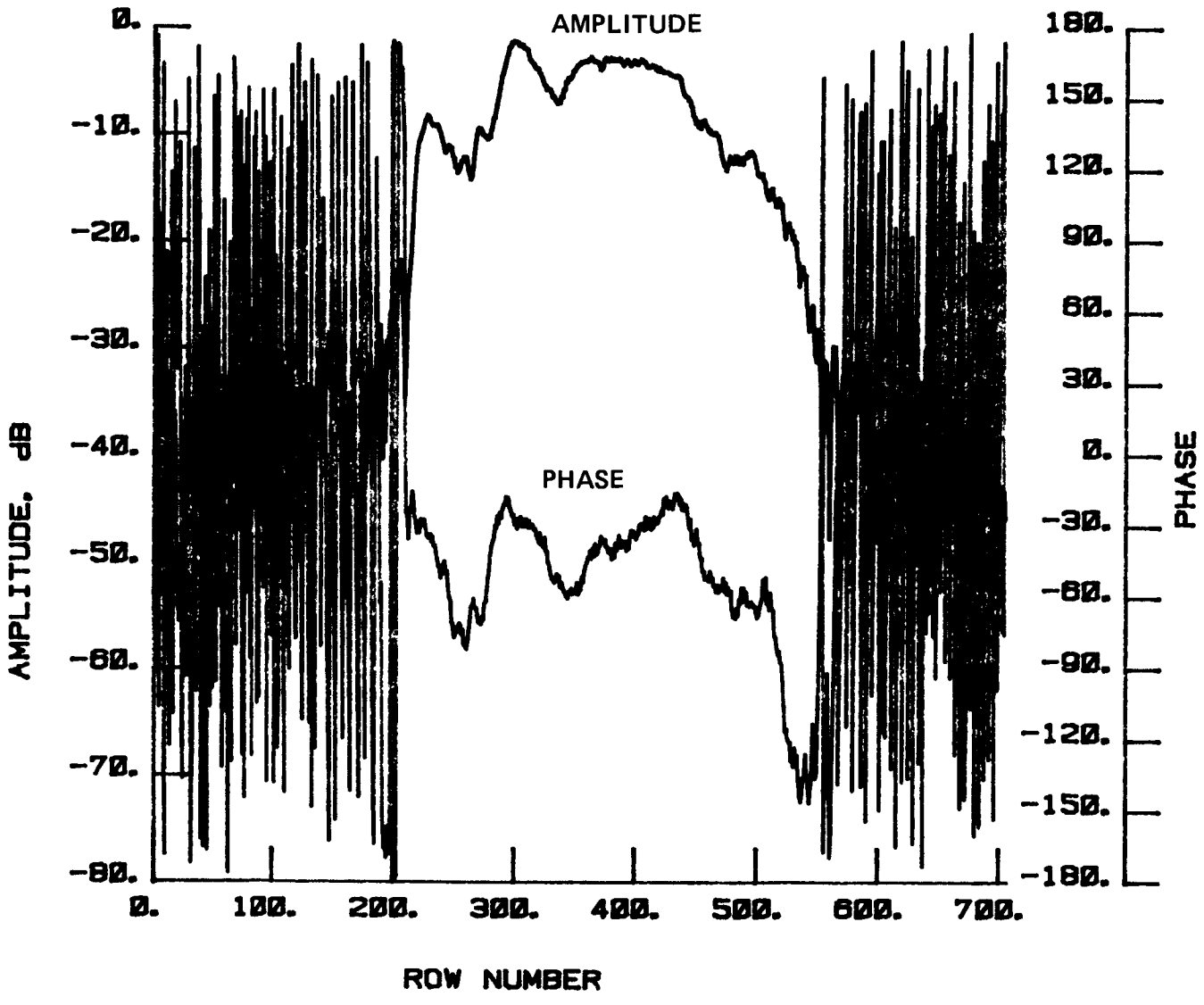

Figure 61 Test 5, 11.60 GHz, Co-Pol, H-Plane, Type 8

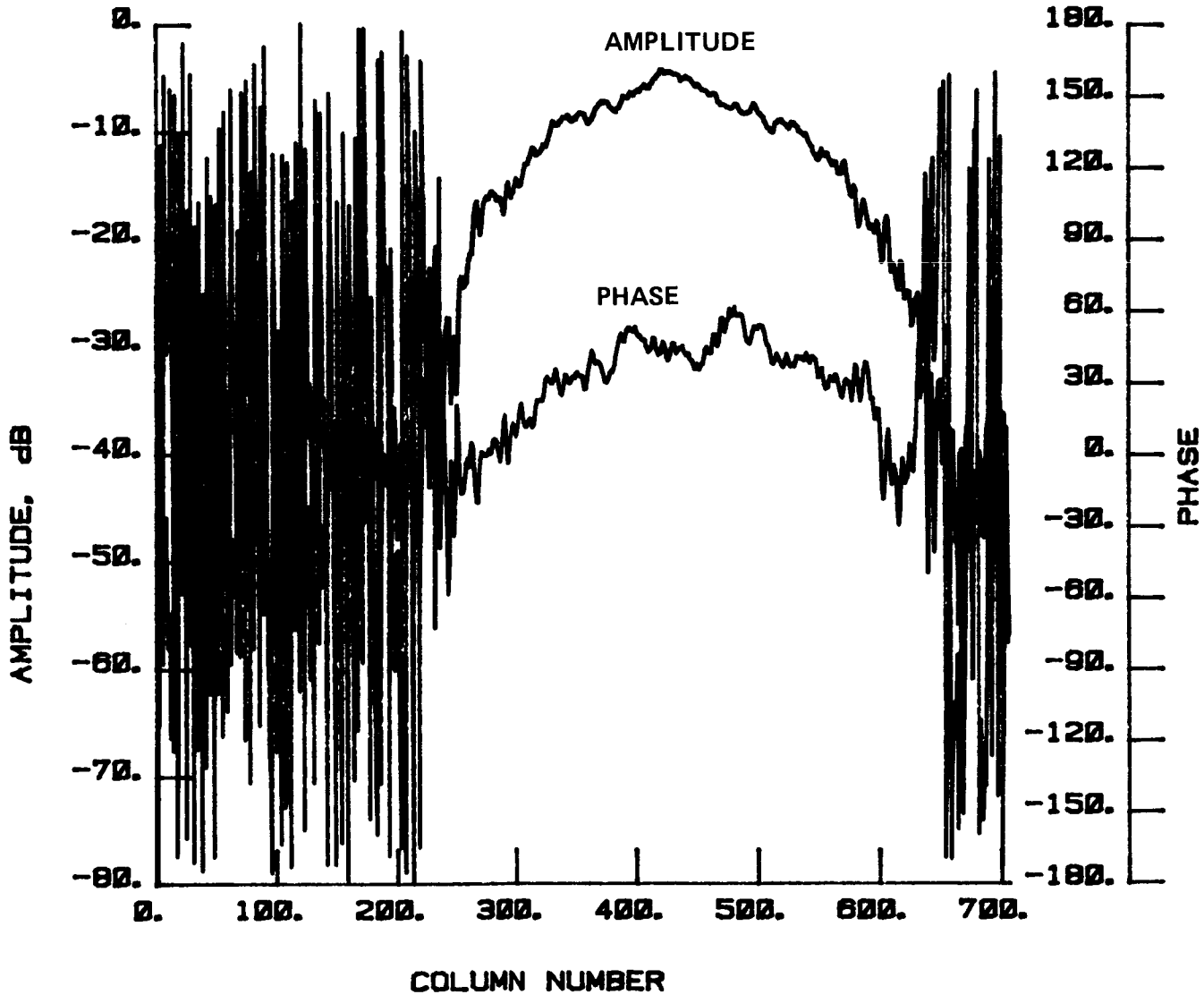

Figure 62 Test 5, 11.60 GHz, Co-Pol, E-Plane, Type 9

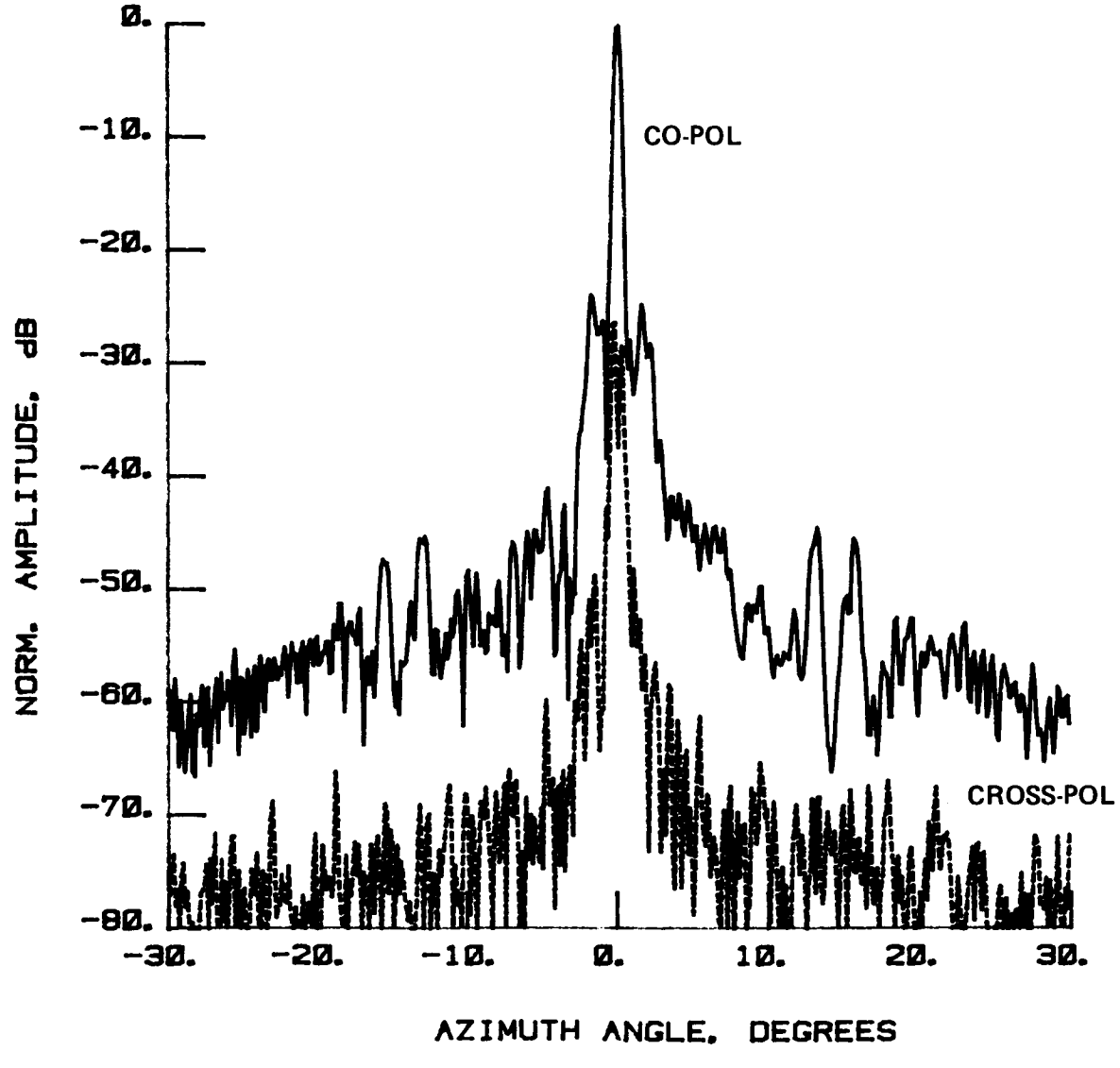

Figure 63 Test 6, 11.60 GHz, Overlay, H-Plane, Type 10

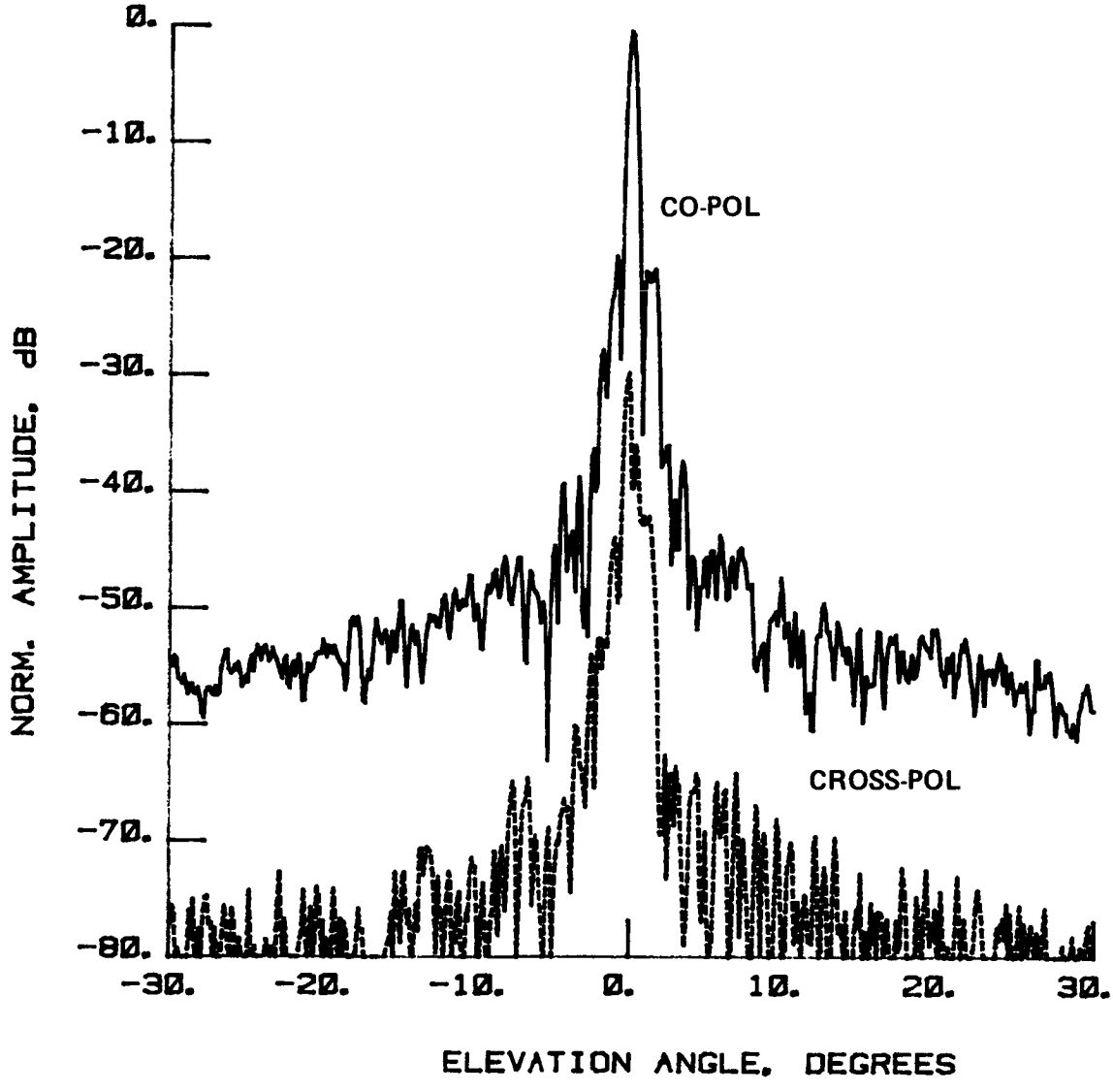

Figure 64 Test 6, 11.60 GHz, Overlay, E-Plane, Type 11

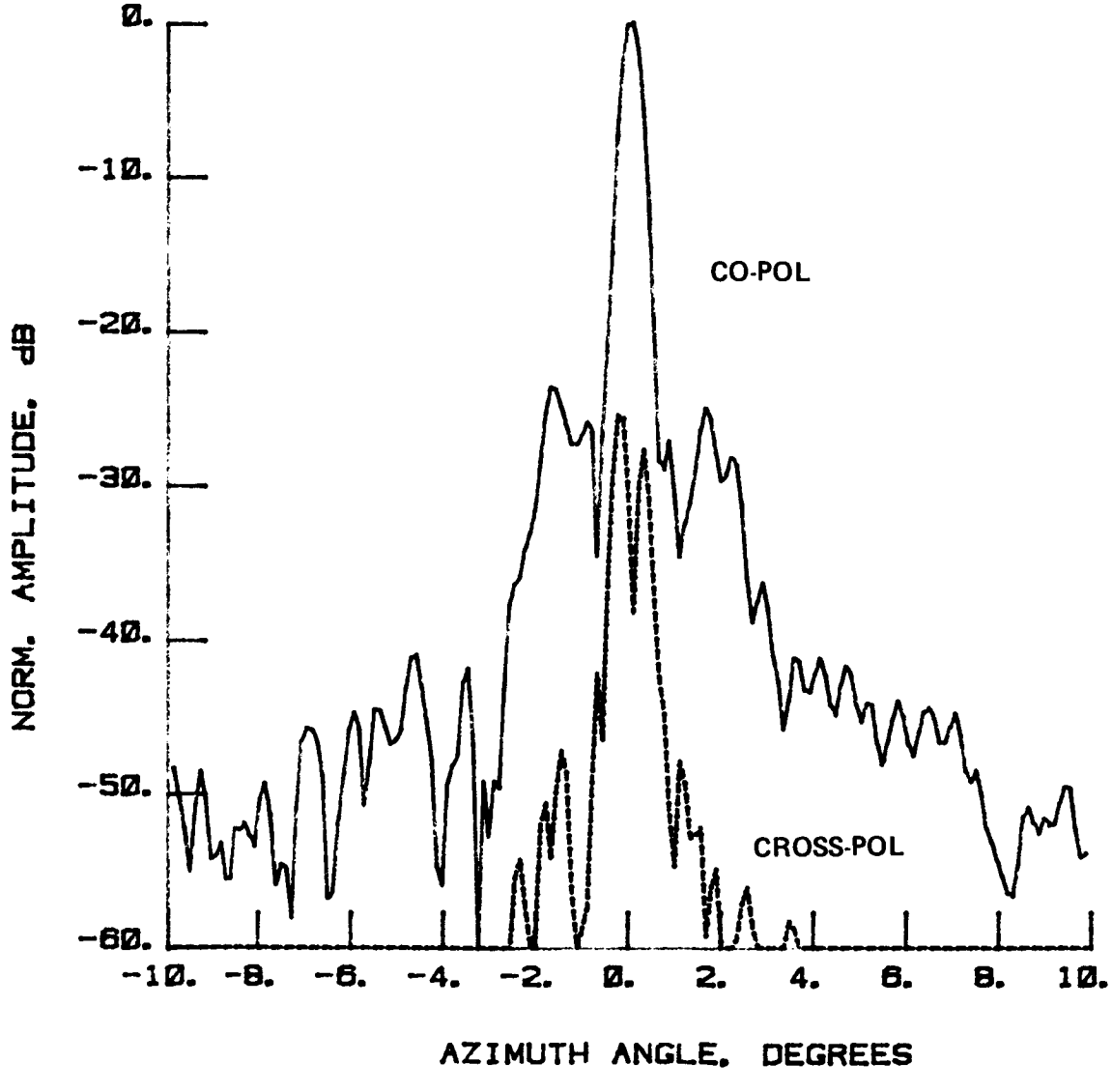

Figure 65 Test 6, 11.60 GHz, Overlay, H-Plane, Type 12

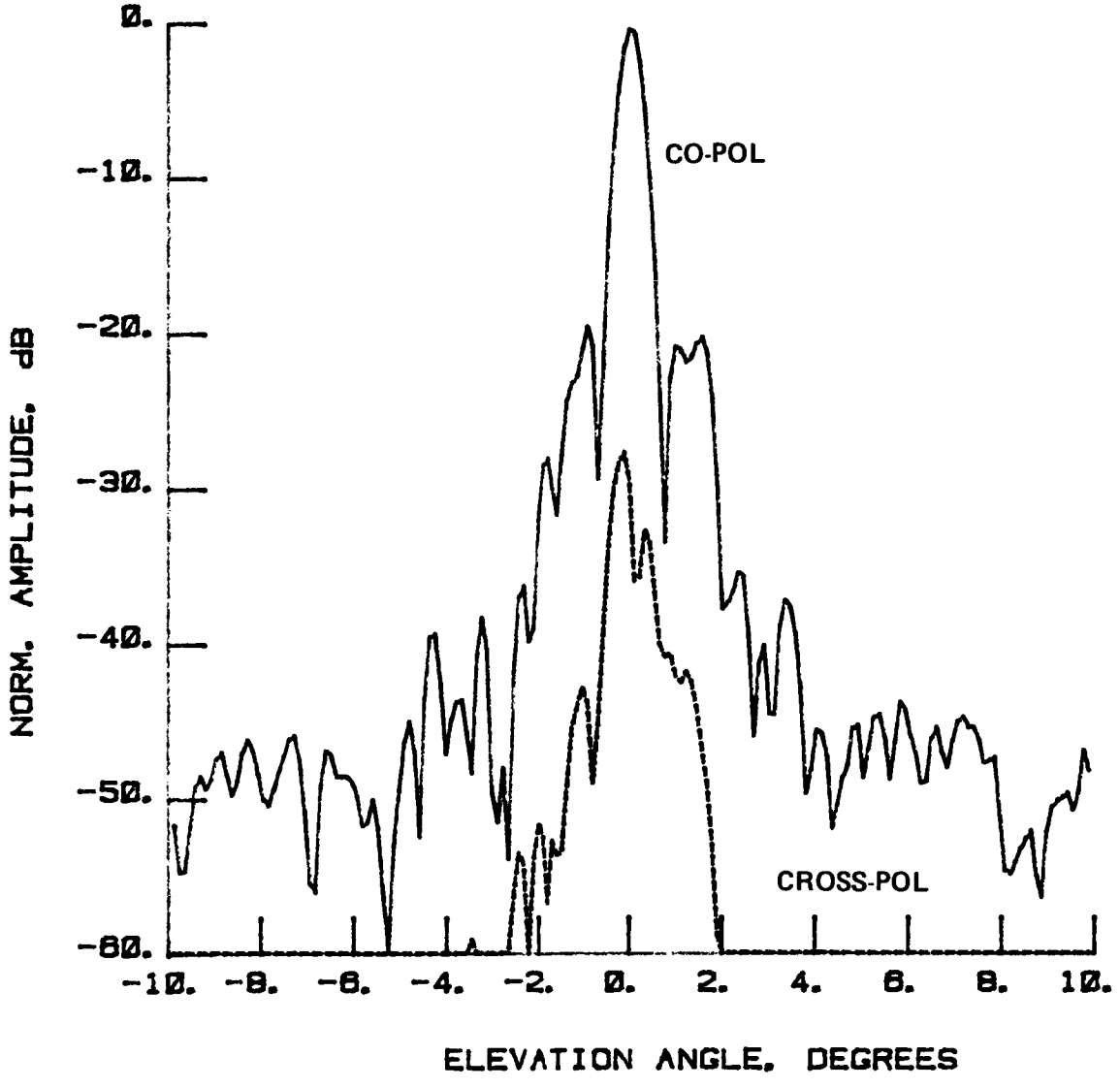

Figure 66 Test 6, 11.60 GHz, Overlay, E-Plane, Type 13

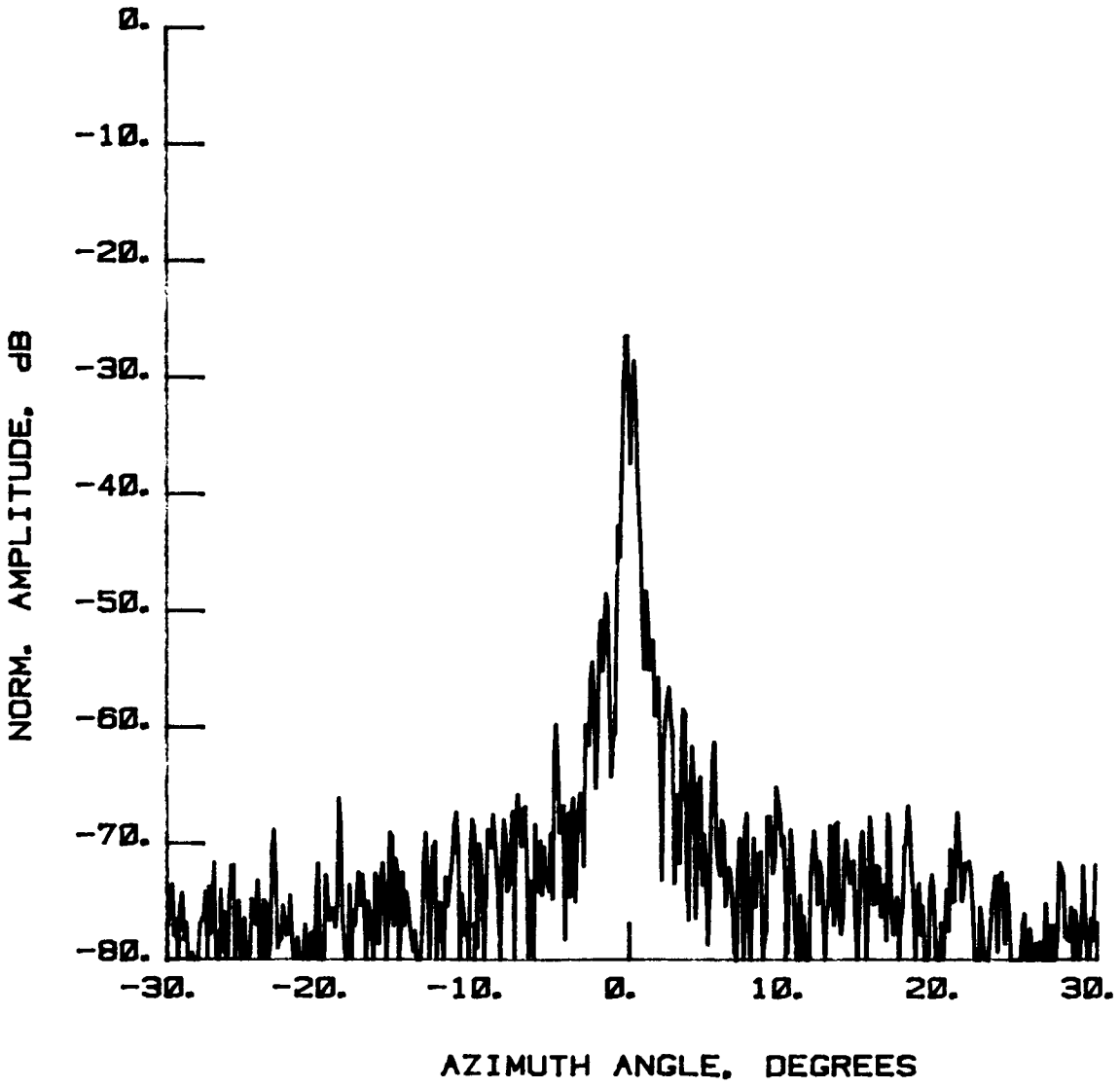

Figure 67 Test 6, 11.60 GHz, Cross-Pol, H-Plane, Type 14

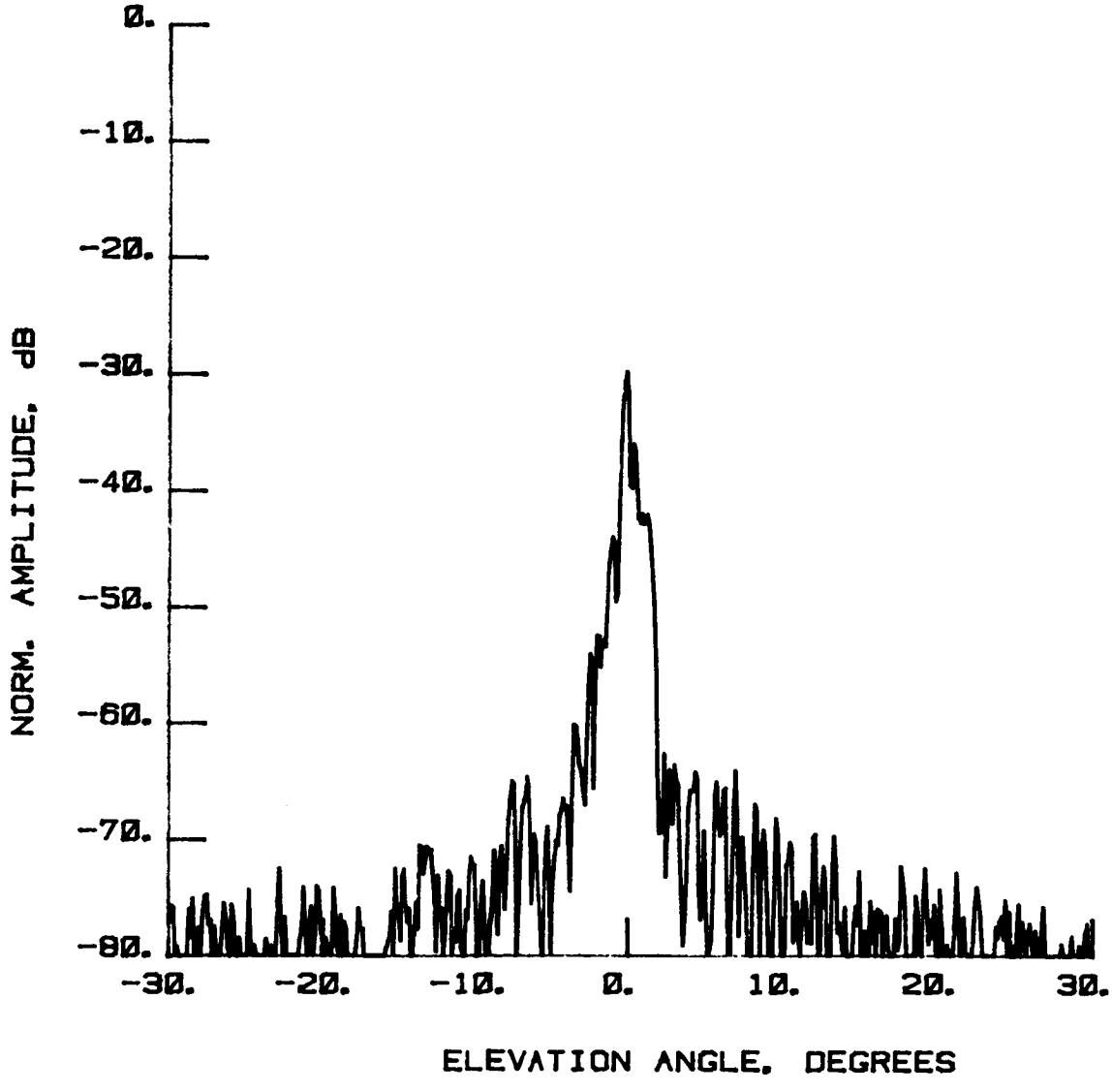

Figure 68 Test 6, 11.60 GHz, Cross-Pol, E-Plane, Type 15

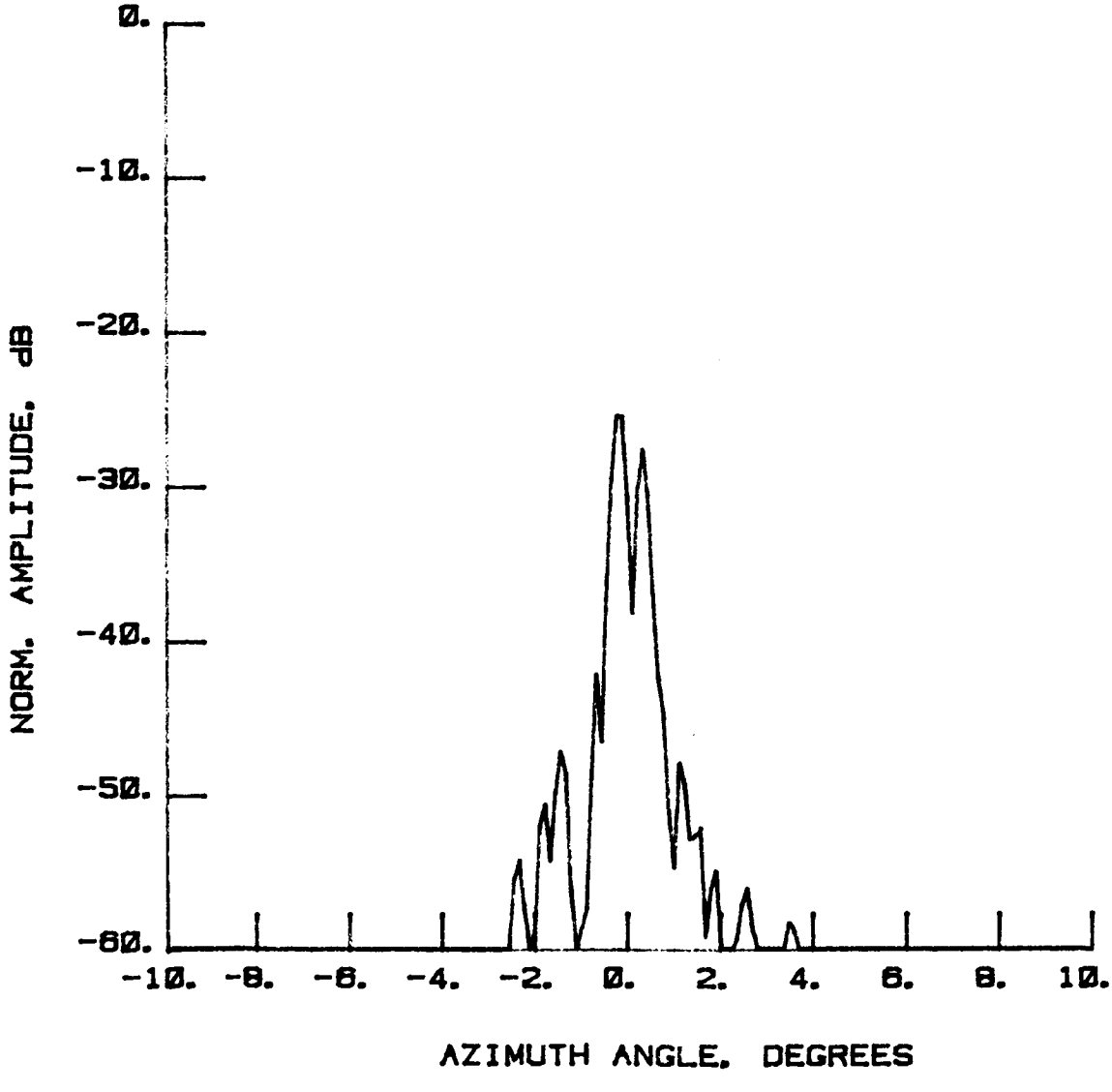

Figure 69 Test 6, 11.60 GHz, Cross-Pol, H-Plane, Type 16

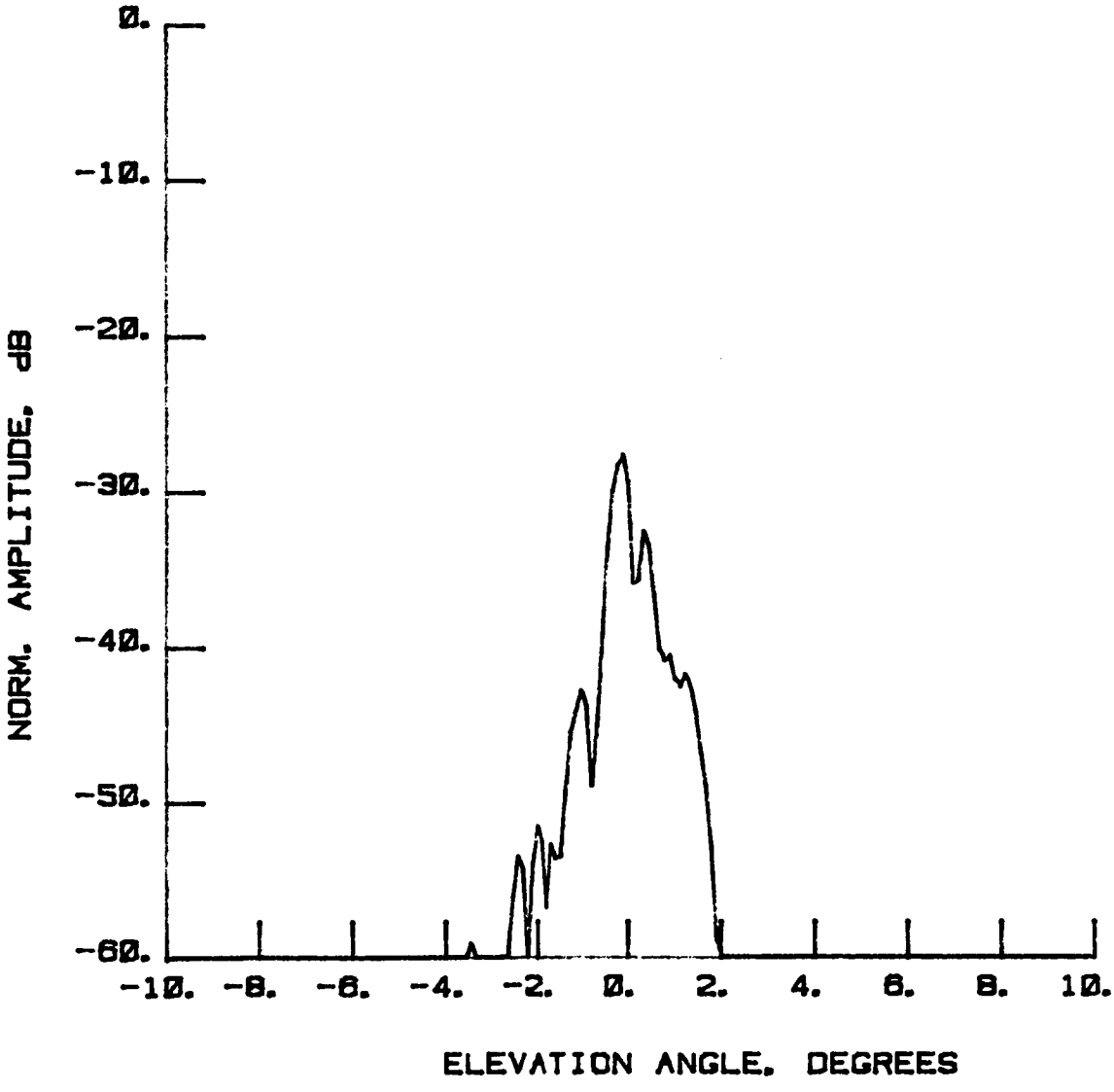

Figure 70 Test 6, 11.60 GHz, Cross-Pol, E-Plane, Type 17

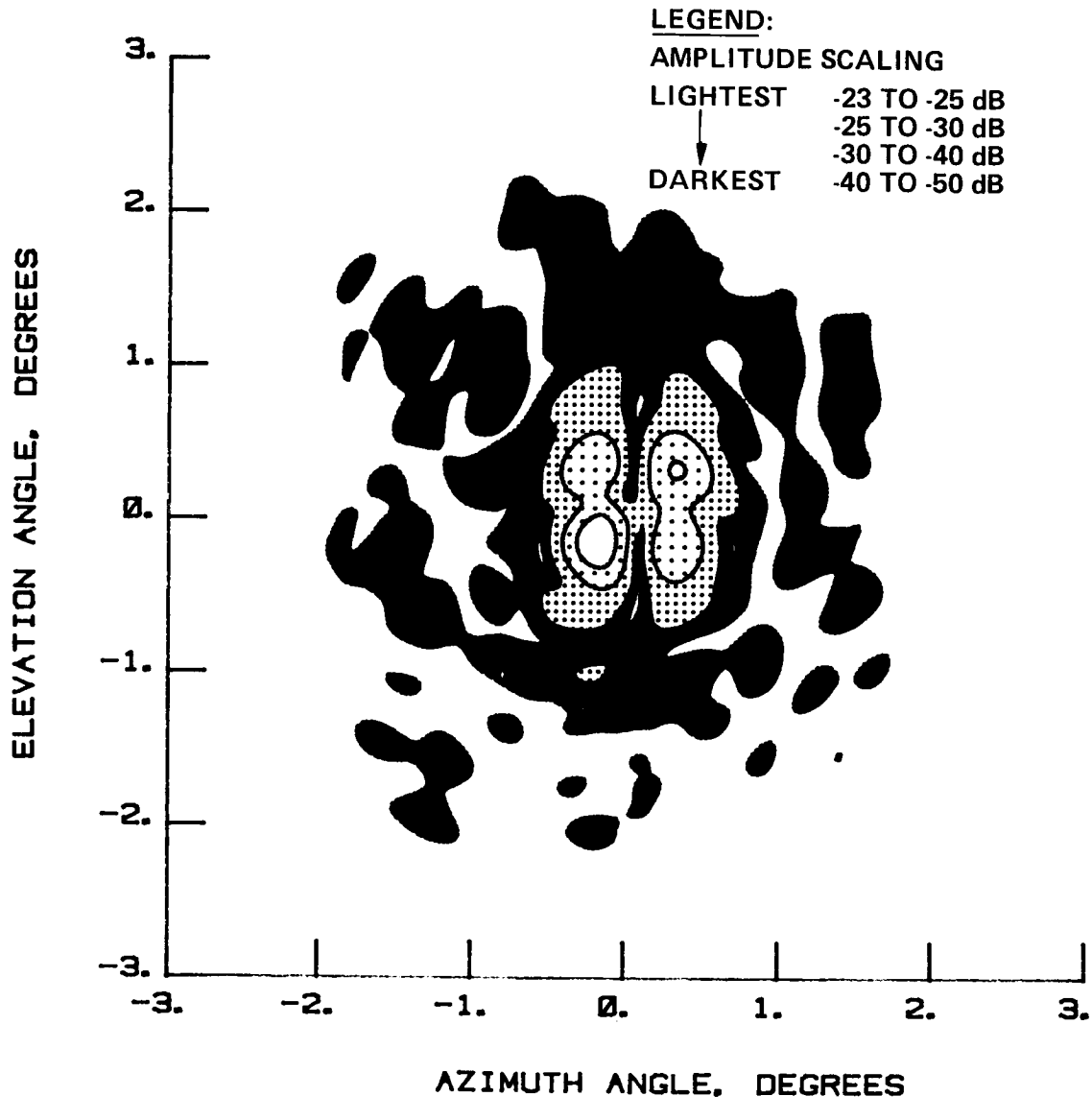

Figure 71 Test 6, 11.60 GHz, Cross-Pol, Contour, Type 18

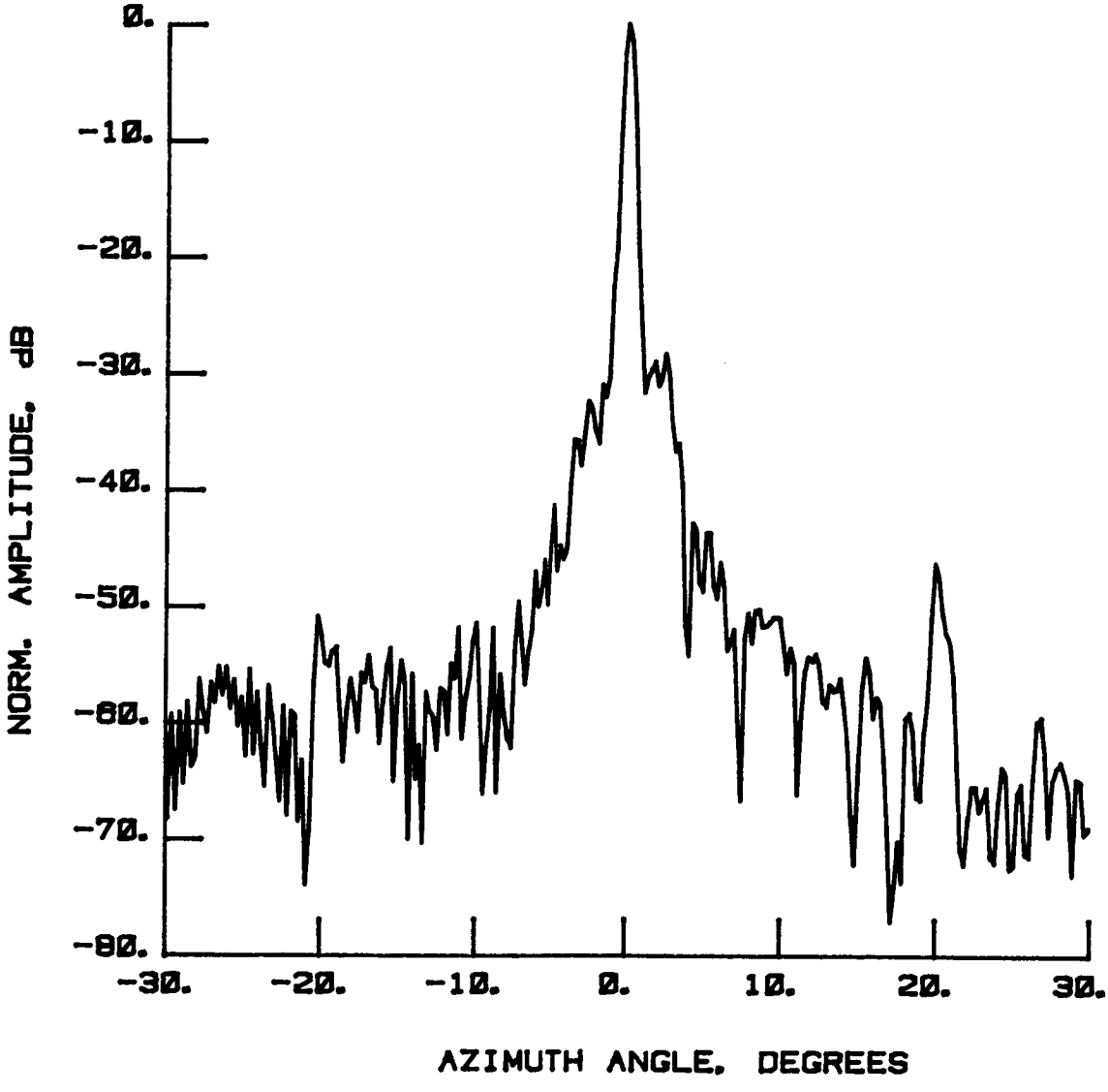

Figure 72 Test 7, 7.73 GHz, Co-Pol, H-Plane, Type 1

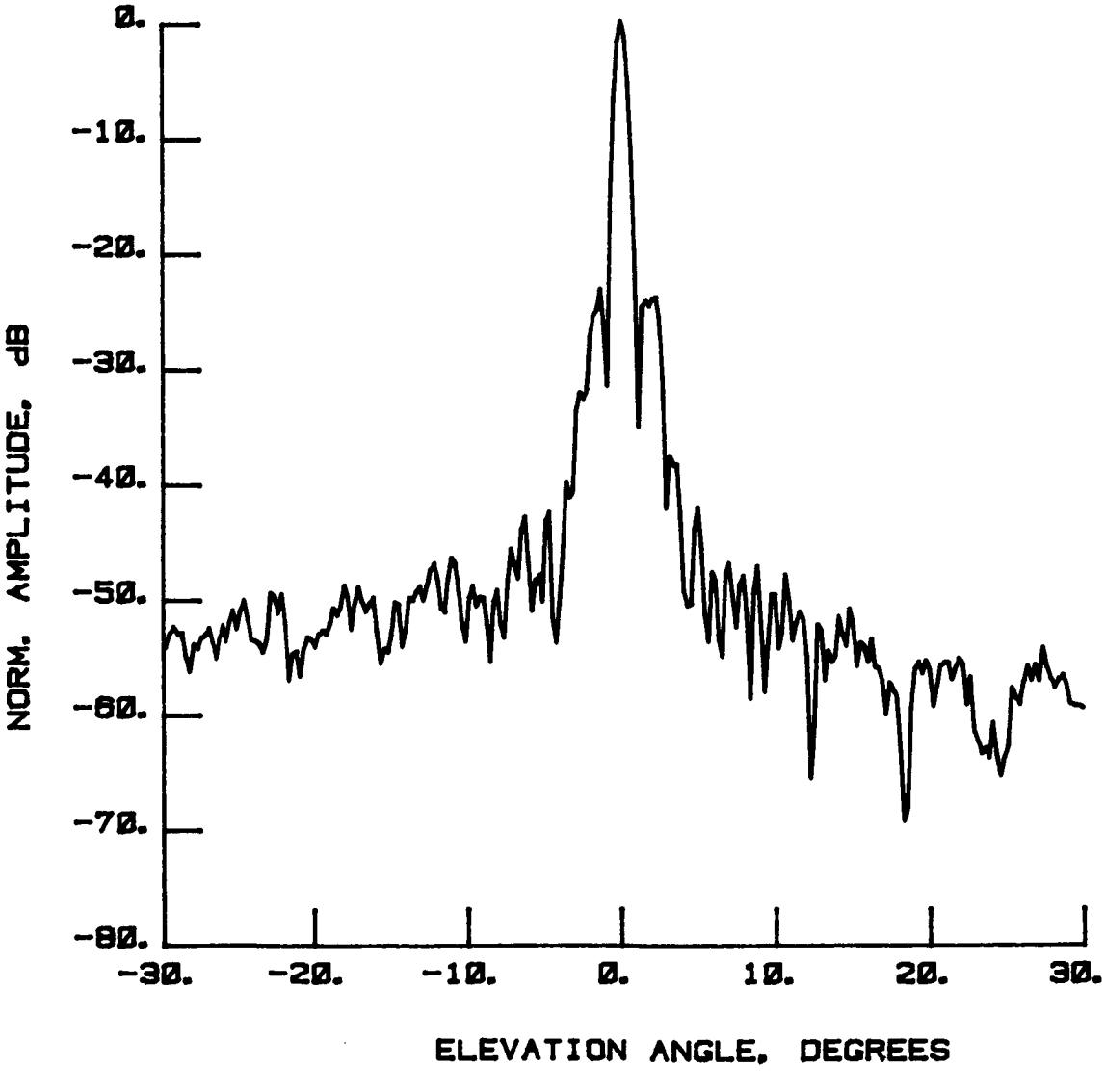

Figure 73 Test 7, 7.73 GHz, Co-Pol, E-Plane, Type 2

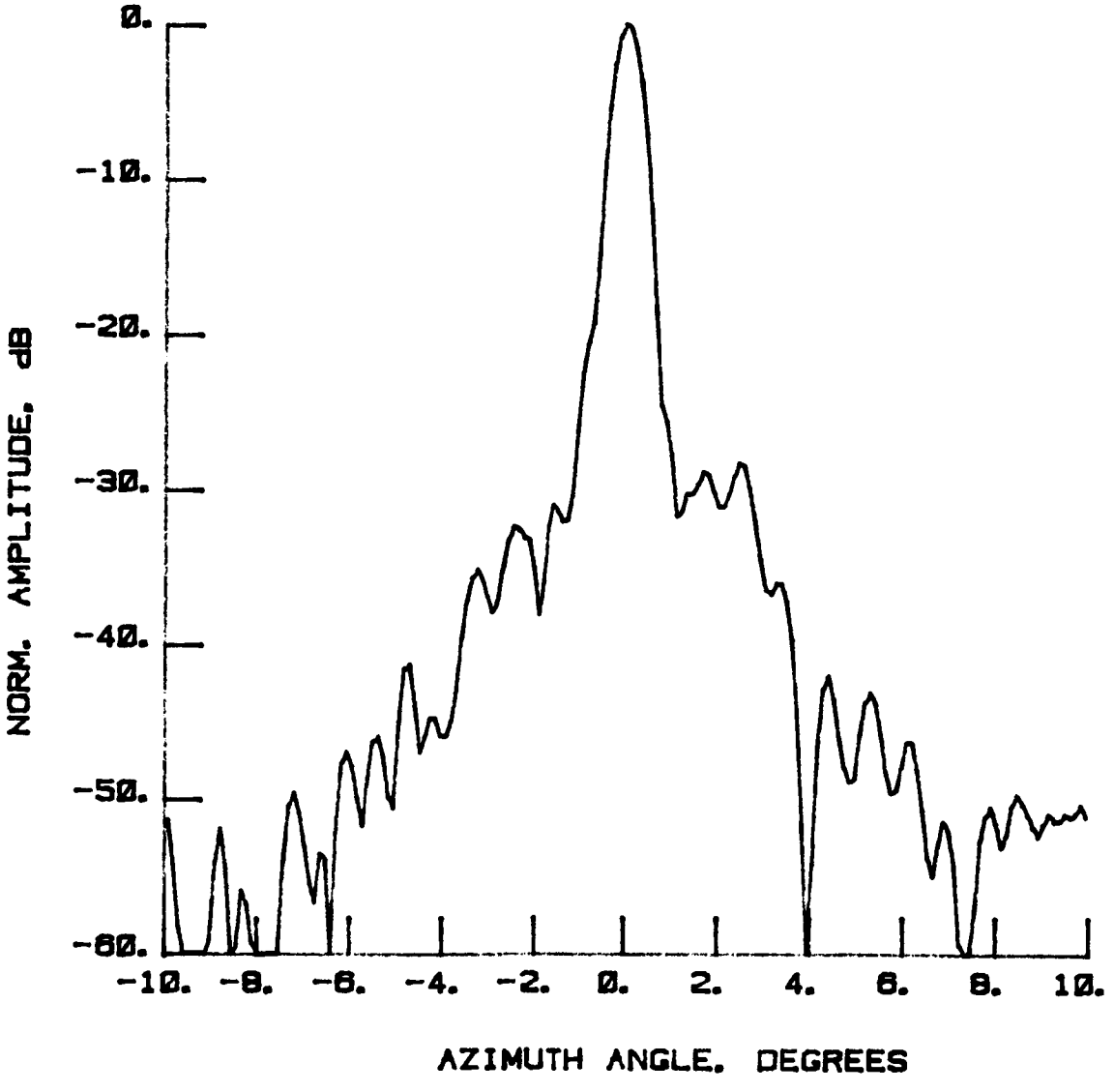

Figure 74 Test 7, 7.73 GHz, Co-Pol, H-Plane, Type 3

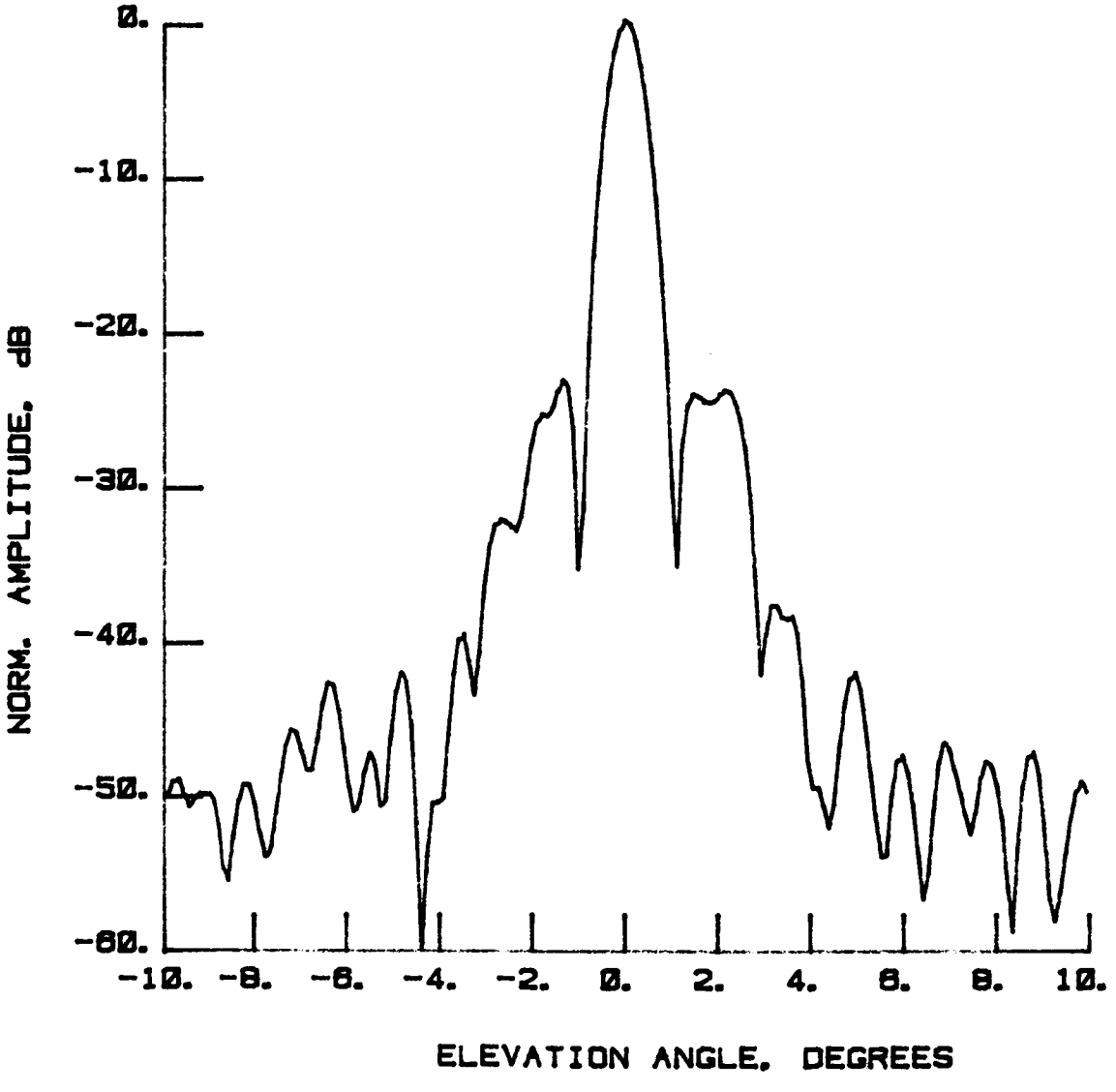

Figure 75 Test 7, 7.73 GHz, Co-Pol, E-Plane, Type 4

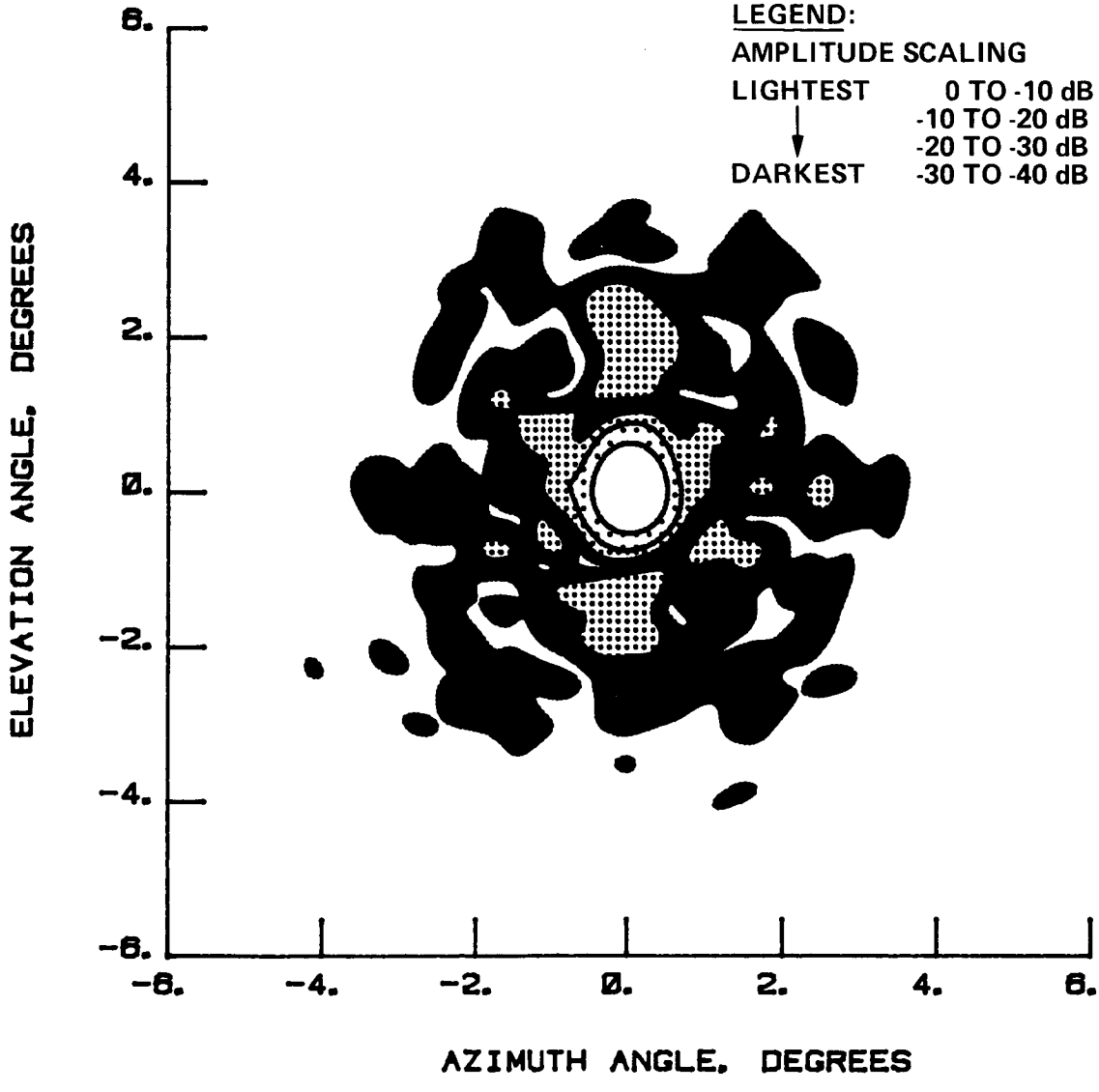

Figure 76 Test 7, 7.73 GHz, Co-Pol, Contour, Type 5

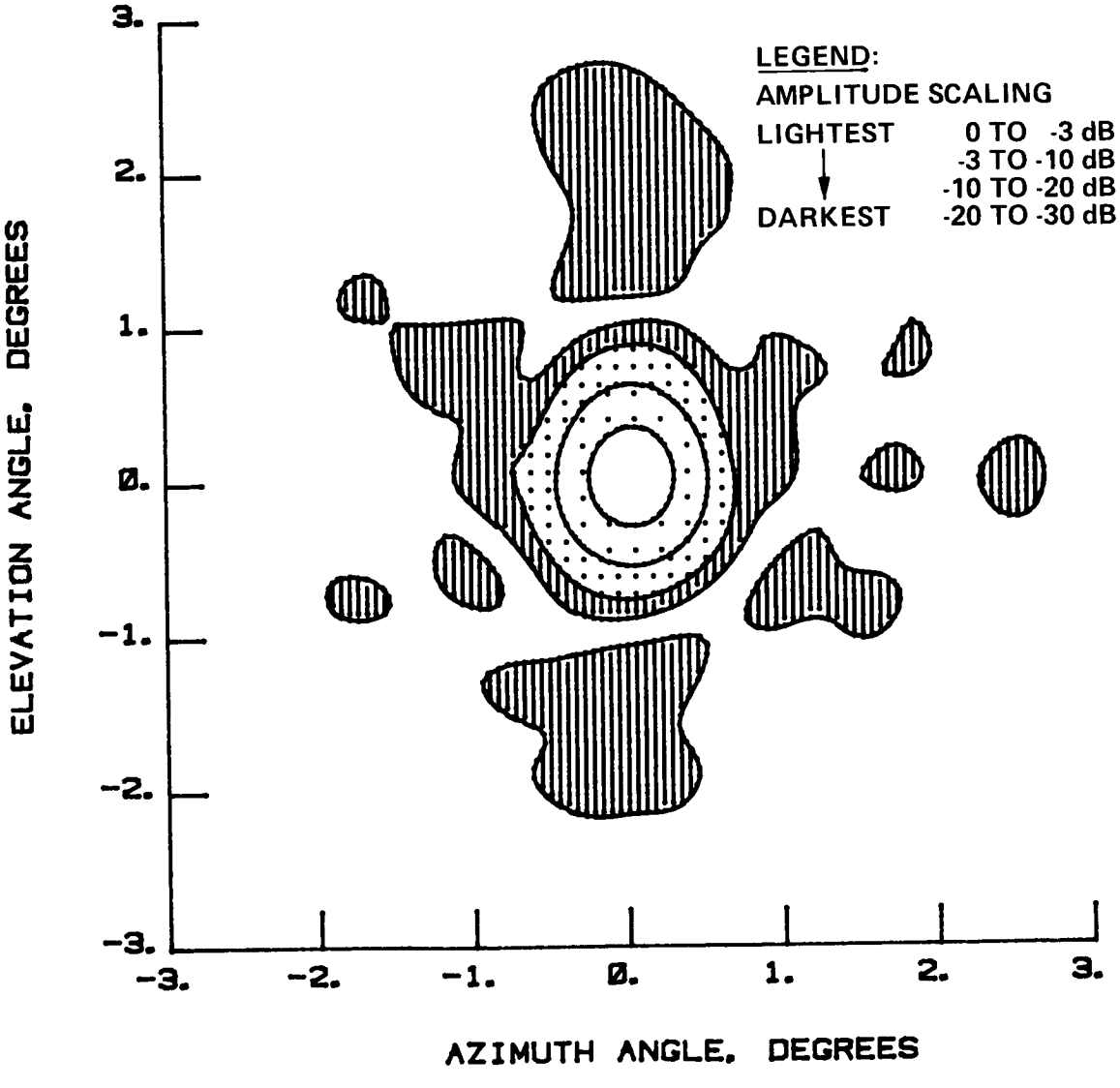

Figure 77 Test 7, 7.73 GHz, Co-Pol, Contour, Type 6

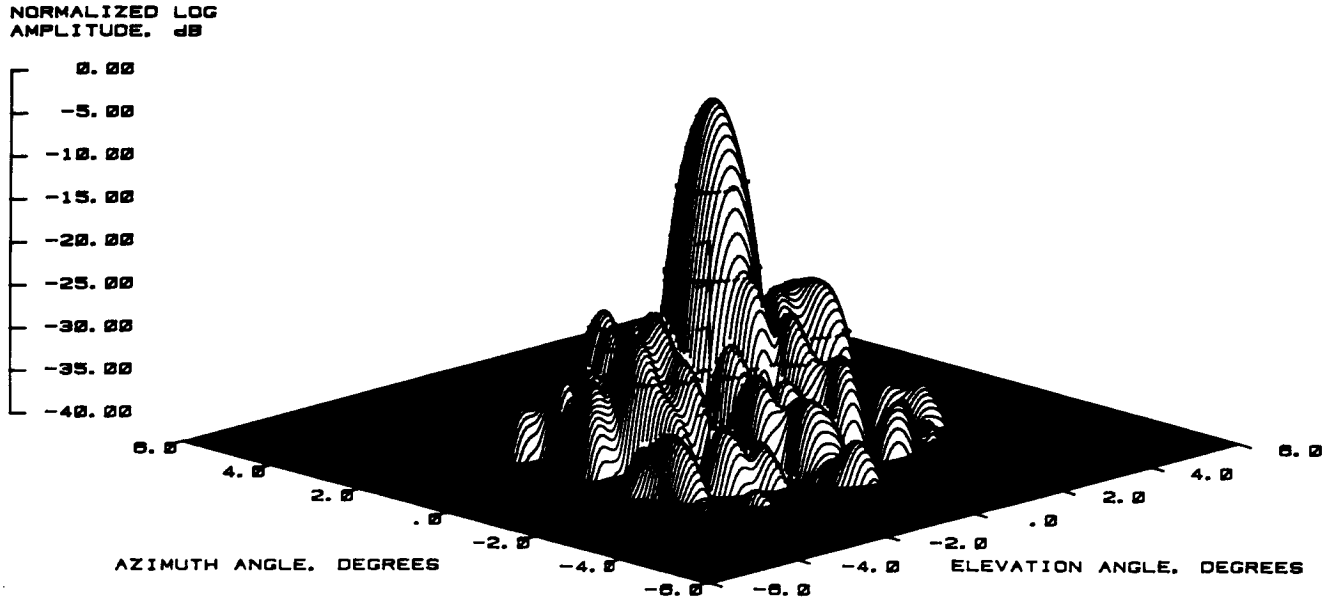

Figure 78 Test 7, 7.73 GHz, Co-Pol, 3-D, Type 7

C-2

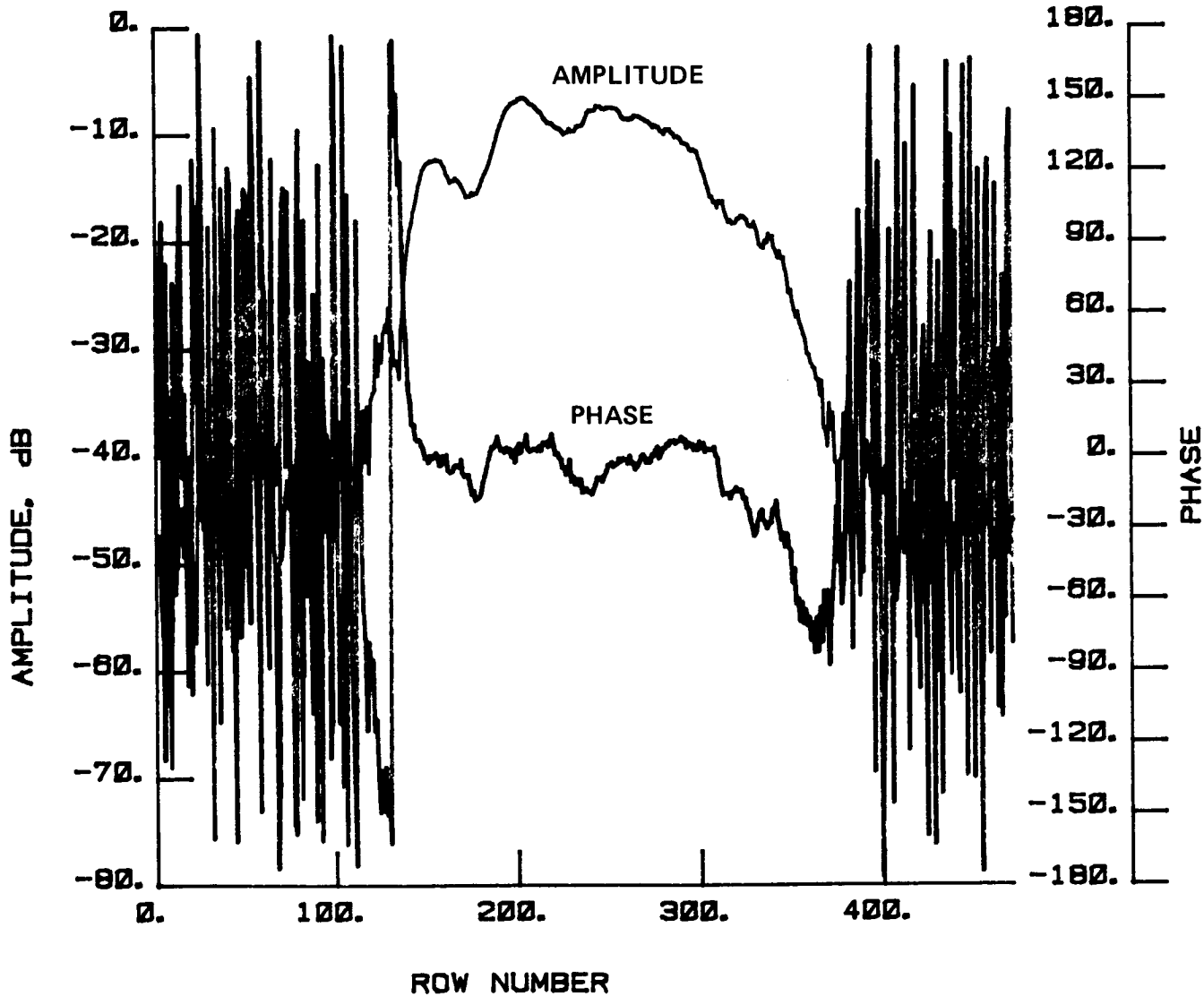

Figure 79 Test 7, 7.73 GHz, Co-Pol, H-Plane, Type 8

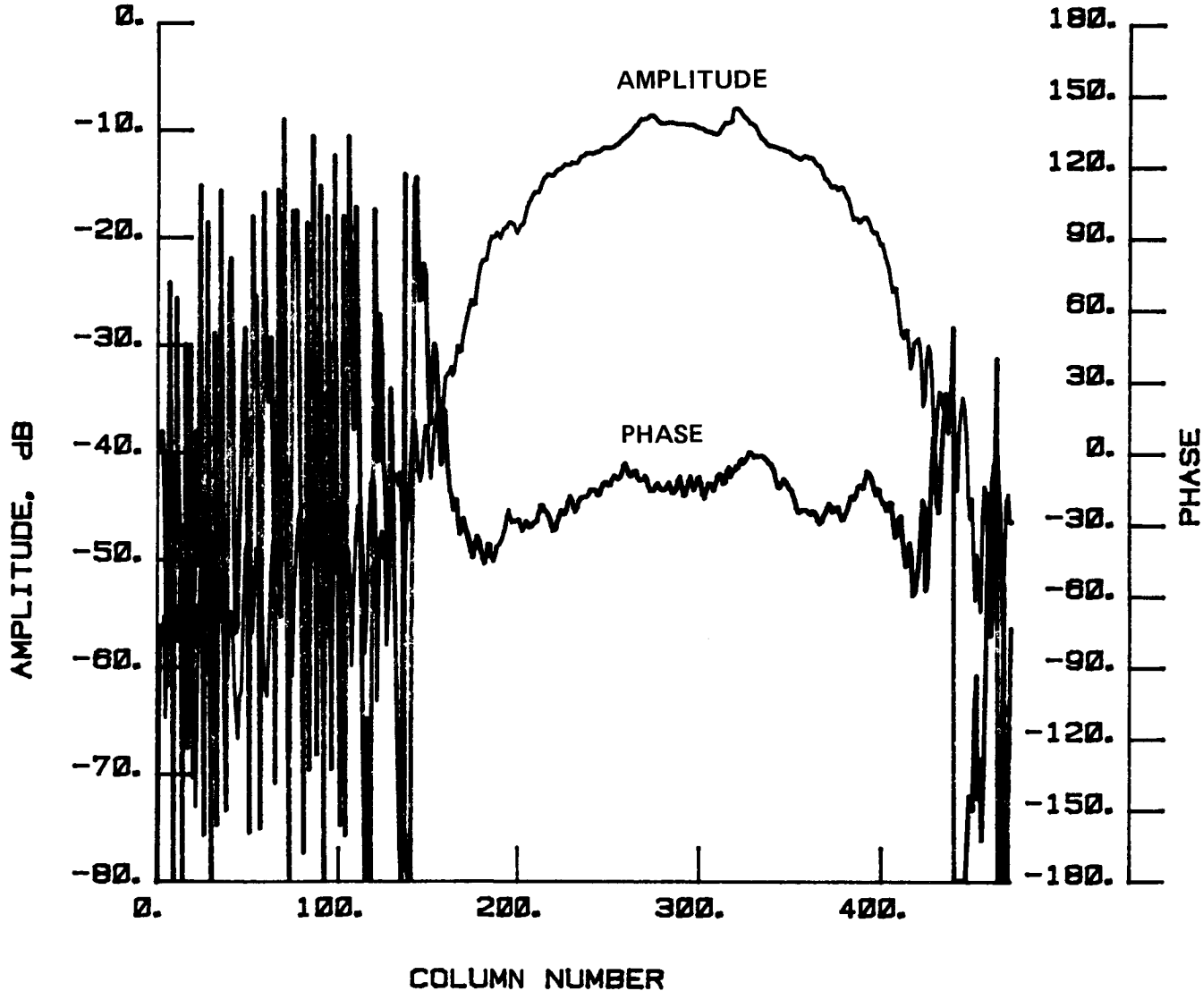

Figure 80 Test 7, 7.73 GHz, Co-Pol, E-Plane, Type 9

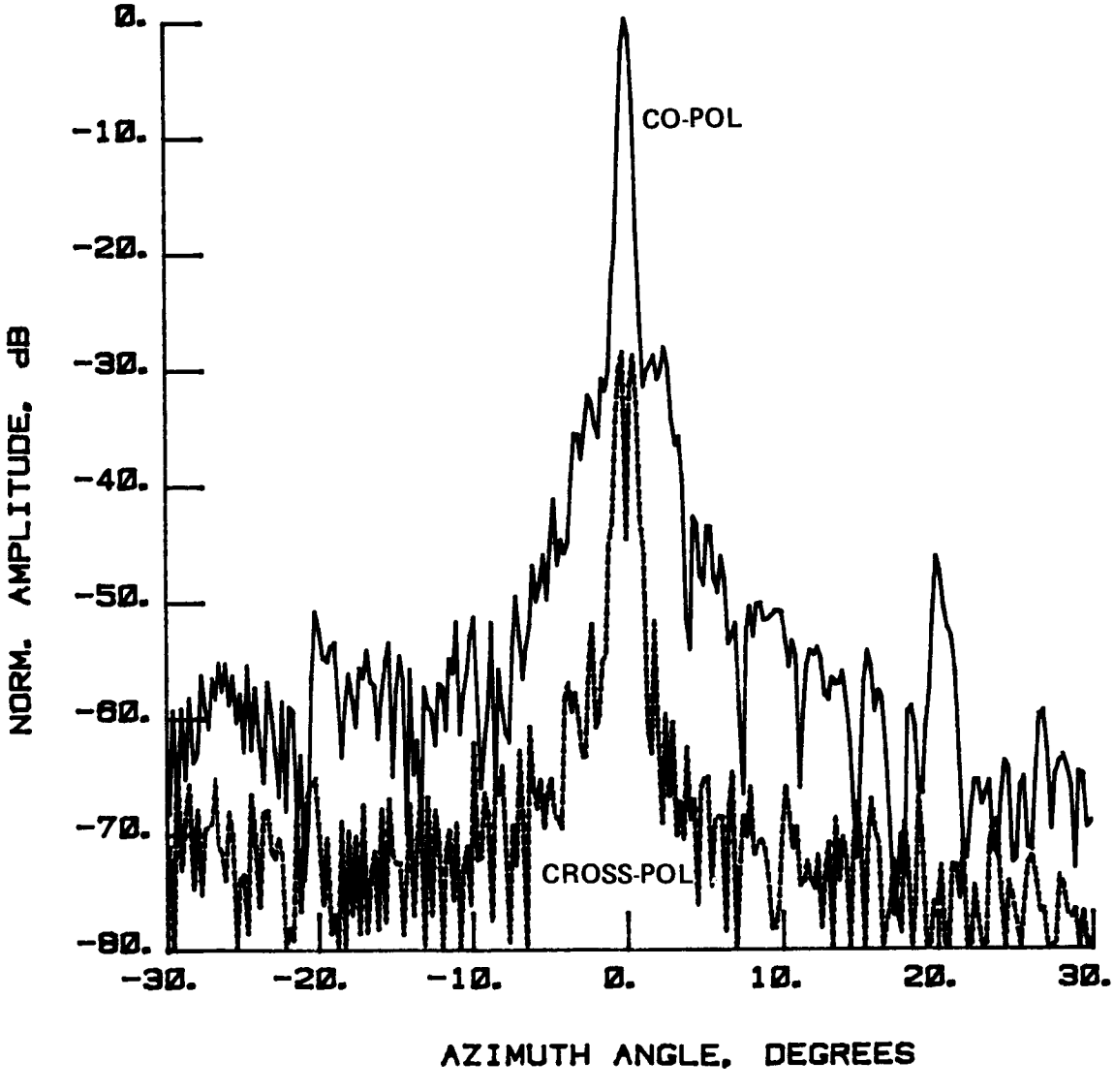

Figure 81 Test 8, 7.73 GHz, Overlay, H-Plane, Type 10

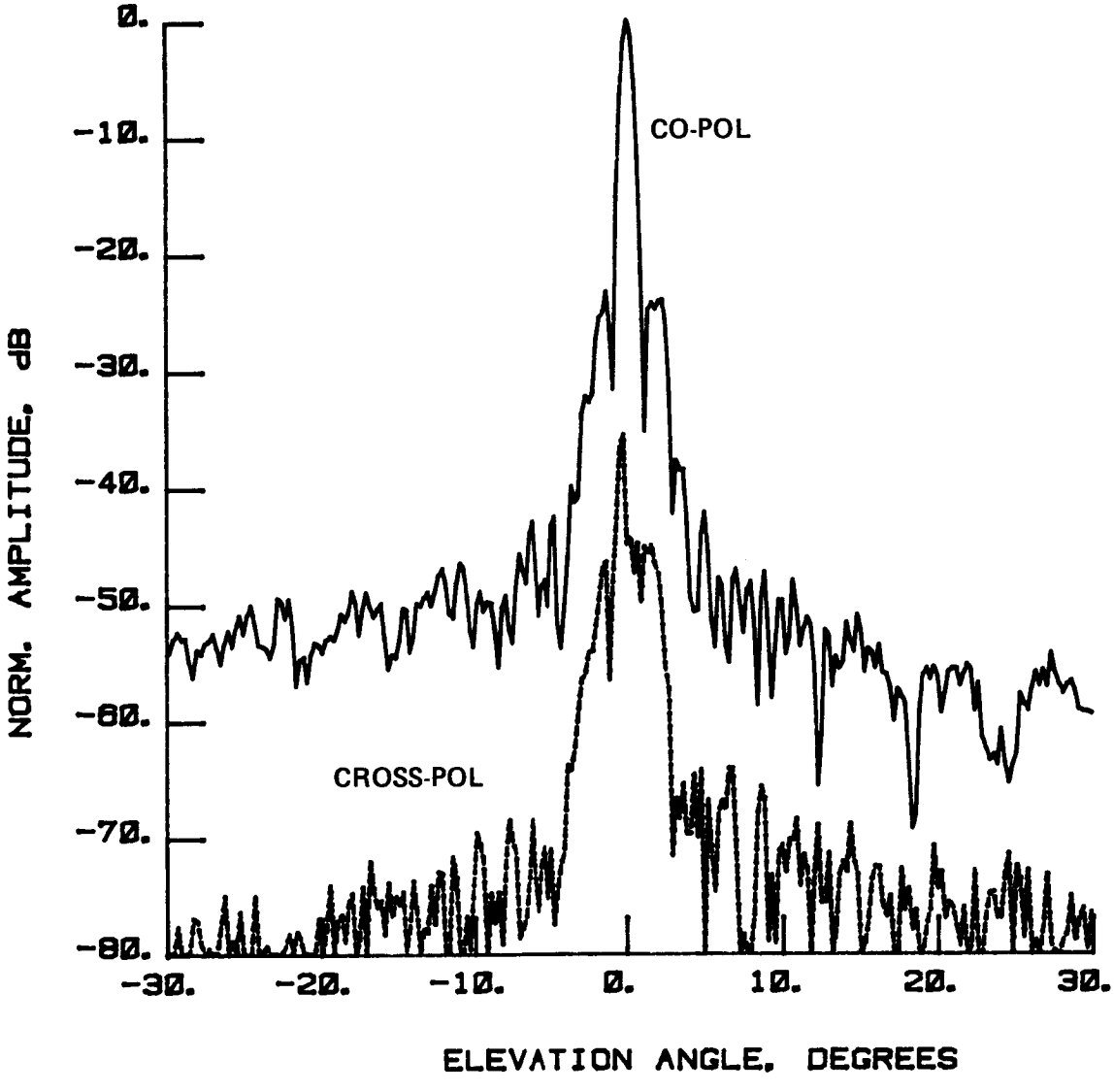

Figure 82 Test 8, 7.73 GHz, Overlay, E-Plane, Type 11

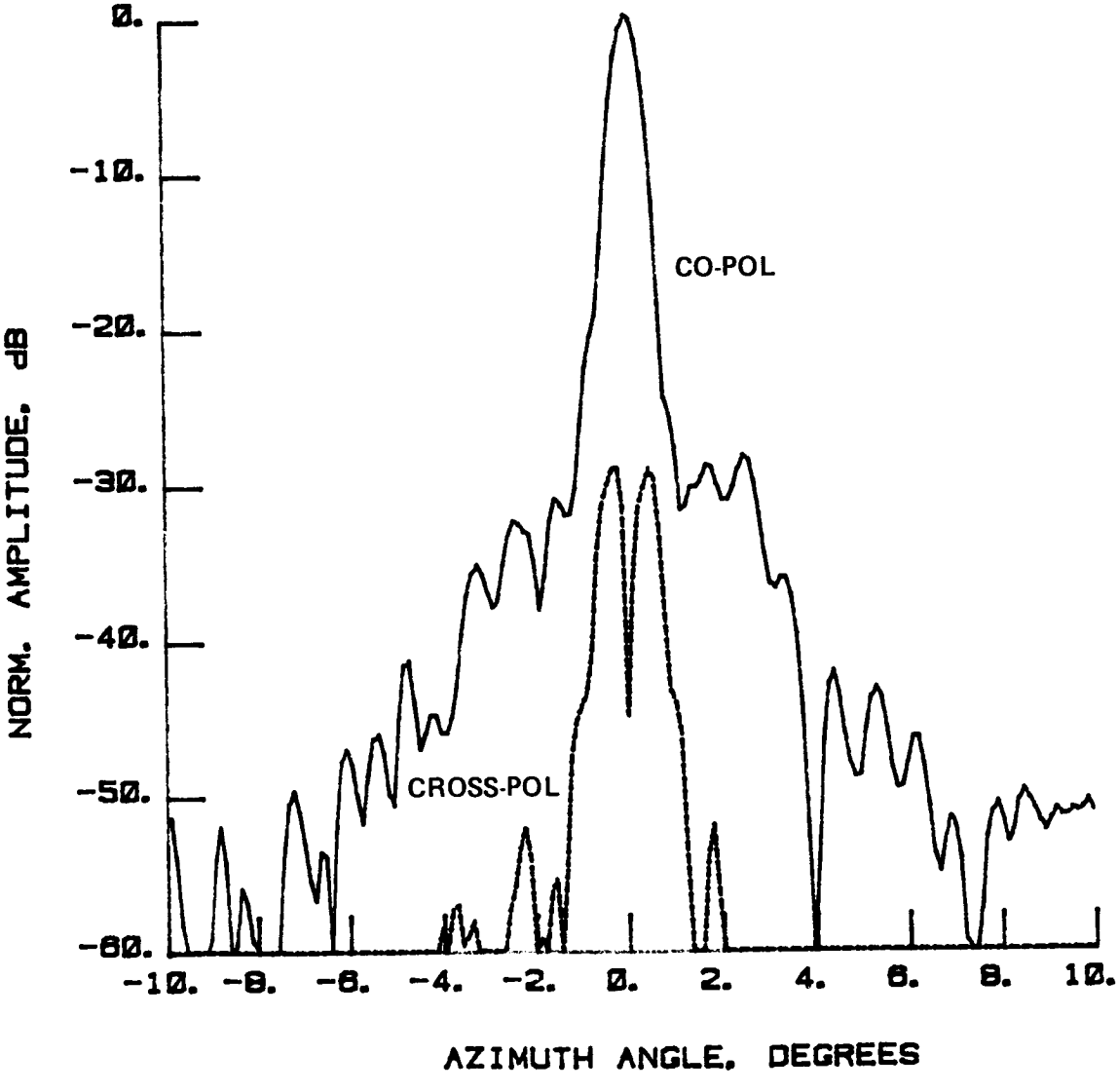

Figure 83 Test 8, 7.73 GHz, Overlay, H-Plane, Type 12

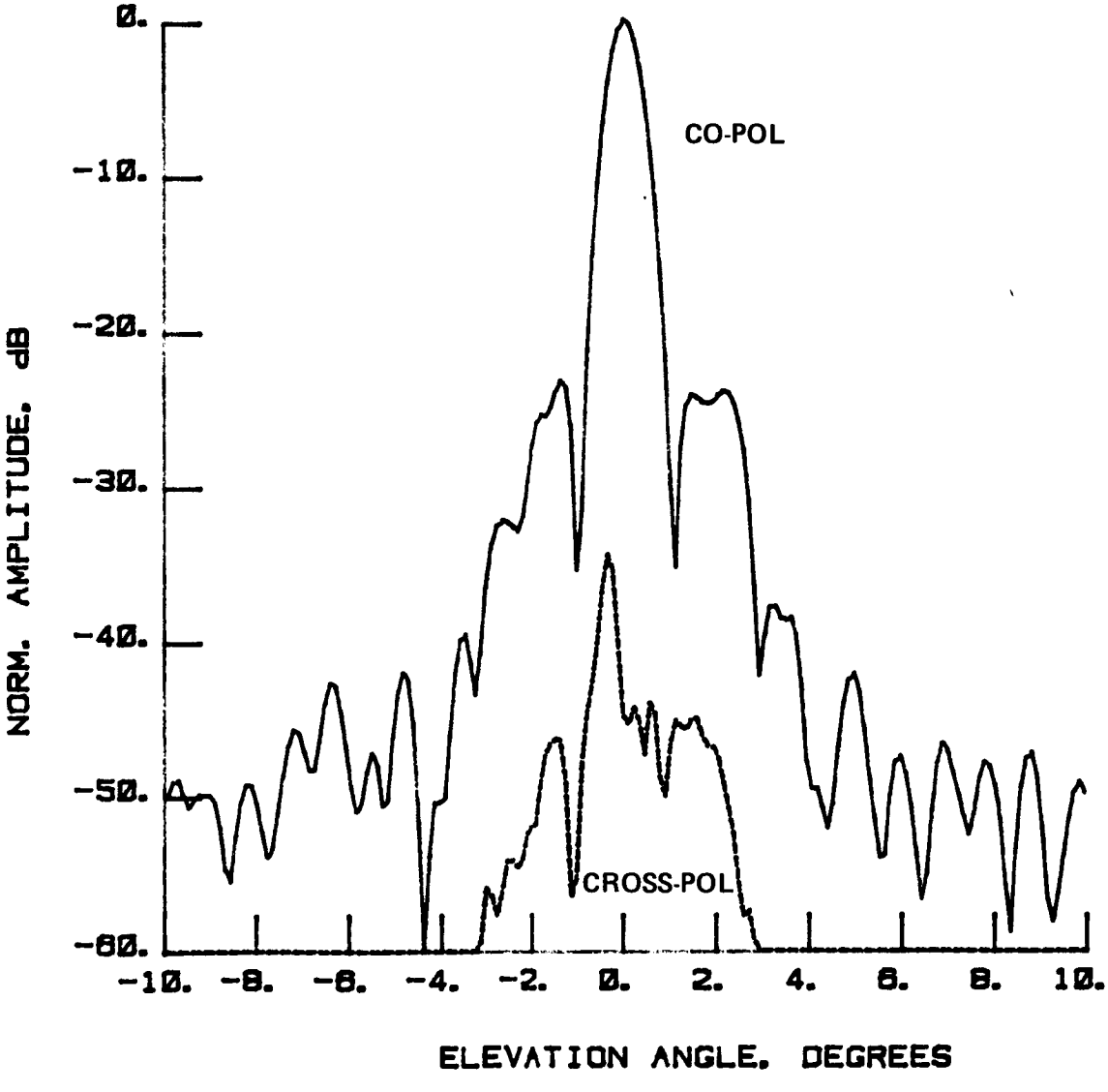

Figure 84 Test 8, 7.73 GHz, Overlay, E-Plane, Type 13

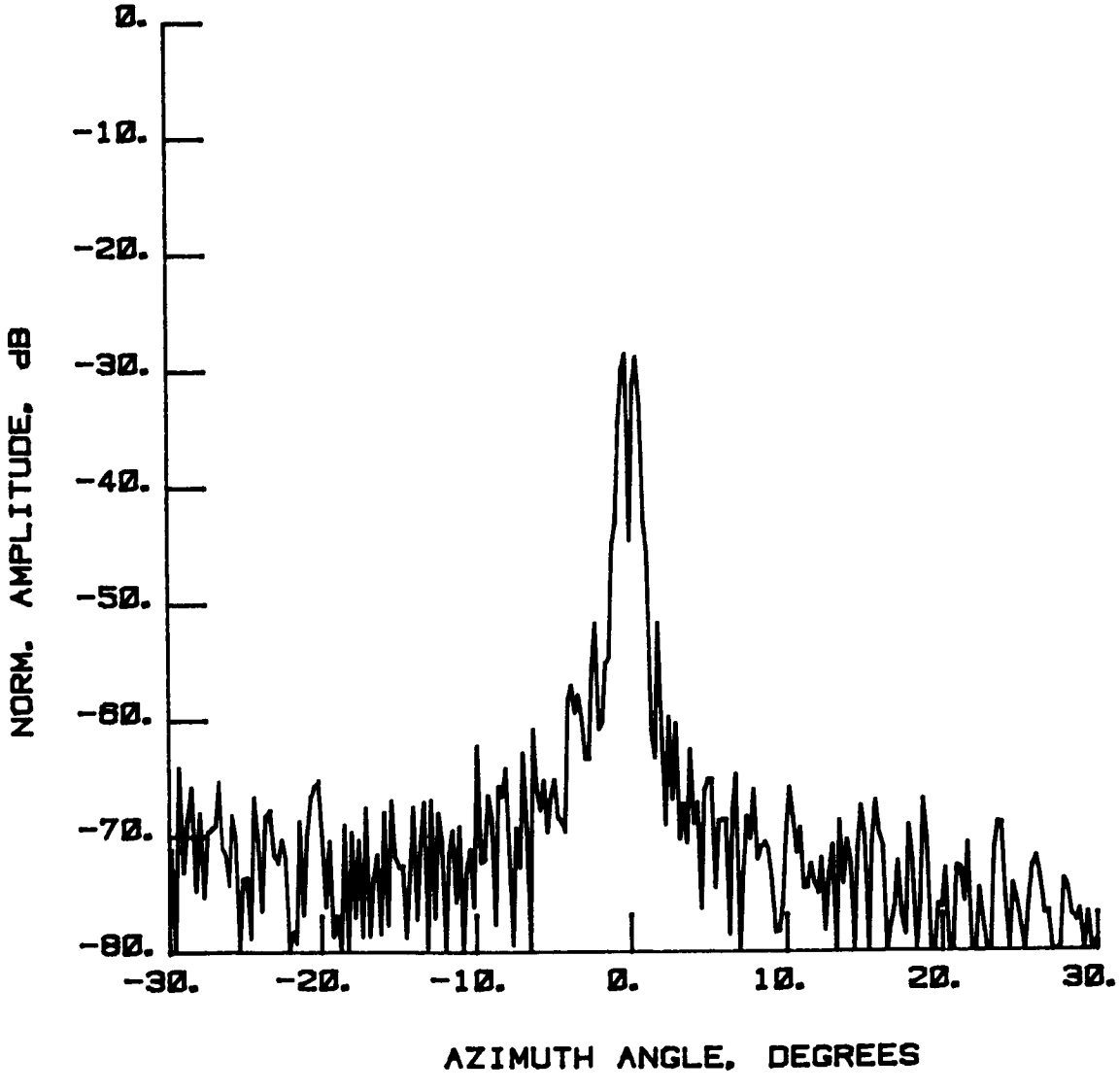

Figure 85 Test 8, 7.73 GHz, Cross-Pol, H-Plane, Type 14

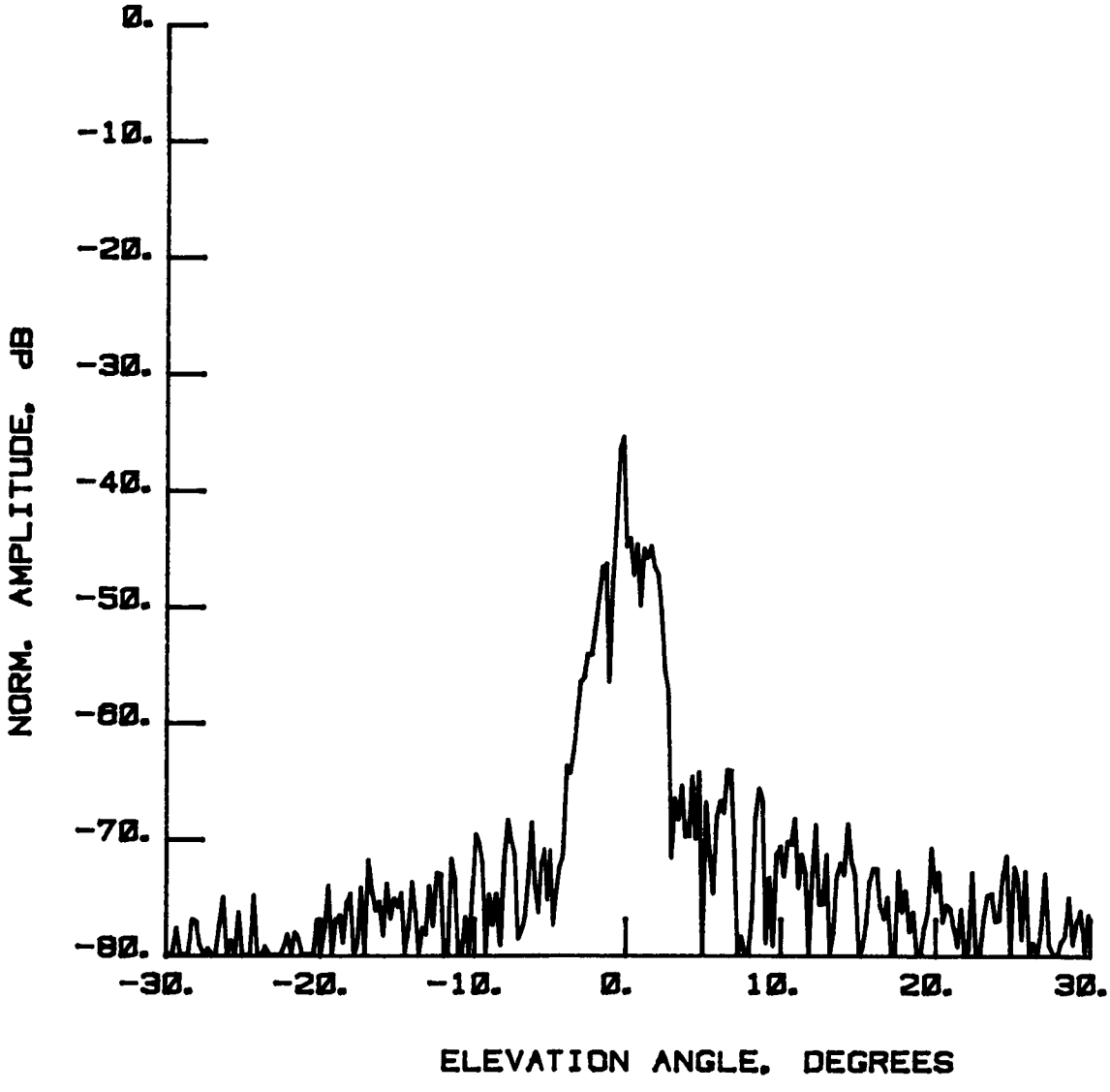

Figure 86 Test 8, 7.73 GHz, Cross-Pol, E-Plane, Type 15

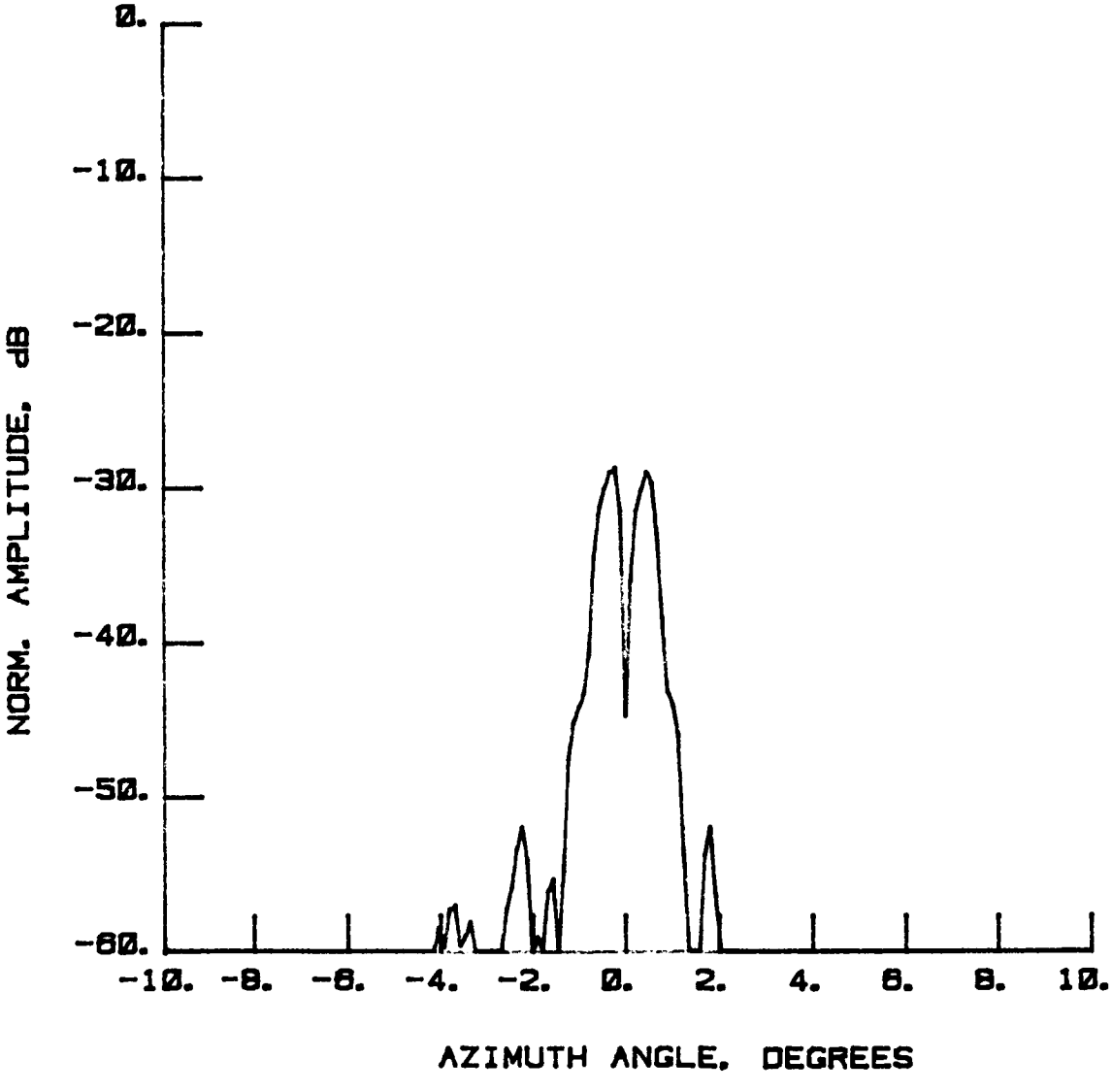

Figure 87 Test 8, 7.73 GHz, Cross-Pol, H-Plane, Type 16

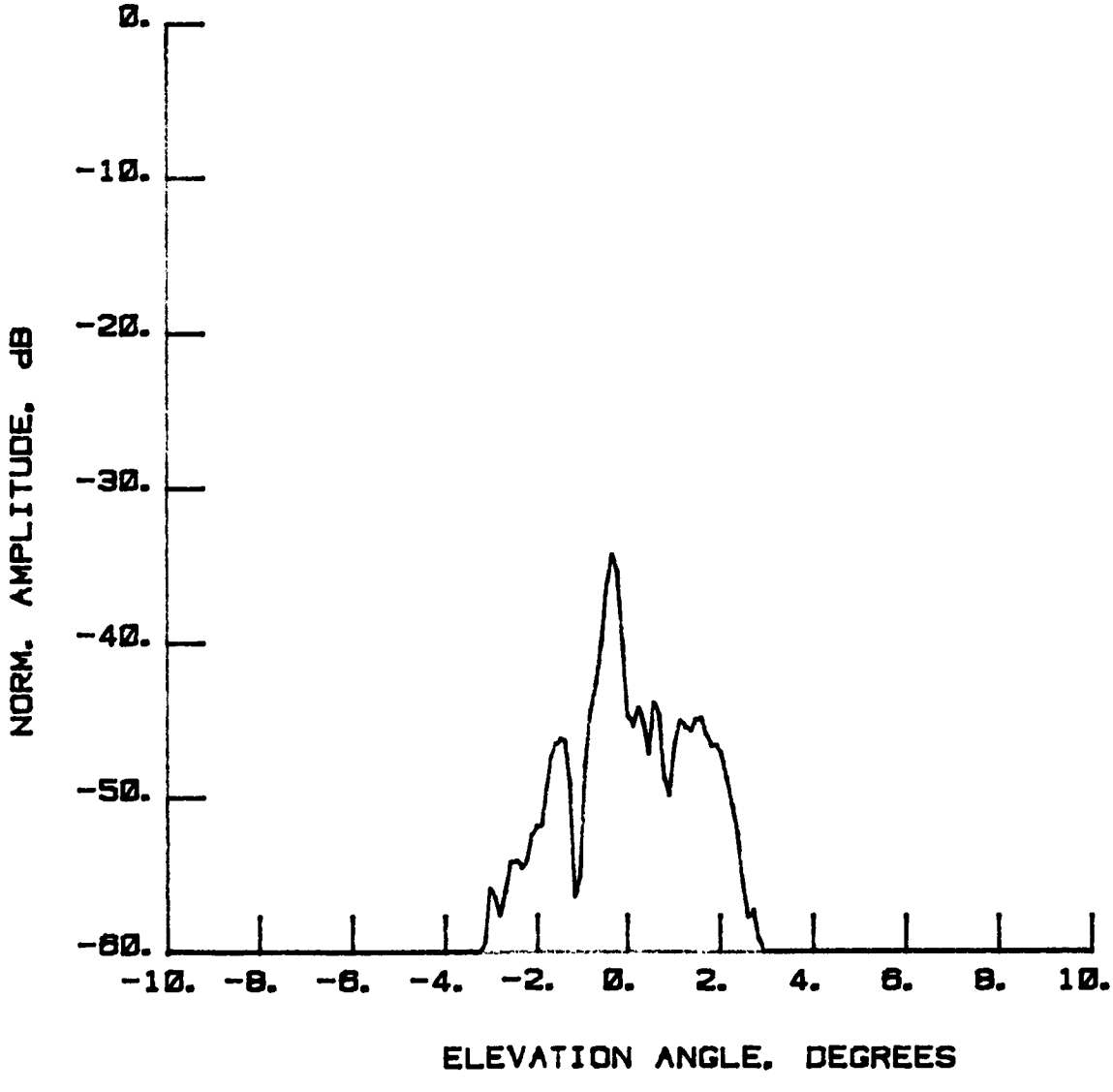

Figure 88 Test 8, 7.73 GHz, Cross-Pol, E-Plane, Type 17

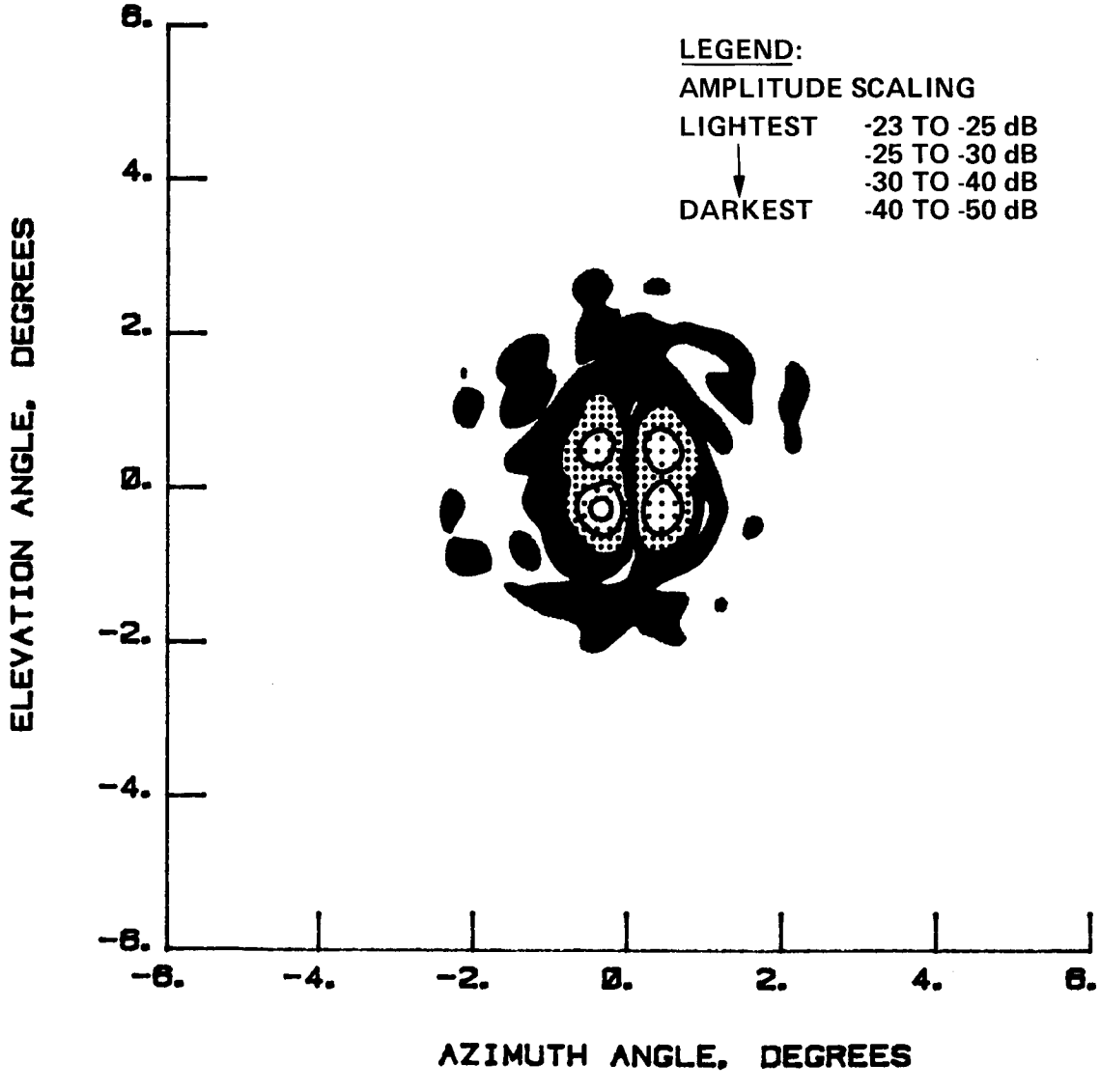

Figure 89 Test 8, 7.73 GHz, Cross-Pol, Contour, Type 18

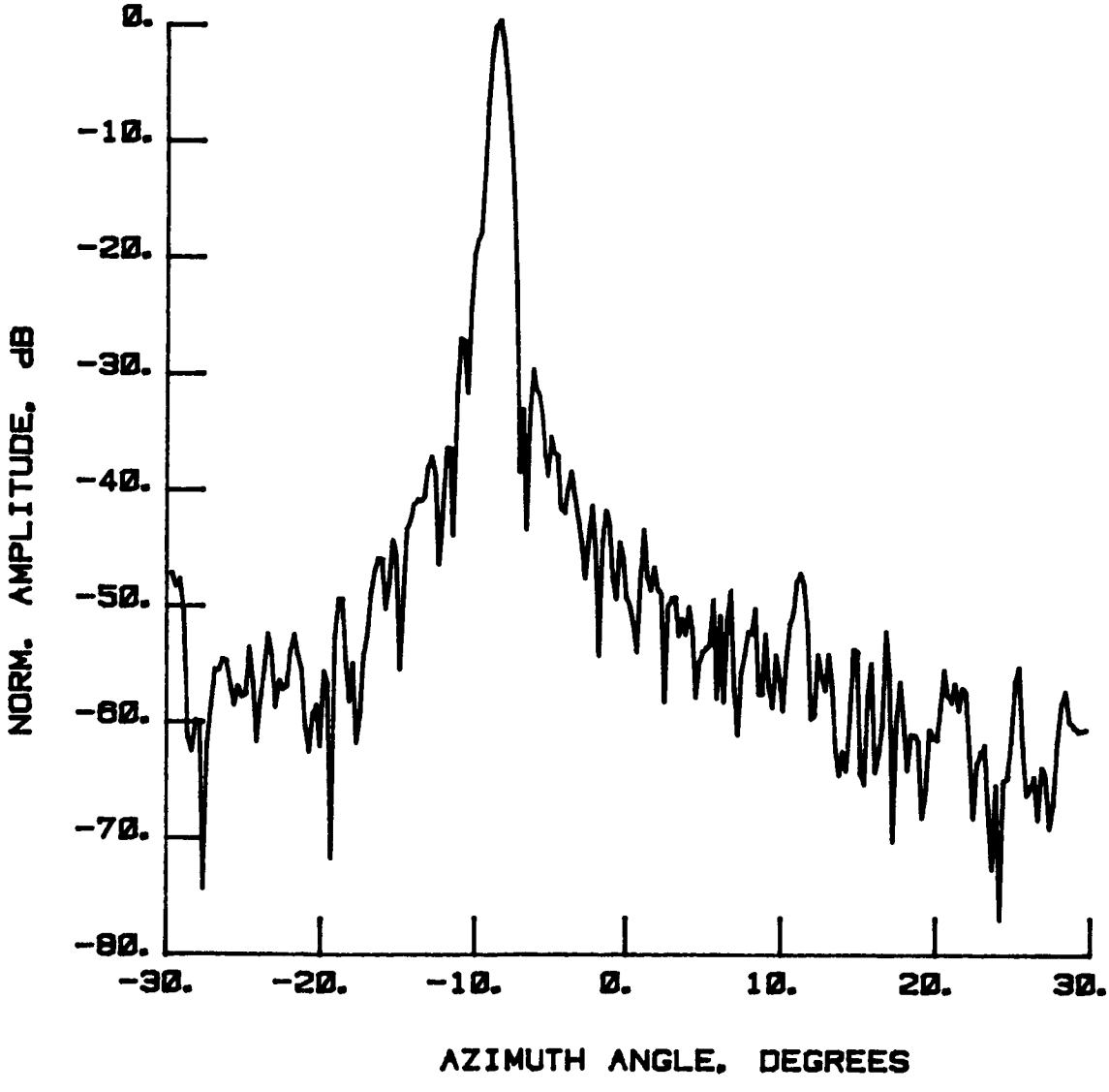

Figure 90 Test 9, 7.73 GHz, Co-Pol, H-Plane, Type 1

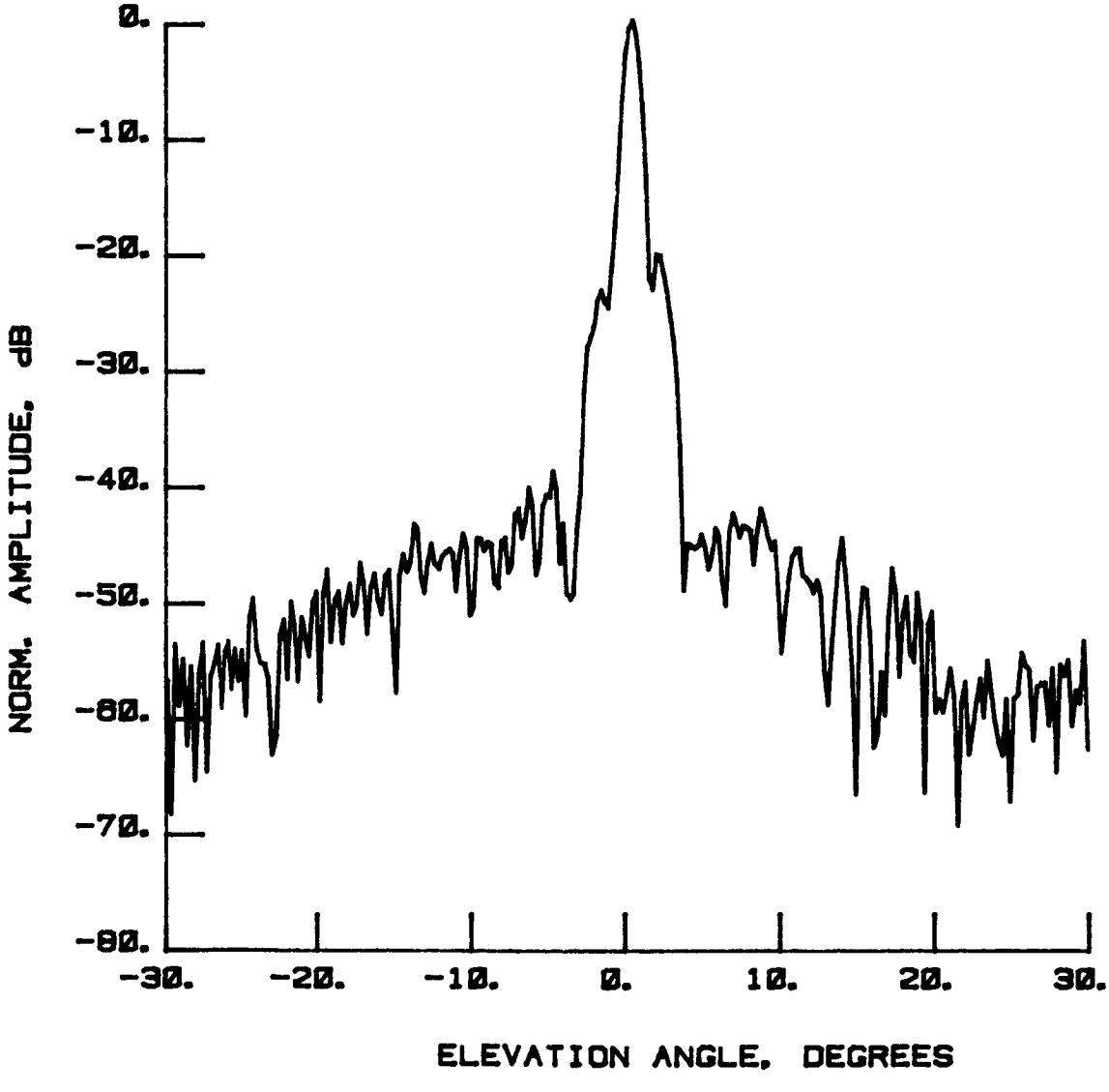

Figure 91 Test 9, 7.73 GHz, Co-Pol, E-Plane, Type 2

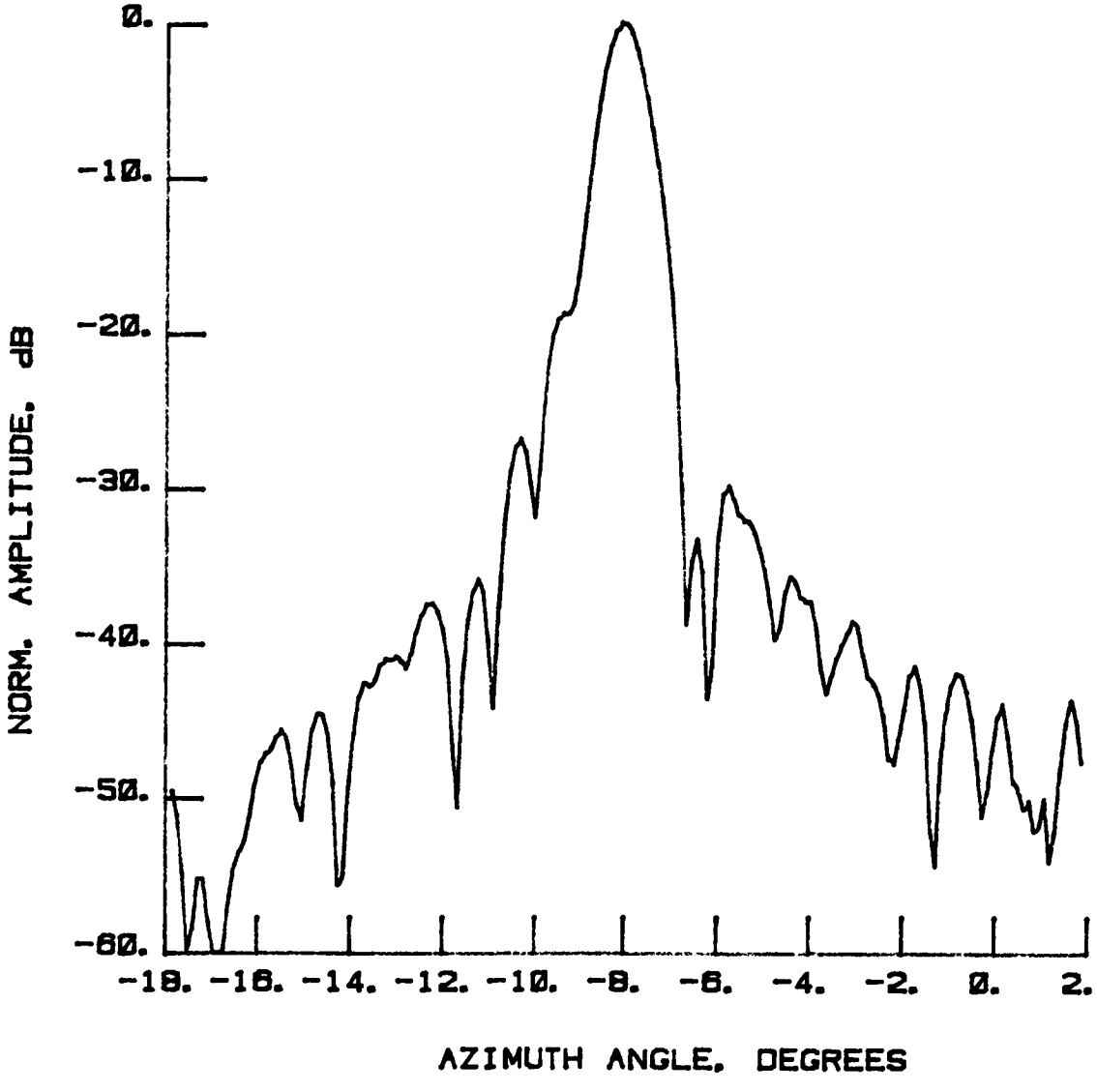

Figure 92 Test 9, 7.73 GHz, Co-Pol, H-Plane, Type 3

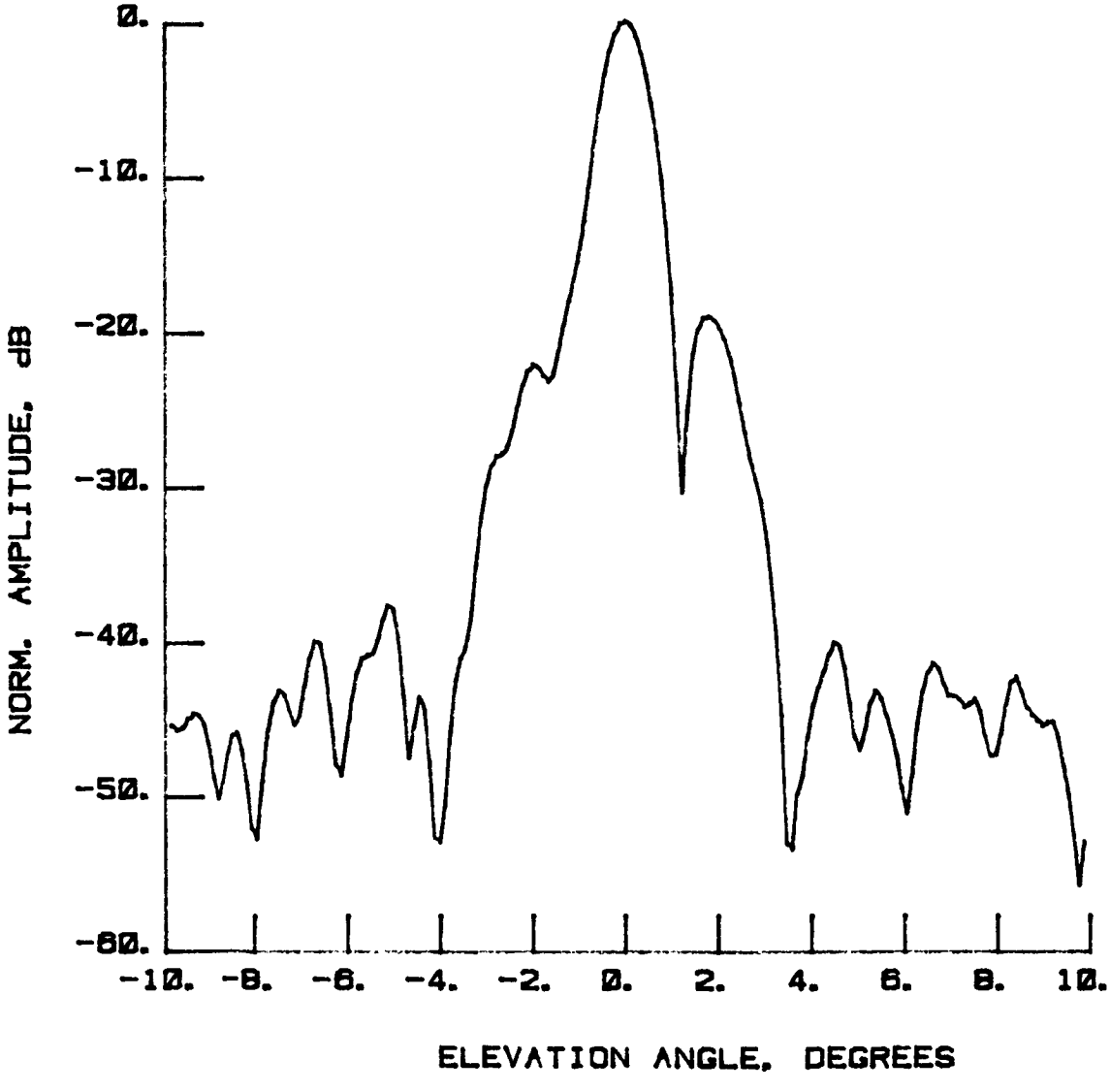

Figure 93 Test 9, 7.73 GHz, Co-Pol, E-Plane, Type 4

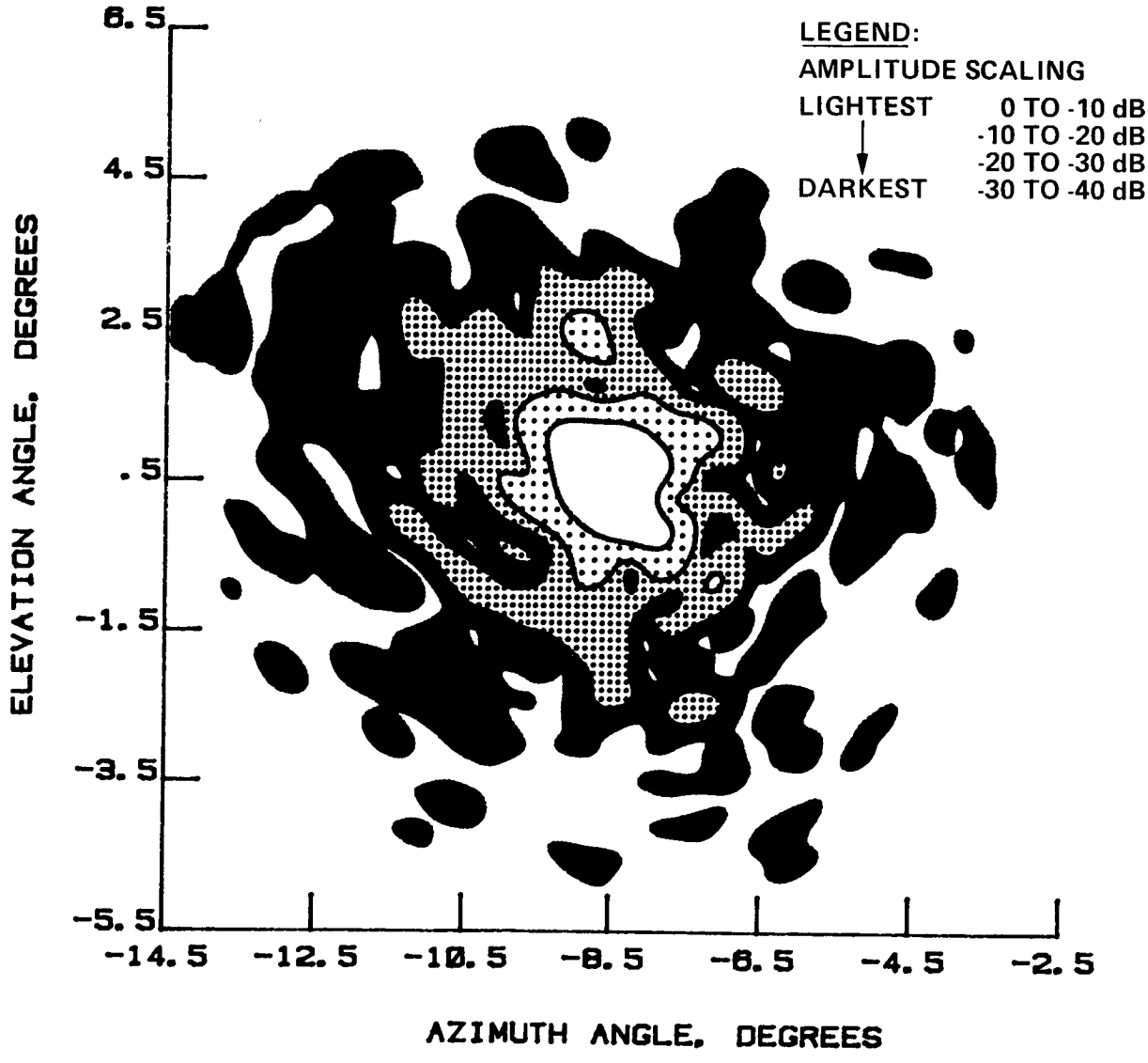

Figure 94 Test 9, 7.73 GHz, Co-Pol, Contour, Type 5

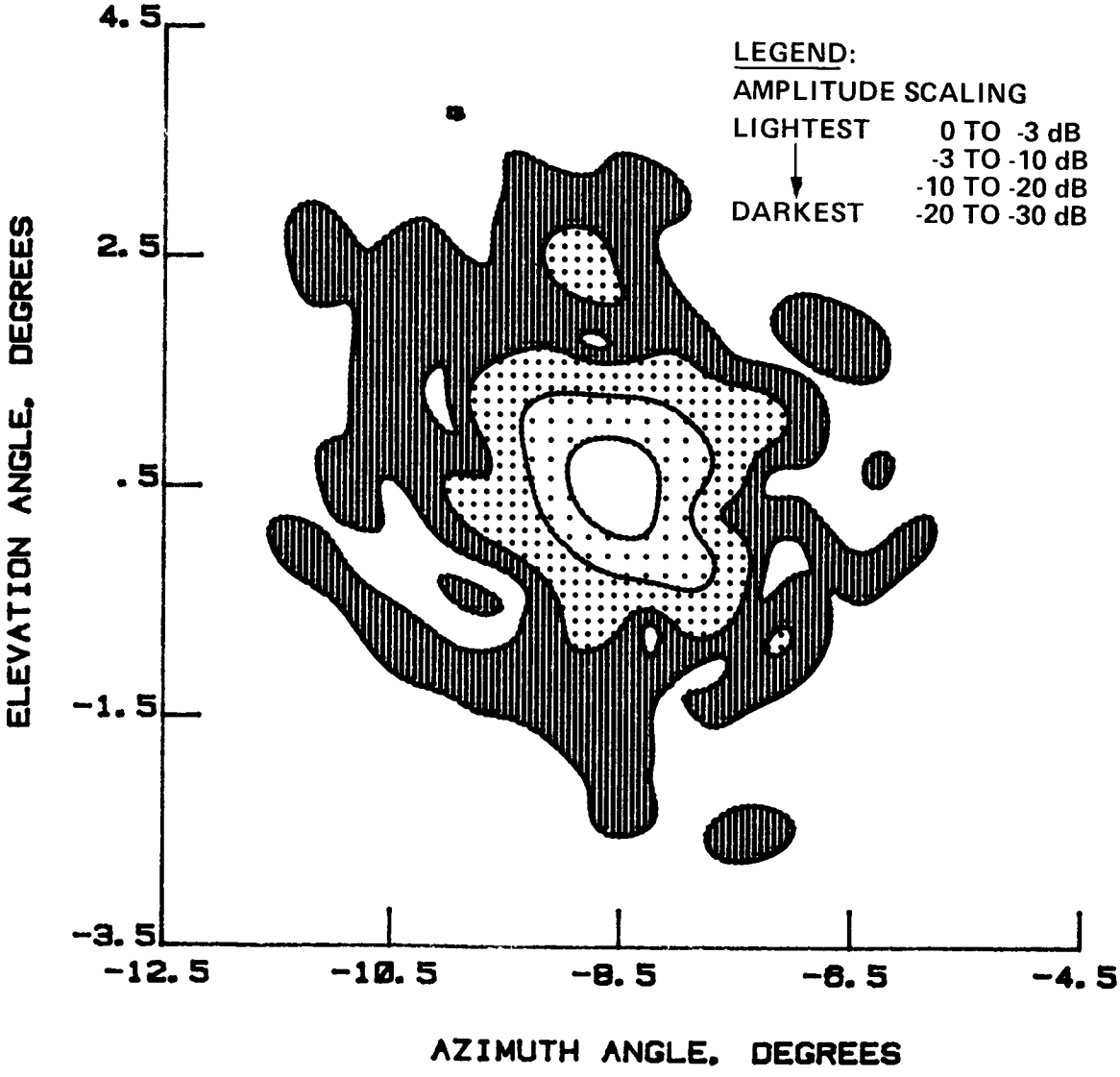

Figure 95 Test 9, 7.73 GHz, Co-Pol, Contour, Type 6

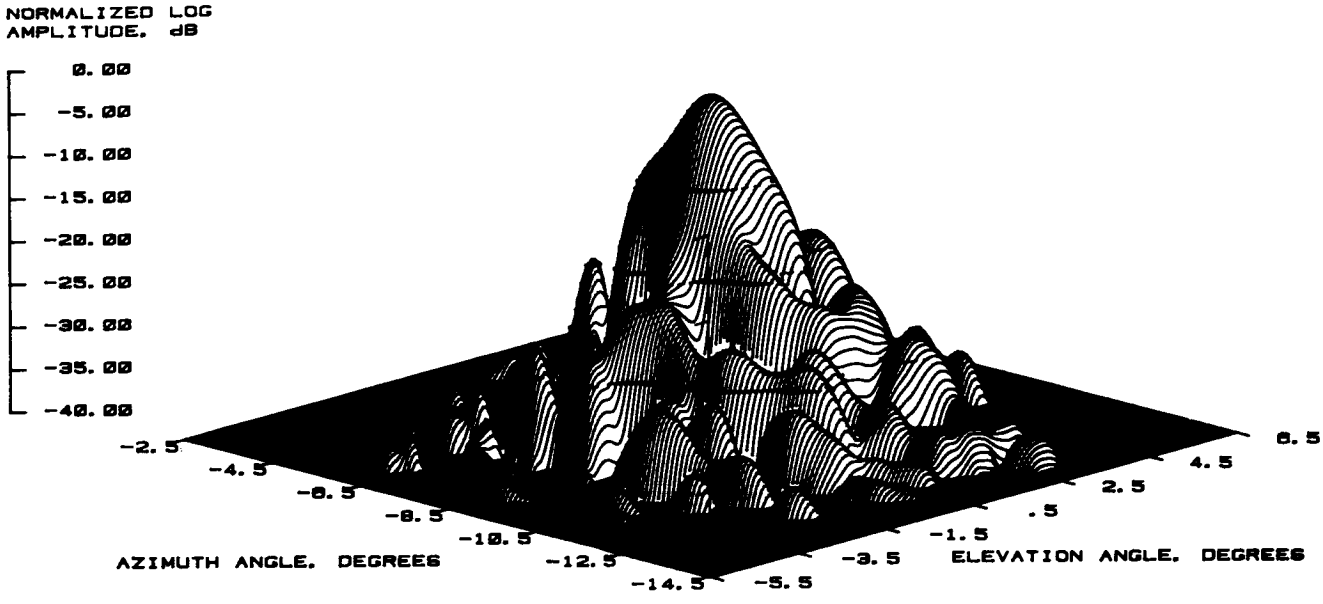

Figure 96 Test 9, 7.73 GHz, Co-Pol, 3-D, Type 7

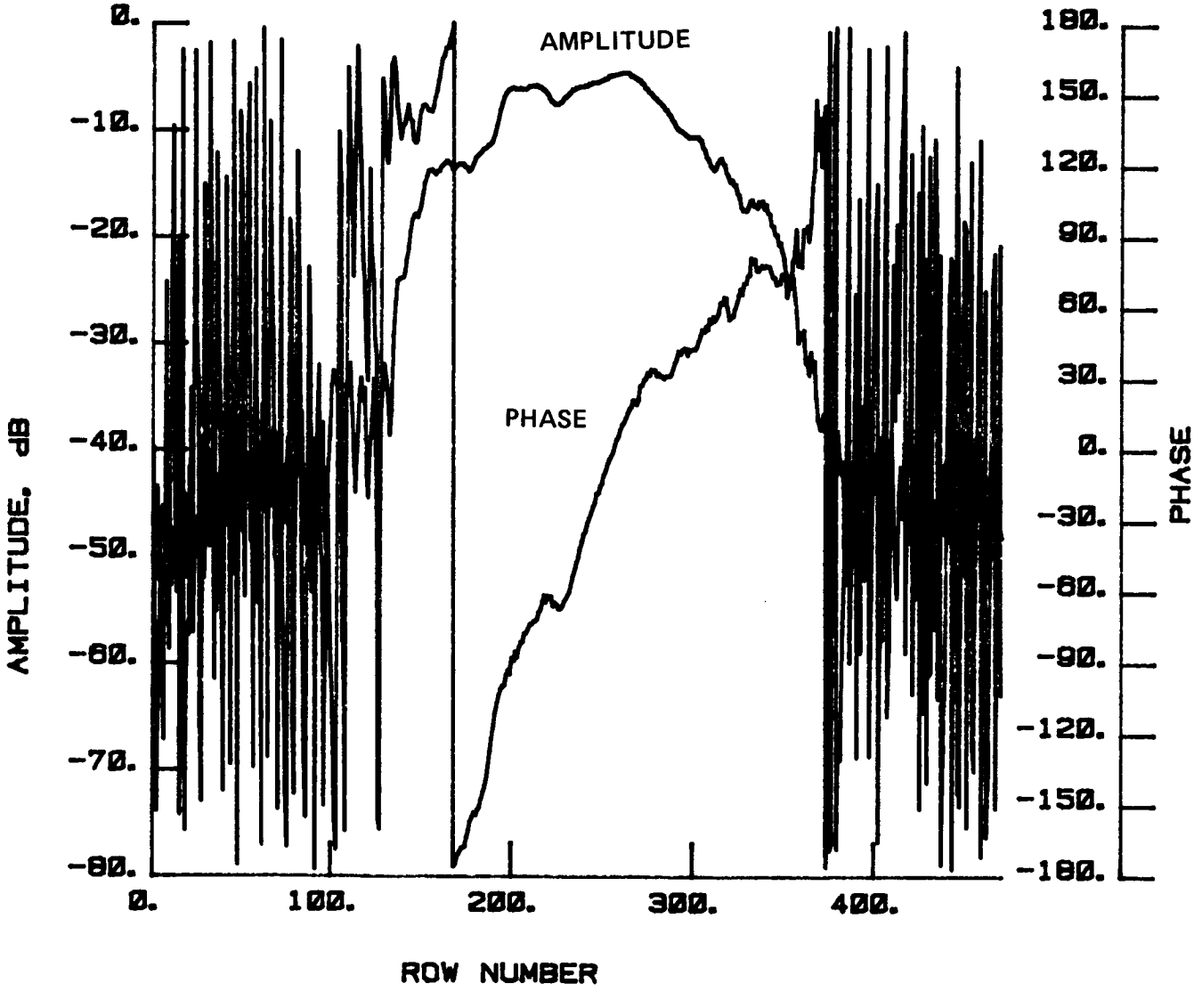

Figure 97 Test 9, 7.73 GHz, Co-Pol, H-Plane, Type 8

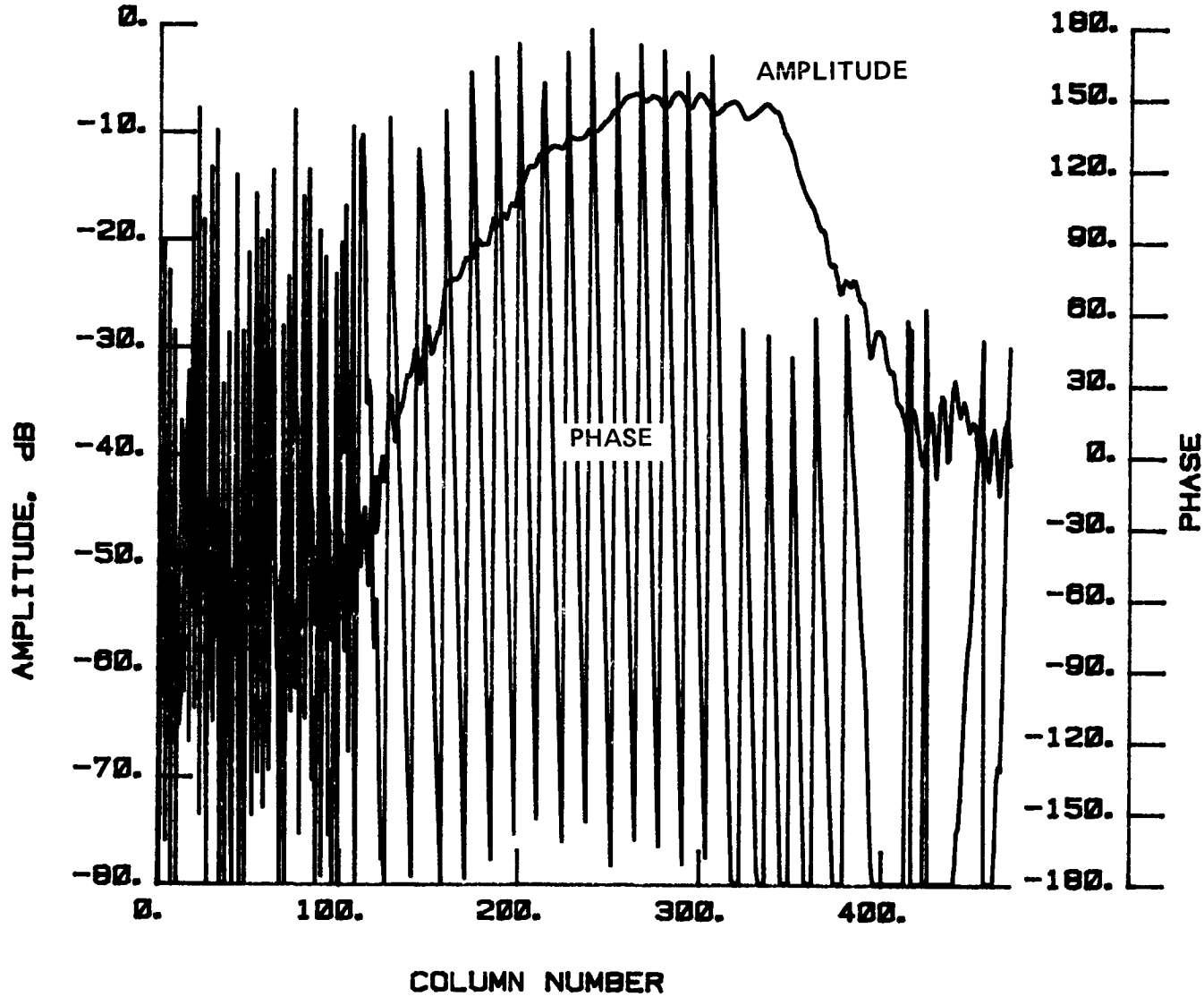

Figure 98 Test 9, 7.73 GHz, Co-Pol, E-Plane, Type 9

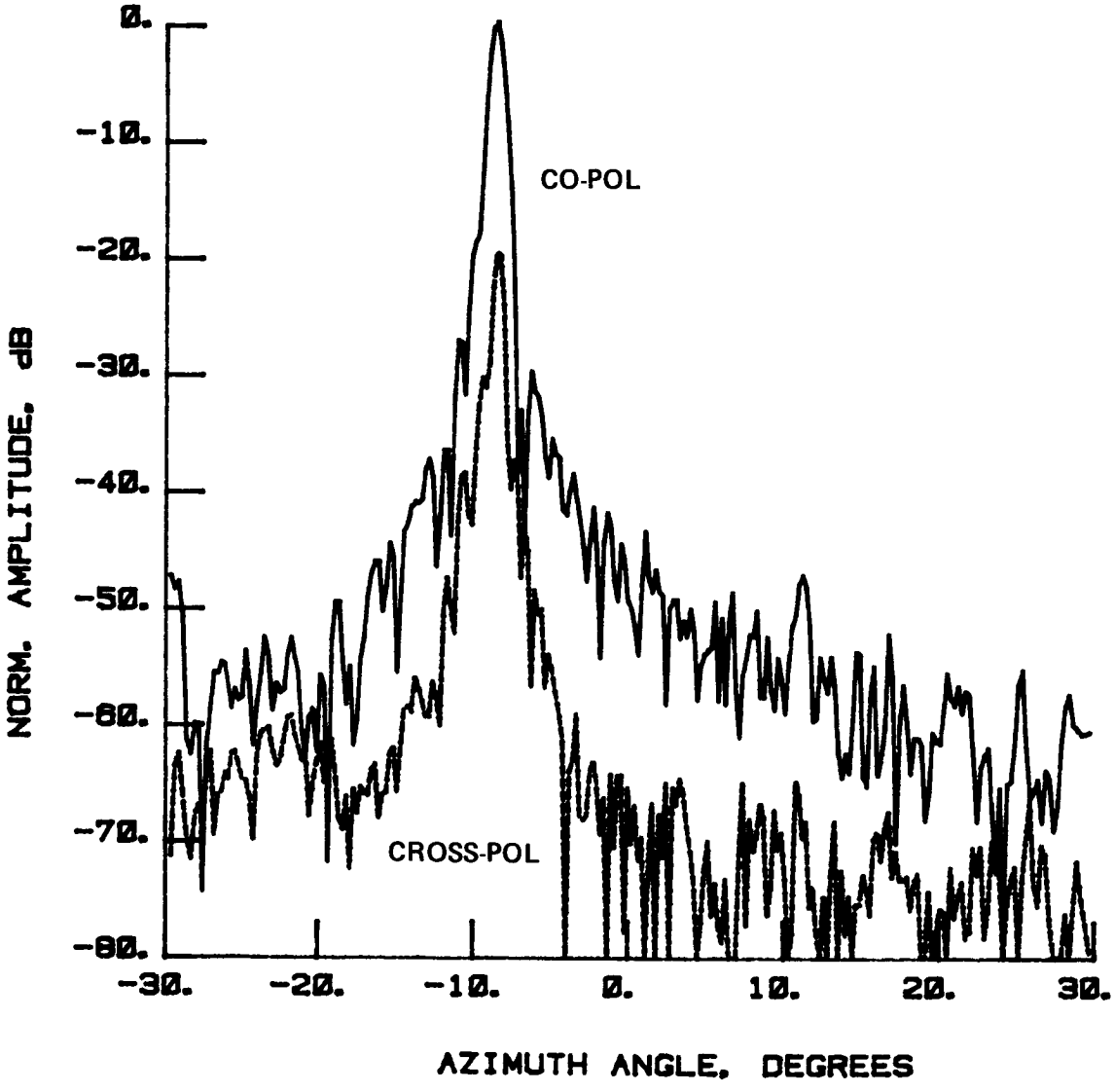

Figure 99 Test 10, 7.73 GHz, Overlay, H-Plane, Type 10

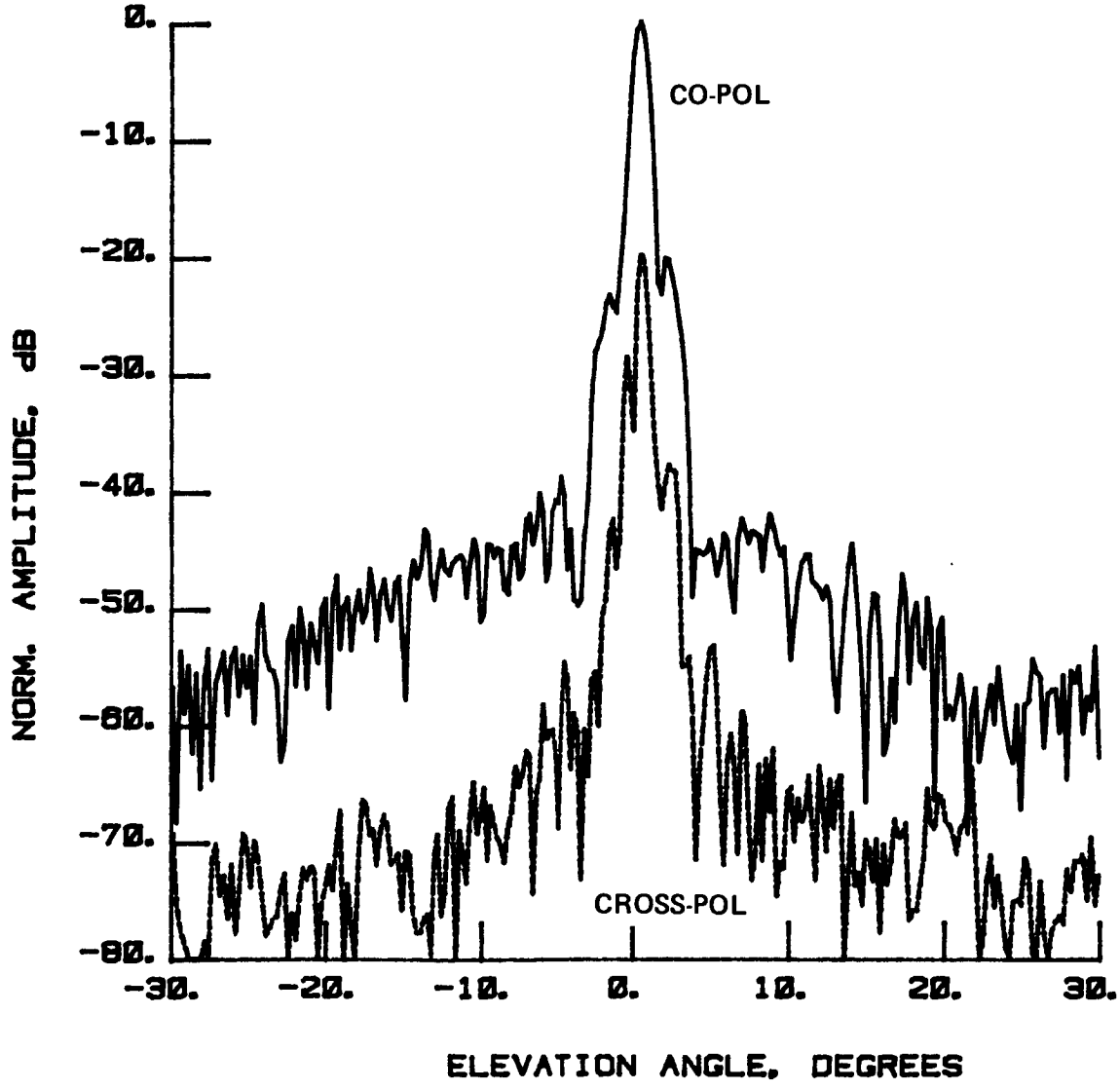

Figure 100 Test 10, 7.73 GHz, Overlay, E-Plane, Type 11

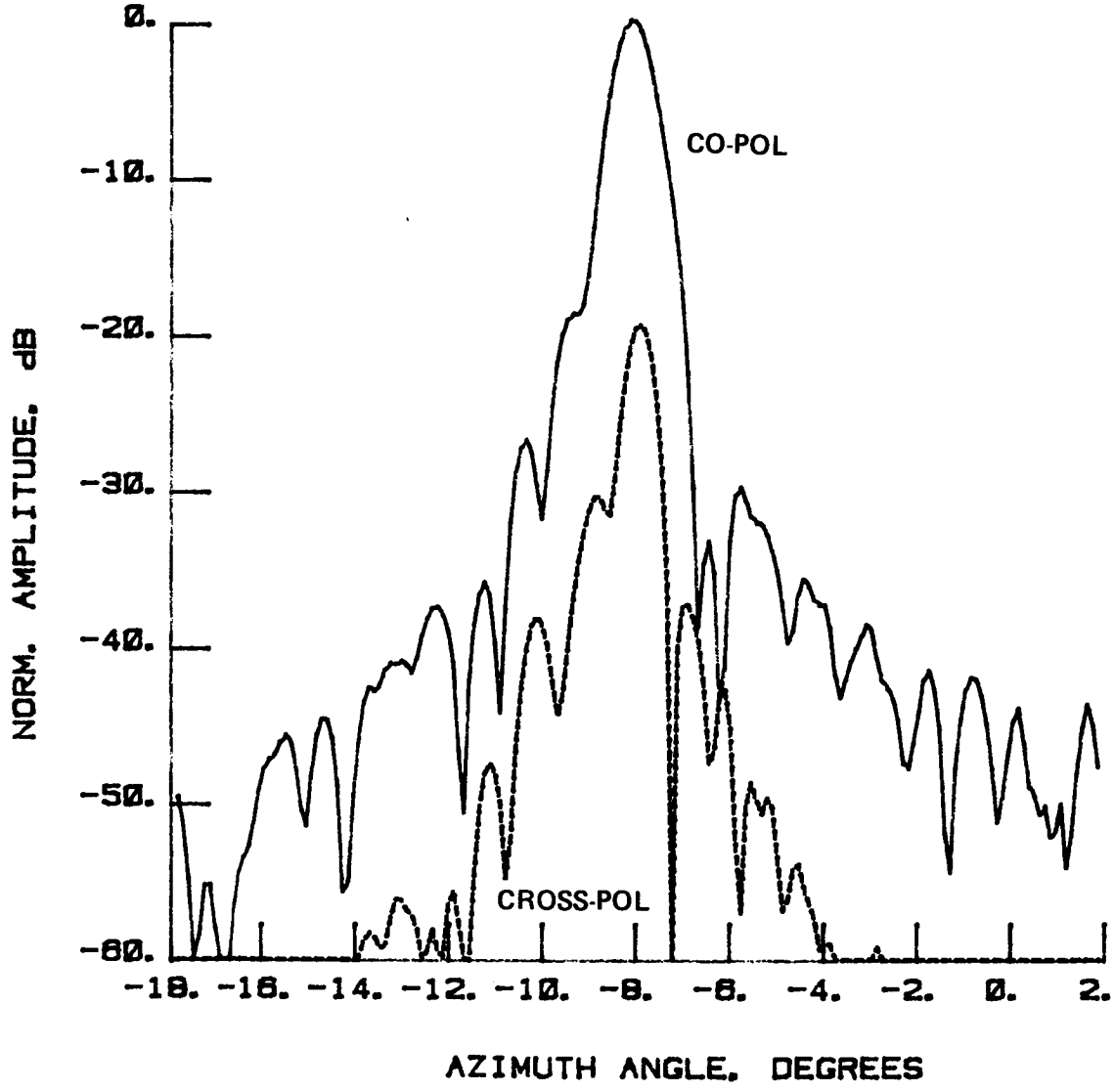

Figure 101 Test 10, 7.73 GHz, Overlay, H-Plane, Type 12

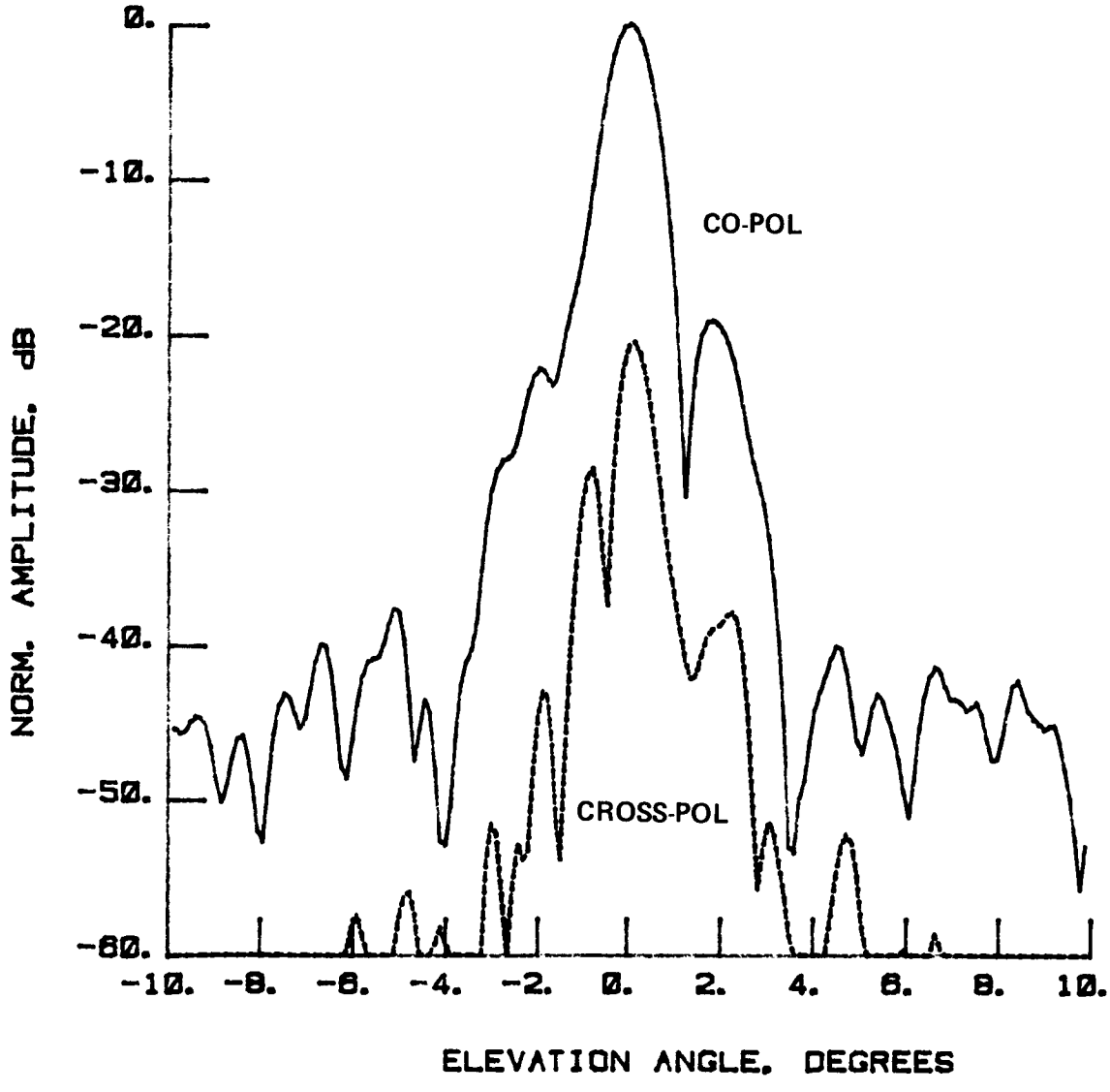

Figure 102 Test 10, 7.73 GHz, Overlay, E-Plane, Type 13

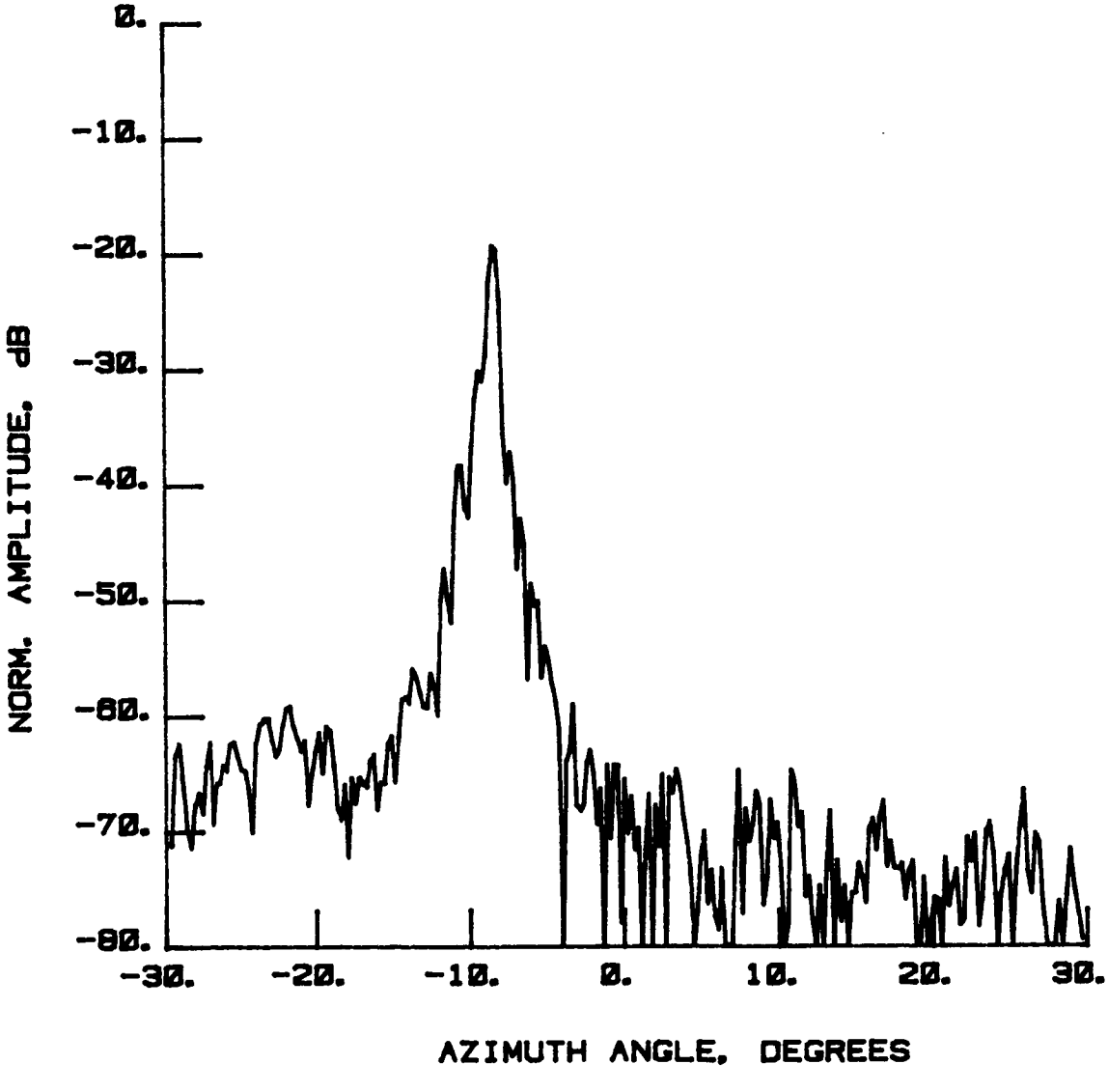

Figure 103 Test 10, 7.73 GHz, Cross-Pol, H-Plane, Type 14

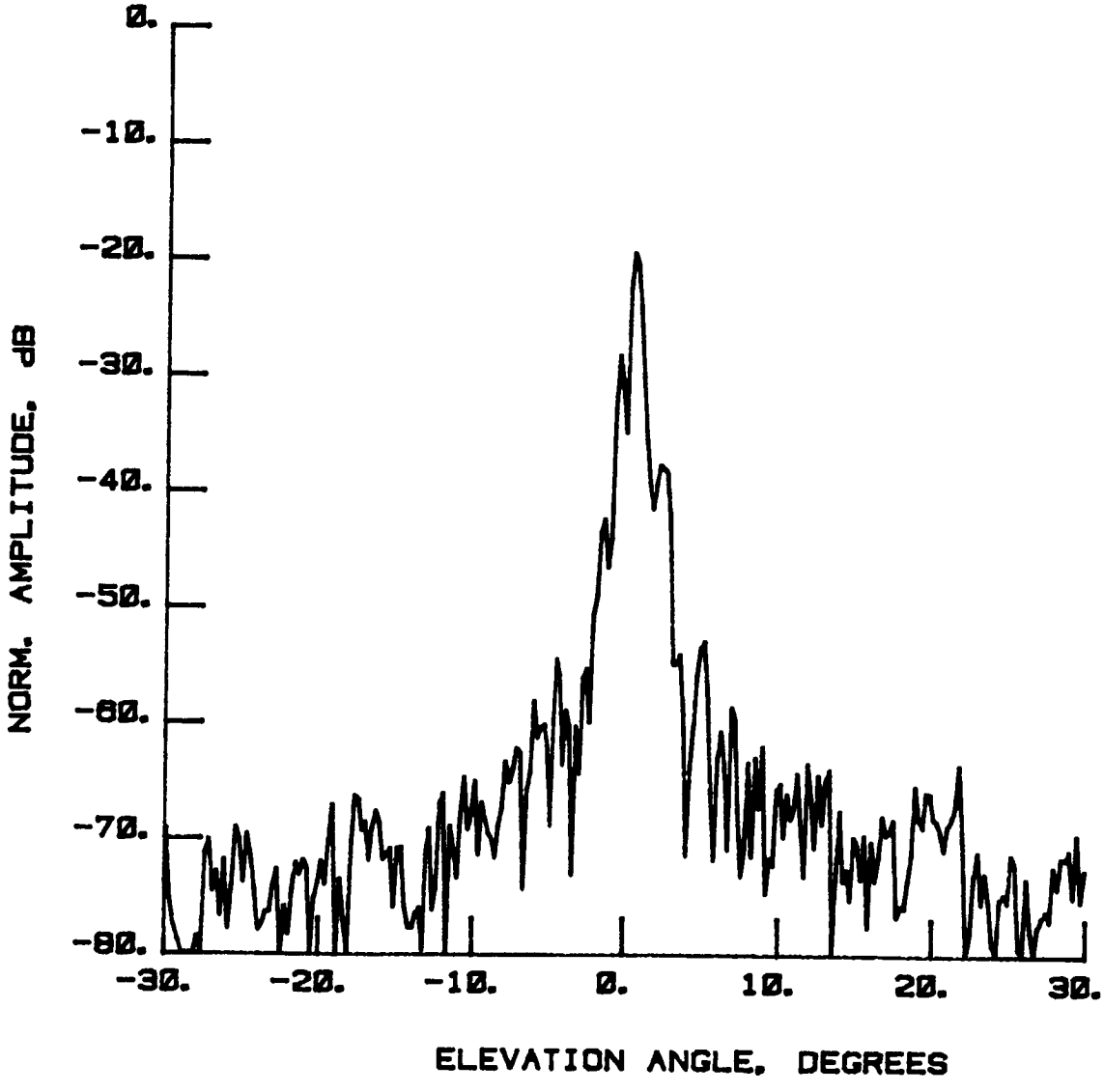

Figure 104 Test 10, 7.73 GHz, Cross-Pol, E-Plane, Type 15

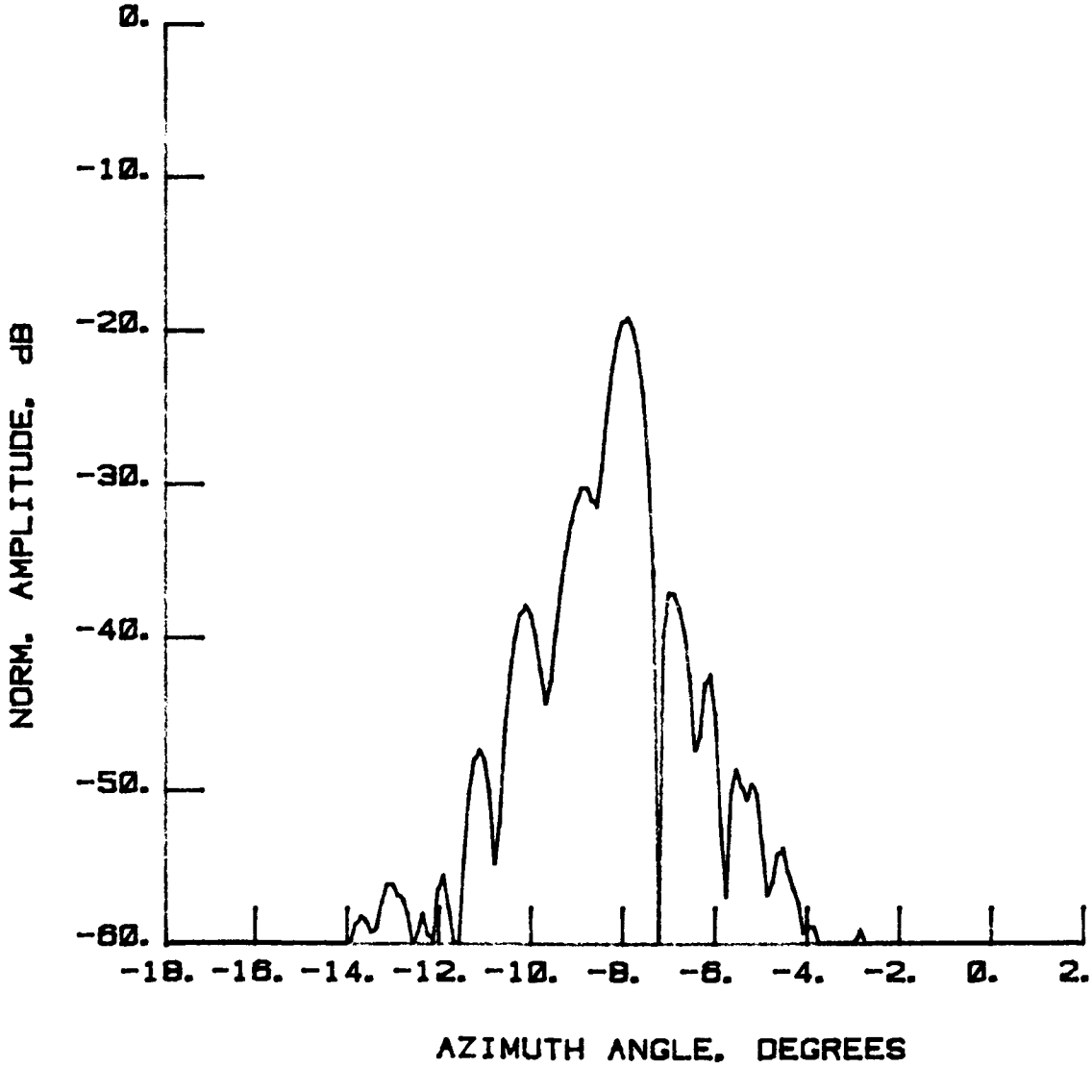

Figure 105 Test 10, 7.73 GHz, Cross-Pol, H-Plane, Type 16

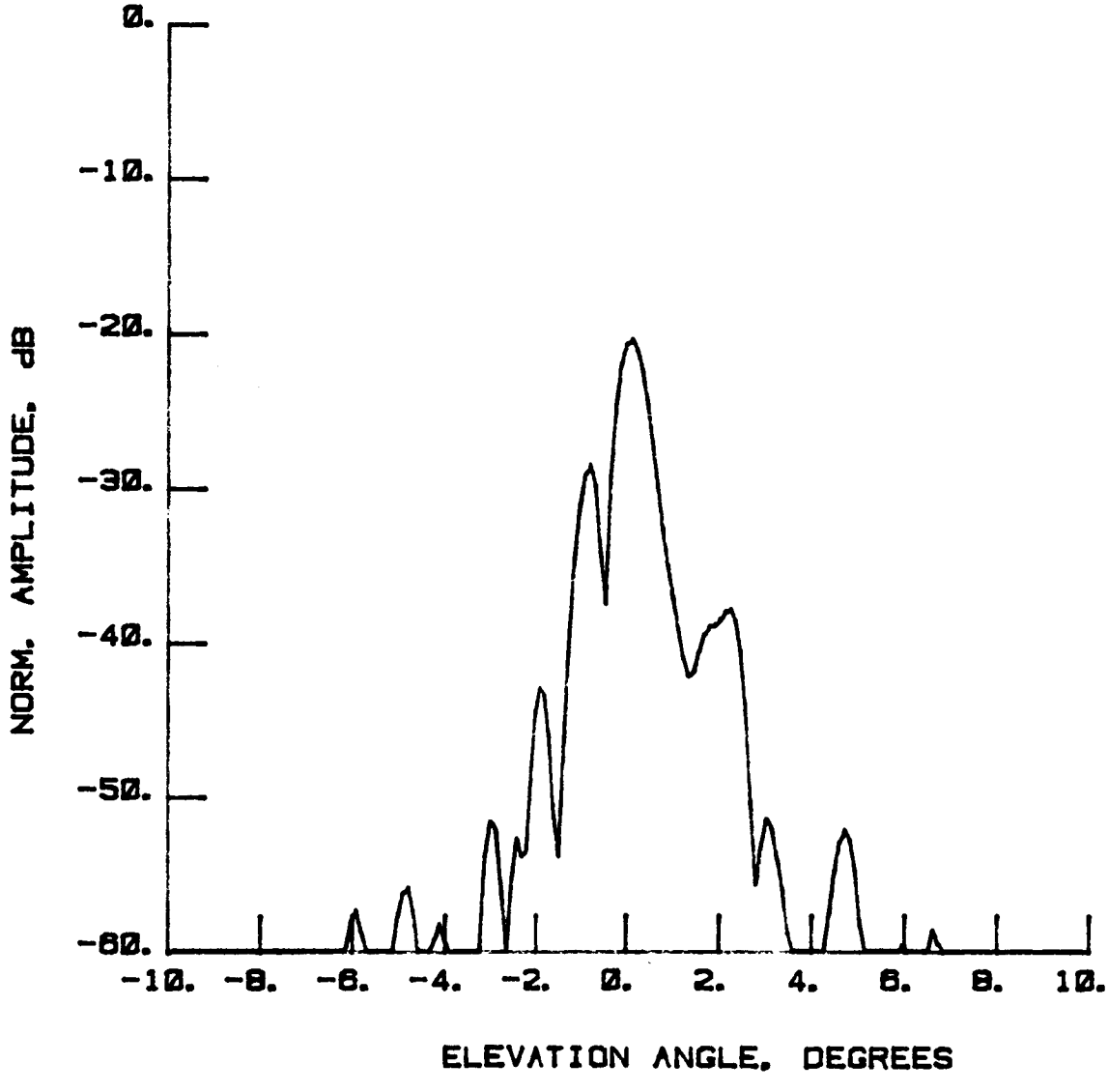

Figure 106 Test 10, 7.73 GHz, Cross-Pol, E-Plane, Type 17

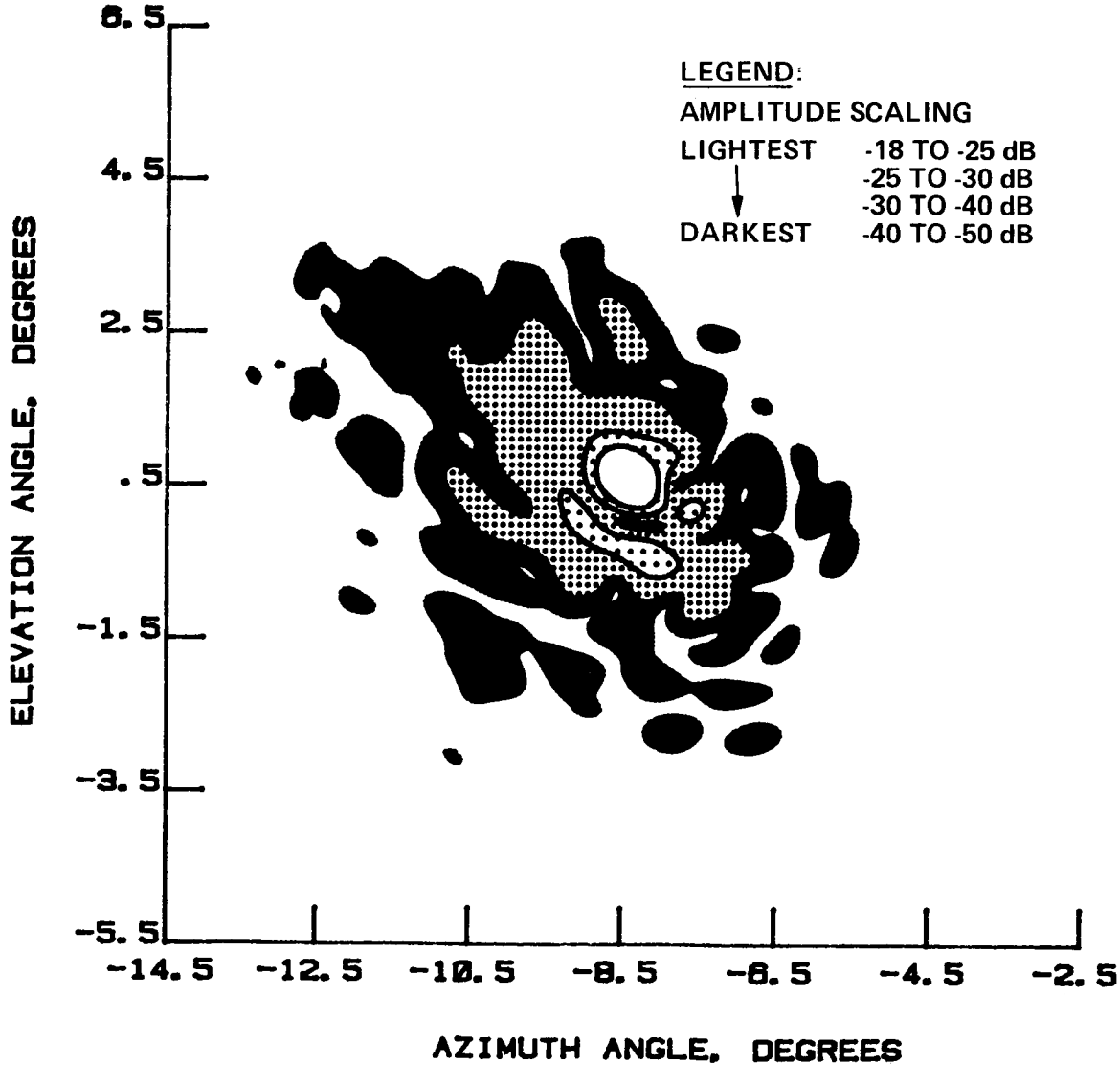

Figure 107 Test 10, 7.73 GHz, Cross-Pol, Contour, Type 18

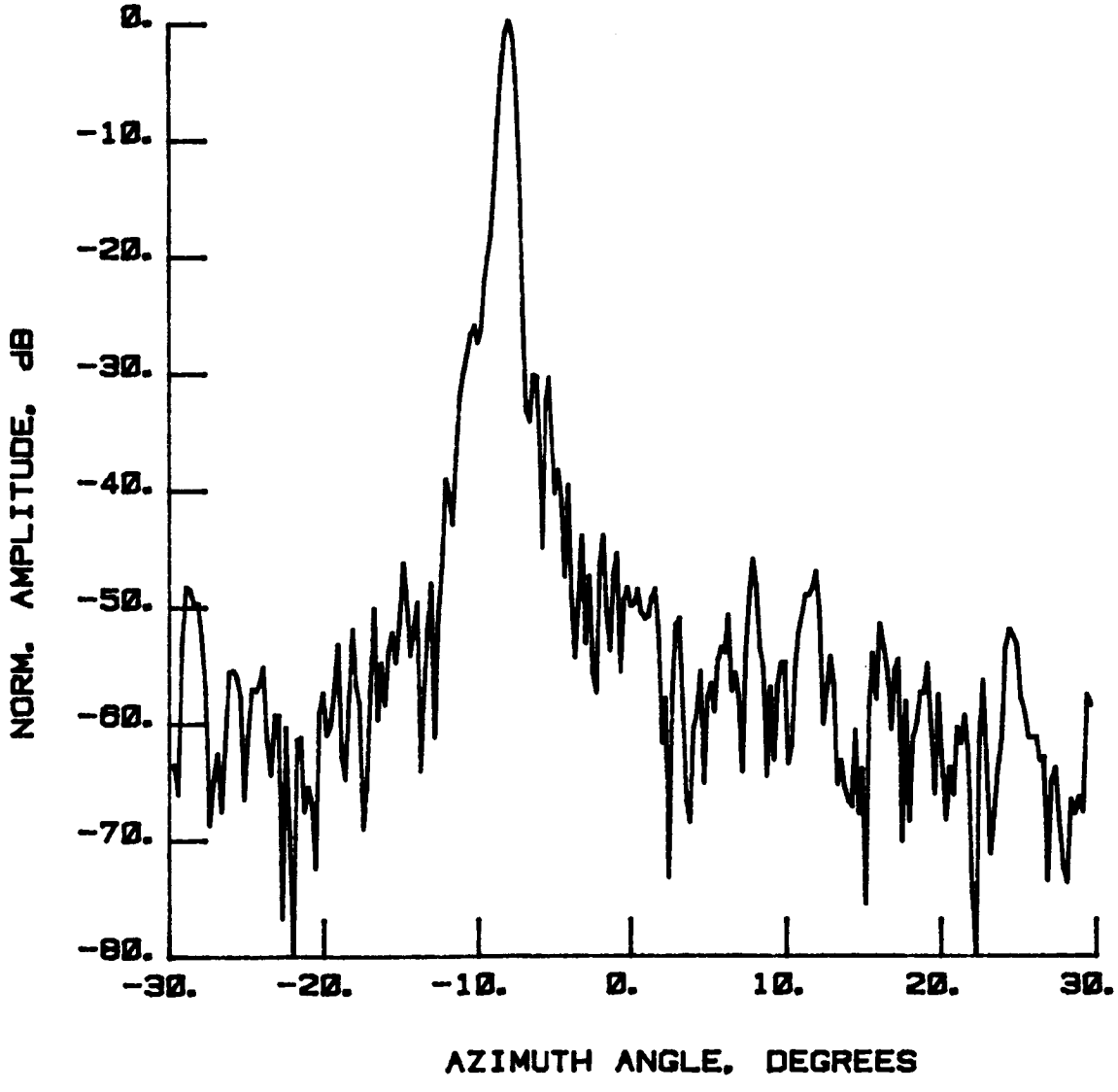

Figure 108 Test 11, 7.73 GHz, Co-Pol, H-Plane, Type 1

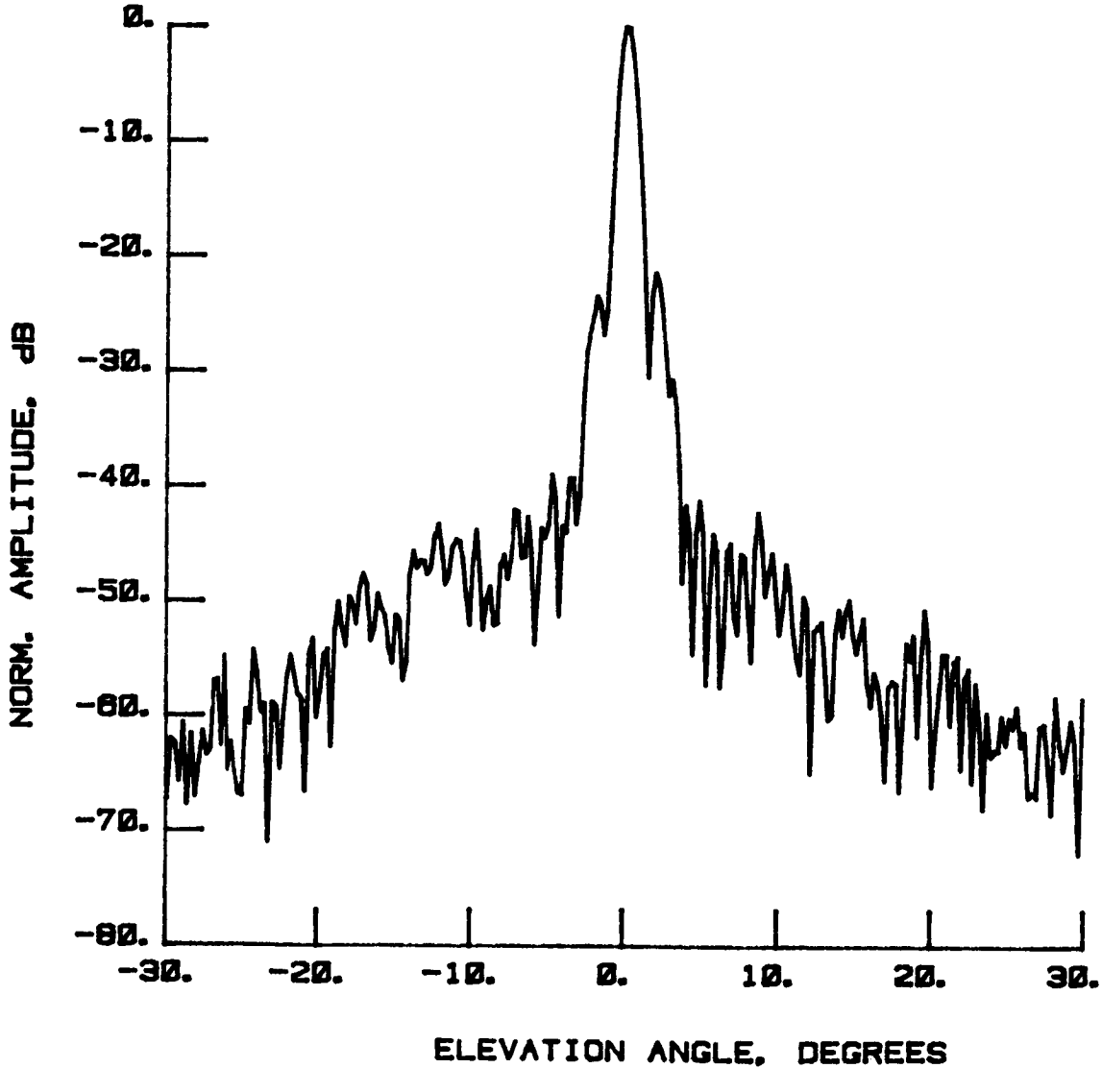

Figure 109 Test 11, 7.73 GHz, Co-Pol, E-Plane, Type 2

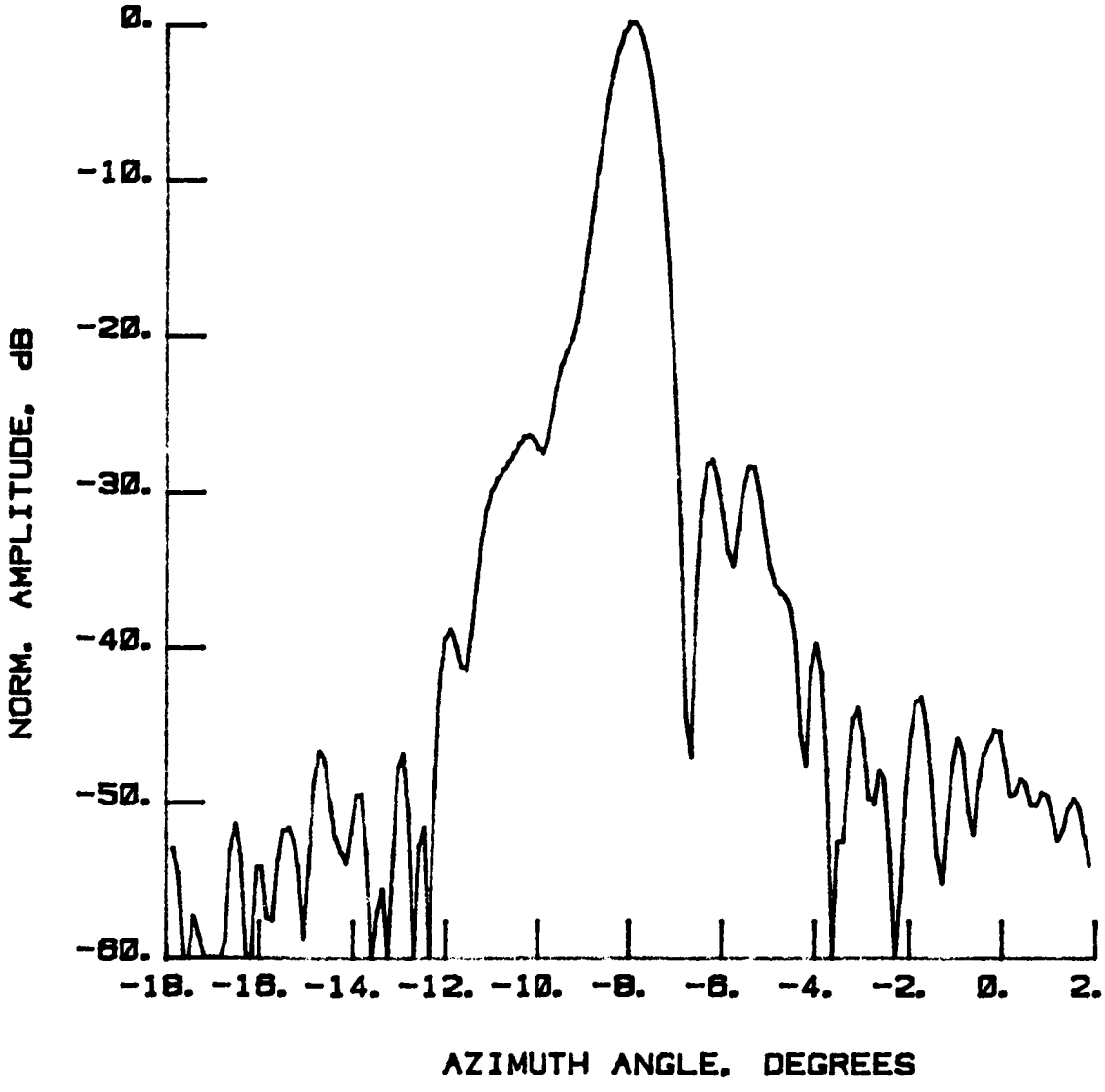

Figure 110 Test 11, 7.73 GHz, Co-Pol, H-Plane, Type 3

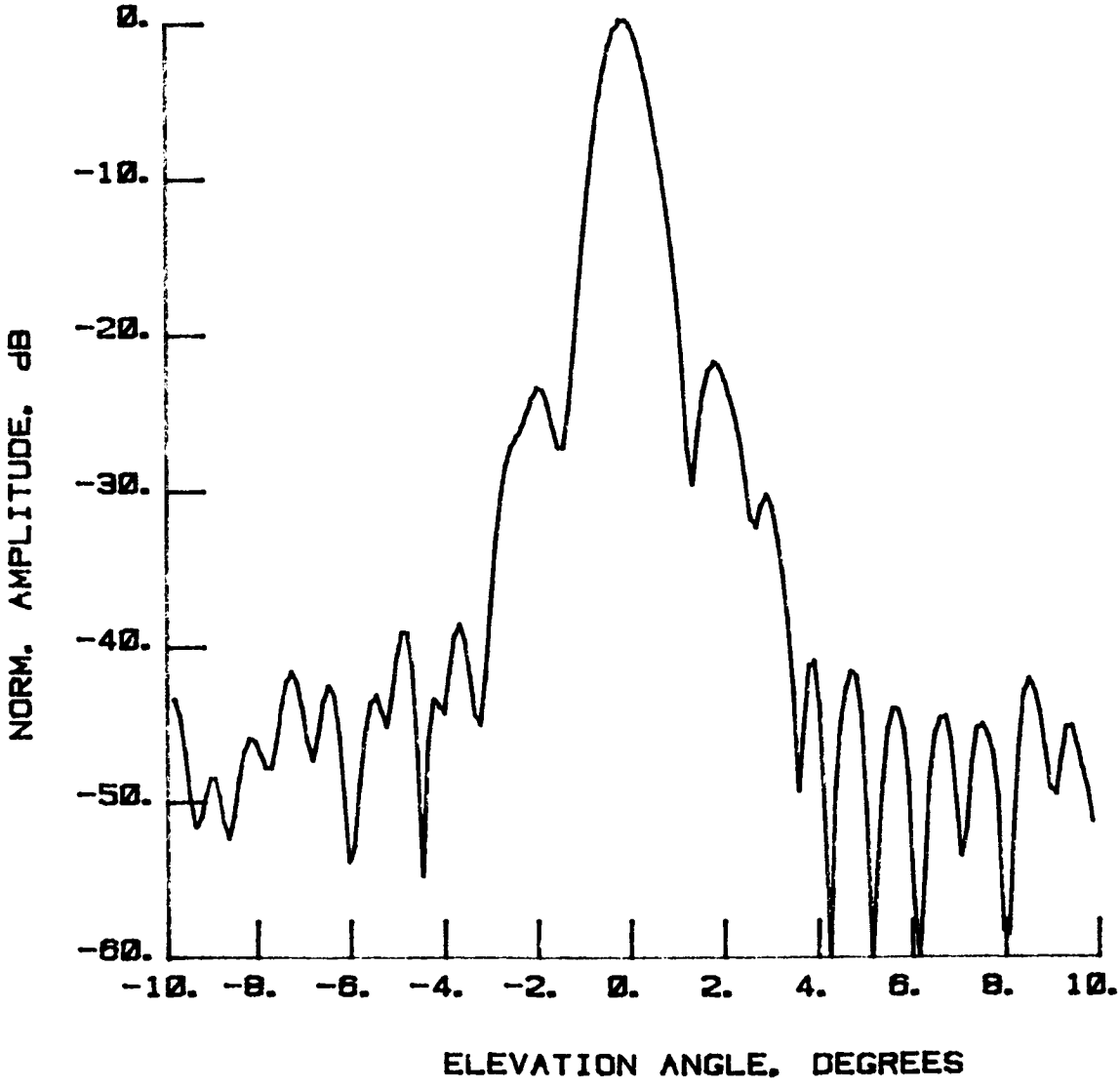

Figure 111 Test 11, 7.73 GHz, Co-Pol, E-Plane, Type 4

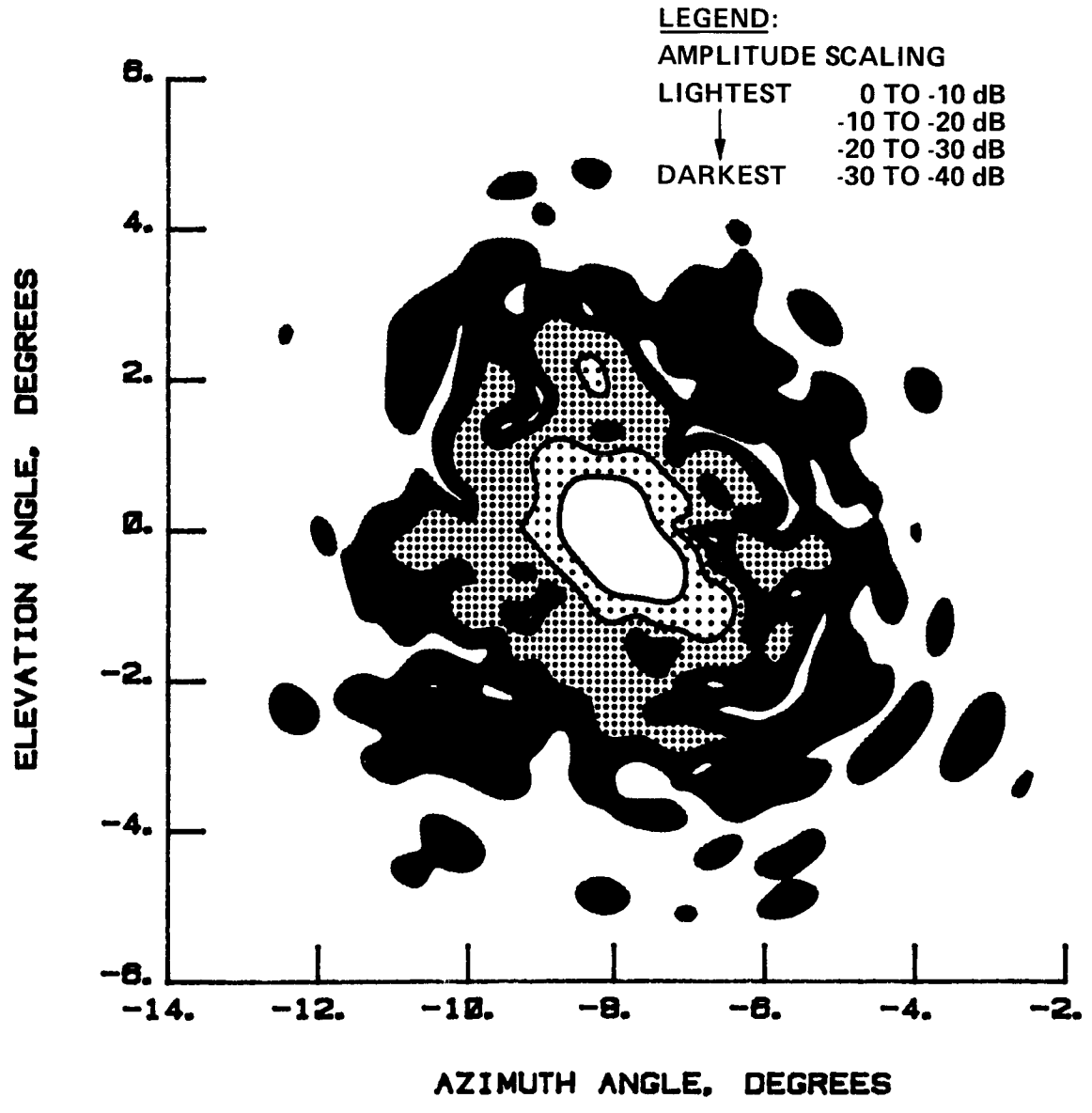

Figure 112 Test 11, 7.73 GHz, Co-Pol, Contour, Type 5

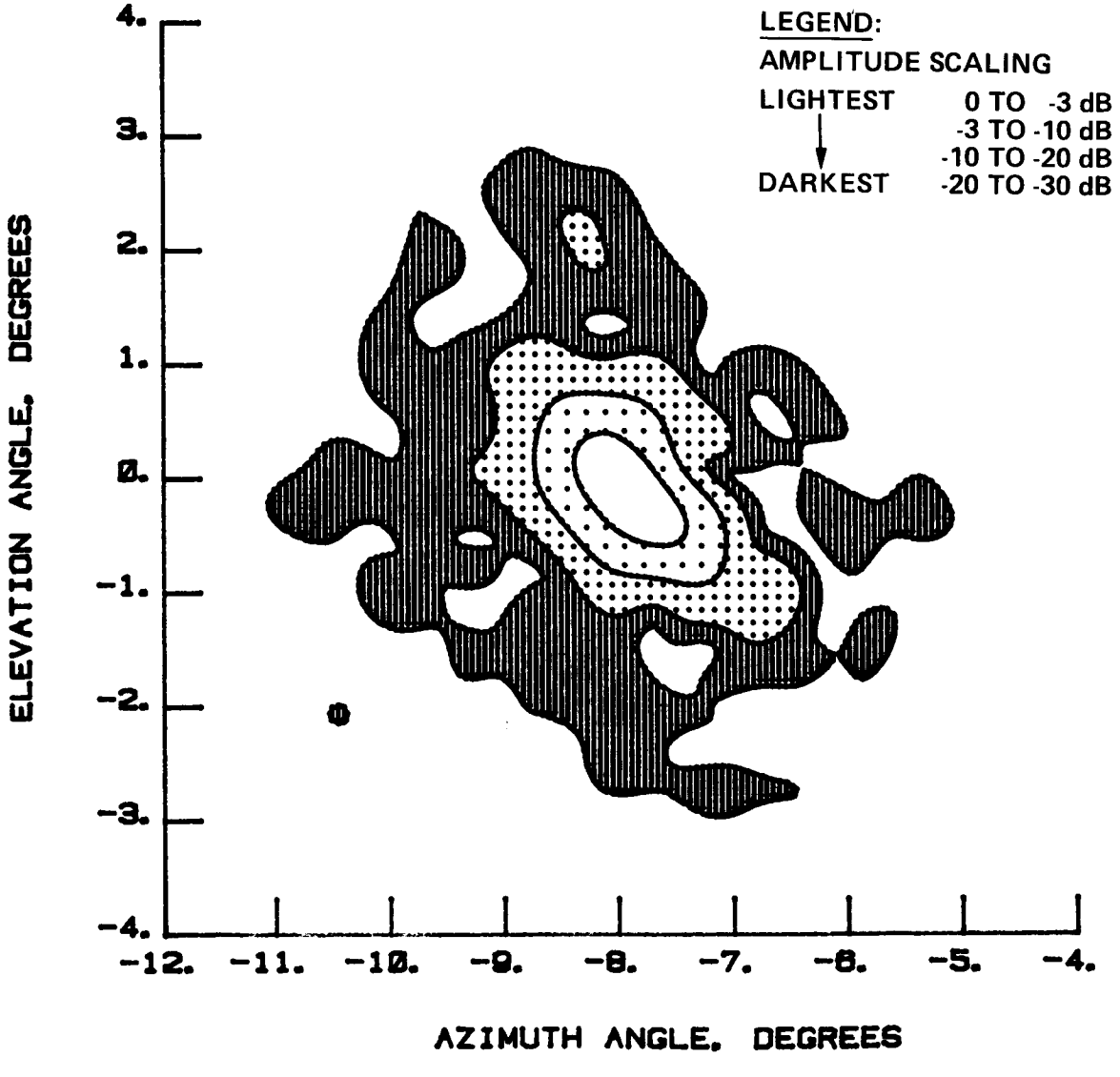

Figure 113 Test 11, 7.73 GHz, Co-Pol, Contour, Type 6

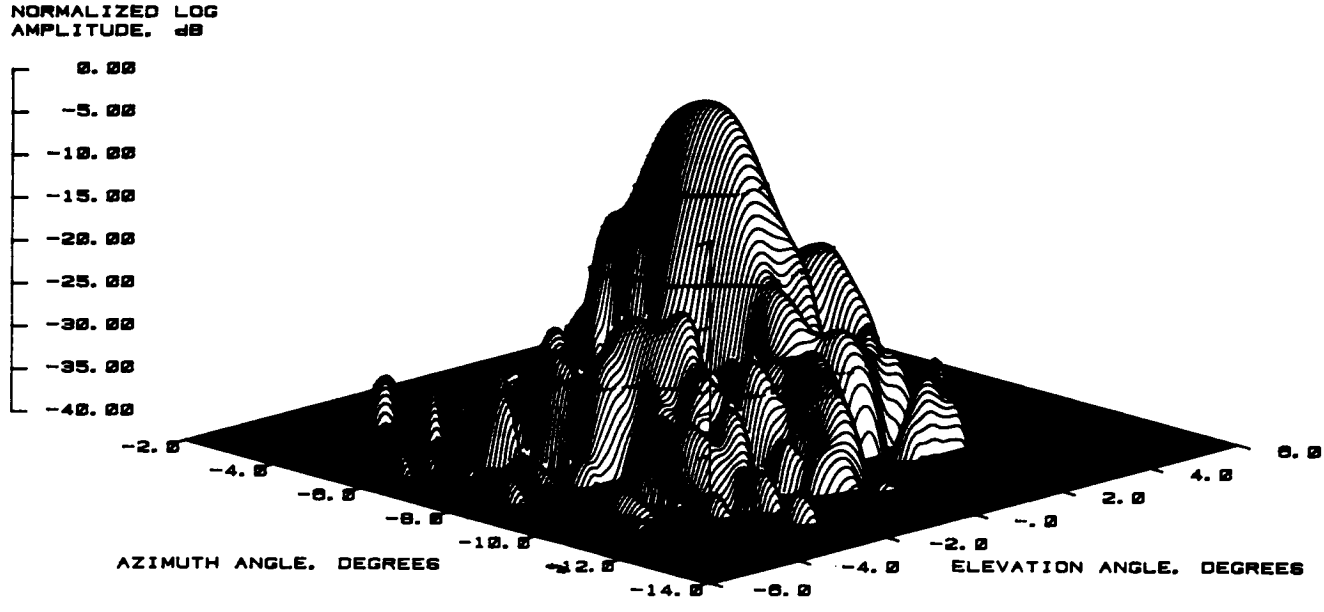

Figure 114 Test 11, 7.73 GHz, Co-Pol, 3-D, Type 7

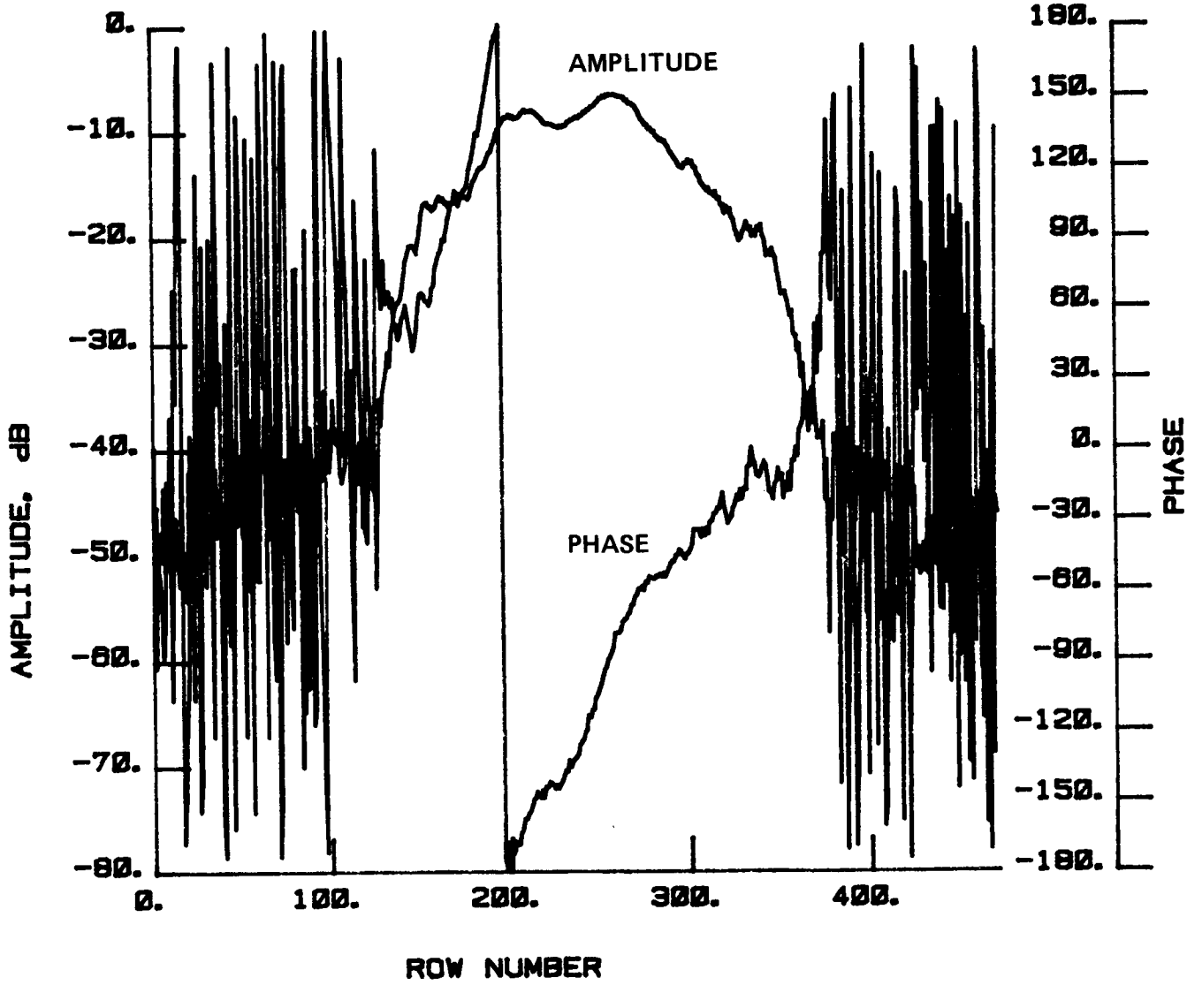

Figure 115 Test 11, 7.73 GHz, Co-Pol, H-Plane, Type 8

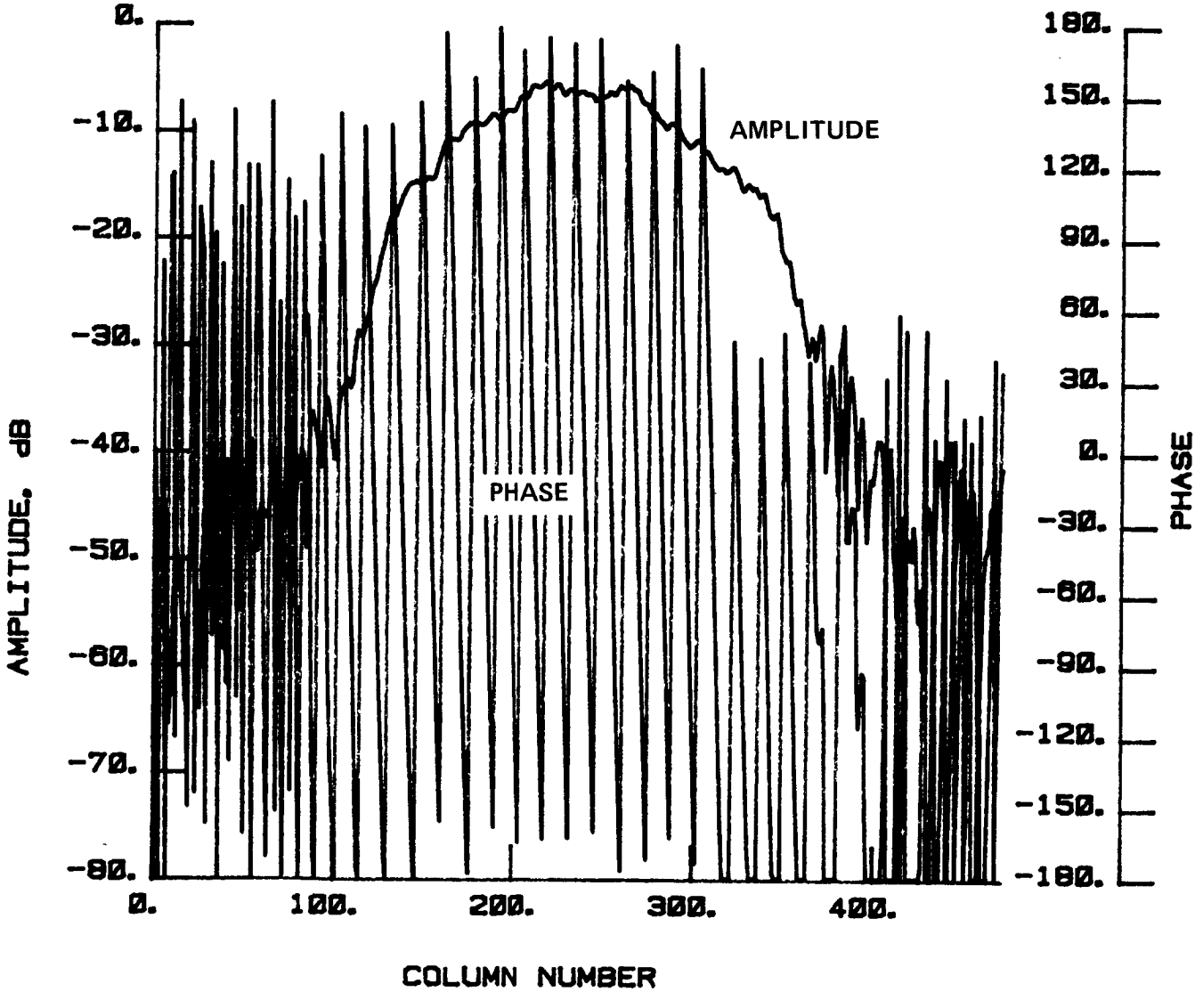

Figure 116 Test 11, 7.73 GHz, Co-Pol, E-Plane, Type 9

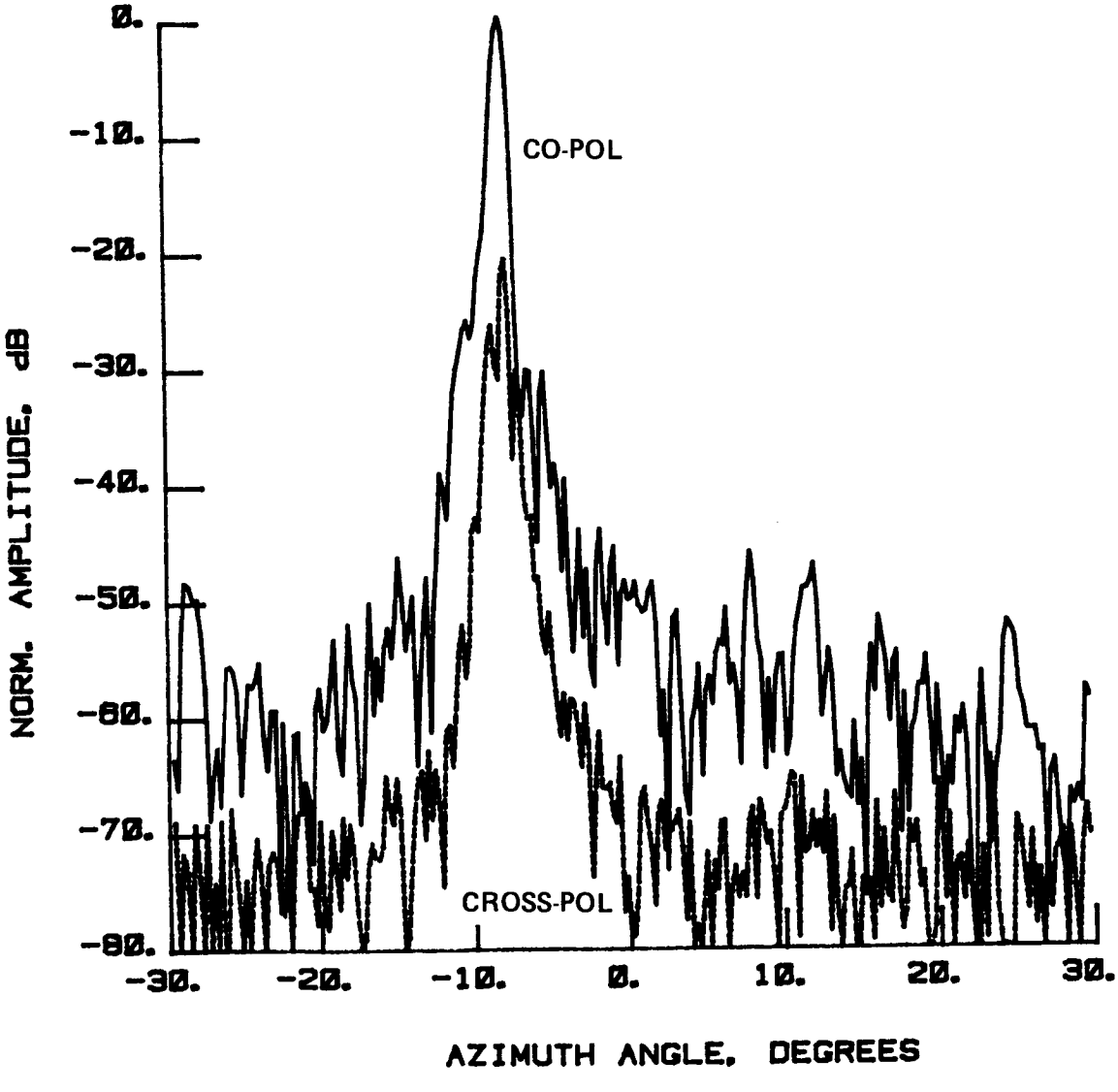

Figure 117 Test 12, 7.73 GHz, Overlay, H-Plane, Type 10

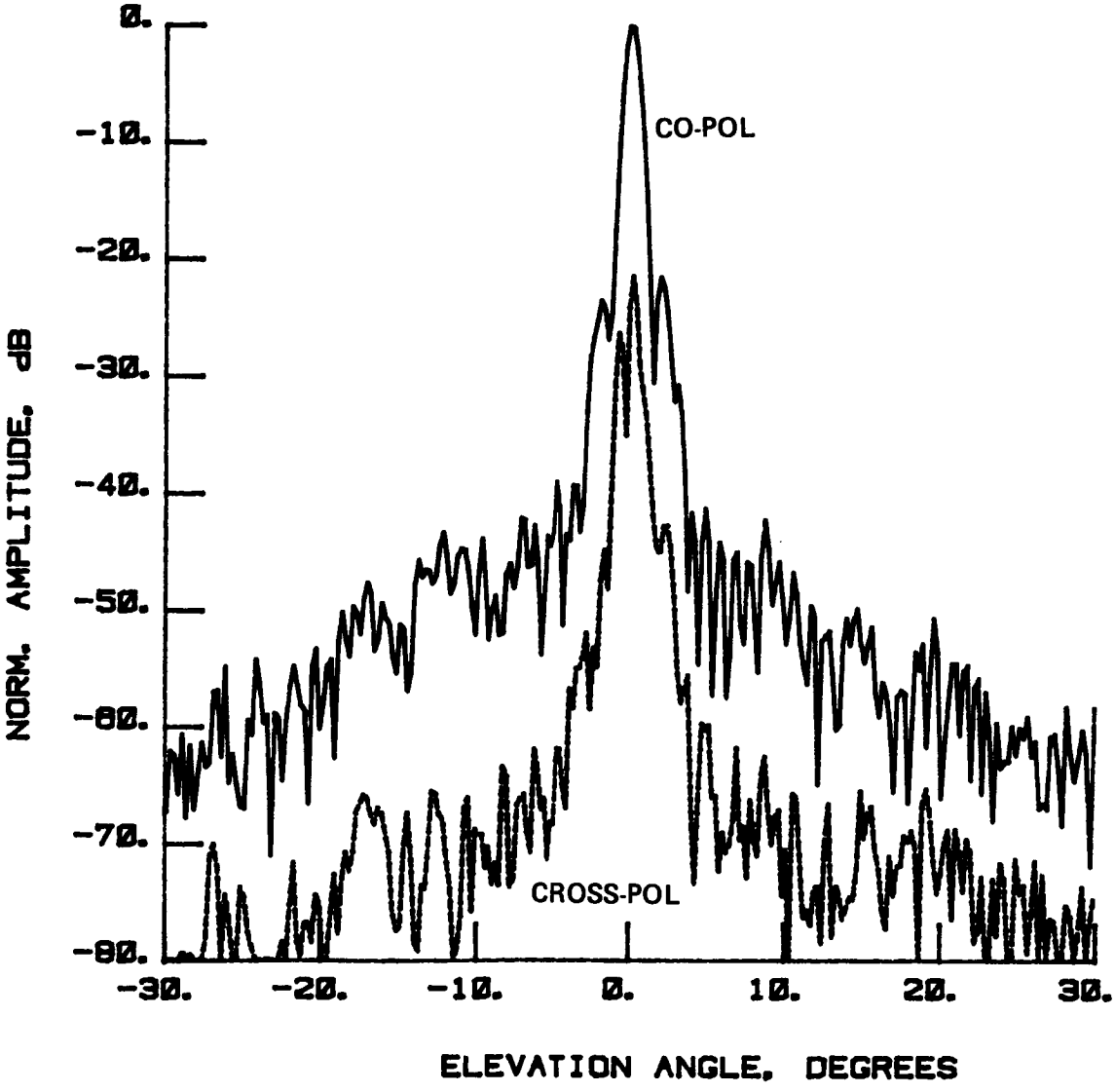

Figure 118 Test 12, 7.73 GHz, Overlay, E-Plane, Type 11

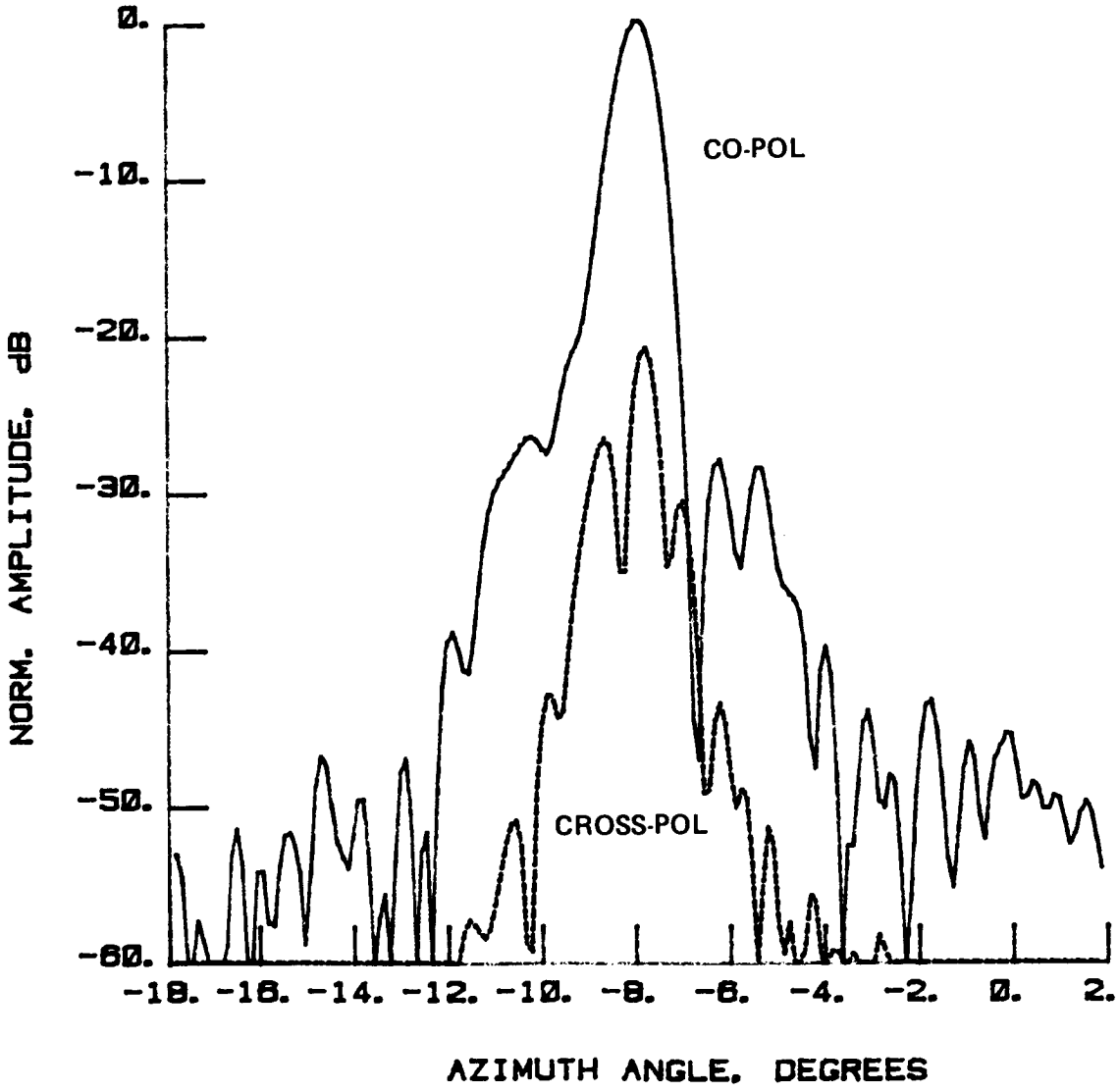

Figure 119 Test 12, 7.73 GHz, Overlay, H-Plane, Type 12

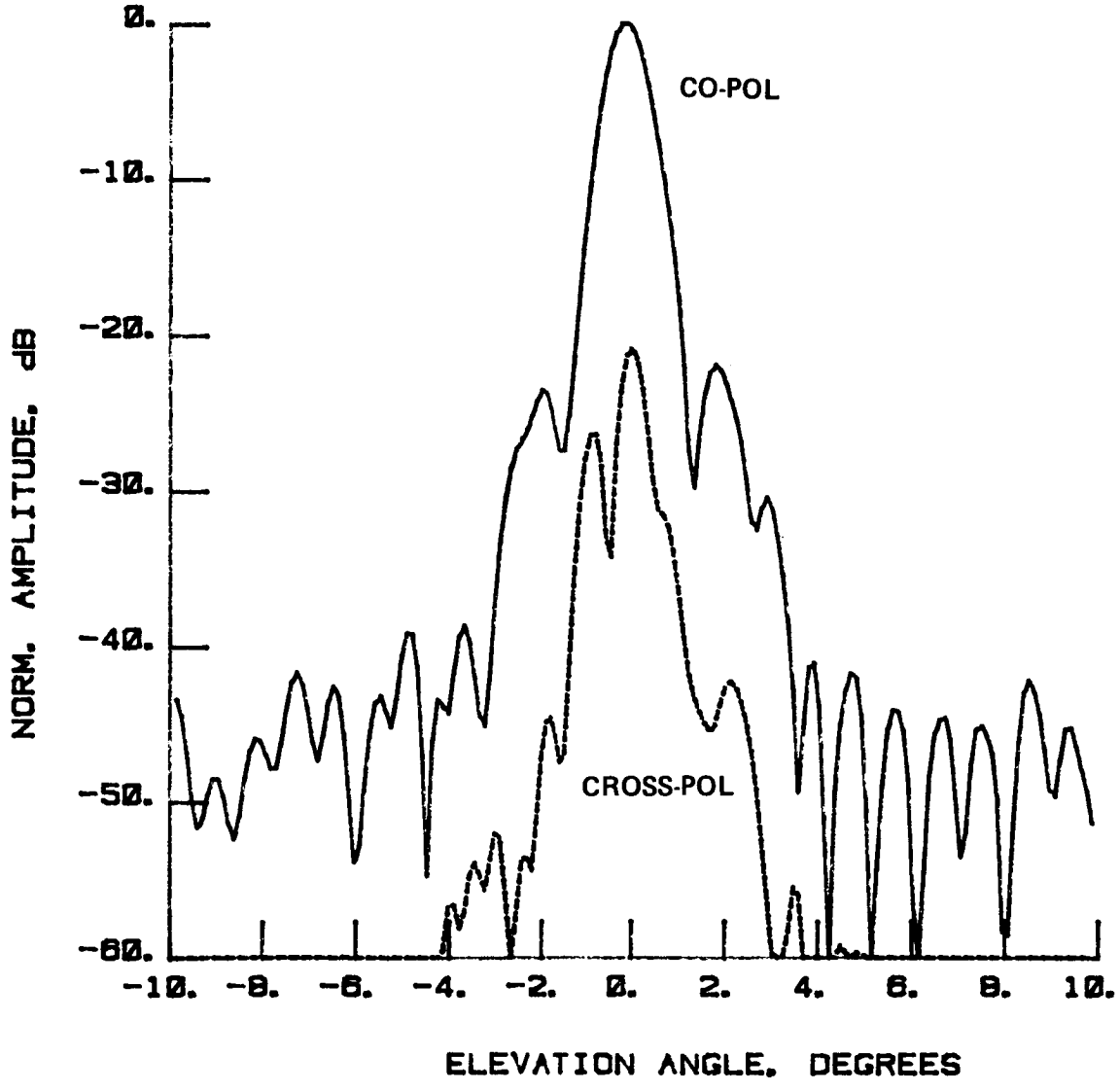

Figure 120 Test 12, 7.73 GHz, Overlay, E-Plane, Type 13

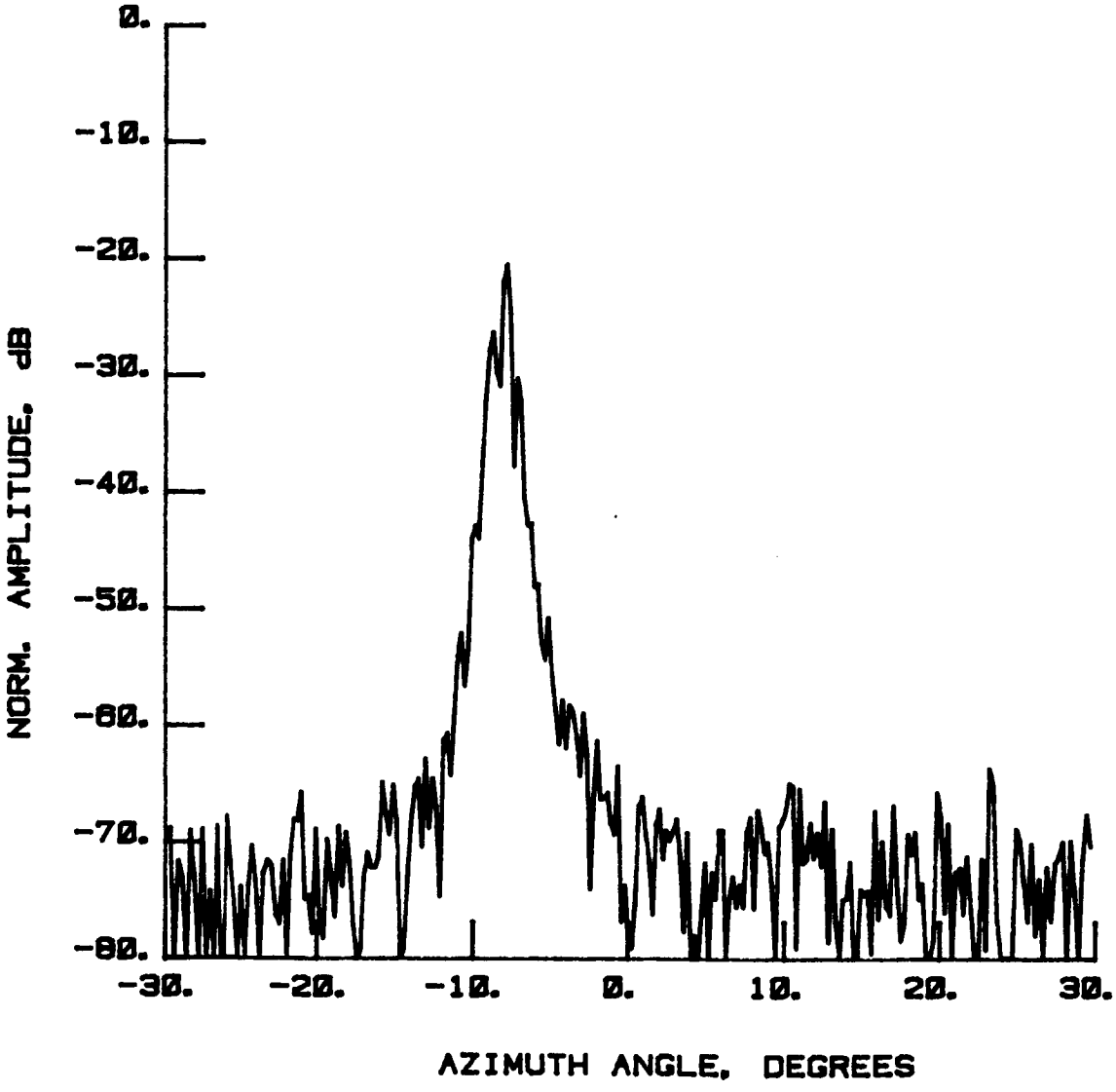

Figure 121 Test 12, 7.73 GHz, Cross-Pol, H-Plane, Type 14

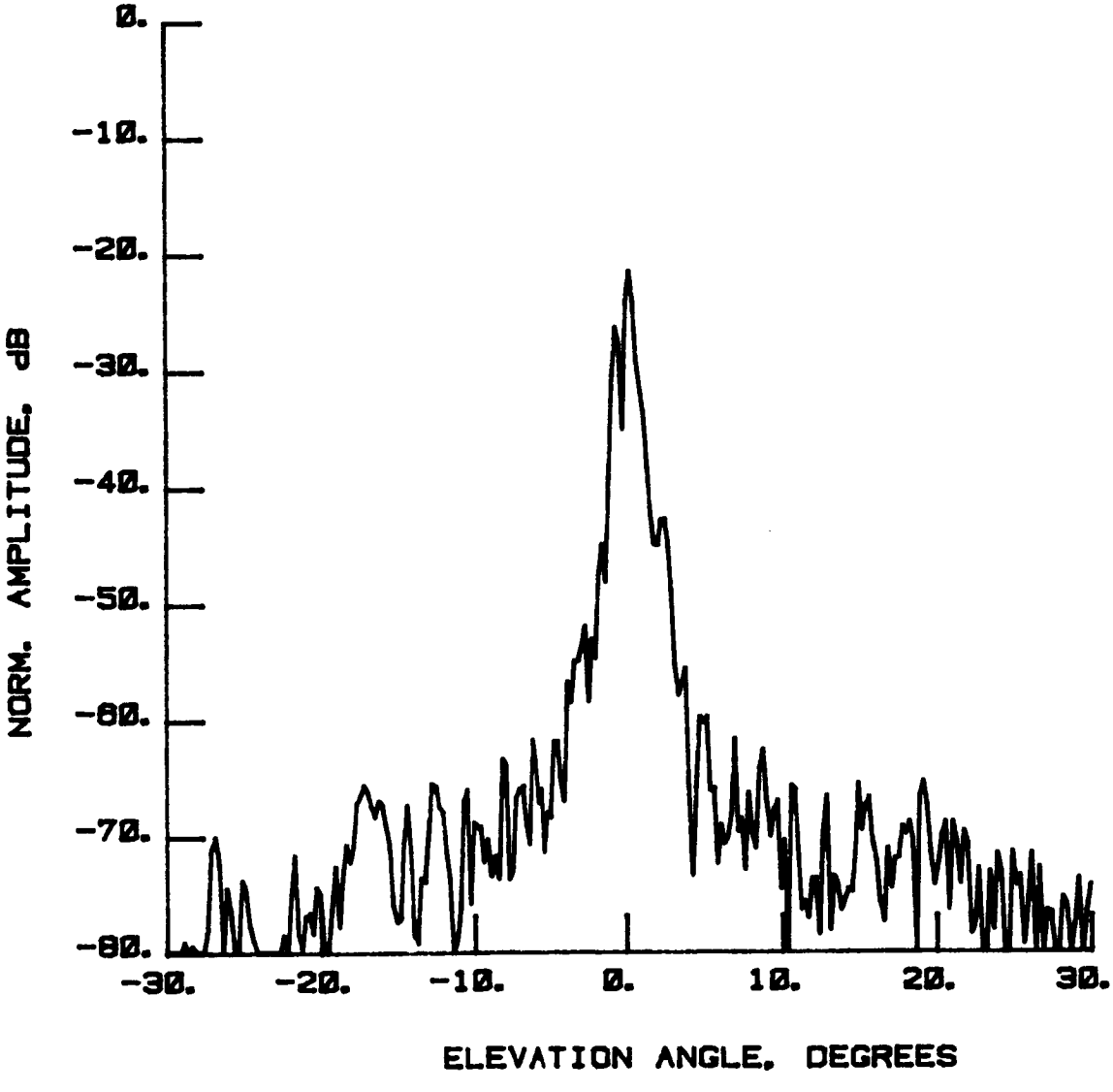

Figure 122 Test 12, 7.73 GHz, Cross-Pol, E-Plane, Type 15

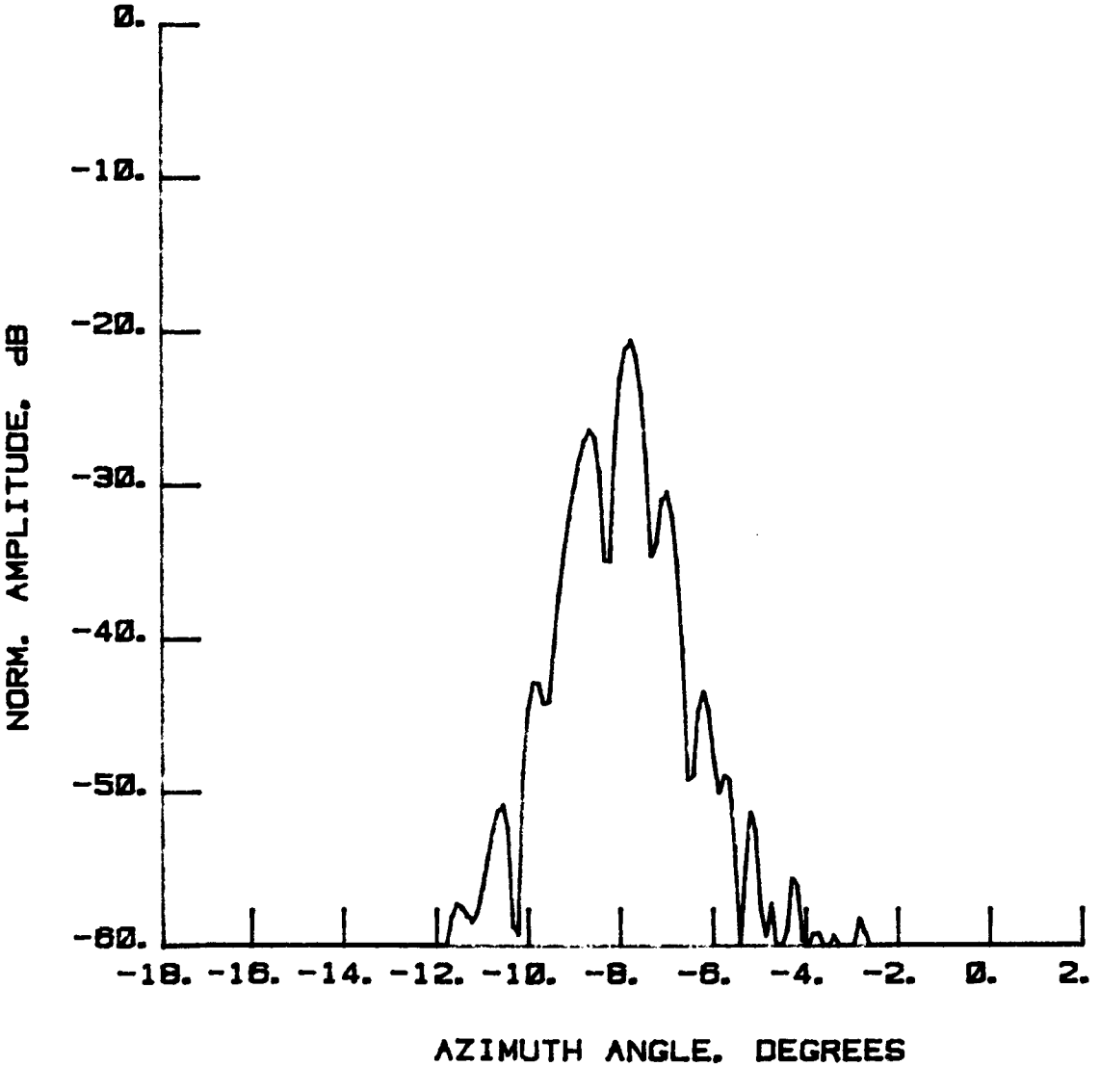

Figure 123 Test 12, 7.73 GHz, Cross-Pol, H-Plane, Type 16

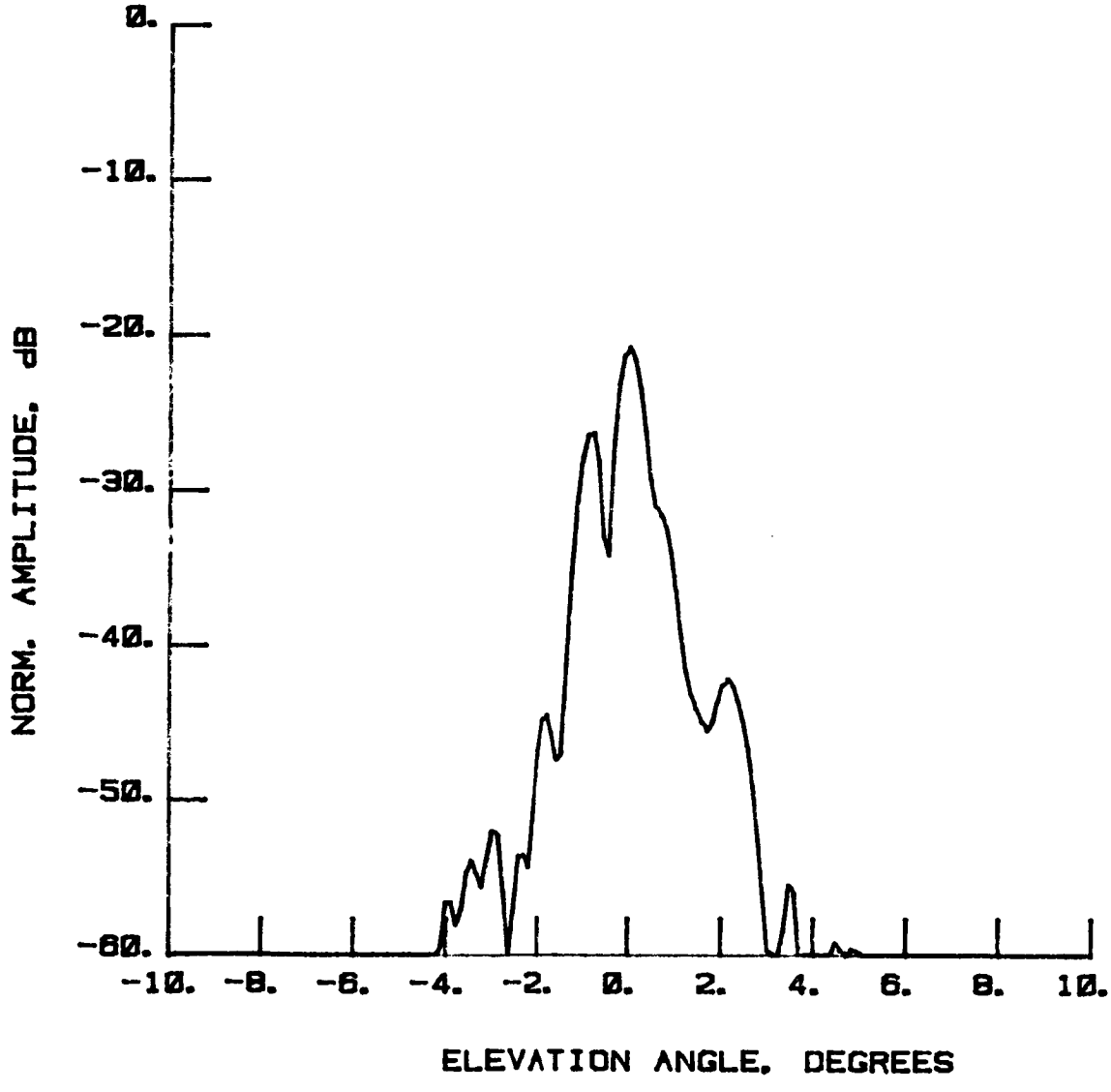

Figure 124 Test 12, 7.73 GHz, Cross-Pol, E-Plane, Type 17

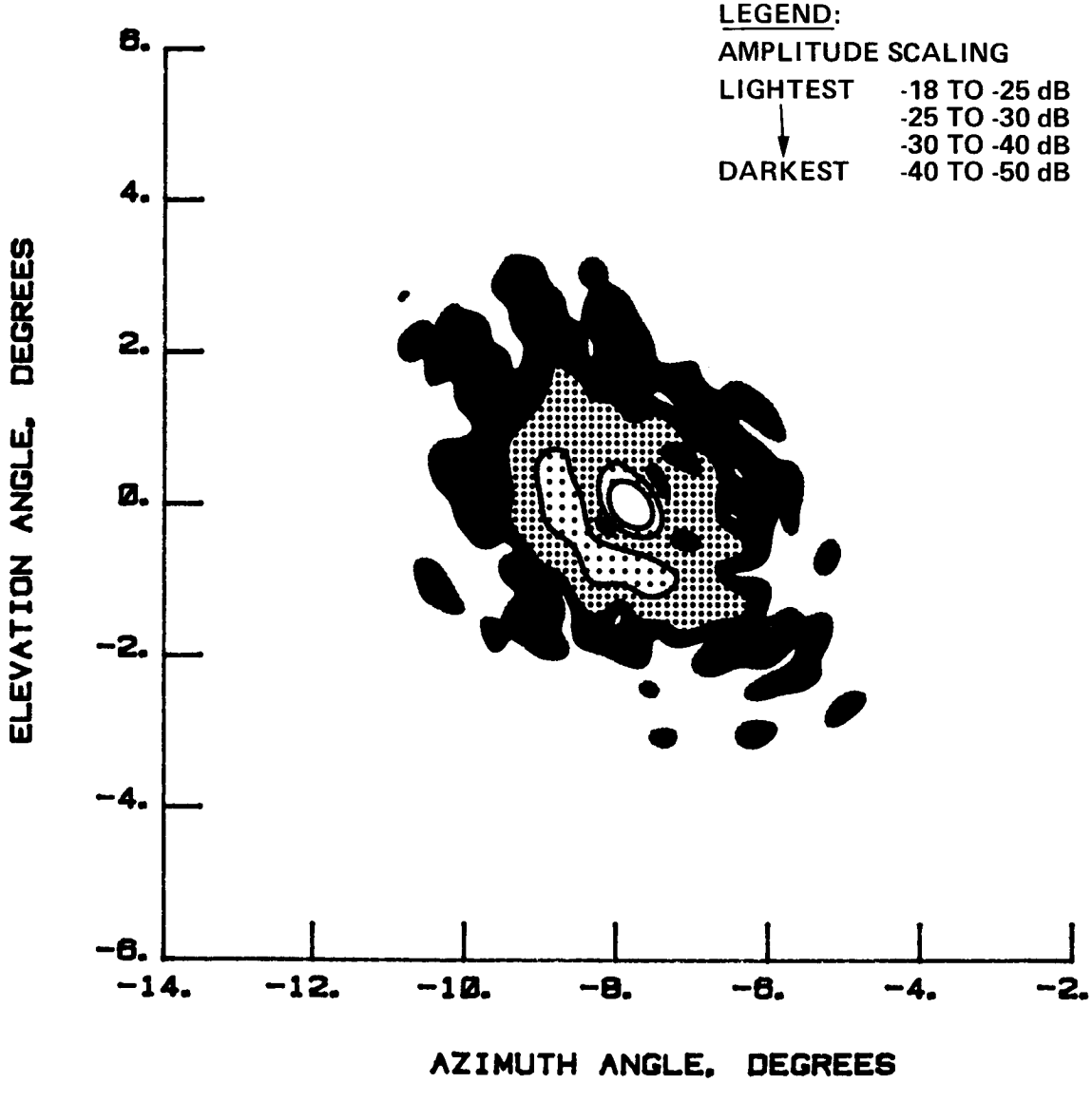

Figure 125 Test 12, 7.73 GHz, Cross-Pol, Contour, Type 18

5.0 DIAGNOSTICS

In addition to generating far-field patterns, the NFTL also analyzed the antenna patterns. This analysis aided in isolating the performance of different components of antenna performance. These components include the feed, electrical surface of the dish, and focusing of the antenna. In order to accomplish this analysis, NFTL developed some fundamental mathematical tools originating from and based on Maxwell's equations. Foremost of these tools, the reconstitution of sources from the far-field found constant use in isolating the determining factors of antenna performance. (See the method described in Ref 1.) This source-reconstitution method bends the far-field phase by a phase taper without changing the amplitude. Unless a source exists that radiates into the front hemisphere between the collection plane and the projected plane (which is distance "d" below the collection plane), a transformation from the far- to near-field using the inverse FFT will produce the lower plane. If a source radiating into the front hemisphere does exist between these two planes, then the NFTL can remove this source using boundary conditions in the region of the source. After removal of the sources, the processing can then continue, using the Fourier transform, until it reconstructs the aperture fields. The aperture fields can then show how the feed illuminated the reflector, the quality of the dish surface, and the accuracy of focusing the reflector.

5.1 DIRECT FEED RADIATION

Tests 1-4 used microstrip patch array designs as feeds. This type of feed has a tendency to produce high grating lobes. Figure 126 shows the near-field amplitude contour at 4.26 GHz using this feed design, and Figure 127 shows this energy projected down 55 in. to the plane of the feed. In Figure 128, an amplitude plot shows these sources isolated in space by a null of more than 30 dB, and shows that the direct radiation converged to a very small high-level source. Although this source has no direct effect on the aperture pattern (as Figures 129 and 130 show), the direct radiation can cause problems when other RF hardware, not protected from electrical interference, is located near the radiating feed. A simple way to reduce the direct radiation of the feed might require enclosing the feed inside a conductor. This would diffuse the direct radiation while changing the aperture illumination only slightly. Figure 131 shows the effect of blocking the direct radiation source.

Since, for the direct radiation, the scanner collected data at approximately 55 in. away from its source, the power levels for Figure 131 approach the level for the reflector cross-pol peak radiation. However, the polarization of these fields may differ because of the actual response of the probe. The probe used at the NFTL, an open-ended waveguide with a low VSWR waveguide-to-coax adapter, has an excellent linear polarization with a low cross-pol near boresight; therefore, it

is a close approximation of an ideal probe. When the probe measures fields such as those in Figure 130, the linear polarization of the probe no longer orients with azimuth elevation components; therefore, the field magnitude may vary 3 dB from the actual level plotted. However, at the levels and angles shown, the critical radiation source in satellite applications would normally be located on the satellite; therefore, this antenna could have high susceptability to the low-level satellite radiation in the configuration used at the NFTL even though boresight performance is excellent.

5.2 ELECTRICAL MAPPING OF THE APERTURE

With the aperture reconstitution method the electrical fields measured in the near-field scan plane can be projected to a plane slightly above the surface. The reflector surface error then correlates with the phase measurements in this plane. Because of the short distance remaining between the surface and the plane containing the phase front, the electrical phase front differs from that of a plane wave over the aperture only as a result of feed defocusing or surface errors directly below the plane. Therefore, if the antenna has a properly focused feed, the surface deviation from a parabola must dominate the phase front's nonplanarity. In this way, the electrical phase map of the aperture becomes equivalent to a plot of surface deviation when scaled to the wavelength of the test. Figure 132 shows a map of the electrical phase over the aperture. This map has equated phase and surface by wavelength. Note that when a reflector becomes part of the antenna, surface errors in the reflector cause twice the shift in phase because the path lengths both to and from the reflector change. The plot in Figure 132 shows that the surface deviation becomes greater than 70 mils (up to 159 mils) in several large areas of the reflector, the important regions being located near the center of the reflector. While these areas may not affect the surface rms because they do not cover a large area, they do dramatically affect the far-field pattern. These surface deviations cause a marked increase in the sidelobes of the antenna when a highly tapered feed illuminates the reflector.

These surface distortions, because of their central location in the reflector, make electrical focusing of the antenna difficult. Normally, the NFTL focuses antennas by checking the near-field scans for quadratic phase errors. Because of this antenna's high f/d, the electrical measurements made at approximately 300 in. from the aperture sometimes yielded misleading results. Even though lateral displacement of the feed for this antenna remained easy to check, axial mispositioning of the feed became difficult to separate from the surface deviations, because a quadratic phase error of only 0.07 wavelengths across the aperture results from an axial mispositioning of one wavelength. Therefore, to accurately focus the antenna, the NFTL had to project the near-field measurement back to the aperture, and even this method only allowed axial focusing accuracy of one inch because surface deviations then began to exceed the effects of quadratic phase error. However, while we could not focus the antenna better electrically, this level of axial defocusing represents less than 0.1 dB in gain loss at 7.73 GHz

and has virtually no effect on the antenna pattern, either cross- or co-pol. Even the gain loss of this level of defocusing remains less than that caused by the surface; the surface loss exceeds 0.3 dB according to the photometric data.

According to metric camera data taken during earlier tests at GDC, the surface had a 13-mil rms roughness as compared to the 30-mil rms now measured. If the effect of the surface deviation on the present aperture phase data is decreased approximately 45%, the result is an approximation of the antenna performance when it had the better surface rms roughness. Figure 133 shows a computed far-field pattern at 7.73 GHz resulting from the approximation. Notice that the highest sidelobe now appears at -30 dB. Gain has improved 0.6 dB, implying that the aperture illumination changed the effective surface losses substantially from the measured rms value. This additional loss, which scales with frequency, must arise from systematic surface errors rather than from the random errors described by surface rms. The errors do cause dramatic changes in the amplitude distribution at the near-field, as shown by comparison of Figures 134 and 135. Changes this pronounced in the amplitude distribution will have a major impact on the gain of the antenna.

5.3 SEAM EFFECTS OF THE REFLECTOR

Figure 136 shows in a contour format the effect that we had noticed in previous H-plane plots at 7.73 GHz and 11.60 GHz. To ensure that this effect arose only from the antenna, the same test was done with the antenna rotated 15° to the scanner. Figure 137 shows the results. After some analysis, the data showed that the source of this broad sidelobe could only occur on the reflector surface. Not only did the effect occur on the reflector, it was also approximately the same width as the reflector diameter. Only two structures on the reflector measure 200 in. long with the narrow width to create sidelobes to 40°. These structures, the seam in the mesh across the center of the reflector and the truss underneath the reflector, satisfy the geometry required for this source. However, it seems more likely that this high-sidelobe region arises from the seam discontinuity in the surface because the mesh has low transmission characteristics and because transmission has to occur through the mesh twice for any reflections below the mesh to appear in the far-field pattern. In order for the seam to produce this sidelobe effect, it would have to cause a step change in the phase over the seam that corresponded to approximately 0.15% of the total field power. This percentage approaches the amount of power received by the reflector over the region of the seam.

This seam effect does not occur in the cross-pol envelope. This probably means that the effect has direct correlation to the aperture illumination. Because the cross-pol illumination approaches a null over the antenna seam, the fields incident on the seam having a cross-pol orientation will not have any effect on the far-field.

5.4 DEFOCUSING EFFECTS OF STEERING

Figure 138 shows the major problem involved in steering parabolic antennas by moving the feed. The plotted phase front shows a cubic phase error caused by steering the antenna 8° in the H-plane. This distortion shows an apparent phase bow of almost a wavelength across the aperture. This phase front nonplanarity will easily cause most of the degradation seen in the far-field patterns of Tests 11 and 12. To reduce this phase error significantly, the use of an adaptive feed to compensate for the phase errors seen at the aperture, while a complex design problem, seems the most likely way to improve the steered antenna pattern under the current geometric configuration.

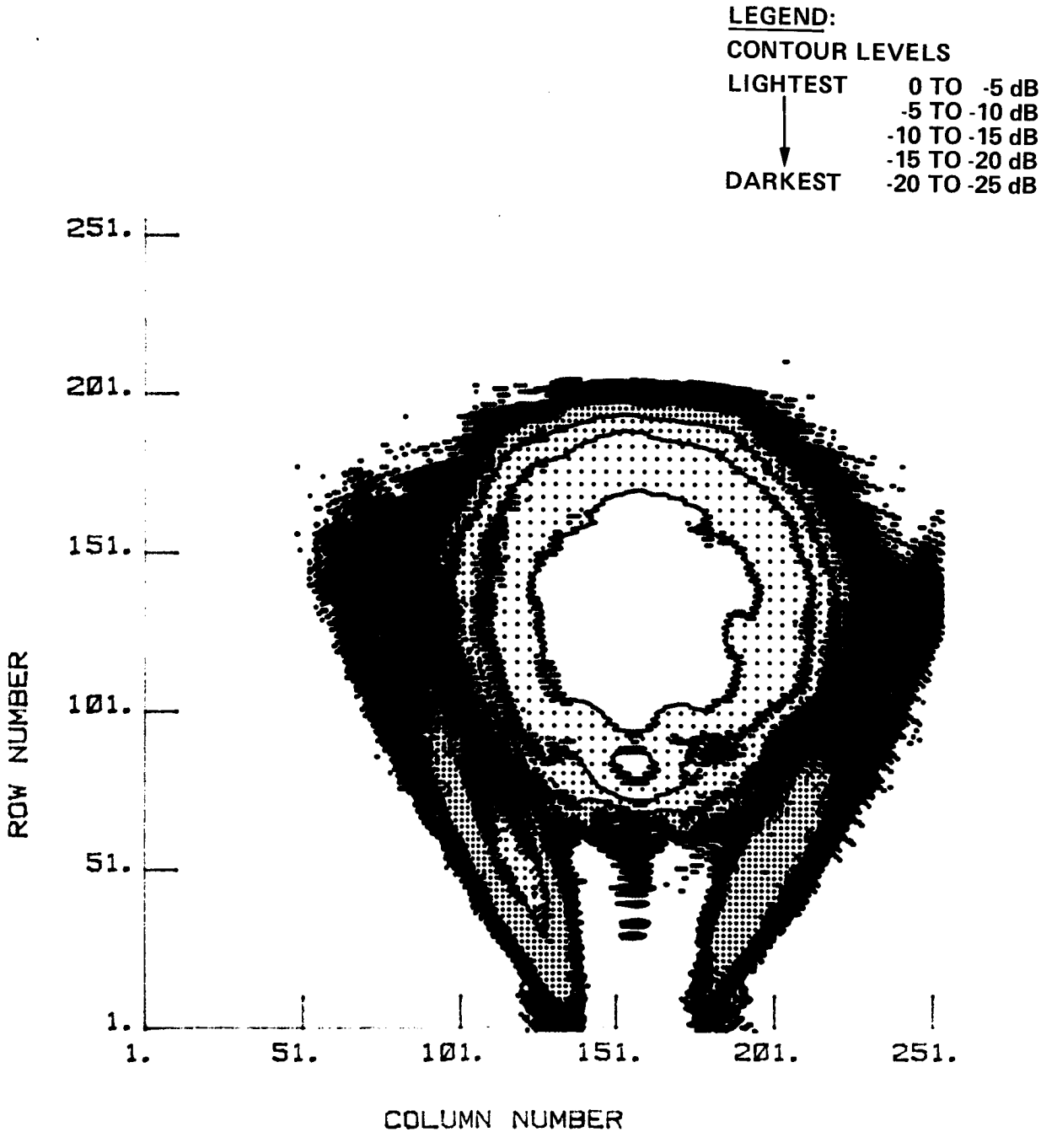

Figure 126 Near-Field Amplitude Contour, 4.26 GHz

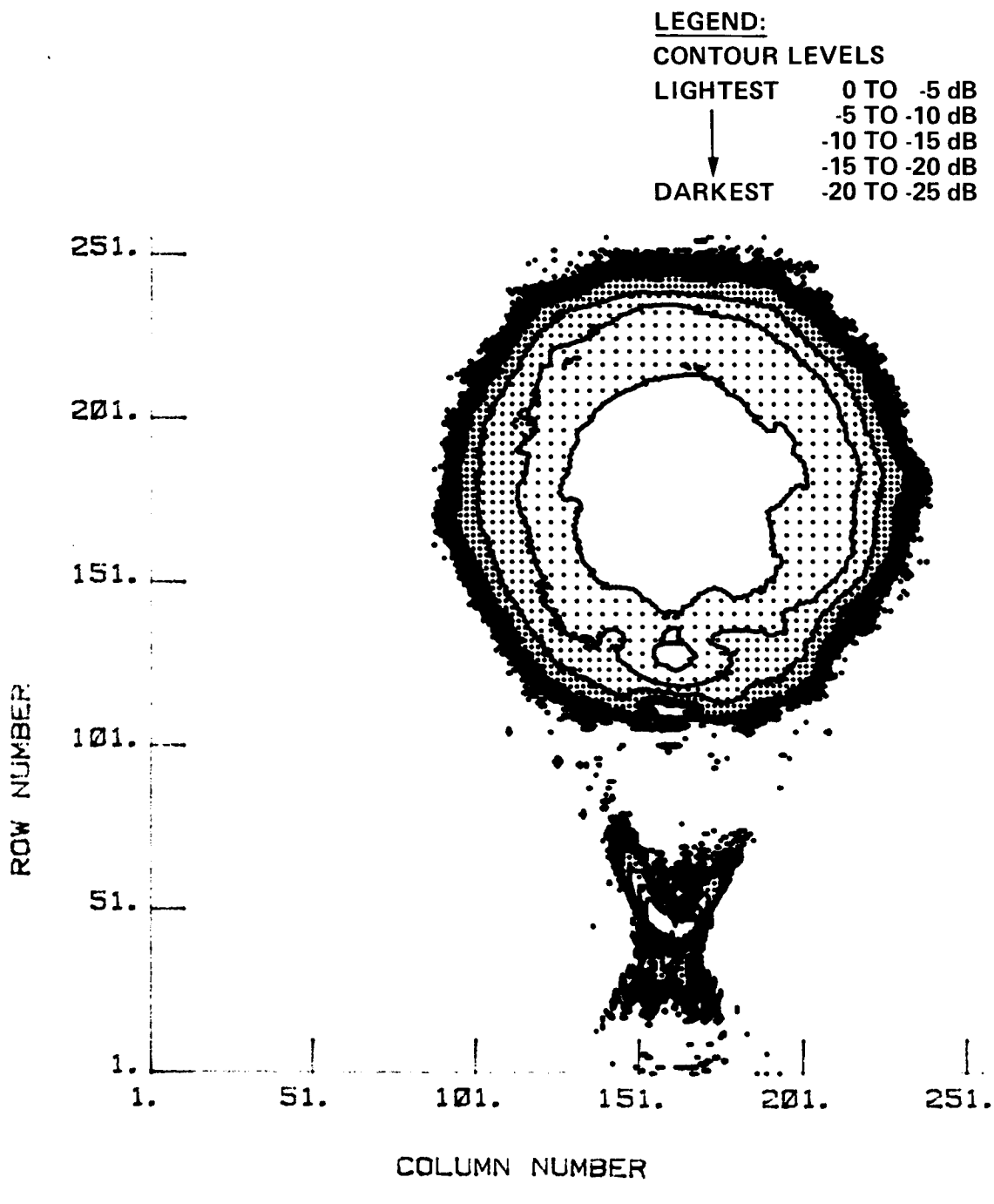

Figure 127 Near-Field Projected Down 55 in. to Feed

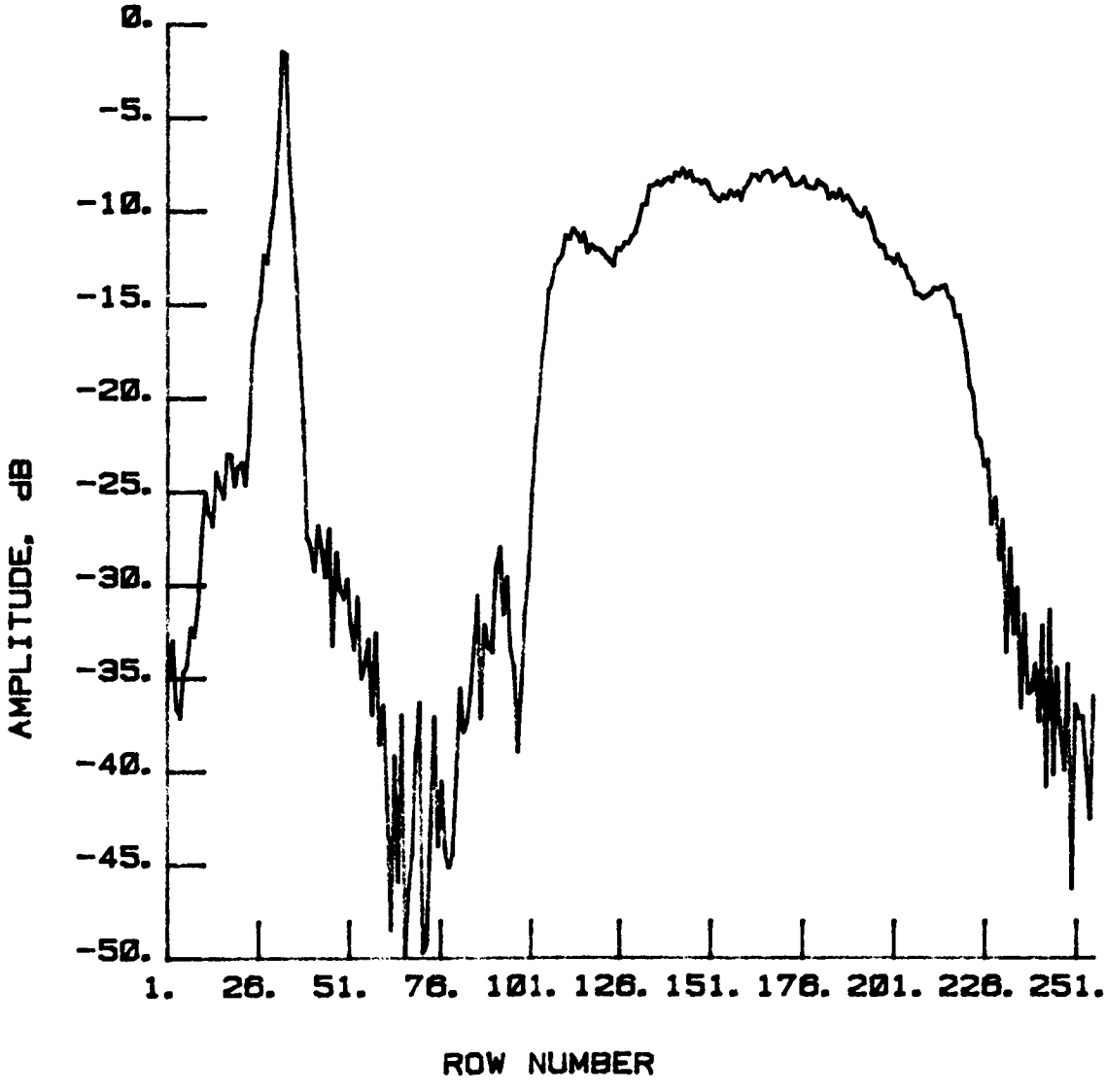

Figure 128 Centerline Showing Feed Radiation

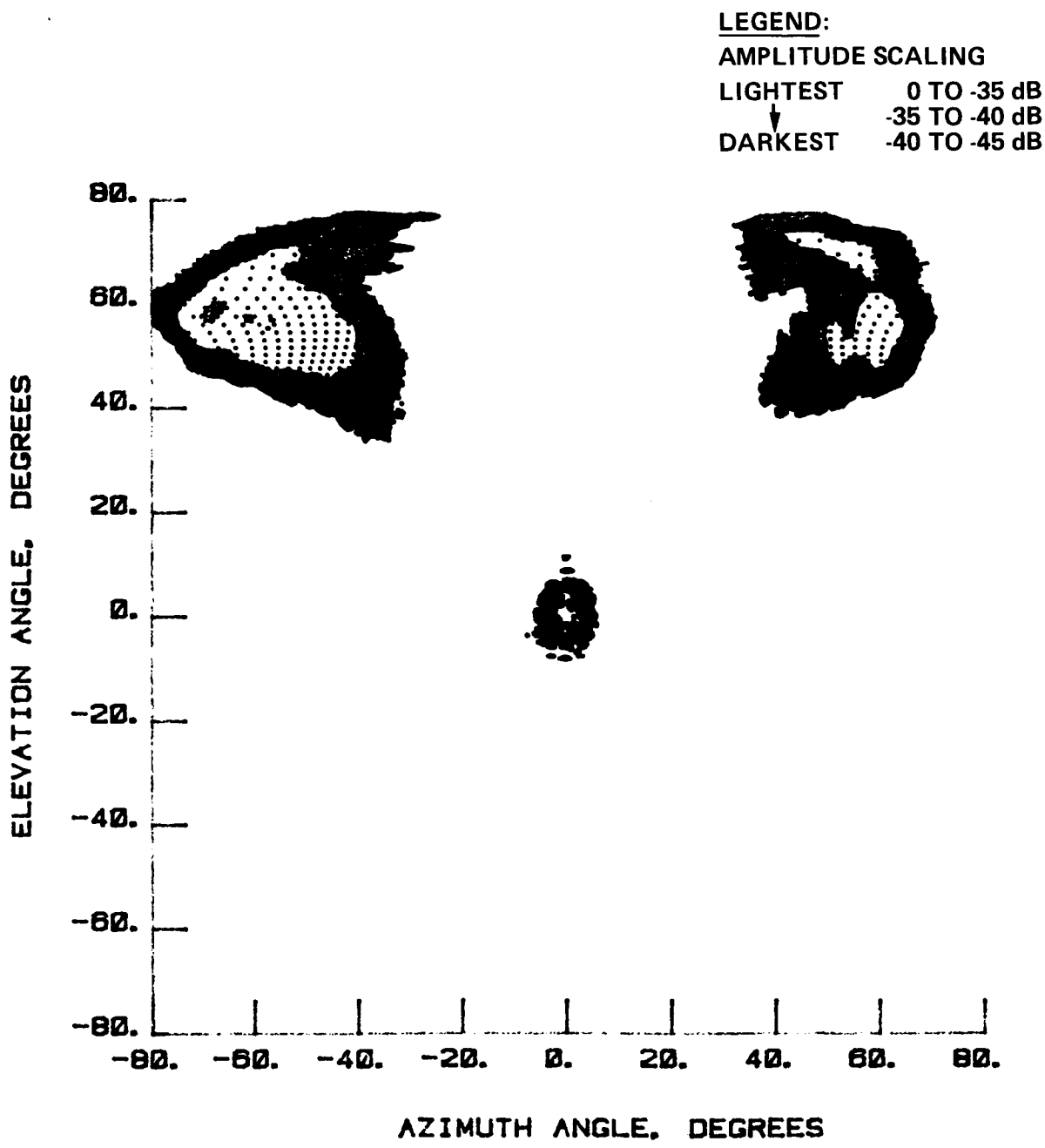

Figure 129 Far-Field Pattern

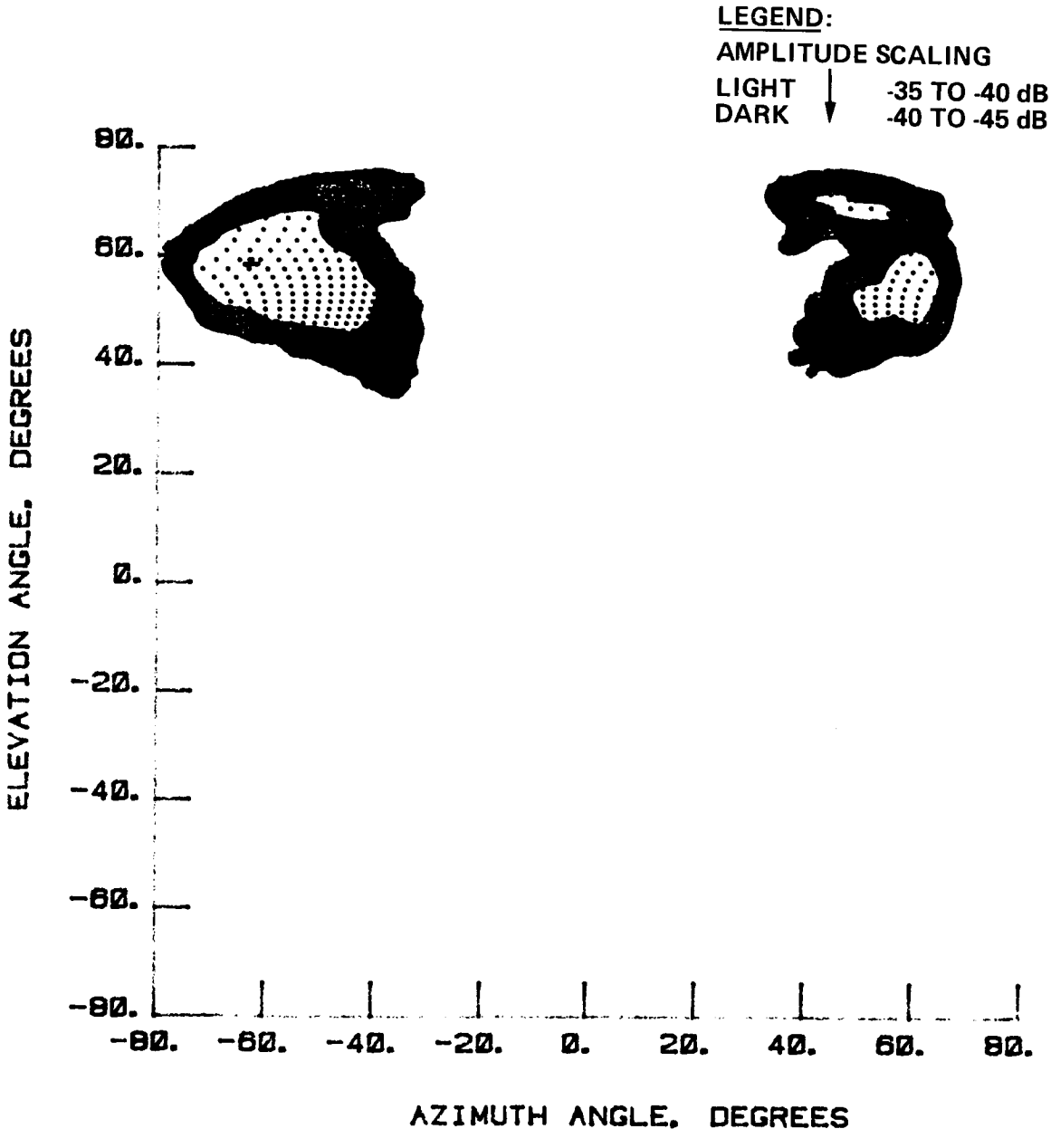

Figure 130 Far-Field Pattern from Direct Feed Radiation

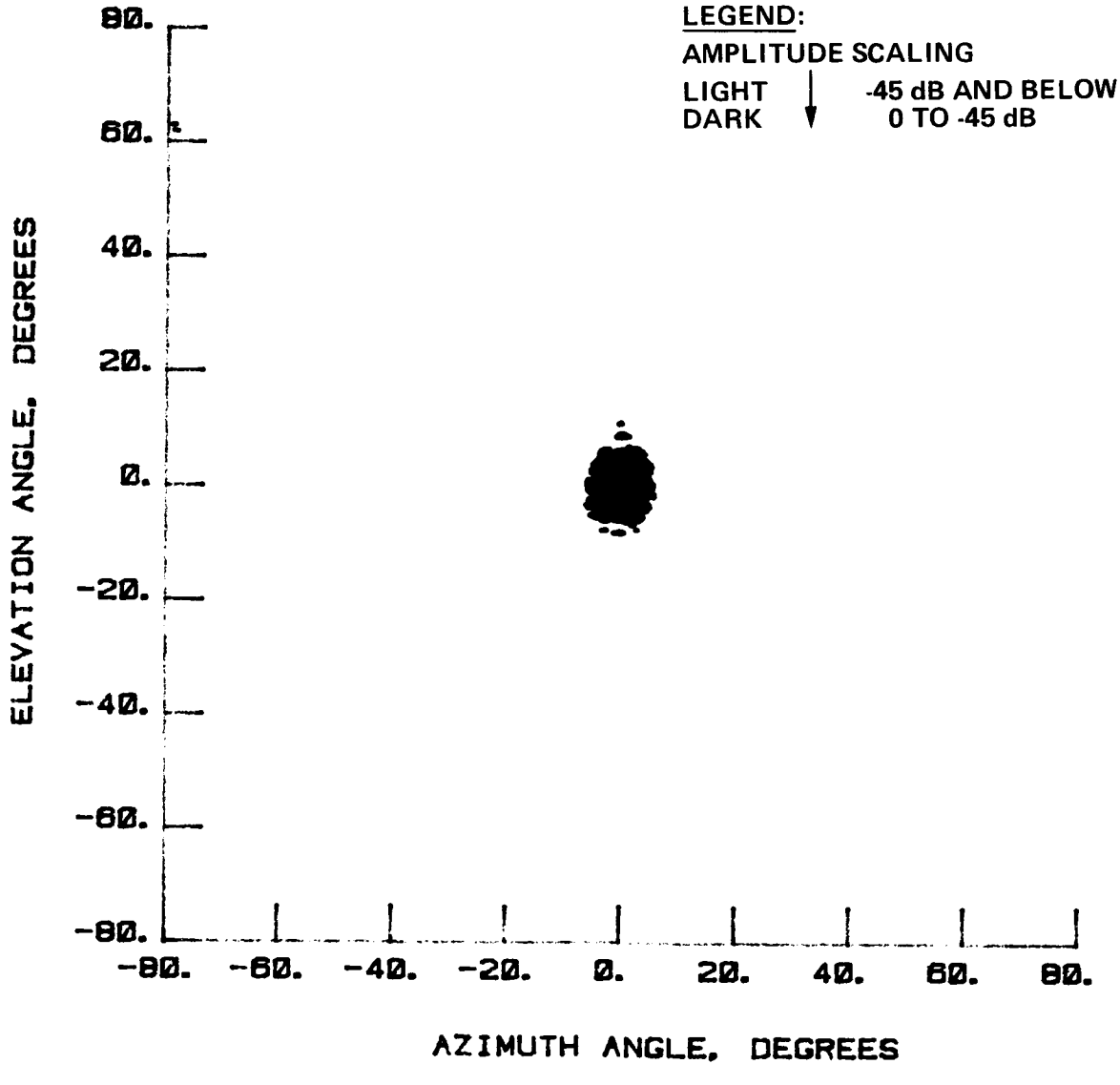

Figure 131 Far-Field Pattern from Reflector

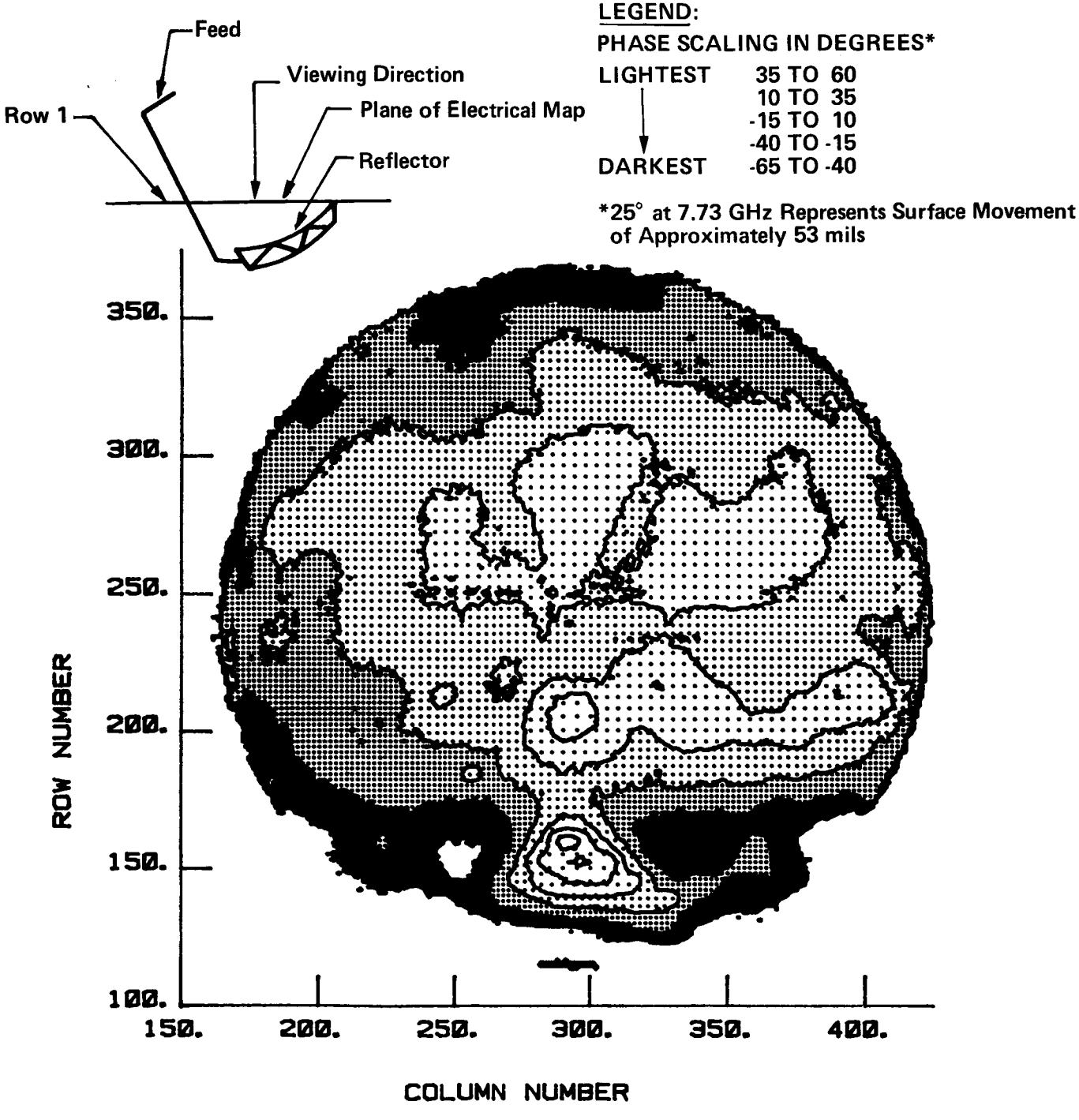

Figure 132 Electrical Map of the Aperture Phase at 7.73 GHz

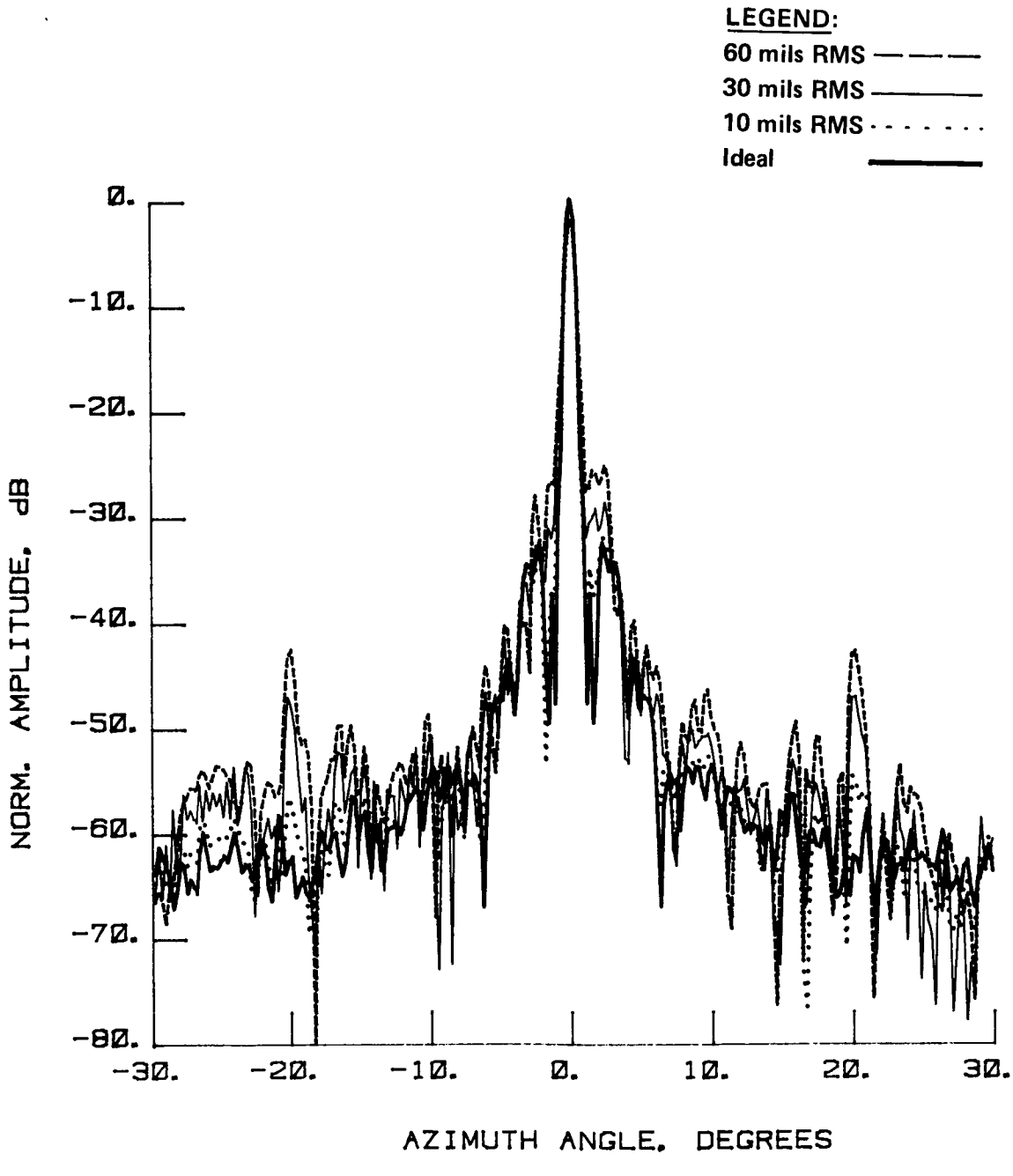

Figure 133 Modeling Surface rms

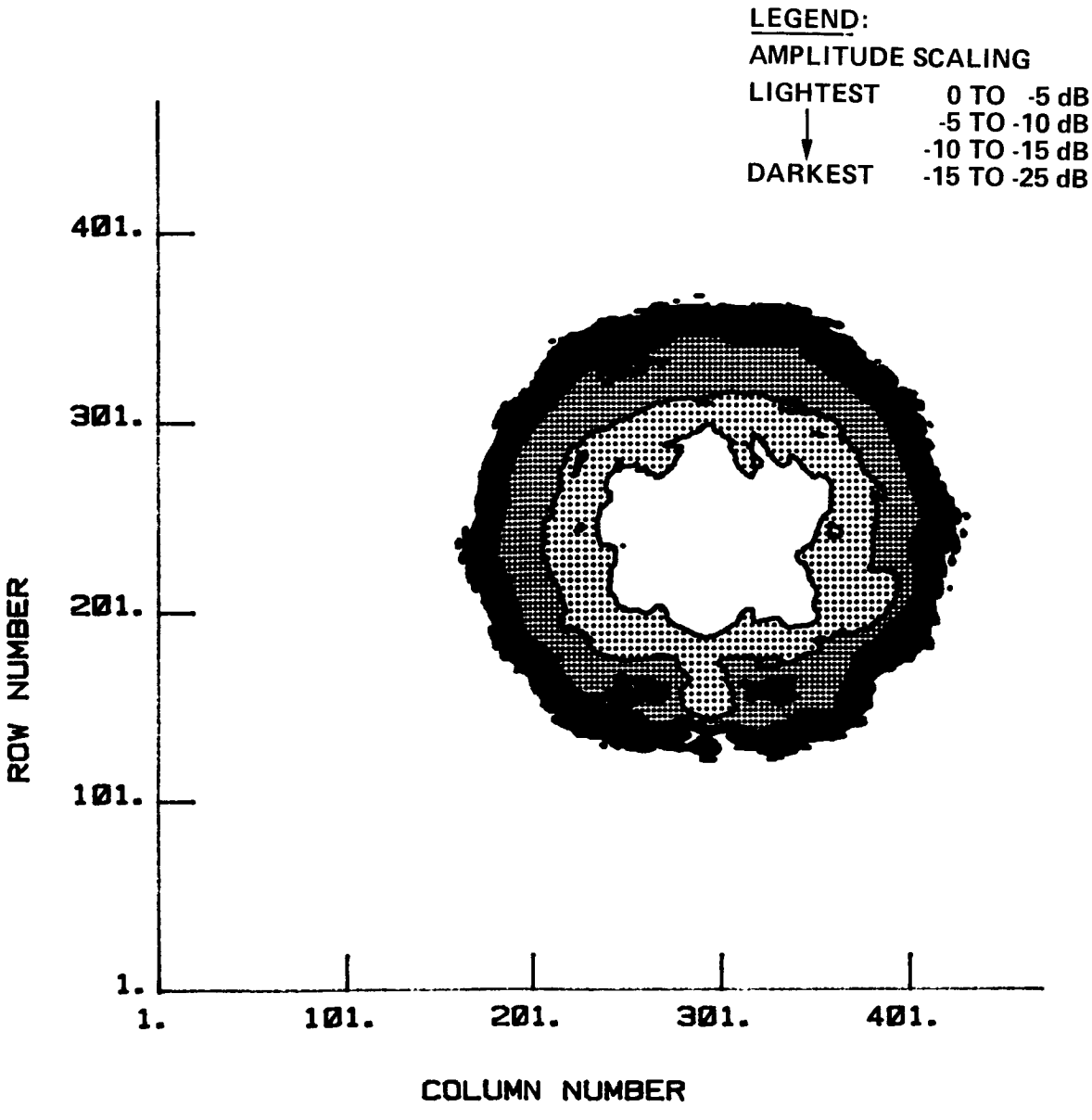

Figure 134 Near Field at 7.73 GHz, Amplitude Contour

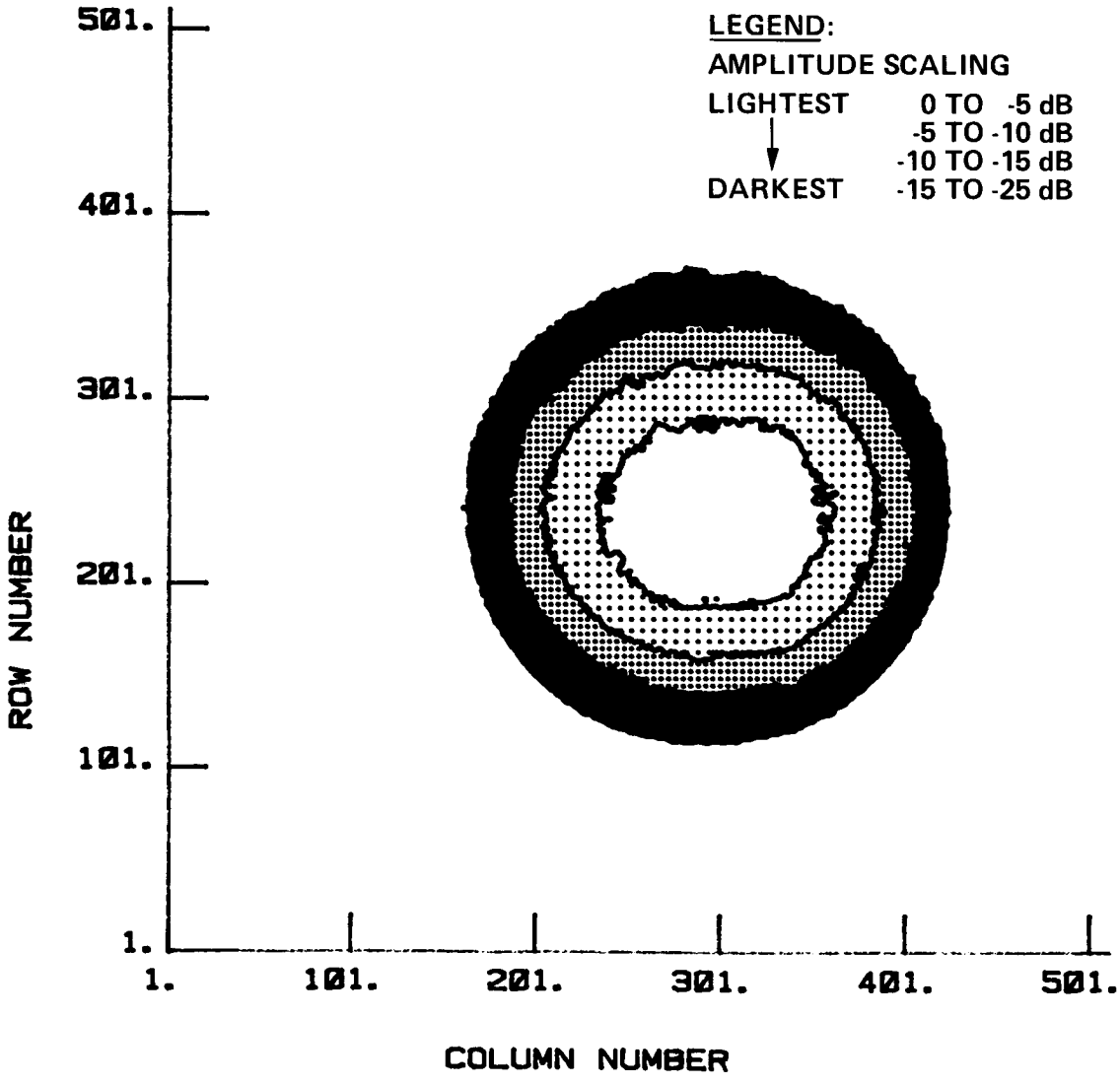

Figure 135 Aperture Field at 7.73 GHz, Amplitude Contour

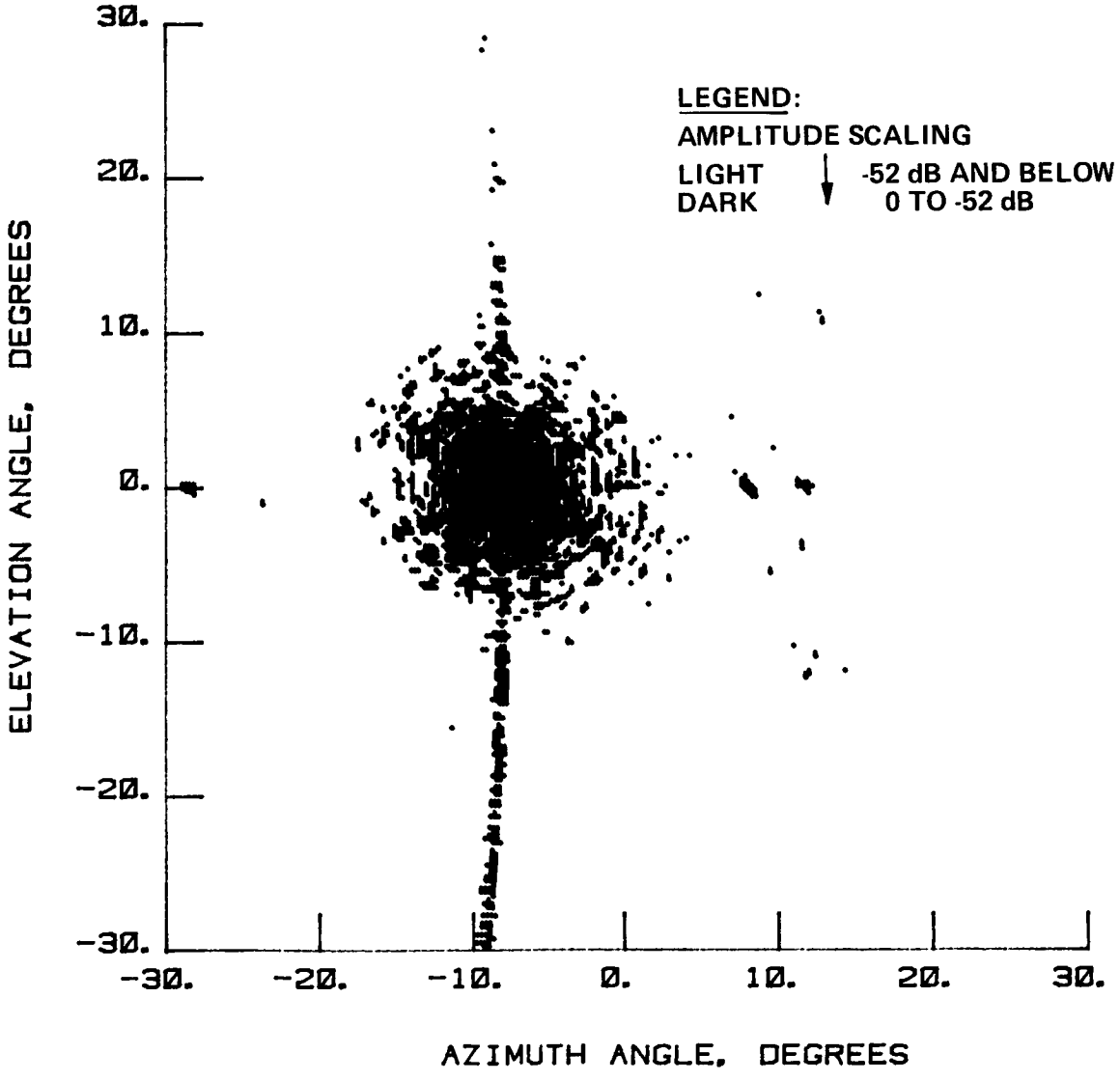

Figure 136 Far-Field Contour at 7.73 GHz of the Seam Effect

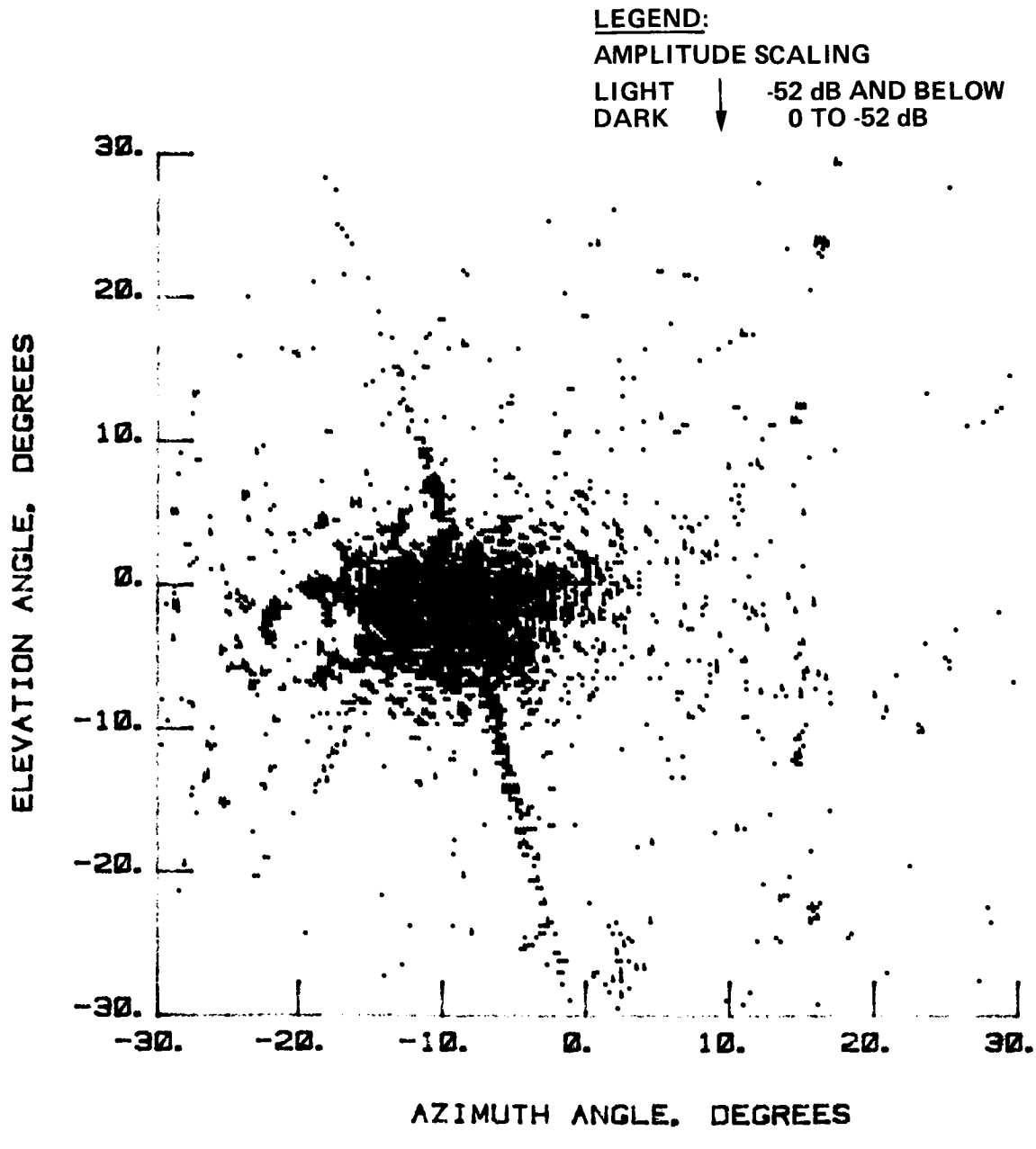

Figure 137 Far Field Generated by Rotating Antenna 15°

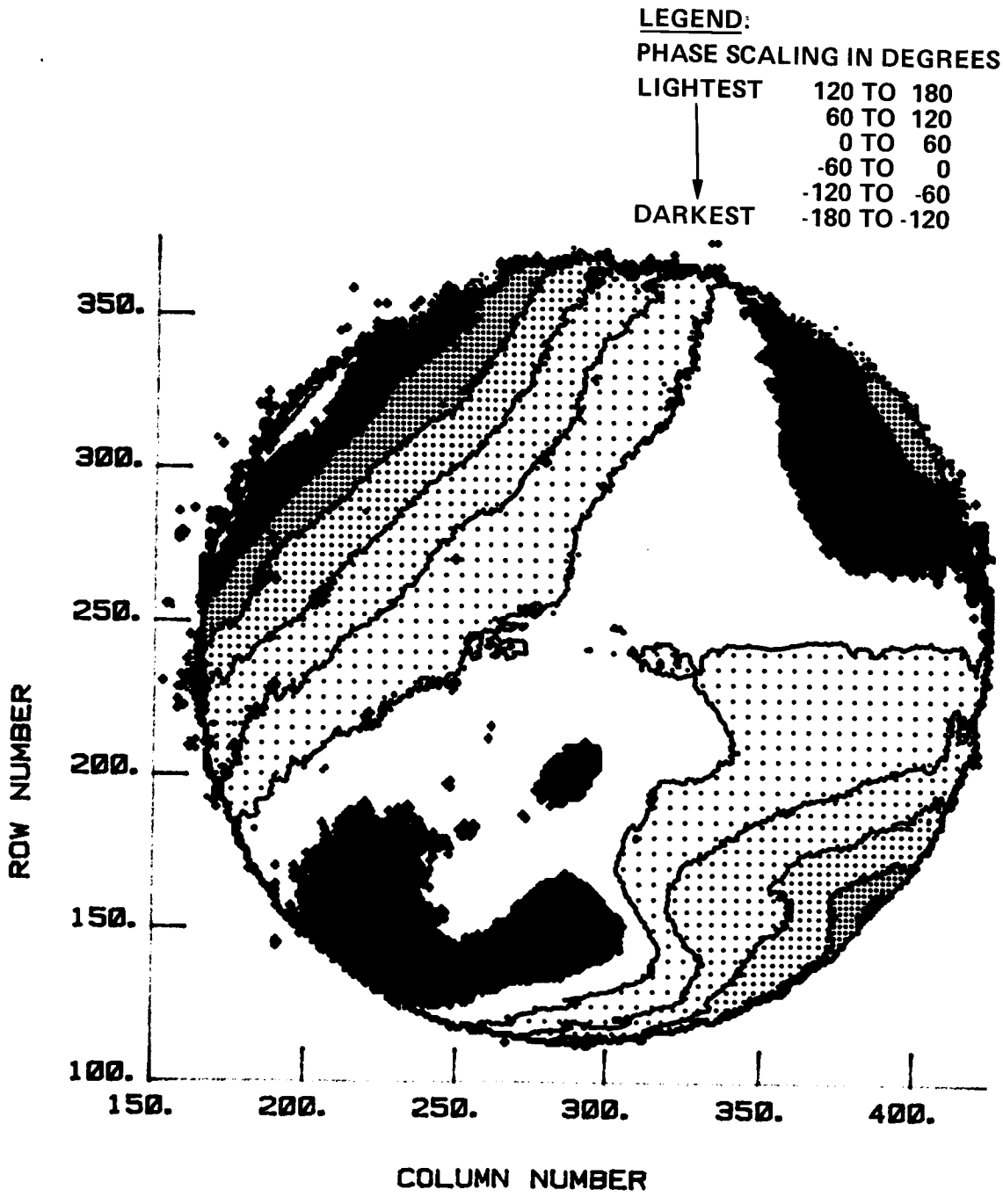

Figure 138 Aperture Phase Resulting from Steering Horn 8°

This Page Intentionally Left Blank

6.0 SUMMARY AND CONCLUSIONS

The GDC antenna has a high efficiency (gain compared to directivity) because of its offset design. The major losses that influenced the antenna gain (surface errors, feed losses, and aperture taper) never cause more than 5 dB total loss. Table 4 states the gain of the antenna for each of the feeds used. The large loss associated with the steered tests arose from a cubic phase error of over 180° caused by the large steering angle. Otherwise, the gains approached expected levels for an antenna of this size.

Table 4 Measured Antenna Performance Parameters

Test Number	Frequency, GHz	Peak Gain, dB	First Sidelobe, dB	Half-Power Beamwidth E-Plane, °	H-Plane, °
1	4.26	42.50	-24	0.99	1.01
2	4.26	20.30	--	--	--
3	2.27	36.54	-28	2.04	1.85
4	2.27	12.32	--	--	--
5	11.60	51.40	-19	0.46	0.38
6	11.60	27.25	--	--	--
7	7.73	49.24	-22	0.64	0.54
8	7.73	25.20	--	--	--
9*	7.73	44.90	-18	0.86	0.80
10*	7.73	25.90	--	--	--
11**	7.73	45.60	-19	0.83	0.77
12**	7.73	25.10	--	--	--

*Steered

**Steered and pointed

The sidelobe performance of the antenna, exceptional for the deployable reflector, demonstrated that a high-quality mesh surface can be maintained after several deployments. Although the surface did not meet the initial design prediction for accuracy, the levels it achieved showed that with minor design modification of components, notably the surface control cords, the surface might easily maintain a 15-mil rms or better after repeated deployments. The peak sidelobes, because of the 30-mil rms, never did exceed -19 dB even at 11.60 GHz, and decreased in proportion to frequency as Table 4 shows. This implies that the design could perform well even in Ku-band.

The surface control used by this reflector differed significantly from the 15-Meter Hoop Column Antenna. The cords used to tension the surface had an average spacing of approximately 4 in. shown by the grating lobes appearing in the electrical measurements. However, these grating lobes appeared at a much lower level than the ones for the 15-Meter Hoop Column Antenna because of the aperiodic control cord spacing, and the smaller spacing reduced the surface errors of pillowing.

The system used to implement surface control on this antenna involved much more complexity than that used for the 15-Meter Hoop Column Antenna, because over 1000 cords must be set individually to adjust the surface as compared to the 96 cords of the 15-Meter Hoop Column Antenna. Metric camera measurements were performed to check surface trueness, which is a function of the cord setting. These metric camera measurements determined that the surface apparently had approximately 30-mils rms when photographed at the NFTL. The surface was not adjusted (as it was for the Hoop Column Antenna) since the control cords were already locked down for the GDC antenna.

The metric camera measurements also correlated well with phase measurements of the antenna aperture, showing that for this type of antenna, design data obtained by surface measurements aid in predicting the electrical performance of the antenna. Although the metric camera data and theodolite data allow the prediction of secondary patterns that agree with the measured data, they can often miss features of the reflector pattern because of the sparseness of targets on the reflector surface. For this reflector, the seam effect and grating lobes are two examples of features not predicted by metric camera measurement data. Therefore, one major conclusion of this program was that electrical measurements will always yield important information on an antenna, even on one with an unblocked reflector such as the 5-Meter Tetrahedral Truss.

7.0 REFERENCES

1. John Hoover, Neill Kefauver, Tom Cencich and Jim Osborn, Near-Field Testing of the 15-Meter Model of the Hoop Column Antenna, Volume I--Final Technical Report. NASA CR-178059, 1986.

2. John Hoover, Neill Kefauver, and Tom Cencich, Near-Field Testing of the 15-Meter Model of the Hoop Column Antenna, Volume II--Near- and Far-Field Plots for the LaRC Feeds. NASA CR-178060, 1986.

3. John Hoover, Neill Kefauver, and Tom Cencich, Near-Field Testing of the 15-Meter Model of the Hoop Column Antenna, Volume III--Near- and Far-Field Plots for the JPL Feeds. NASA CR-178061, 1986.

4. Martin Marietta Denver Aerospace: "Antenna Pattern Measurement Description." Interim Progress Report, Project No. 1-28-1570.2379, April 9, 1985.

5. Martin Marietta Denver Aerospace: "Measurements Error Analysis." Interim Progress Report, Project No. 1-28-1570.2379, June 1985.

6. Allen C. Newell, "Upper Bound Errors in Far-Field Antenna Parameters Determined from Planar Near-Field Measurements, Part 2: Analysis and Computer Simulation." Lecture Notes for National Bureau of Standards Short Course, Boulder, Colorado, July 1975.

7. Arthur D. Yaghjian, Planar Near-Field Measurement Techniques on High Performance Array, Part 1: Error Analysis for Nonscanning Beam Patterns. AFAL-TR-75-67, July 1974.

Standard Bibliographic Page

1. Report No.	2. Government Accession No.	3. Recipient's Catalog No.
NASA CR-178147		

4. Title and Subtitle	5. Report Date
Near-Field Testing of the 5-Meter Model of the Tetrahedral Truss Antenna	August 1986
	6. Performing Organisation Code
7. Author(s)	8. Performing Organisation Report No.
Neill Kefauver, Tom Cencich, Jim Osborn, and J. T. Osmanski	MCR-85-640
9. Performing Organisation Name and Address	10. Work Unit No.
Martin Marietta Denver Aerospace P.O. Box 179 Denver, CO 80201	11. Contract or Grant No. NAS1-18016
12. Sponsoring Agency Name and Address	13. Type of Report and Period Covered
National Aeronautics and Space Administration Washington, DC 20546	Contractor Report
	14. Sponsoring Agency Code 506-58-23-01

15. Supplementary Notes

Technical Monitor - Lyle C. Schroeder, NASA Langley Research Center, Hampton, VA 23665-5225

16. Abstract

This report documents the technical results from near-field testing of the General Dynamics 5-meter model of the tetrahedral truss antenna at the Martin Marietta Denver Aerospace facility. A 5-meter square side of the tetrahedral served as the perimeter of the antenna, and a mesh surface and extensive surface contouring cord network was used to create a parabolic aperture shape to within an rms accuracy of 30 mils or better. Pattern measurements were made with offset feed systems radiating at frequencies of 7.73, 11.60, 2.27, and 4.26 (all in GHz). This report discusses the method of collecting the data, system measurement accuracy, the test data compiled, and diagostics and isolation of causes of pattern results. The technique of using near-field phase for measuring surface mechanical tolerances is included. Detailed far field antenna patterns and their implications are provided for all tests conducted.

17. Key Words (Suggested by Authors(s))	18. Distribution Statement
Large-Space Deployable Antenna Tetrahedral Truss Antenna Near-Field Antenna Patterns Offset Feeds Microwave Frequencies	Unclassified - Unlimited Subject Category 15

19. Security Classif.(of this report)	20. Security Classif.(of this page)	21. No. of Pages	22. Price
Unclassified	Unclassified	167	A08

For sale by the National Technical Information Service, Springfield, Virginia 22161